UNIVERSITÀ DEGLI STUDI DI MILANO

FACOLTÁ DI SCIENZE MATEMATICHE, FISICHE E NATURALI

Dipartimento di Chimica Inorganica, Metallorganica ed Analitica

"Lamberto Malatesta"

Dottorato di Ricerca In Chimica Industriale - CHIM/03

XXIII Ciclo

TESI DI DOTTORATO DI RICERCA

GLUCOSE ELECTROOXIDATION

Dott. Mauro PASTA

Matricola R07837

Tutore: Chiar.mo Prof. Michele ROSSI

Coordinatore: Chiar.ma Prof.ssa Dominique ROBERTO

Anno Accademico 2009/2010

TABLE OF CONTENTS

PREFACE

Glucose electrooxidation is a complex topic that needs a multidisciplinary approach to be deeply investigated; organic chemistry, electrochemistry, material science and catalysis backgrounds are certainly required. It is directly related to some important issues of the modern society: renewable bio-energy, energy recovery and healthcare. Concerning the above mentioned matters, glucose fuel cells, wastewater treatment in microbial fuel cells as well as glucose sensors are the key applications. My PhD work was devoted to research and develop such devices.

The thesis is divided into six chapters, so to keep the narration as clear as possible. It starts with an introduction where glucose, the main character of the dissertation, is presented and it continues with an overview on glucose electrooxidation from both theoretical classification and practical applications point of view. In chapter two, the mechanism of glucose non-enzymatic electrooxidation is discussed, focusing on the mechanism at gold electrodes, which I deeply studied in my PhD. Chapter three is dedicated to glucose sensing and its relation to Diabetes Mellitus, introducing a new approach to glucose determination. In chapter four glucose-gluconate alkaline fuel cells are discussed; after a basic study on the optimization of the operating conditions, performed on a commercially available cell, the superior electrocatalytic activity of gold nanoparticles is demonstrated and applied to the development of a new anode material. Chapter five is entirely dedicated to the emerging technology of microbial fuel cells applied to energy recovery from wastewater: new, promising anode and cathode materials based on textiles conformally coated with carbon nanotubes (CNT/textile) are proposed. Finally, chapter six deals with synthesis and physicochemical characterization of the CNT/textile material utilized in both chapters four and five; its application to the development of stretchable, porous, conductive textiles for the wearable electronics industry is also discussed.

There has been times, especially during my first year, when the complexity of the system seemed to be overwhelming, but now I am glad to have worked on this subject because it helped me improve my ability to overcome problems and it introduced me (from the backdoor) to the fascinating world of electrochemistry.

On the basis of this work about eight papers on international journals have been or are going to be published soon.

Mauro Pasta

CHAPTER I: INTRODUCTION

Chapter I: Introduction

In this first chapter D(+)-glucose molecule, the main character of the dissertation, is introduced describing its chemistry, occurrence, industrial production and utilization. Obviously the details of its biological fundamental role are only mentioned. Glucose electrooxidation will then be discussed starting from its history, classification and definitions emphasizing the most important applications involving this topic.

1.1 Glucose: chemistry, occurrence and industrial production (adapted from [1])

Glucose, a monosaccharide (or simple sugar), is an important carbohydrate in biology. The living cell uses it as a source of energy and metabolic intermediate. Glucose is one of the main products of photosynthesis and starts cellular respiration in both prokaryotes and eukaryotes. The name comes from the Greek word *glykys* (γλυκύς), which means "sweet", plus the suffix "-ose" which denotes a carbohydrate.

Two stereoisomers of the aldohexose sugars are known as glucose, only one of which (D-glucose) is biologically active. D-glucose is often referred to as dextrose monohydrate, or, especially in the food industry, simply dextrose (from *dextrorotatory glucose*). The mirror-image of the molecule (L-glucose) cannot be phosphorylated by hexokinase, the first enzyme in the glycolysis pathway, and so it is not broken down by living organisms to release energy.

Since L-glucose is sweet (a bit less sweet than D-glucose), but cannot be used as source of energy, it had been proposed as a low-calorie sweetener. L-Glucose was also found to be a laxative, and proposed as a colon-cleansing agent. Its derivative, L-glucose pentaacetate, was found to stimulate insulin release.

Glucose is commonly available in the form of a white substance or as a solid crystal. It can also be commonly found as an aqueous solution. The main chemical, physicochemical and thermochemical properties of D-(+) glucose can be found in Appendix A.

1.1.1 Structure

Glucose ($C_6H_{12}O_6$) contains six carbon atoms one of which is part of an aldehyde group so it is therefore referred to as an aldohexose. The glucose molecule can exist in both open-chain (acyclic) and ring (cyclic) form the latter being the result of a covalent bond between the aldehyde C atom and the C-5 hydroxyl group to form a six-membered cyclic hemiacetal. In water solution both forms are in equilibrium and at pH 7 the cyclic form is predominant. As the

ring contains five carbon atoms and one oxygen atom, which resembles the structure of pyran, the cyclic form of glucose is also referred to as glucopyranose. In this ring, each carbon is linked to a hydroxyl side group with the exception of the fifth atom, which links to a sixth carbon atom outside the ring, forming a CH_2OH group.

1.1.2 Isomers

Aldohexose sugars have 4 chiral centers giving $2^4 = 16$ stereoisomers. These are split into two groups, L and D, with 8 sugars in each. Glucose is one of these sugars, and L and D-glucose are two of the stereoisomers. Only 7 are found in living organisms, of which D-glucose (Glu), D-galactose (Gal) and D-mannose (Man) are the most important. These eight isomers (including glucose itself) are all diastereoisomers in relation to each other, and all belong to the D-series.

An additional asymmetric center at C-1 (called *the anomeric carbon atom*) is created when glucose cyclizes and two ring structures, called anomers are formed — *α*-glucose and *β*-glucose. These anomers differ structurally with respect to the relative positioning of their hydroxyl group linked to C-1 and the group at C-6, which is termed the reference carbon. When D-glucose is drawn as a Haworth projection or in the standard chair conformation, the designation *α* means that the hydroxyl group attached to C-1 is positioned trans to the -CH_2OH group at C-5, while *β* means it is cis. Another popular method of distinguishing *α* from *β* is by observing whether the C-1 hydroxyl is below or above the plane of the ring, respectively, but this method is an inaccurate definition and may fail if the glucose ring is drawn upside down or in an alternative chair conformation. The *α* and *β* forms interconvert over a timescale of hours in aqueous solution, to a final stable ratio of *α*:*β* 36:64, in a process called *mutarotation* Figure 1.

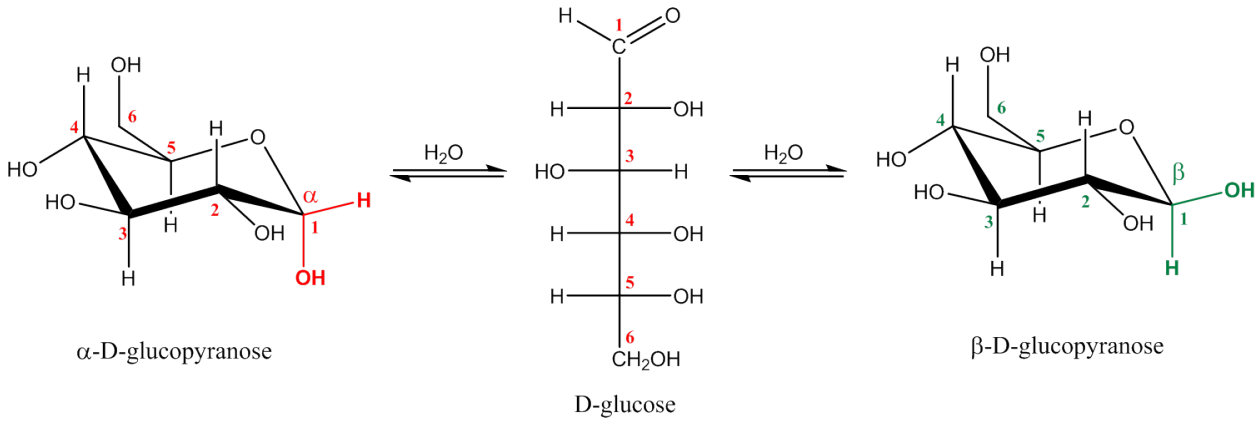

Figure 1. Glucose mutarotation.

1.1.3 Rotamers

Within the cyclic form of glucose, rotation may occur around the O6-C6-C5-O5 torsion angle (termed the ω-angle) to form three rotamer conformations as shown in the diagram below. Referring to the orientations of the ω-angle and the O6-C6-C5-C4 angle the three stable staggered rotamer conformations are termed *gauche-gauche* (gg), *gauche-trans* (gt) and *trans-gauche* (tg). For methyl *α*-D-glucopyranose at equilibrium the ratio of molecules in each rotamer conformation is reported as 57:38:5 gg:gt:tg. This tendency for the ω-angle to prefer a *gauche* conformation is attributed to the gauche effect.

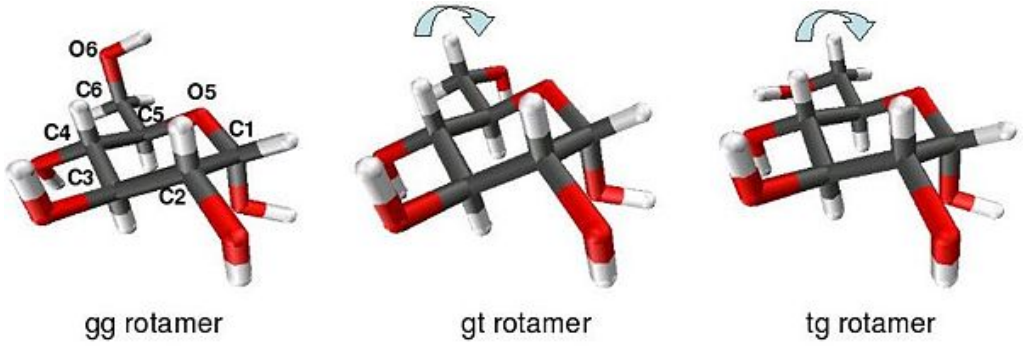

Figure 2. Rotamer conformations of α-D-glucopyranose.

1.1.4 Production

Natural

Glucose is one of the products of photosynthesis in plants and some prokaryotes.

In animals and fungi, glucose is the result of the breakdown of glycogen, a process known as glycogenolysis. In plants the breakdown substrate is starch.

In animals, glucose is synthesized in the liver and kidneys from non-carbohydrate intermediates, such as pyruvate and glycerol, by a process known as gluconeogenesis.

Commercial

Glucose is produced via the enzymatic hydrolysis of starch. Many crops can be used as the source of starch. Maize, rice, wheat, potato, cassava, arrowroot, and sago are all used in various parts of the world. In the United States, cornstarch (from maize) is used almost exclusively.

This enzymatic process has two stages. Over the course of 1-2 hours near 100 °C, enzymes hydrolyze starch into smaller carbohydrates containing on average 5-10 glucose units each. Some variations on this process briefly heat the starch mixture to 130 °C or hotter one or more times. This heat treatment improves the solubility of starch in water, but deactivates the enzyme, and fresh enzyme must be added to the mixture after each heating.

In the second step, known as "saccharification", the partially hydrolyzed starch is completely

hydrolyzed to glucose using the glucoamylase enzyme from the fungus *Aspergillus niger*. Typical reaction conditions are pH 4.0–4.5, 60 °C, and a carbohydrate concentration of 30–35% by weight. Under these conditions, starch can be converted to glucose at 96% yield after 1–4 days. Still higher yields can be obtained using more dilute solutions, but this approach requires larger reactors and processing a greater volume of water, and is not generally economical. The resulting glucose solution is then purified by filtration and concentrated in a multiple-effect evaporator. Solid D-glucose is then produced by repeated crystallizations.

1.1.5 Function

We can speculate on the reasons why glucose, and not another monosaccharide such as fructose (Fru), is so widely used in evolution, ecosystem and metabolism. Glucose can form from formaldehyde under abiotic conditions, so it may well have been available to primitive biochemical systems. Probably more important to advanced life is the low tendency of glucose, by comparison to other hexose sugars, to non-specifically react with the amino groups of proteins. This reaction (glycation) reduces or destroys the function of many enzymes. The low rate of glycation is due to glucose preference for the less reactive cyclic isomer. Nevertheless, many of the long-term complications of diabetes (e.g., blindness, kidney failure, and peripheral neuropathy) are probably due to the glycation of proteins or lipids. In contrast, enzyme-regulated addition of glucose to proteins by glycosylation is often essential to their function.

1.1.6 As an energy source [2]

Glucose is a ubiquitous fuel in biology. It is used as energy source in most organisms, from bacteria to humans. Use of glucose may be by either aerobic or anaerobic respiration (fermentation). Carbohydrates are the human body key source of energy, through aerobic respiration, providing approximately 4 kilocalories (17 kilojoules) of food energy per gram. Breakdown of carbohydrates (e.g. starch) yields mono- and disaccharides, most of which is glucose. Through glycolysis and later in the reactions of the Citric acid cycle (TCAC), glucose is oxidized to eventually form CO_2 and water, yielding energy, mostly in the form of ATP. The insulin reaction, and other mechanisms, regulates the concentration of glucose in the blood. A high fasting blood sugar level is an indication of pre-diabetic and diabetic conditions (see Appendix C). Glucose is a primary source of energy for the brain, and hence its availability influences psychological processes. When glucose is low, psychological processes requiring mental effort (e.g., self-control) are impaired.

1.1.7 Glucose in glycolysis [2]

The use of glucose as energy source in cells is via aerobic or anaerobic respiration. Both of these start with the early steps of the glycolysis metabolic pathway. The first step is the phosphorylation of glucose by hexokinase to prepare it for later breakdown to provide energy.

Table 1. Glucose phosphorylation.

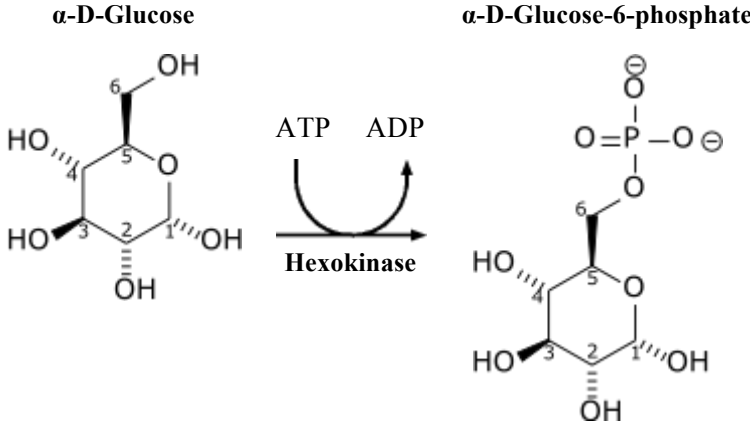

The major reason for the immediate phosphorylation of glucose by hexokinase is to prevent diffusion out of the cell. The phosphorylation adds a charged phosphate group so the glucose 6-phosphate cannot easily cross the cell membrane. Irreversible first steps of metabolic pathway are common for regulatory purposes.

1.1.8 As a precursor [2]

Glucose is critical in the production of proteins and in lipid metabolism. Also, in plants and most animals, it is a precursor for vitamin C (ascorbic acid) production. It is modified for use in these processes by the glycolysis pathway.

Glucose is used as a precursor for the synthesis of several important substances. Starch, cellulose, and glycogen ("animal starch") are common glucose polymers (polysaccharides). Lactose, the predominant sugar in milk, is a glucose-galactose disaccharide. In sucrose, another important disaccharide, glucose is joined to fructose. These synthesis processes also rely on the phosphorylation of glucose through the first step of glycolysis.

1.1.9 Sources and absorption

All major dietary carbohydrates contain glucose, either as their only building block, as in starch and glycogen, or together with another monosaccharide, as in sucrose and lactose. In the lumen

of the duodenum and small intestine, the oligo- and polysaccharides are broken down to monosaccharides by the pancreatic and intestinal glycosidases. Glucose is then transported across the apical membrane of the enterocytes by the sodium/glucose cotransporter 1 (SLC5A1), and later across their basal membrane by the sodium/glucose cotransporter 2 (SLC2A2). Some of the glucose goes directly toward fuelling brain cells and erythrocytes, while the rest makes its way to the liver and muscles, where it is stored as glycogen, and to fat cells, where it can be used to power reactions which synthesize some fats. Glycogen is the body auxiliary energy source, tapped and converted back into glucose when there is need for energy.

1.2 Glucose electrooxidation

Glucose electrooxidation was firstly studied about one hundred years ago in sulphuric acid electrolyte [3], attracting a lot of interest due to its potential application in several areas such as the development of blood sugar sensor and biological fuel cells [4,5].

Glucose electrooxidation can be divided into three main categories according to the catalytic material enabling the electrode reactions: enzymatic, microbial, and abiotical (non-enzymatic).

- *Enzymatic* electrooxidation employs enzymes such as glucose oxidase and glucose dehydrogenase in their isolated forms.
- *Non-enzymatic* electrooxidation makes use of non-biological catalysts, e.g., noble metals or activated carbon.
- *Microbial* electrooxidation employs the whole enzymatic system of an electroactive microorganism.

An overview on each of these branches is reported in the next paragraphs.

1.2.1 The Enzymes of Glucose Electrooxidizing Anodes [4]

The two families of enzymes that are most widely used in the electrooxidation of glucose are glucose oxidases (GOx) and PQQ-glucose dehydrogenases (PQQ-GDH).

The wild-type enzymes were originally derived, respectively, from Aspergillus niger and Acinetobacter calcoaceticus. The wild-type enzymes were replaced by engineered enzymes, produced in other organisms. The purpose of their mutation and expression in different organisms was to increase enzyme yield, facilitate enzyme purification, enlarge specific activity, improve the enzyme stability, and enhance selectivity for glucose.

The two enzyme families differ in redox potentials, strengths of the bonds between their protein-devoid apoenzymes and their cofactors, co-substrates, turnover rates, Michaelis constants (*Km*),

and selectivity for glucose.

The FAD cofactor of GOx is strongly bound to apo-GOx; $FADH_2$-GOx reacts with O_2 to yield FAD-GOx and H_2O_2. The apparent formal redox potential of GOx at 25 °C and pH 5.3 is -0.063 V (0.011 V versus SHE); at pH 9.3 it is -0.200 V (0.010 V versus SHE). Nevertheless, according to a recent re-estimate the apparent formal redox potential of GOx at pH 7.2 is -0.048 V versus SHE. GOx is relatively specific for glucose. In the electrochemically relevant half-reaction in which glucose is oxidized by FADGOx, about $5 \cdot 10^3$ glucose molecules are oxidized per second.

PQQ-GDH catalyzes not only the oxidation of glucose, but also of other sugars; the PQQ cofactor is moderately well bound to the apoenzyme in the presence of Ca^{2+}excess, which also stabilizes the binding of the PQQ-cofactor by the apoenzyme. Its redox potential at pH 7.0, in the presence of Ca^{2+} excess, is 10.5 mV (4 mV versus SHE). Unlike the $FADH_2$ of GOx, the $PQQH_2$ of GDH is not oxidized by O_2. In the half-reaction of PQQ-GDH, in which glucose is oxidized, 11800 glucose molecules are oxidized per second.

In addition to PQQ-GDH, two other members of the dehydrogenase family have begun to be applied in electrochemical glucose detection. These are NAD-dependent GDH and FAD-dependent GDH. These enzymes combine the oxygen independence of PQQ-GDH with the specificity of GOx, and it is likely that they will be more widely used in the future.

1.2.2 Direct, non-enzymatic electrooxidation of glucose [4]

Glucose was directly electrooxidized to gluconic acid in a sulfuric acid solution at a lead anode in 1909 by Walther Loeb. In 1937, the Atlas Powder Company manufactured sorbitol commercially by electroreducing glucose in a $NaOH$-Na_2SO_4 solution at an amalgamated lead electrode in a diaphragm cell. Studies of direct electrooxidation and electroreduction of glucose in basic (pH > 11) and acidic (pH < 1) solutions continue to date. At pH 7.4 glucose has been directly electrooxidized, at a current density of 1 mA cm^{-2}, on an electrode coated with a 4,4′,4″,4‴-tetrasulfophthalocyanine complex of molybdenum oxide. Nevertheless, partial oxidation products of glucose irreversibly adsorb on and poison most electrocatalysts. Hence, electrochemical assays of biological glucose solutions utilize glucose oxidation-catalyzing enzymes.

1.2.3 Microbial electrooxidation of glucose [6]

The first study on mediatorless microbial electrooxidation of glucose is directly associated with the discovery of *R. ferriducens*.

R. ferrireducens was isolated from anoxic subsurface sediments of Oyster Bay, Virginia, USA, as dissimilatory Fe(III)-reducing microorganism. It is able to grow in the temperature range at 4-30 °C, the optimum temperature being 25 °C.

Although its substrate range was originally reported to be limited to organic acids, further evaluation demonstrated that it could oxidize glucose to carbon dioxide with Fe(III) serving as the sole electron acceptor and could conserve energy to support growth from this metabolism. *R. ferrireducens* does not grow on glucose in the absence of Fe(III) and glucose does not react with Fe(III) in the absence of the bacterium. The stoichiometry of glucose utilization and Fe(III) reduction is consistent with the reaction:

$$C_6H_{12}O_6 + 6\ H_2O + 24\ Fe(III) \rightarrow 6\ CO_2 + 24\ Fe(II) + 24\ H^+$$

Fructose is oxidized in a similar manner. This is the first time that complete oxidation of sugars coupled to Fe(III) reduction has been observed in an organism capable of growing at circumneutral pH.

Recent studies have demonstrated that Fe(III)-reducing microorganisms in the family *Geobacteraceae* can also directly transfer electrons onto electrodes. However, the range of electron donors that these organisms can use is limited primarily to simple organic acids, such as acetate. Thus, they rely on fermentative microorganisms to produce their required electron donors from sugars and other more complex organic compounds. To determine whether *R. ferrireducens* might transfer electrons to an electrode with glucose as the electron donor, the bacterium was inoculated into the anode compartment of an anaerobic two-chambered vessel with each side containing a graphite electrode and the two chambers connected by a cation-selective membrane. The anode was poised at +200 mV against an Ag/AgCl reference electrode. Glucose (2 mM) in the anode medium was consumed with the production of current and the growth of *R. ferrireducens*. Once the current generation reached a plateau, about the 10% inoculums from the anode chamber was transferred to a new chamber.

Enzymatic electrooxidation was deeply studied in the past and many researchers are working on it nowadays, therefore it will not be discussed in this thesis. For an overview of the topic I suggest the review of Heller and Feldman [4] and a good biochemistry book [2].

During my PhD I focused my attention on non enzymatic electrooxidation at gold electrodes and on microbial electrooxidation applied to microbial fuel cells for wastewater treatment applications.

1.3 Practical applications

Electrochemical oxidation of glucose has generated much interest over the years. It has been extensively studied for applications in glucose sensors, [4] whose optimization (in terms of response time, lifetime, sensitivity and selectivity) is required to improve the treatment of Diabetes Mellitus, a chronic disease affecting millions of people around the world [7]. Most studies on this subject have involved the use of the enzymes to catalyze the oxidation of glucose to δ-gluconolactone [4]. Although enzymatic detection usually shows good selectivity and high sensitivity, the enzyme is easily denatured during its immobilization process. The most serious problem of such sensors is the inherent lack of stability due to the sensitive nature of enzymes, especially in implantable devices that represent the new frontier in diabetes management. Non-enzymatic glucose sensors have been studied in order to develop effective enzyme-free sensors.
Much attention has also been paid to the electrocatalytic oxidation of glucose for the construction of glucose-air biofuel cells and abiotically catalyzed fuel cells. In comparison with other fuel cells, this new type is powered with glucose derived from degradable biomass. Moreover, the direct glucose fuel cell is of high energy-density. Theoretically, glucose can be completely oxidized to CO_2 and H_2O, releasing 24 electrons per glucose molecule, although the transfer of 24 electrons has not yet been achieved [8]. In recent years enzymatic glucose biofuel cells have received more attention than the non enzymatic ones because of the high power densities as compared with their abiotically catalyzed counterparts. The key technological problem for improving the performance of abiotically catalyzed fuel cells is to develop high efficiency electrocatalysts for the glucose oxidation. Microbial fuel cells (MFCs) harness the metabolism of microorganisms, converting chemical potential energy into electrical energy. Applications include energy recovery not only from glucose but also from reducing matter contained in waste, such as organic matter in wastewater, marine sediment, or human excrement in space. All of these subjects will be discussed in details in the following chapters.

CHAPTER II: MECHANISM OF GLUCOSE ELECTROOXIDATION

Chapter II: Mechanism of glucose electrooxidation

Before going into the details of glucose electrooxidation applications, it is necessary to understand the mechanism with which the process happens in order to easily identify and overcome all the potential problems encountered in its use.

This chapter deals with the *non-enzymatic* mechanism of glucose electrooxidation. After a brief introduction on the previously proposed mechanisms, the complex oxidation of glucose at the surface of gold electrodes will be discussed in detail in different conditions of pH, buffer and halide concentration. As observed in previous studies, an oxidative current peak occurs during the cathodic sweep showing highly linear dependence on glucose concentration, when other electrolyte conditions are unchanged. The effect of the different conditions on the intensity of this peak has stressed the limitations of the previously proposed mechanisms. A mechanism able to explain the presence of this oxidative peak will be proposed. The mechanism takes into account ion-sorption and electrochemical adsorption of OH^- as well as buffer species (K_2HPO_4/KH_2PO_4) and halides.

2.1 State of the art

The electrocatalytic oxidation of glucose at noble metal electrodes has been broadly explored, mainly for its potential application to biofuel cells or as a way to transform interesting biomass resources into valuable chemicals. These studies were based on mechanistic considerations and there is a certain agreement on the first step of action which is (at Pt electrodes) commonly believed to proceed through a dehydrogenation step upon adsorption of glucose.

Beden at al. [9] deeply studied the mechanism of glucose electrooxidation at platinum electrodes, by means of SPAIRS (single potential-alteration surface infrared spectroscopy) [10] and SNIFTIRS (Subtractively normalized interfacial Fourier transform infrared spectra) [11], proposing the following mechanism.

In the hydrogen region (Low Potential ~ -0.5 V): The first step is the chemisorption of glucose, associated with the first voltammetric peak:

(1) 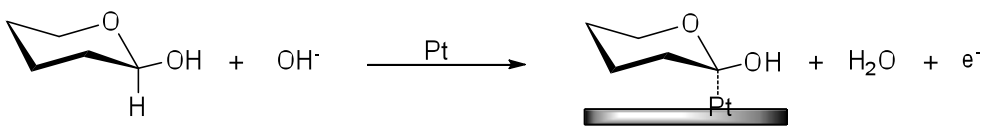

Process (1) takes place at the free Pt sites due to hydrogen oxidation:

(2) $Pt{-}H + OH^- \longrightarrow Pt + H_2O + e^-$

In the hydrogen and double layer region, the adsorbed dehydrated intermediate can be further oxidized to weakly adsorbed gluconate, the configuration of which depends on the potential:

(3) 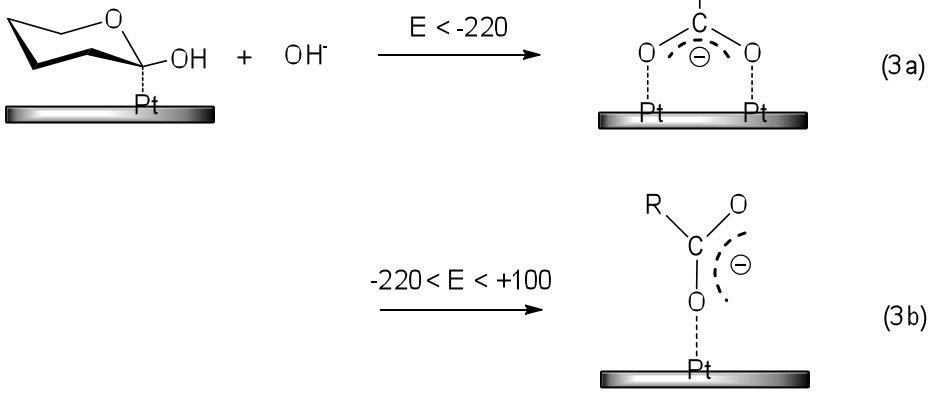

Weakly adsorbed gluconate species can desorb, forming solution gluconate.

At potentials greater than 0.1 V and up to the anodic limit, the adsorbed dehydrogenated intermediate formed by reaction (1) leads by oxidation to a δ-gluconolactone structure, *i.e.*, no breaking of the C-O-C bond is observed on the surface.

(4) 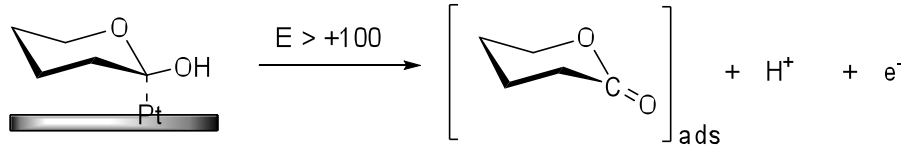

Desorption of lactone occurs slowly (5), leading to gluconate by hydrolysis (6).

(5) 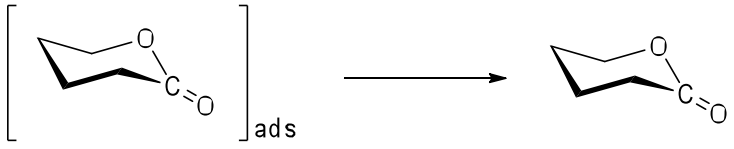

(6) 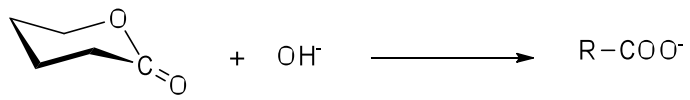

During the negative potential sweep, the surface lactone production remains the dominant

process on the oxidized surface. When the potential is cathodic enough to reduce the surface, reactive OH^- are released in the immediate vicinity of the surface by reaction. Breaking of the C-O-C bond occurs, the oxidation process leads to weakly bonded gluconate.

(7) 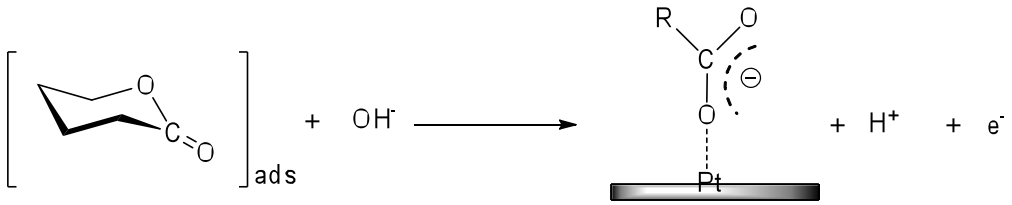

Weakly bonded gluconate desorbs into solution (8).

(8) 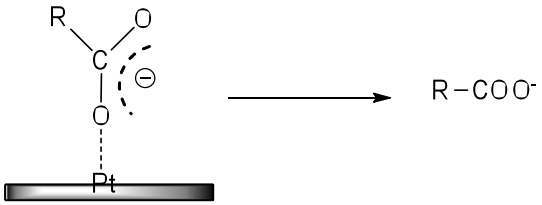

In the hydrogen region, the same processes occur, except that reactive OH^- are produced by water reaction (reverse of reaction (2)).

On the basis of this study we proposed a mechanism of glucose electrooxidation at gold electrodes.

2.2 Mechanism of glucose electrooxidation at gold electrodes [12]

2.2.1 Introduction

The electrocatalytic oxidation of glucose in alkaline medium was investigated using Cu, Ni, Fe, Pt and Au electrodes [13]. Among them, platinum has been the most widely studied [14-18]; in particular Beden *et al.* applied a reflectance IR spectroscopic technique to study the electrooxidation process of D-glucose at platinum electrodes in alkaline medium [9]. However, platinum also proved to be extremely non-selective and susceptible to poisoning by various components of blood and other physiological media over extended use [18-20].

Gold is an attractive metal for the oxidation of glucose, because its oxidation potential in neutral and alkaline medium is more negative compared to the other metals [21,22] and therefore has been extensively examined [13,22-31].

Nikolaeva *et al.* proposed a mechanism for glucose electrooxidation at high potentials, in which

a layer of gold oxide formed on the surface of a gold electrode could have a great catalytic effect on glucose oxidation [32]. The suggested mechanism was the following:

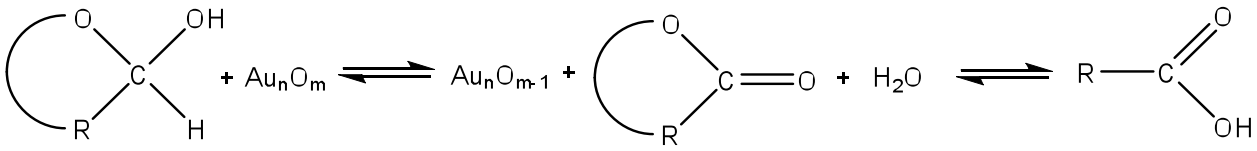

or

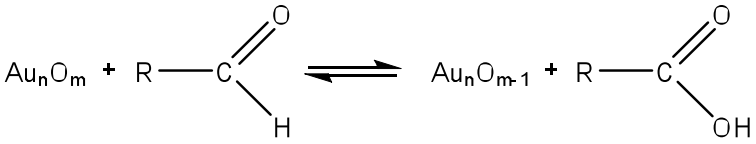

This reaction was followed by rapid electrochemical regeneration of the surface oxide:

$$AunOm{-}1{+}\ 2OH{-} \rightleftharpoons AunOm{+}H2O{+}2e{-}$$

In a subsequent study, Makovos *et al.* first identified a positive current peak during the cathodic sweep in cyclic voltammetry and highlighted a highly linear dependence between the maxima of current values and glucose concentration in a wide potential range depending on the medium composition [33]. They also proposed a different mechanism for the peak generation, claiming that the one provided by Nikolaeva *et al.* did not account for the fact that the reaction proceeds only when the potential favors a partial reduction of the gold oxide:

$$AunOm{+}\ 2e{-} \rightleftharpoons AunOm{-}1{+}O2{-}$$

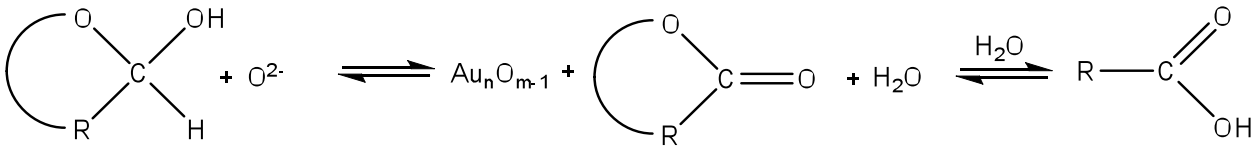

Followed by:

$$AunOm{-}1{+}\ 2OH{-} \rightleftharpoons AunOm{+}H2O{+}2e{-}$$

Chlorides, amino acids, and human albumin were observed to inhibit the reaction whereas urea and L-ascorbic acid contributed a stabilizing effect to the performance of the electrode. They concluded that gold oxide might be successfully utilized as catalyst for glucose oxidation in glucose sensors or biological fuel cells, if a proper separation of the inhibitors was achieved. In fact, this is the basis of the pulsed amperometric detection technique (PAD) at gold electrodes which, coupled with liquid chromatography (LC), gained prominence for the analysis of complex mixtures of polyalcohols and carbohydrates in alkaline medium [34].

Nevertheless the presence of the previously reported inhibitors forbids the direct application of this system in blood, where it is mainly required. Among these inhibiting species, chlorides are the most problematic because they are present in a high concentration in the blood (about 0.1 M) and their separation from glucose is difficult to achieve.

Makovos *et al.* attempted to use a gold electrode in media containing chloride ions, but discovered that chloride ions, even at trace levels, strongly inhibit any response toward glucose. They suggested that the presence of Cl^- ions caused gold to dissolve instead of forming an oxide layer:

$$Au + 4Cl^- \rightleftharpoons AuCl4^- + 3e^-$$

Consequently, the unoxidized gold has no electro-catalytic activity with respect to the oxidation of glucose.

Many questions remain unanswered by the mechanisms proposed by Nikoleava and Makovos:

1) If these mechanisms are correct, the charge under the cathodic oxidative peak current should show a dependence on the oxide thickness, not on the glucose concentration;
2) The last step proposed in both mechanisms is gold re-oxidation, however it is difficult to imagine this re-oxidation taking place at such a low potential (down to 0.0 V vs. RHE) when the same reaction (initial formation of the oxide) in the anodic sweep start at 0.8 V vs. RHE;
3) The peak onset is very sharp, but there is also a long tail after the main peak which is difficult to explain with the proposed mechanism: it seems instead that the reduction of the oxide enables the oxidation of the glucose;
4) The data does not conclusively suggest that gold oxide that is really what is formed in these conditions.

In the present study we investigated the effects of varying chloride concentration, pH and buffer conditions on the electrooxidation of glucose at a gold electrode, proposing a new mechanism

for the positive current peak formation during the cathodic sweep. The comprehension of the mechanisms behind the formation of this peak was necessary to correctly lay the groundwork for upcoming work concerning glucose sensing. The experimental details can be found in Appendix D.

2.2.2 Results and discussion

Figure 3 shows a typical cyclic voltammogram of glucose electrooxidation in alkaline solution. The discussion of the overall mechanism is not the aim of this work; a deep analysis has been already discussed by Beden and coworkers at platinum electrodes and low temperature [9]. The aim of the present work is to understand the influence of different species in the electrolyte on the generation of peak (*) in Figure 3.

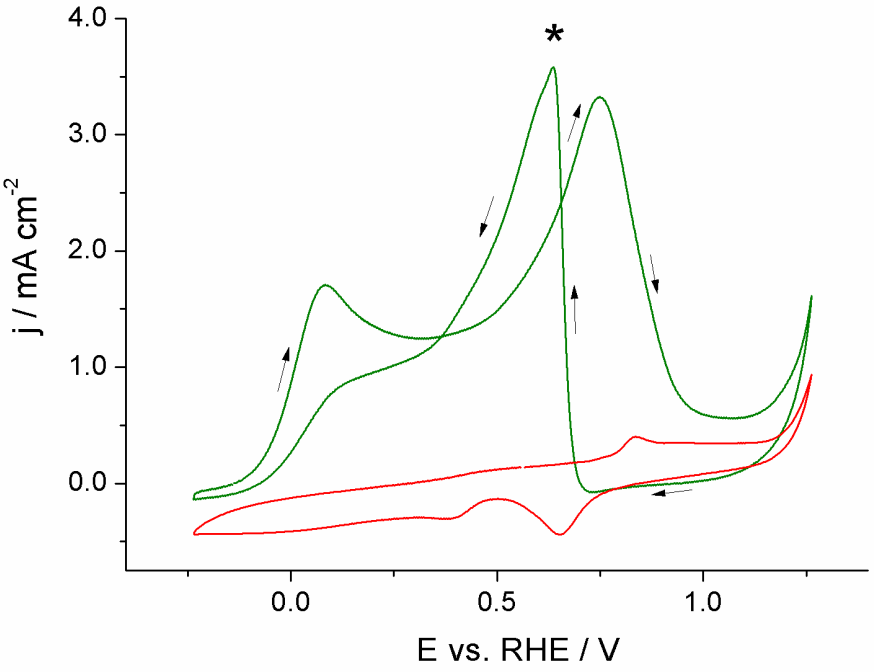

Figure 3. Cyclic voltammetry at gold pin electrode in 0.1 M KOH without (red curve) and with (green curve) 10 mM glucose; scan rate 100 mV s^{-1}.

The Pourbaix diagram of Au in aqueous solutions (see Figure 3) stresses that in the pH range 7-12, gold is oxidized to Au(III) hydroxide, the oxidation potential decreasing as the pH is increased. Above pH 12.5, gold is oxidized to the water-soluble ion $HAuO_3^{2-}$.

Accordingly to the diagram, cyclic voltammetry measurements performed at a gold pin working electrode in a 100 mM K_2HPO_4-K_3PO_4 solution without glucose at different pH values (see Figure 5) show a peak relative to the formation of the gold hydroxide (around 1 V vs. RHE),

which is successively reduced in the negative sweep (0.75 V vs. RHE).

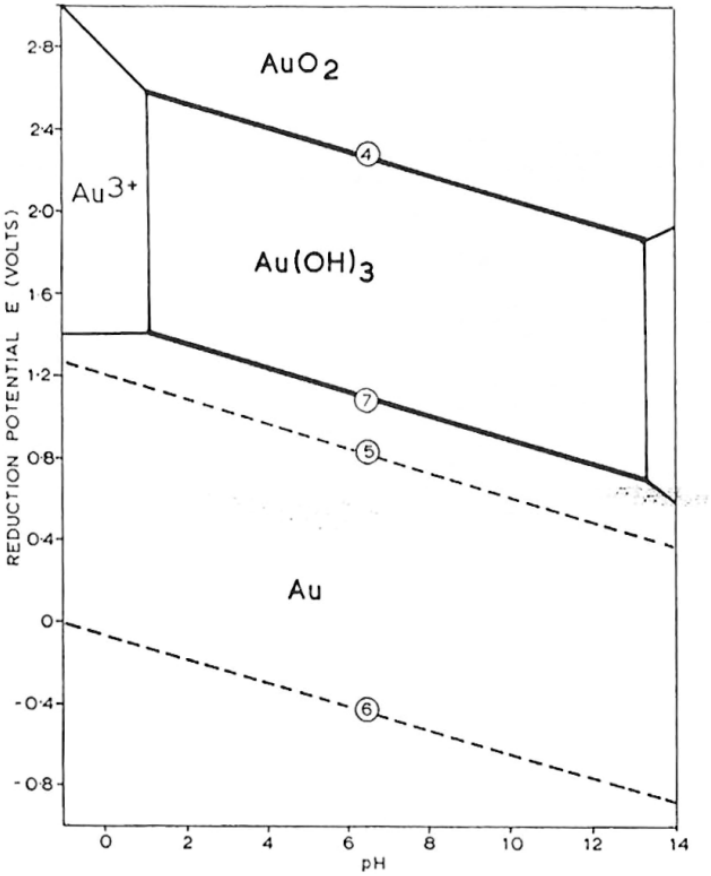

Figure 4. Potential versus pH diagram for gold in aqueous solution at 25 °C. The concentration of all the soluble species is 10^{-4} M. Extract from [35].

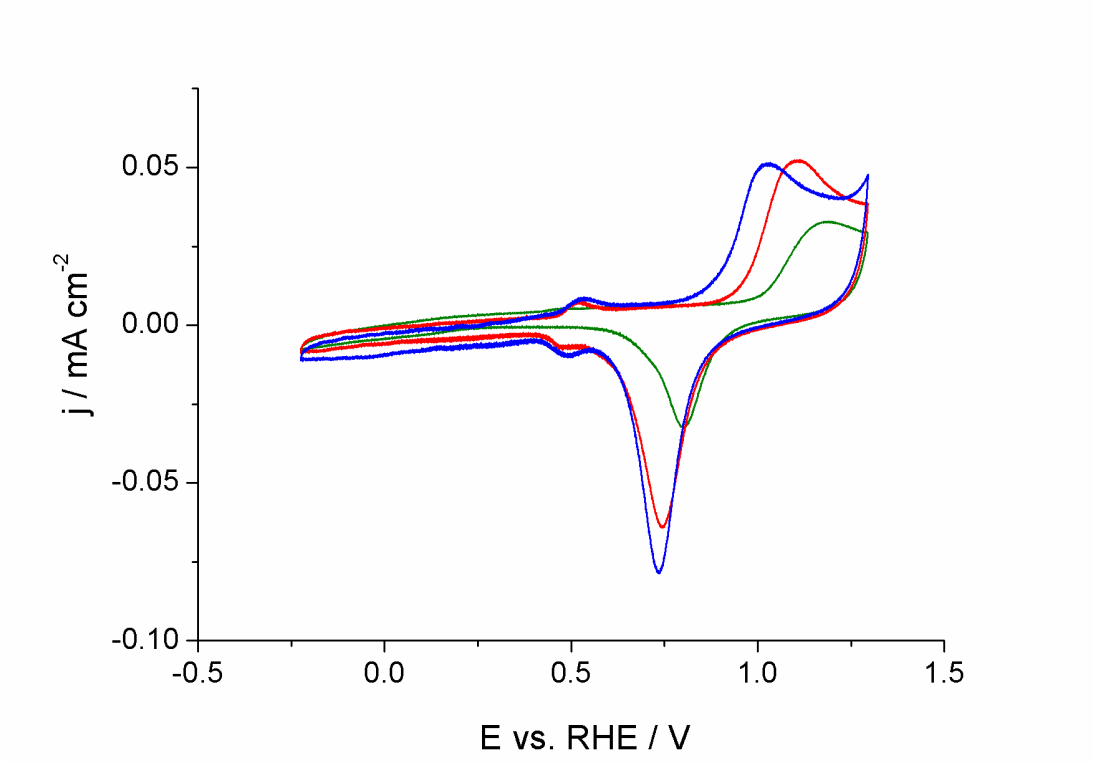

Figure 5. Cyclic voltammetry at gold pin electrode 100 mM buffer (K_2HPO_4-K_3PO_4) at different pH: 7.5

(green curve); 9.5 (red curve); 11.5 (blue curve). Scan rate 20 mV s^{-1}.

Two other peaks, one in the oxidative (0.55 V vs. RHE) and the other in the reductive scan (0.5 V vs. RHE) (both clearly visible at pH 11.5) has been attributed to the chemisorption of the hydroxide ion to the Au surface [36].

When glucose (10 mM) is added to the electrolyte (Figure 6) the oxidative peak (*) appears. Its current density depends strongly on the pH of the solution.

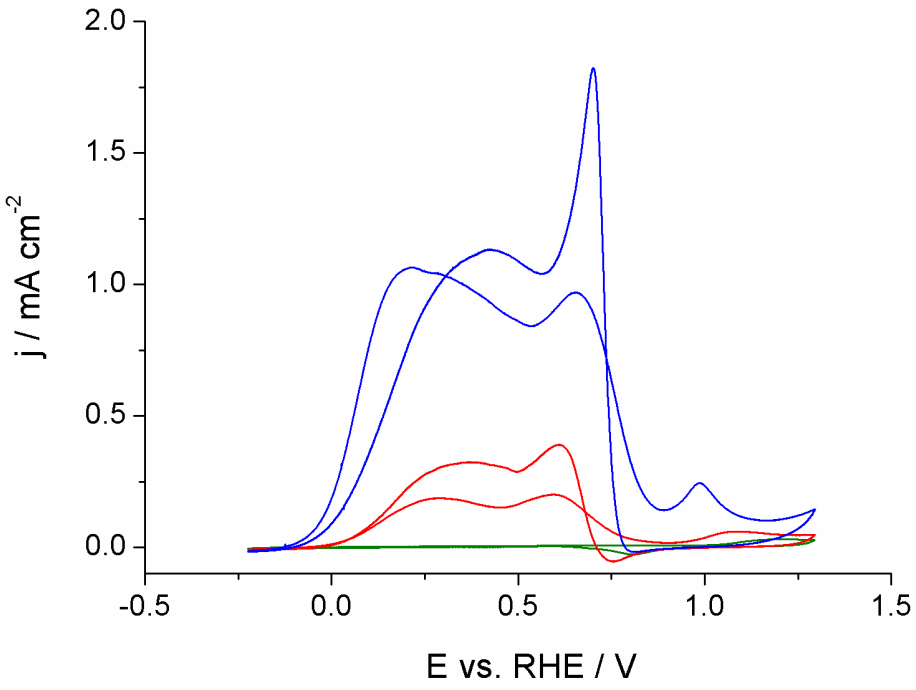

Figure 6. Cyclic voltammetry at gold pin electrode in 100 mM buffer (K_2HPO_4-K_3PO_4) and in the presence of glucose (10 mM) solution at different pH: 7.5 (green curve); 9.5 (red curve); 11.5 (blue curve). Scan rate 20 mV s^{-1}.

Figure 7 shows the Pourbaix diagram of Au in 2 M Cl^- aqueous solution. The reason indicated by Makovos *et al.* for the inactivity of gold in presence of Cl^- is the dissolution of Au to $AuCl_4^-$ which prevents the formation of the oxide. However the Pourbaix diagram shows that above pH 9, gold is directly oxidized to $Au(OH)_3$ thus avoiding the formation of the tetrachloroaurate ion. This means that above pH 9, $Au(OH)_3$ should be formed, even in the presence of chlorides.

To demonstrate this, CV measurements at pH 11.5 (buffered, 100 mM) in 10 mM glucose solution have been performed at different chloride concentrations (Figure 8). As expected, in these conditions the chloride ions do not completely prevent the generation of peak (*), but the intensity of the peak does decrease as the concentration of Cl^- increases.

The mechanism proposed by Makovos [33] cannot explain this phenomenon.

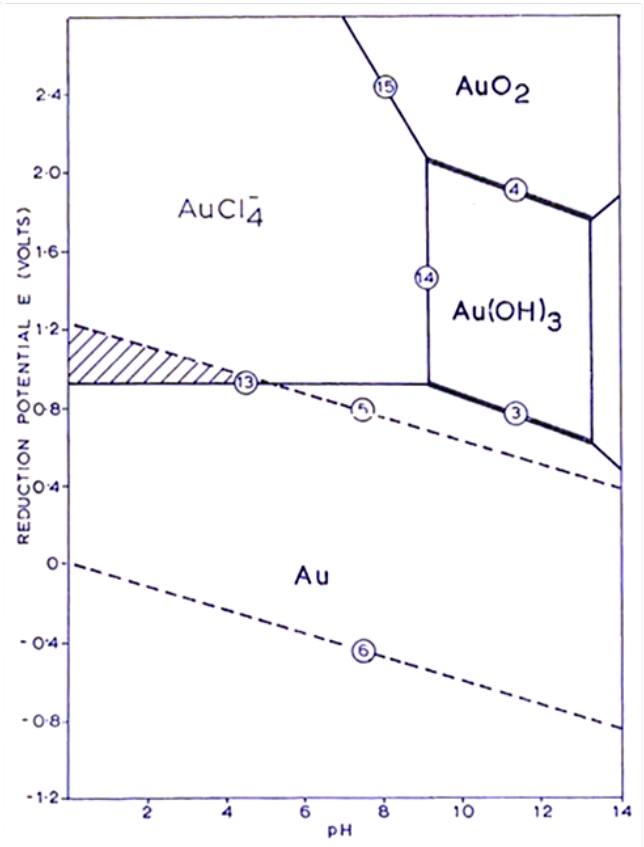

Figure 7. Pourbaix diagram for the system Au-H_2O-Cl- at 25 °C. [Au(III)] = 10^{-2} M, [Cl^-] = 2 M, pO_2 = pH_2 = 1 atm. Extract from [35].

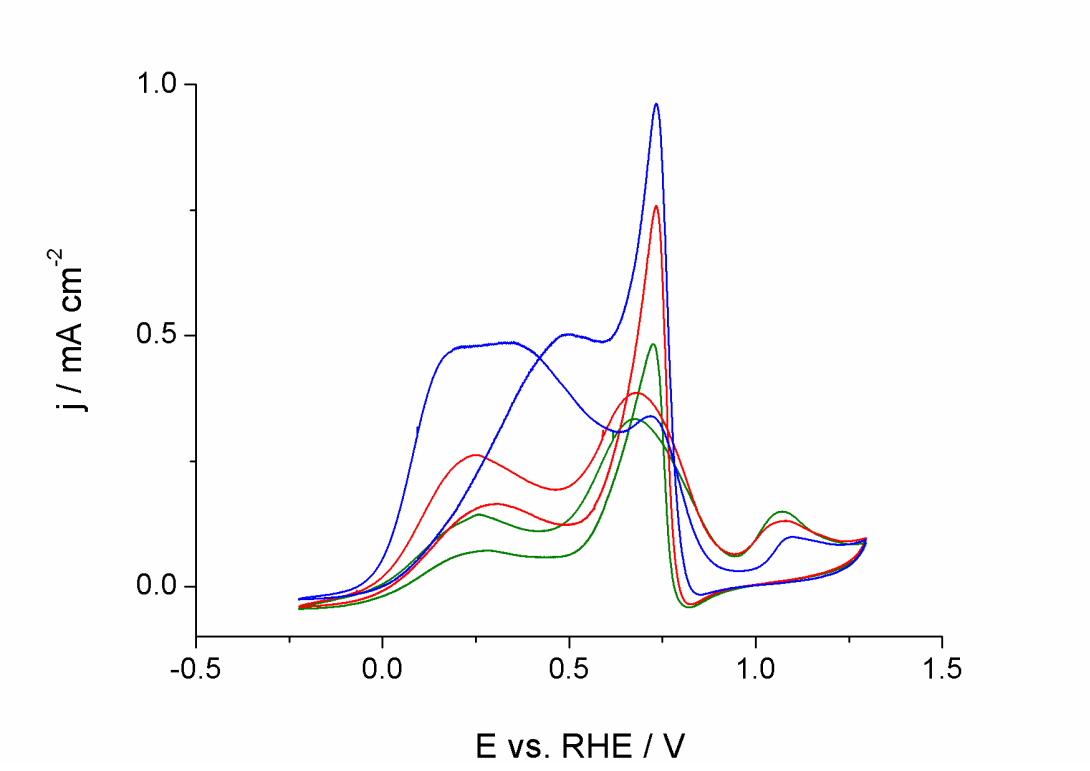

Figure 8. Cyclic voltammetry at gold pin electrode in 10 mM glucose solution in the presence of 100 mM buffer (K_2HPO_4-K_3PO_4) at pH 11.5 and different chloride concentrations: (blue) without chloride ions, (red) 50 mM, (green) 100 mM. Scan rate 20 mV s^{-1}.

For this reason we propose another mechanism: the chloride ions can strongly adsorb to the gold active sites thus inhibiting the oxidative adsorption of glucose, a key step in the overall oxidation process. To prove the adsorption of the chlorides to the surface, electrochemical impedance spectroscopy (EIS) techniques has been employed at fixed frequency and potential, while increasing the concentration of Cl^-. EIS at high frequency enables the gold/electrolyte interface to be studied. An adsorption of Cl^- to the surface should increase the differential capacitance; as consequence the negative imaginary part of the impedance (-Z(im)) should decrease. A preliminary EIS was performed in the range from 100 kHz -100 mHz to establish the optimal working frequency (5 kHz). The experiment was performed recording the impedance every 10 seconds (Figure 9).

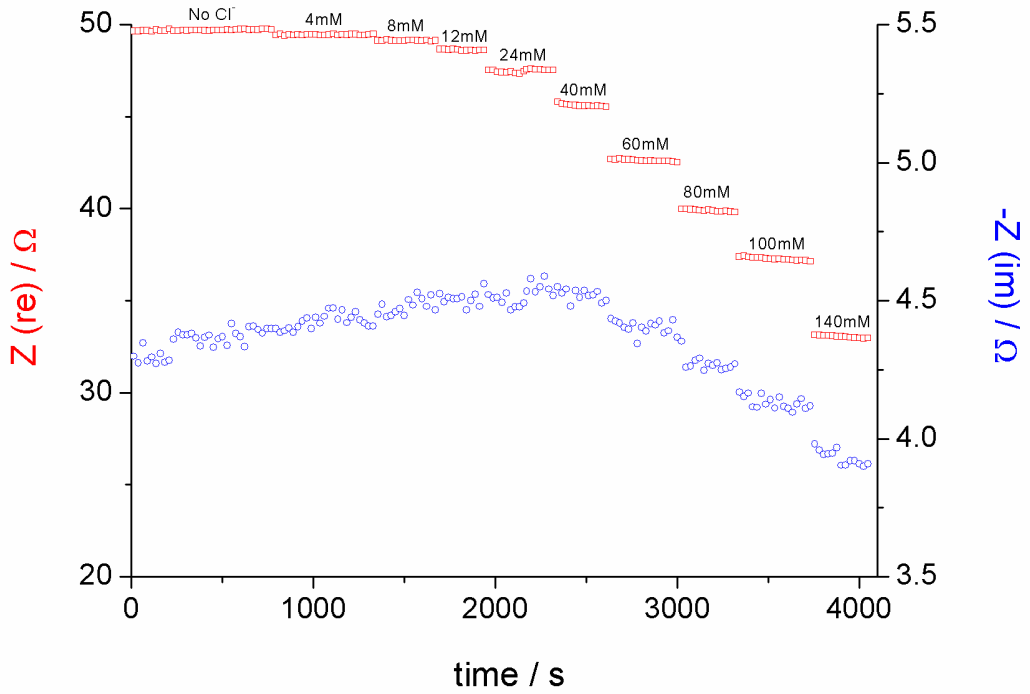

Figure 9. Continuous EIS measurement at 5 kHz on Au pin electrode in 100 mM buffer (K_2HPO_4-K_3PO_4), pH 11.5 with increasing chloride concentration. Z(re) red squares and -Z(im) blue circles.

Obviously a decrease of the Z(re) is observed when increasing the KCl concentration, due to the increase of the conductivity. Accordingly to the results, after an initial period in which the value of -Z(im) slightly increases, it decreases for concentrations higher than 40 mM Cl^-.

The suspected importance of the adsorbed ions on the glucose overall oxidation mechanism was confirmed by the replacement of Cl^- with F^-. It is expected that the interaction between a very hard ion, such as fluoride, with a soft element, like gold, is hindered, thus -Z(im) should remain constant in response to increasing fluoride concentration. The cyclic voltammograms after successive fluoride additions are reported in Figure 10.

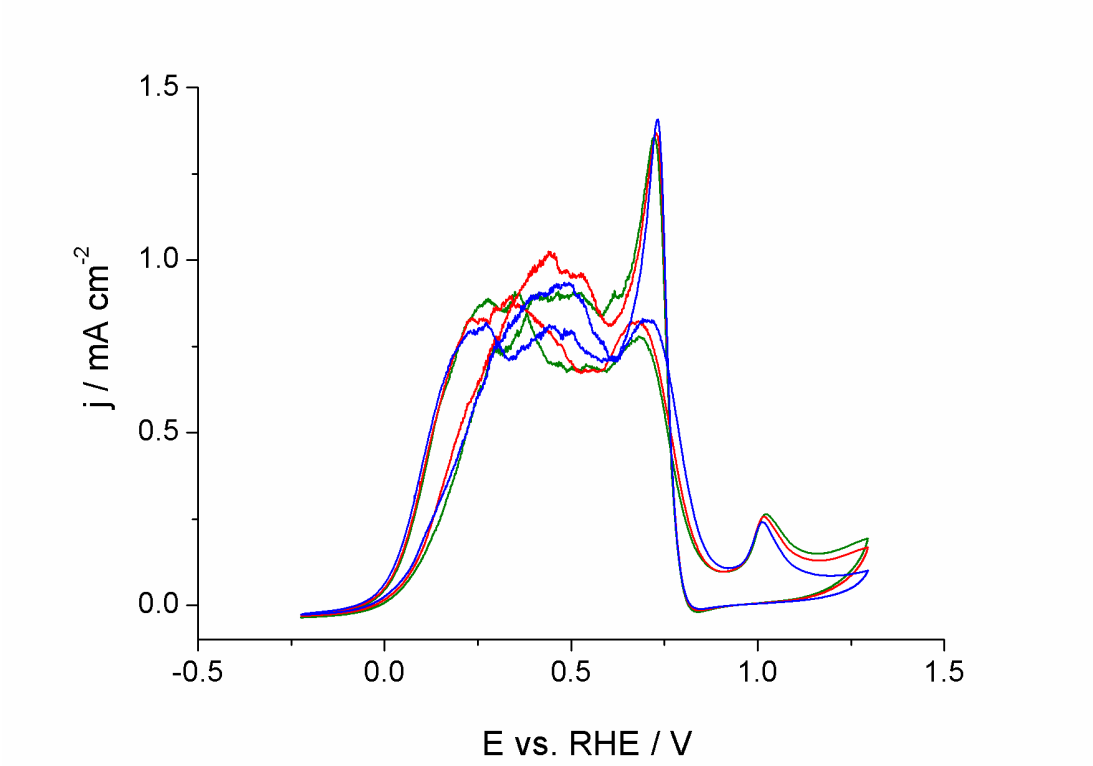

Figure 10. Cyclic voltammetry at gold pin electrode in 10 mM glucose solution in presence of 100 mM buffer (K_2HPO_4-K_3PO_4) at pH 11.5 and different fluoride concentrations: (red) without fluoride ions, (blue) 50 mM, (black) 100 mM. Scan rate 20 mV s^{-1}.

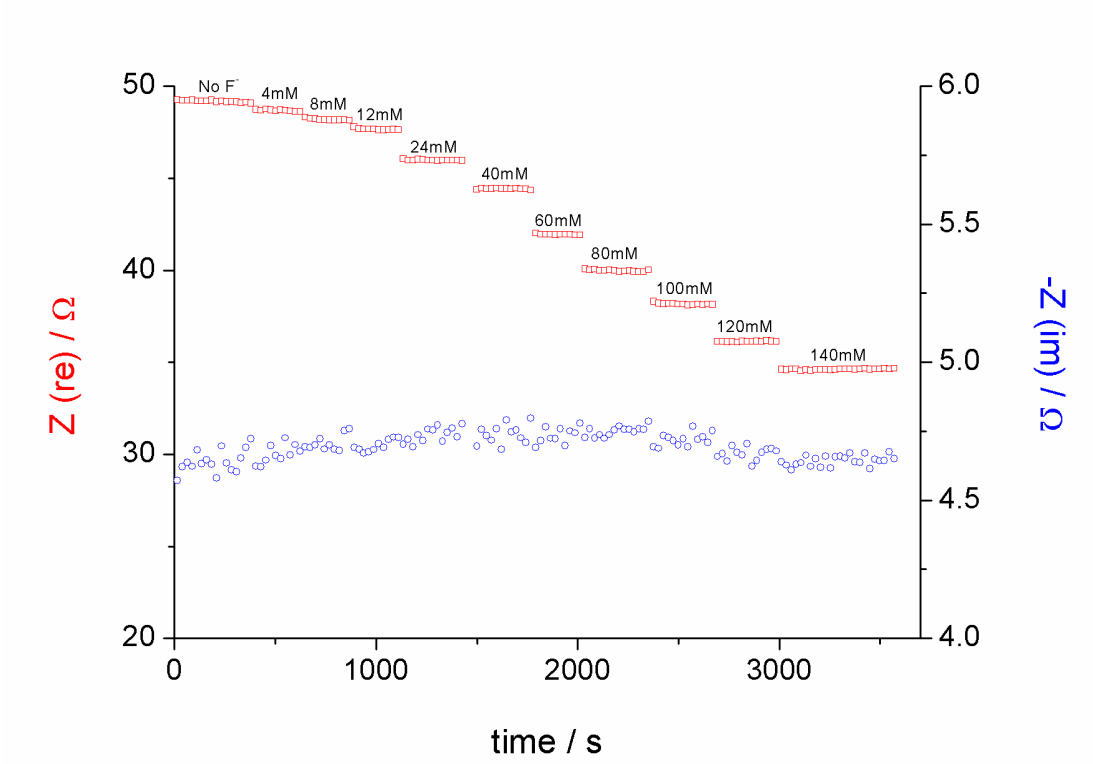

Figure 11. Continuous EIS measurement at 5 kHz on Au pin electrode in 100 mM (K_2HPO_4-K_3PO_4), at pH 11.5 with increasing fluoride concentration. Z(re) red squares and -Z(im) blue circles.

As expected, the addition of fluorides does not affect the features of the cyclic voltammogram, meaning that the adsorption of F^- is negligible. This conclusion has been confirmed with the EIS measurement at fixed frequency and potential, while increasing the concentration of F^- (Figure 11). In this case we can observe a decrease of the Z(re) value, while -Z(im) is constant.

The very importance of the adsorbed species on the glucose oxidation gives rise to questions about the possible limitations generated by other species in solution, like the buffer. To address this question, cyclic voltammetry of glucose oxidation was performed using only NaF (100 mM) as supporting electrolyte (Figure 12).

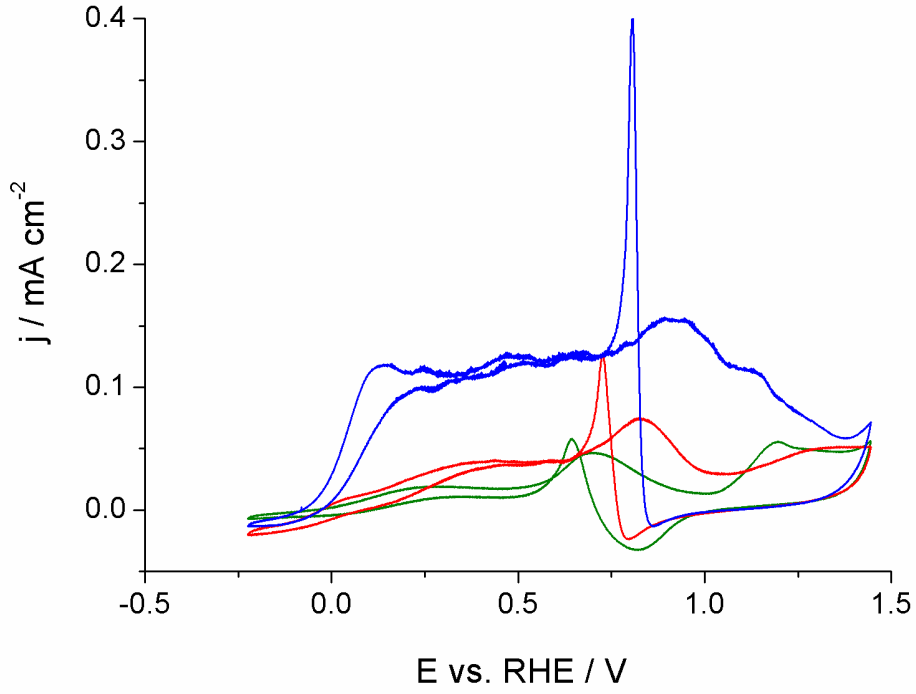

Figure 12. Cyclic voltammetry at gold pin electrode in 100 mM NaF solutions in presence of 1 mM (K_2HPO_4-K_3PO_4) buffer and glucose (10 mM), at different pH: 7.5; 9.5; 11.5. Scan rate 20 mV s^{-1}.

The presence of a very low buffer (K_2HPO_4-K_3PO_4) concentration (1 mM) was necessary to obtain reproducible cyclic voltammetries. The anodic limit was also shifted 150 mV toward more positive potentials with respect to the 100 mM buffer measurement to allow the $Au(OH)_3$ oxidation peak formation.

Interesting conclusions can be drawn by comparing Figure 6 and Figure 12. At pH 7.5 without buffer it is possible to observe the presence of the cathodic peak which is practically invisible with 100 mM buffer. This effect stresses that the buffer is also adsorbed on the active sites.

The effect at higher pH is also very interesting. It is clearly visible that in presence of fluorides as the supporting electrolyte the peak current density is about 5 times lower. This can be easily

explained by considering the real purpose of the buffer: to maintain a constant pH near the gold surface [9]. This process is very slow when only fluorides ions are present, being OH^- ions provided only through transport. So the buffer has two contrasting effects: it adsorbs to the surface, decreasing the active sites for the glucose oxidation, and it also keeps constant the pH at the surface of the electrode. This second effect is predominant at high pH values.

On the basis of the experimental data and considerations reported in this section, a new mechanism of the generation of the oxidative peak (*) is proposed in the next section.

2.2.3 New model of glucose oxidation

Here the electrochemical oxidation of glucose to gluconate is analyzed in mechanistic detail. The aim is to understand the origin of the oxidative peak in the reductive sweep of the cyclic voltammetry, a peculiar feature already studied for its implication in glucose sensing [33]. The mechanism proposed is based on previous studies on platinum electrodes at low temperatures [9]. Figure 13 summarizes the mechanism and the main species involved.

At first, the glucose molecule is electrochemically adsorbed at the surface of the electrode by dehydrogenation (reaction 1). The dehydrogenated molecule can be transformed to gluconate by direct oxidation (reaction 2), which involves the production of a hydroxide ion and the elimination of an H^+. An alternative path is the oxidization of the dehydrogenated glucose to δ-gluconolactone (reaction 3). The δ-gluconolactone is then transformed to gluconate after reacting with a hydroxide ion.

$$G'_{(I)} + H_2O_{(\varepsilon)} + e_{(\beta)}^- \underset{k_{1,O}}{\overset{k_{1,R}}{\rightleftharpoons}} G_{(\varepsilon)} + OH_{(\varepsilon)}^- \qquad (1)$$

$$G''^-_{(I)} + H^+_{(\varepsilon)} + e_{(\beta)}^- \underset{k_{2,O}}{\overset{k_{2,R}}{\rightleftharpoons}} G'_{(I)} + OH_{(\varepsilon)}^- \qquad (2)$$

$$G'''_{(I)} + H^+_{(\varepsilon)} + e_{(\beta)}^- \underset{k_{3,O}}{\overset{k_{3,R}}{\rightleftharpoons}} G'_{(I)} \qquad (3)$$

Here the subscript I indicates the inner Helmholtz layer of the interface, ε the solution and β the electrode. The electrochemical reactions are written following the electrochemical convention of reduction as the direct reaction and oxidation as the inverse one.

The molecules represented by the symbols G, G', G'', and G''' are reported in Figure 13, and are glucose, dehydrogenated glucose, gluconate, and δ-gluconolactone, respectively.

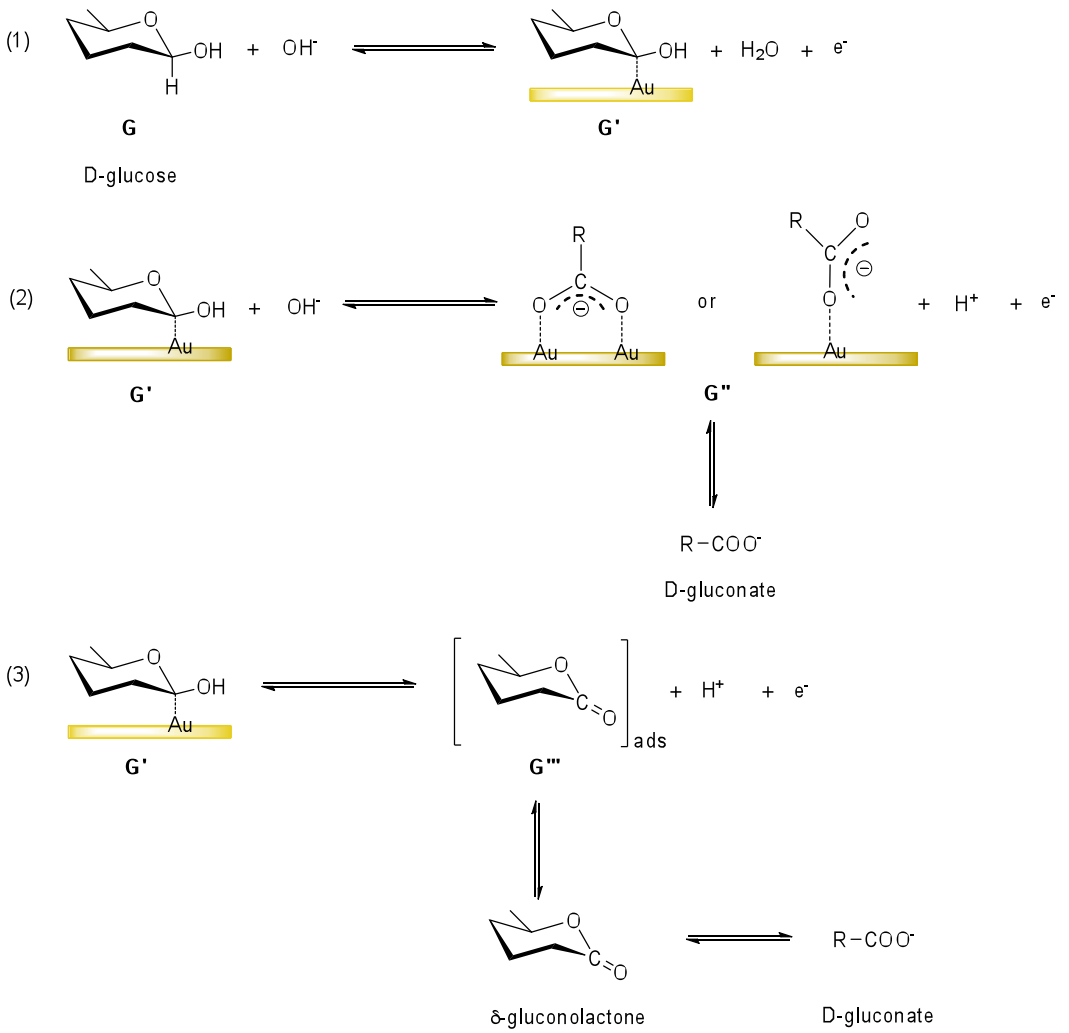

Figure 13. Proposed mechanism at gold electrodes. G = D-glucose (β-D-glucopyranose formed predominantly in water), G'= dehydrogenated glucose (intermediate generated by anomeric carbon dehydrogenation), G''= D-gluconate, G'''= δ-gluconolactone.

Our electrochemical experiments confirm that the glucose oxidation of glucose is blocked at the surface of the gold hydroxide, as previously pointed out by Xieng *et al.* [37]. We described the reaction rates for the i-th reaction, r_i, as:

$$\begin{aligned} r_1 &= k_{1,R} N_I \gamma' - k_{1,O} a_G{}^{\varepsilon} a_{OH}{}^{\varepsilon} \left(1-\gamma'-\gamma''-\gamma'''\right)\left(a_{Au}\right)^m \\ r_2 &= k_{2,R} N_I \gamma'' a_H{}^{\varepsilon} - k_{2,O} N_I \gamma' a_{OH}{}^{\varepsilon} \\ r_3 &= k_{3,R} N_I \gamma''' a_H{}^{\varepsilon} - k_{3,O} N_I \gamma' \end{aligned} \qquad (4)$$

where N_I is the number of sites available in the inner Helmholtz layer, γ', γ", γ"' are the fraction of sites occupied by the dehydrogenated glucose, gluconate and δ-gluconolactone, respectively, aG^{ε} is the activity of glucose molecules in the electrolyte, $a_{OH^{\varepsilon}}$ the activity of hydroxide ions in the electrolyte, $a_{H^{\varepsilon}}$ the activity of protons in the electrolyte, and a_{Au} the activity of gold at the

surface of the electrode. The exponent m of a_{Au} is dependent on the number of gold atoms necessary to coordinate the oxidation of the glucose. Empirically, it should be greater than 1. The kinetic constants of the electrochemical reactions (1-3) are dependent on the electric potential distribution at the interface according to:

$$\frac{k_{1,R}}{k_{1,R,0}} = \exp\left[-\frac{F\left(\Phi_0{}^{\beta} - \Phi_H{}^{\varepsilon}\right)}{2RT}\right] \qquad \frac{k_{1,O}}{k_{1,O,0}} = \exp\left[\frac{F\left(\Phi_0{}^{\beta} - \Phi_H{}^{\varepsilon}\right)}{2RT}\right]$$
$$\frac{k_{2,R}}{k_{2,R,0}} = \exp\left[-\frac{F\left(\Phi_0{}^{\beta} + \Phi_I - 2\Phi_H{}^{\varepsilon}\right)}{2RT}\right] \qquad \frac{k_{2,O}}{k_{2,O,0}} = \exp\left[\frac{F\left(\Phi_0{}^{\beta} + \Phi_I - 2\Phi_H{}^{\varepsilon}\right)}{2RT}\right] \quad (5)$$
$$\frac{k_{3,R}}{k_{3,R,0}} = \exp\left[-\frac{F\left(\Phi_0{}^{\beta} - \Phi_H{}^{\varepsilon}\right)}{2RT}\right] \qquad \frac{k_{3,O}}{k_{3,O,0}} = \exp\left[\frac{F\left(\Phi_0{}^{\beta} - \Phi_H{}^{\varepsilon}\right)}{2RT}\right]$$

where F is the Faraday constant, R the universal gas constant, T the absolute temperature, $\Phi_0{}^{\beta}$ the electric potential at the surface of the electrode, $\Phi_H{}^{\varepsilon}$ the electric potential of the solution at the Helmholtz plane (d_H in Figure 14), and Φ_I the electric potential in the inner Helmholtz layer.

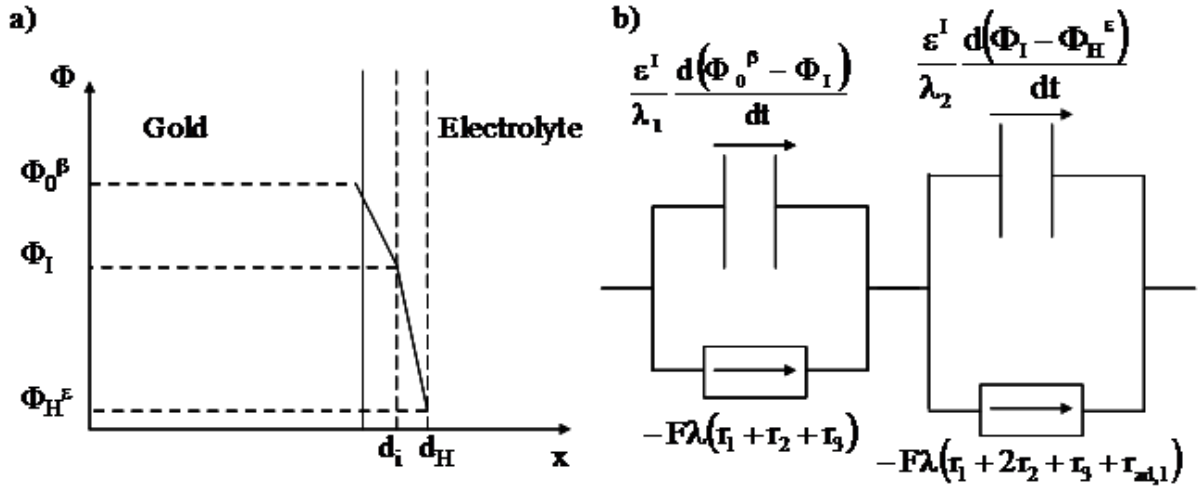

Figure 14. (a) Potential distribution at the solid phase/electrolyte interface. (b) Current flow through the gold/electrolyte interface.

The electric field in the inner Helmholtz layer is not constant, due to the presence of the gluconate, which is a charged species (see Figure 14). The correlation between the fraction of the occupied sites of the different compounds and the reaction rates is given by:

$$\begin{aligned} \lambda N_I \frac{d\gamma'}{dt} &= -\lambda r_1 + \lambda r_2 + \lambda r_3 \\ \lambda N_I \frac{d\gamma''}{dt} &= -\lambda r_2 - \lambda r_{ad,1} \\ \lambda N_I \frac{d\gamma'''}{dt} &= -\lambda r_3 - \lambda r_{ad,2} \end{aligned} \qquad (6)$$

where λ is the distance between the surface of the electrode and the Helmholtz plane, and $r_{ad,1}$ and $r_{ad,2}$ are the reaction rates of the gluconate and the δ-gluconolactone desorption respectively. The desorption reaction rates can be expressed by:

$$\begin{aligned} r_{ad,1} &= k_{ad,1,R} N_I \gamma'' - k_{ad,1,O} a_{G''}{}^{\varepsilon} \left(1 - \gamma' - \gamma'' - \gamma'''\right) \left(a_{Au}\right)^m \\ r_{ad,2} &= k_{ad,2,R} N_I \gamma''' - k_{ad,2,O} a_{G'''}{}^{\varepsilon} \left(1 - \gamma' - \gamma'' - \gamma'''\right) \left(a_{Au}\right)^m \end{aligned} \qquad (7)$$

with the kinetic parameters equal to:

$$\frac{k_{ad,1,R}}{k_{ad,1,R,0}} = \exp\left[-\frac{F\left(\Phi_I - \Phi_H{}^{\varepsilon}\right)}{2RT}\right] \quad \frac{k_{ad,1,O}}{k_{ad,1,O,0}} = \exp\left[\frac{F\left(\Phi_I - \Phi_H{}^{\varepsilon}\right)}{2RT}\right] \quad \frac{k_{ad,2,R}}{k_{ad,2,R,0}} = 1 \quad \frac{k_{ad,2,O}}{k_{ad,2,O,0}} = 1 \qquad (8)$$

We want to stress that the reaction of gluconate desorption involves charged species, therefore passage of reductive current, as reported in Figure 14. On the other hand, δ-gluconolactone desorption of does not involve any passage of charged species.

To prove that the proposed mechanism can justify the presence of the oxidative peak (*), glucose oxidation simulations of were performed by a program compiled with MATLAB 7.0. From an intuitive point of view, when the activity of gold at the surface decreases (due to the formation of gold hydroxide), the reaction rates r_1, r_2, and r_3 slow down, while reaction $r_{ad,1}$ and $r_{ad,2}$ become more positive. The result is a decrease of the adsorbed species. When the oxide is reduced, the naked gold surface is ready to oxidize the glucose. We will demonstrate that the ratio of the reaction rates of the two alternative mechanisms of formation of the gluconate (reaction 2 and 3) is relevant in observing the oxidative peak (*) (see Figure 3). The simulations include neither transport phenomena, nor the activity coefficients of the species, therefore it is not expected to completely reproduce the experimental cyclic voltammetry curves. Nevertheless, the main features (number of peaks and the peak (*)) should be reproduced.

The fixed parameters of the simulations are given in Table 2. The parameter r is the ratio between $k_{d,2}$ and $k_{d,3}$.

Table 2. Summary of fixed simulation parameters.

$k_{1,R,0}$	$k_{1,O,0}$	$k_{2,R,0}+k_{3,R,0}$	$k_{2,O,0}/k_{2,R,0}$	$k_{3,O,0}/k_{3,R,0}$
10^{-10}	10^{-7}	$8\cdot10^{-1}$	1	1
$k_{ad,1,R,0}$	$k_{ad,2,R,0}$	N_I / mol cm^{-3}	λ / cm	λ_2 / cm
10^{-7}	$8\cdot10^{-3}$	10^{-1}	$4\cdot10^{-8}$	$2\cdot10^{-8}$

In Figure 15 the simulations for different values of r are reported.

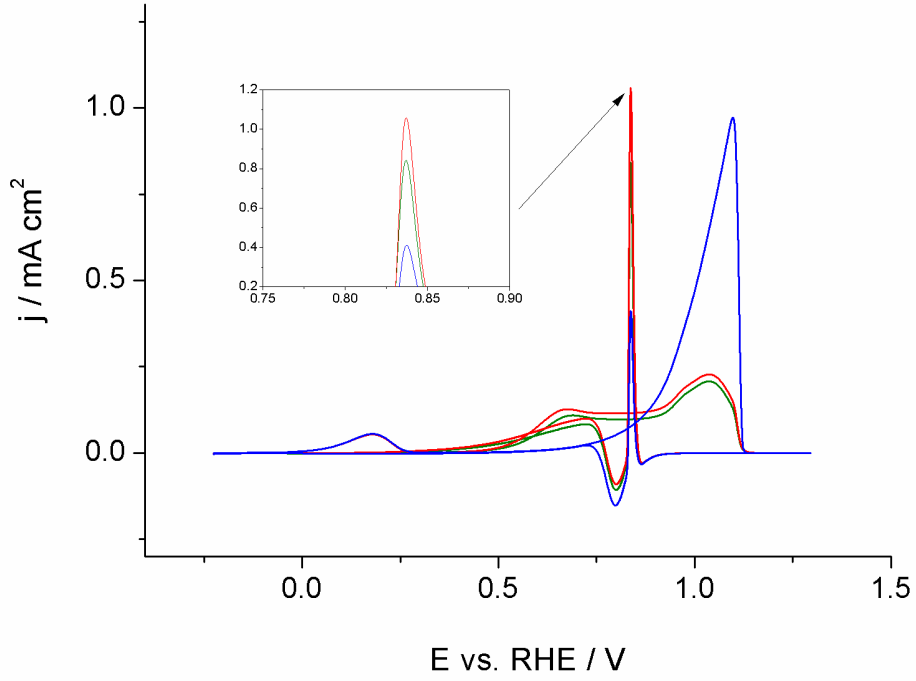

Figure 15. Simulation of the electrochemical oxidation of glucose; no absorption process considered. Parameters are given in table I. Green r = 1, red r = 0, blue r = ∞.

Absorption of other ions except glucose is neglected (like in the fluorides). The simulations should be compared with Figure 12. The effect of the parameter r on reaction 1 is negligible, while it is very important in the shape of the cyclic voltammetry curve above 0.3 V vs. RHE. When r = ∞, most of the dehydrogenated glucose is oxidized to δ-gluconolactone near 0.6 V vs. RHE. The desorption of δ-gluconolactone does not involve current flow; a limiting current is

reached. After the formation of gold hydroxide (at 1.05 V vs. RHE) the oxidation of glucose stops, and the surface desorbs all the adsorbed species. Decreasing the potential, the reduction of gold hydroxide generates new gold surface, active to the oxidation of glucose (Figure 16).

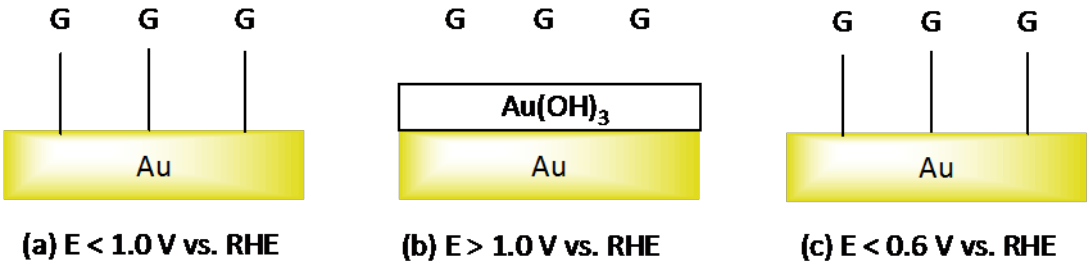

Figure 16. Schematic of the formation of the oxidative peak in the cathodic scan. (a) As long as the potential of the electrode is below 1.05 V vs. RHE glucose can adsorbe to the gold surface, first step of the oxidation reaction. (b) At potential higher than 1.05 V vs. RHE gold surface is oxidized to gold hydroxide, inactive towards glucose electrooxidation (c) during the cathodic scan gold is reduced at potentials around 0.6 V vs. RHE, glucose can adsorbe again and get oxidized, generating the oxidative peak in the cathodic scan. The different in potential for gold hydroxide formation and reduction is due to overpotential.

The peak (*) is observed in the simulations. Its intensity is much higher than in experimental data, due to the fact that diffusion has not been considered. Under these conditions, the limiting reactant is the number of active sites at the gold surface, which is immediately saturated. By decreasing the value of r, the peak (*) intensity decreases, an effect due to the gluconate. The gluconate is a negatively charged species, and therefore is attracted to the surface of the electrode at high voltages. When the potential of the electrode is increased, the gluconate desorbs much more slowly than the δ-gluconolactone, therefore less active sites are available when the glucose oxidation starts again.

The results concerning the simulation of the adsorption effect on the peak (*) are reported in Figure 17. Two curves, simulating the presence of no adsorption (F^- ions in solution) and chemisorption (Cl^- ions in solution) respectively are shown. As expected from the experimental data, the presence of Cl^- partially blocks the active sites, thus decreasing the intensity of the peak (*). We want to stress that in the case of Cl^- adsorption, the reaction rate for each step in the glucose oxidation decreases, as observed in the experimental section (see Figure 8). The simulations support the mechanism we have proposed for the generation of the peak (*) as well as the influence of the other species in the electrolyte on its intensity.

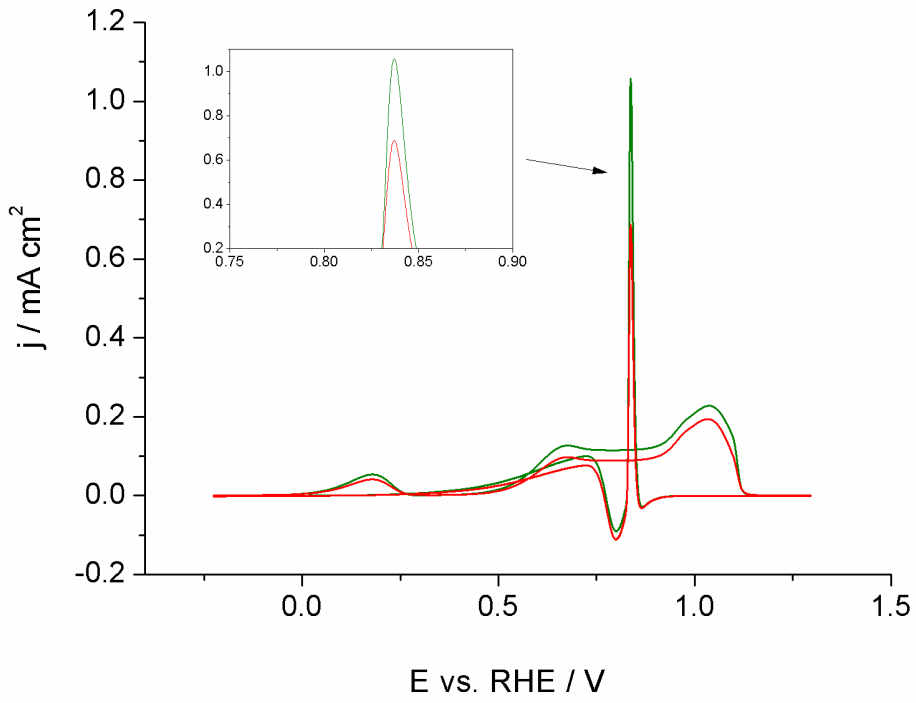

Figure 17. Simulation of the electrochemical oxidation of glucose, with r = 0. Green no adsorption, red adsorption (100 mM).

2.2.4 Conclusions

The new proposed mechanism is able to explain the presence of glucose oxidation peak in the cathodic scan at gold electrodes in which the key step is the competitive adsorption at the active sites of the ionic species present in the solution (phosphate buffer, chlorides and OH^-) and the substrate (glucose). Simulations of the proposed mechanism have supported the plausibility of the mechanism. The study represented the basis for the work on glucose sensing at gold electrodes described in the following chapter.

CHAPTER III: GLUCOSE SENSING

Chapter III: Glucose Sensing

Glucose meters are devices for the determination of the approximate concentration of D(+)-glucose in the blood; they are necessary to cure Diabetes Mellitus, a disease affecting millions of people around the world. In this chapter the glucose meters state of the art will be discussed and the new approach to glucose sensing at gold electrode we developed introduced.

3.1 Introduction [4]

Glucose sensors are of great interest for the medical application of blood glucose sensing. Their optimization (in terms of response time, lifetime, sensitivity and selectivity) is highly necessary to improve the treatment of *Diabetes Mellitus* (Appendix C), a chronic disease affecting millions of people around the world [7]. The concentration of glucose in the blood is called glycemia, it is usually expressed in mg/dl and it fluctuates physiologically within a narrow range. Excessively low levels (e.g. fasting glycemia of 70 mg/dl or below) are classed as hypoglycemia. These may result from poor diet, or as a side effect of diabetes medication. Excessively high levels (e.g., 250 mg/dl or more) are classed as hyperglycemia and are a particular threat to diabetes sufferers. Diabetes mellitus is a group of metabolic diseases in which a person has high blood sugar, producing the classical symptoms of polyuria (frequent urination), polydipsia (increased thirst) and polyphagia (increased hunger).

There are two main types of diabetes:

- Type 1 diabetes: results from the body's failure to produce insulin, and presently requires the person to inject insulin.
- Type 2 diabetes: results from insulin resistance, a condition in which cells fail to use insulin properly, sometimes combined with an absolute insulin deficiency.

All forms of diabetes have been treatable since insulin became available in 1921, and type 2 diabetes may be controlled with medications.

3.2 Glucose meters (adapted from [38])

A glucometer is a medical device for determining the approximate concentration of glucose in the blood (Figure 18). It is a key element of home blood glucose monitoring (HBGM) for people with diabetes mellitus or proneness to hypoglycemia. A small drop of blood, obtained by pricking the skin with a lancet, is placed on a disposable test strip, which the meter reads and uses to calculate the blood glucose level (in mg/dl or mmol/l).

Figure 18. Blood glucose testing, showing the size of blood drop required by modern meters.

Since approximately 1980, the primary goal of the diabetes management has been the achievement of closer-to-normal levels of glucose in the blood for as much of the time as possible, guided by HBGM several times a day. The benefits include a reduction in the occurrence rate and severity of long-term complications from hyperglycemia as well as a decrease, in the short-term, of the potentially life-threatening complications of hypoglycemia.

3.2.1 Characteristics

There are several glucose meters characteristics that may differ from model to model:

- Size. The average size is now approximately the dimension of the palm of the hand, though some are smaller or larger. They are battery-powered.
- Test strips. A consumable element containing chemicals that react with glucose in the drop of blood is used for each measurement. For some models this element is a plastic strip with a small spot impregnated with glucose oxidase and other components. Instead of strips, some models use discs that may be used for several measurements.
- Coding. Since test strips may vary from batch to batch some models needs to be calibrated. Such procedure requires the user to enter a code (that may be found on the vial of test strips) or a chip (that comes with the test strip). If the calibration is omitted or incorrectly carried out, the measurement is up to 4 mmol/L inaccurate. The implications of an incorrectly coded meter can be serious, placing patients at increased risk of hypoglycaemia.
- Blood sample volume. The blood drop size needed varies from 0.3 to 10 μl by different models. Older models required larger blood samples, usually defined as a "hanging drop" from the fingertip. Smaller volume requirements reduce the frequency of unproductive pricks.

- Alternative site testing. Smaller drop volumes have enabled "alternate site testing" *i.e.* pricking the forearms or other less sensitive areas instead of the fingertips. Although less uncomfortable, readings obtained from forearm are slower than fingertip in reflecting changing of glucose levels in the rest of the body.
- Testing times. The response time can range from 3 to 60 seconds for different models.
- Display. The glucose value, in mg/dl or mmol/l, is displayed on a small window. The preferred measurement unit varies by country: mg/dl is preferred in the US, mmol/l in Canada and Europe. Many devices can toggle between both types of measurements and there have been a couple of published instances in which someone with diabetes has been misled into the wrong action by assuming that a reading in mmol/l was really a very low reading in mg/dl, or the converse. Recent production U.S.-marketed machines are pre-set at the factory for mg/dl and cannot be changed.
- Glucose vs. Plasma glucose. Glucose levels in plasma are generally 10%–15% higher than glucose measurements in whole blood (and even more after eating). This is important because home blood glucose meters measure the glucose in whole blood while most lab tests determine the glucose in plasma. Currently, there are many meters that convert the measured whole blood glucose as "plasma equivalent" by an algorithm built into the meter allowing to easily compare the glucose amount between lab and home test.
- Clock/memory. All meters now include a clock and a memory for past test results, keeping a record of management and looking for trends and patterns in blood glucose levels over days. Most memory chips can display an average of recent glucose readings.
- Data transfer. Many meters now have sophisticated data handling capabilities: they can be downloaded by a cable or infrared to a computer that has diabetes management software to display the test results. Some meters allow entry of additional data throughout the day, such as insulin dose, amounts of carbohydrates eaten, or exercise. Furthermore they have been combined with other devices, such as insulin injection devices, PDAs, and even Game Boys. A radio link to an insulin pump allows automatic transfer of glucose readings to a calculator that assists the wearer in deciding the appropriate insulin dose. One model also measures beta-hydroxybutyrate in the blood to detect ketoacidosis (ketosis).
- Hospital glucose meters. Special glucose meters for multi-patient hospital management are now used. These provide more elaborate quality control records, and the data handling capabilities are designed to transfer glucoses into electronic medical records and into laboratory computer systems for billing purposes.

3.2.2 Cost

The cost of home blood glucose monitoring is substantially due to the test strips. In 2006, the consumer cost of each strip ranged from about $0.35 to $1.00. Manufacturers often provide meters at no cost to induce use of the profitable test strips. Type 1 diabetics may test as often as 10 to 12 times a day due to the dynamics of insulin adjustment, whereas type 2 typically test less frequently, especially when insulin is not part of treatment.

3.2.3 Accuracy

Accuracy is a common topic of clinical concern. Nearly all of the meters have similar accuracy (±10-15%) when optimally used; however, a variety of factors can affect it: calibration, ambient temperature, pressure use to wipe off strip (if applicable), size and quality of the blood sample, high levels of certain drugs (such as ascorbic acid = vitamin C) in blood, hematocrit, dirt on meter, humidity, and aging of test strips. Models vary in their susceptibility to these factors, and in their ability to prevent or warn of inaccurate results with error messages. The Clarke error grid has been the common way of analyzing and displaying accuracy of readings related to management consequences. More recently an improved version of the Clarke error grid, known as the Consensus Error Grid, has come into use.

3.2.4 History

In 1962, Clark and Lyons at the Cincinnati Children's Hospital developed the first glucose enzyme electrode. It consisted of a thin layer of glucose oxidase immobilized onto an oxygen electrode. The sensor worked by measuring the oxygen amount consumed by the enzyme[39].

Another early glucose meter was the Ames Reflectance Meter by Anton H. Clemens. It was used in American hospitals in the 70's. It was about 10 inches long, it needed connection to an electrical outlet for the power and a moving needle indicated the blood glucose concentration after about a minute.

Home glucose monitoring was demonstrated to improve glycemic control of type 1 diabetes in the late 1970s, and the first meters were marketed for home use around 1980. The two models initially dominant in North America were the “Glucometer” whose trademark is owned by Bayer and the Accu-chek meter (by Roche). Consequently, these brand names became synonymous with the generic product to many healthcare professionals. In Britain, a healthcare professional and indeed a patient may refer to "taking a BM", "Mrs X's BM is 5" etc. BM stands for Boehringer Mannheim, now called Roche, who produced test strips called 'BM-test'.

Test strips that changed color and could be read "visually", without a meter, were also widely used in the 1980s; nevertheless as meter accuracy and insurance coverage improved, they lost popularity and are no longer marketed.

For over a decade, in North America hospitals resisted the adoption of glucose meters for inpatient diabetes care. Managers of laboratories argued that the superior accuracy of the laboratory measurement outweighed the advantage of immediate availability and made glucose meters measurements unacceptable for diabetic inpatients management. Patients with diabetes and their endocrinologists eventually persuaded acceptance. Some healthcare policy makers still resist the idea that the society would be well advised to pay the consumables (reagents, lancets etc.) needed.

Home glucose testing was adopted for type 2 diabetes more slowly than for type 1, and a large proportion of people with type 2 diabetes have never been instructed in home glucose testing.

3.2.5 Future

Development of non-invasive devices may enable continuous monitoring. Research is being done on non-invasive methods for measuring blood glucose, such as using infrared or near-infrared light and ultrasound.

There is one non-invasive glucose meter that has been approved by the food & drug administration FDA: the GlucoWatch G2 Biographer, designed to be worn on the wrist, uses electric fields to draw out body fluid for testing. This device does not replace conventional blood glucose monitoring. One limitation is that the GlucoWatch system is not able to cope with perspiration at the measurement site. The sweat must be allowed to dry before measurement can resume. Due to some important limitations and others, the product is no longer on the market.

The market introduction of noninvasive blood glucose measurement by spectroscopic measurement methods, in the field of near-infrared (NIR), by extracorporeal measuring devices, failed so far because at the present time, the devices measure tissue sugar, in body tissues, and not the blood sugar in blood fluid. To determine blood glucose, the measuring beam of infrared light has to penetrate the tissue for measurement of blood glucose.

It is speculated that within the next decade, meters may be replaced with continuous glucose sensors for many people with diabetes. This will likely decrease complications found in people with diabetes by limiting problems associated with hyperglycemia and hypoglycemia.

There are currently 2 continuous glucose monitoring systems (CGMS) available. The first is Medtronic's Minimed Paradigm RTS with a sub-cutaneous probe attached to a small transmitter (roughly the size of a quarter) that sends interstitial glucose levels to a small pager sized receiver

every 5 minutes. As well, the DexCom STS System (2Q 2006) is a hypodermic probe with a small transmitter. The receiver, having about the size of a cell phone, can operate up to five feet from the transmitter. Aside from a two hour calibration period, monitoring is logged at five-minute intervals for up to 72 hours; high and low glucose alarms are user-settable.

Currently, there is an effort to develop integrated treatment systems with glucose meter, insulin pump and wrist controller, as well as an effort to integrate a glucose meter in a cell phone. These glucose meter/ mobile phones combinations are under testing and cost around$149.00 USD retail. Testing strips are proprietary and available only through the manufacturer (no insurance availability). Three "Glugophones" varieties are currently offered: as dongle for the iPhone, add-on pack for LG model UX5000, VX5200, and LX350 cell phones, as well as add-on pack for the Motorola Razr. This limits providers to AT&T for the iPhone and Verizon for the others. Similar systems have been tested for longer time in Finland.

3.2.6 Technology

Many glucose meters employ the oxidation of glucose to δ-gluconolactone catalyzed by glucose oxidase (GOx) or glucose dehydrogenase (GDH). The latter has the advantage of higher sensitivity over glucose oxidase, but is more susceptible to interfering reactions with other substances. The first generation devices relied on the same colorimetric reaction that is still used nowadays in glucose test strips for urine. Besides glucose oxidase, the test kit contains a benzidine derivative, which is oxidized to a blue polymer by the hydrogen peroxide formed in the oxidation reaction. The disadvantage of this method was that the test strip had to be developed after a precise interval (the blood had to be washed away), and the meter needed to be calibrated frequently.

Most glucose meters today use an electrochemical method. Test strips contain a capillary that sucks up a reproducible amount of blood. The glucose in the blood reacts with an enzyme electrode containing glucose oxidase (or dehydrogenase). The enzyme is reoxidized with an excess of a mediator reagent such as ferricyanide ions, a ferrocene derivatives or osmium bipyridyl complexes. The mediator in turn is electrochemically reoxidized and total charges (coulombometric method) or limiting currents (amperometric method) are proportional to the glucose amount in the blood.

The same principle is used in test strips for the detection of Diabetic Ketoacidosis (DKA) in which beta-hydroxybutyrate-dehydrogenase enzyme is used instead of a glucose oxidising one. Such determination helps to treat some of the complications that can result from prolonged hyperglycaemia.

Blood alcohol sensors using alcohol dehydrogenase enzymes have been tested and patented; unfortunately they have not yet been successfully commercially developed.

Figure 19. Four generations of blood glucose meter, ca. 1993–2005. Sample sizes vary from 30 to 0.3 µl.

3.2.7 Meter use for hypoglycemia

A common problem of clinical concern arising from the method regards accuracy and ratio between false positive and negative results in the case of hypoglycemia (glycemia < 70 mg/dl). The inaccuracy of ±15% is less of a problem for high glucose levels than low. There is little difference in the management of a glucose of 200 mg/dl compared with 260 (*i.e.*, a "true" glucose of 230±15%), but a ±15% error margin at low glucose concentrations brings greater ambiguity with regards to glucose management.

The inaccuracy is compounded by the relative likelihoods of false positives and negatives in populations with and without diabetes, respectively.

People with type 1 diabetes usually have glucose levels above normal, often ranging from 40 to 500 mg/dl (2.2 to 28 mmol/l), and when a meter reading of 50 or 70 (2.8 or 3.9 mmol/l) is accompanied by their usual hypoglycemic symptoms, there is little uncertainty about the reading representing a "true positive" and little harm done if it is a "false positive." However, the incidence of hypoglycemia unawareness, hypoglycemia-associated autonomic failure (HAAF) and faulty counterregulatory response to hypoglycemia make the need for greater reliability at low levels particularly urgent in patients with type 1 diabetes mellitus, while this is seldom an issue in the more common form of the disease, type 2 diabetes mellitus.

In contrast, people who do not have diabetes may periodically have hypoglycemic symptoms but

may also have much higher rate of false positives to true, and the meter is not accurate enough to base a diagnosis of hypoglycemia. The meter can occasionally be useful in the monitoring of severe types of hypoglycemia (e.g., congenital hyperinsulinism), to ensure that the average glucoses when fasting remain above 70 mg/dl (3.9 mmol/l).

3.3 A new approach to glucose sensing at gold electrodes [40]

Since Clark and Lyons reported the first enzyme electrode in 1962 [39], most studies on this subject have involved the use of the enzymes glucose oxidase (GOD) and glucose dehydrogenase (GDH), both of which catalyze the oxidation of glucose to δ-gluconolactone [4].
Although enzymatic detection usually shows good selectivity and high sensitivity, the enzyme is easily denatured during its immobilization process. The most serious problem of such sensors is the inherent lack of stability due to the sensitive nature of enzymes, especially in implantable devices that represent the new frontier in diabetes management; providing continuous information, they help to reduce the occurrence of complications [41].
Non enzymatic glucose sensors have been studied in order to develop effective enzyme-free sensors; in particular the direct electrochemical oxidation of glucose in alkaline medium was investigated at Cu, Ni, Fe, Pt and Au electrodes [13]. Of these electrodes, platinum was the most promising [14-18], but it proved to be extremely non-selective and susceptible to poisoning by various components of blood and other physiological media over extended use [18-20]. (Appendix B, constituent of human blood). Attempts have been made to overcome these drawbacks by modifying the electrode substrate with ad-metals and nanoparticles, or by using different kinds of electrode materials, since the key factor that affects both the sensitivity and selectivity of glucose detection is the electrocatalytic activity of the electrode materials [28,42-47].
A different approach to the subject has been developed by Makovos *et al.* [33]. By performing a cyclic-voltammetric study of glucose oxidation at a gold electrode, they observed the occurrence of a positive current peak during the cathodic sweep, and highlighted a highly linear dependence between current value maxima and glucose concentration. On the basis of their study, pulsed amperometric detection (PAD) at gold electrodes coupled with HPLC gained prominence for analysis of complex mixtures of polyalcohols and carbohydrates [34].
The application of the method in blood glucose sensing has been hindered by the presence of inhibitors; as already outlined by Makovos, chlorides, amino acids, and human albumin were observed to inhibit the reaction [33]. Among them, chlorides are the most problematic because of their high concentration in the blood, (about 0.1 M) and the difficulty inherent in trying to separate them from glucose.

In order to overcome this problem in chapter II we extensively investigated the mechanism of glucose oxidation at gold electrodes (see paragraph 2.2), and in particular the influence of chloride ion, pH and buffer concentration on the oxidative peak in the cathodic sweep [12].

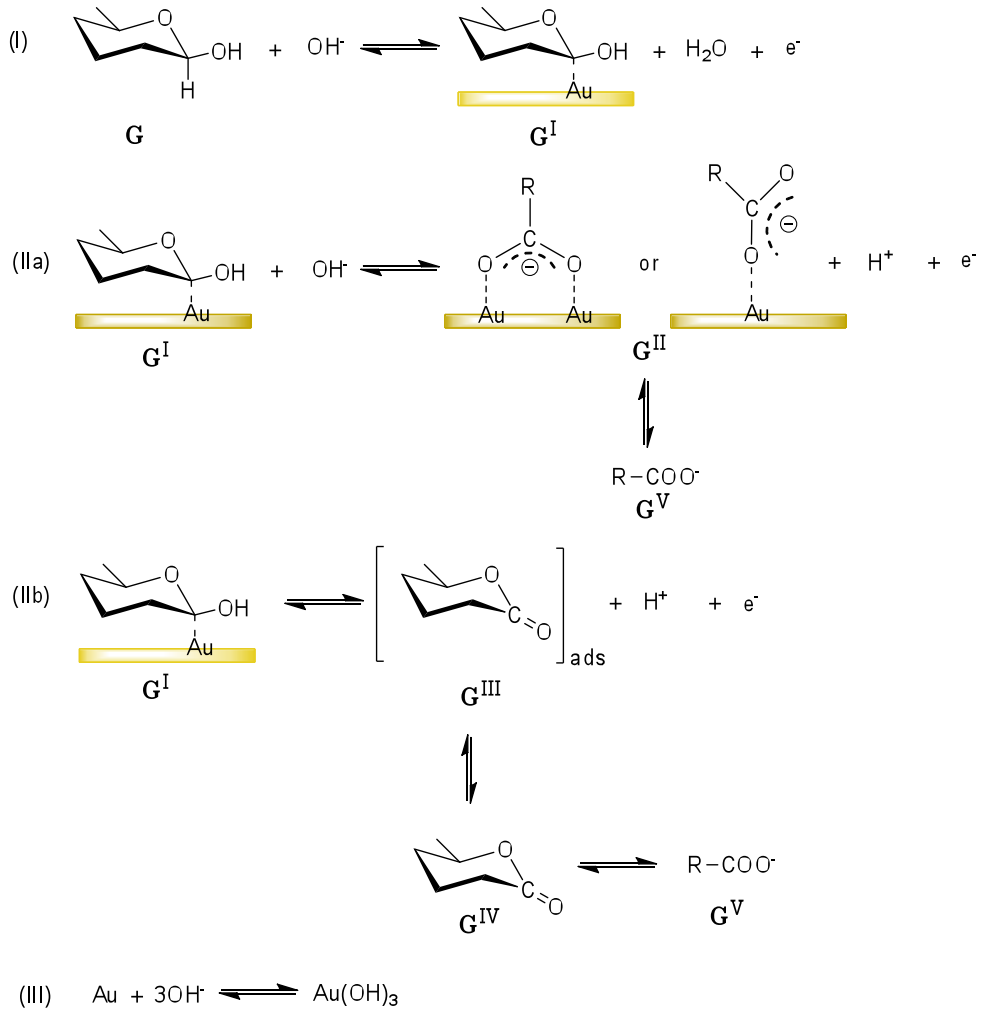

Scheme 1. Proposed mechanism at gold electrodes [46]. G = D-glucose (β-D-glucopyranose, predominant form in water), G^{I}= dehydrogenated glucose (intermediate generated by anomeric carbon dehydrogenation), G^{II}= adsorbed D-gluconate (two possible forms), G^{III}= adsorbed δ-gluconolactone, G^{IV}= δ-gluconolactone and G^{V}= δ-gluconolactone. Adapted from [48].

In the proposed mechanism (Scheme 1), the glucose molecule is first electrochemically adsorbed at the surface of the electrode by dehydrogenation (reaction I, peak I in Figure 20a). The dehydrogenated molecule can be transformed to gluconate either by direct oxidation (reaction IIa) or through a δ-gluconolactone intermediate step (reaction IIb). At room temperature these two processes cannot be distinguished (peak II in Figure 20a). At higher potentials, the gold surface is oxidized to gold hydroxide (reaction III, peak III in Figure 20a), which is inactive towards glucose electrooxidation.

During the cathodic scan, gold hydroxide is reduced, and therefore glucose can be readsorbed and oxidized, generating the oxidative peak in the cathodic scan (peak IV in Figure 20a).

According to our previously reported study (paragraph 2.2), chloride ions inhibit the formation of the "sensing peak" in two ways (Scheme 2):

1) In the presence of chlorides gold gets oxidised to gold tetrachloroaurate instead of forming the hydroxide (reaction III).
2) Chlorides, adsorbing at gold active sites, inhibit glucose oxidative adsorption (reaction I), first and key step of the oxidation mechanism.

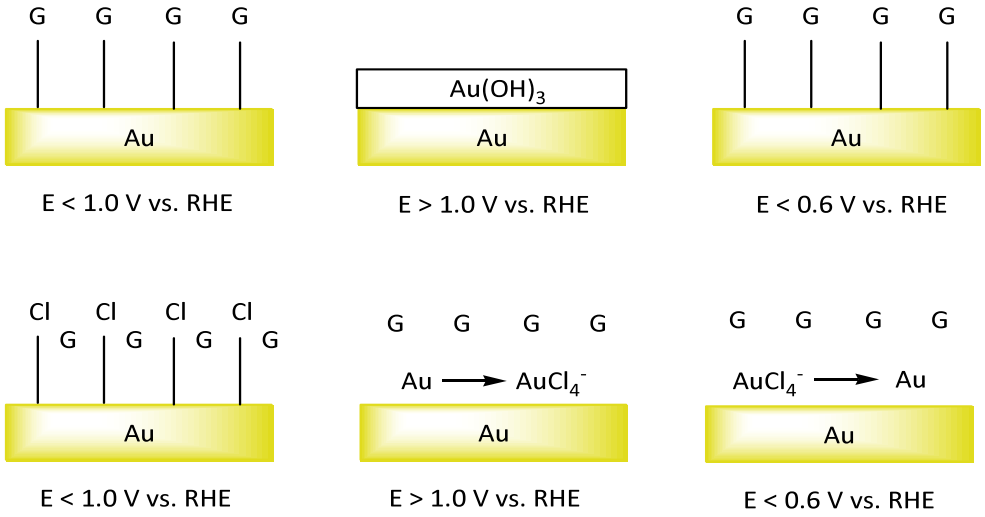

Scheme 2. Schematic representation of the chloride inhibition problem.

In the following, we propose a solution to this problem involving a three electrodes setup, and a four steps pulsed electrochemical detection technique.

3.3.1 Results and discussion

Figure 20a shows cyclic voltammetries performed in a 50 mM buffer (K_2HPO_4/K_3PO_4), of pH 11.5 at different glucose concentrations ranging from 1 to 20 mM, corresponding to 18-360 mg/dl glycemia range. According to our previous study, these are the best operating conditions for optimal sensitivity of the return peak. In fact, glucose electrooxidation is favored by increasing the OH^- concentration, but on the other hand, glucose is unstable at pH values higher than 11-11.5, due to secondary reactions [3,49]. We also demonstrated that the buffer has multiple effects on the reaction that can be summarized as follows:

- improves the reaction by increasing the ionic conductivity of the solution;
- maintains a constant pH value near the electrode surface, which would otherwise be decreased to glucose oxidization to gluconic acid;

- at higher concentrations, the buffer itself can be adsorbed to the gold surface and occupy active sites thus limiting the adsorption of glucose, first step of glucose electrooxidation.

We found that a 50 mM concentration is the best compromise in optimizing these contrasting effects.

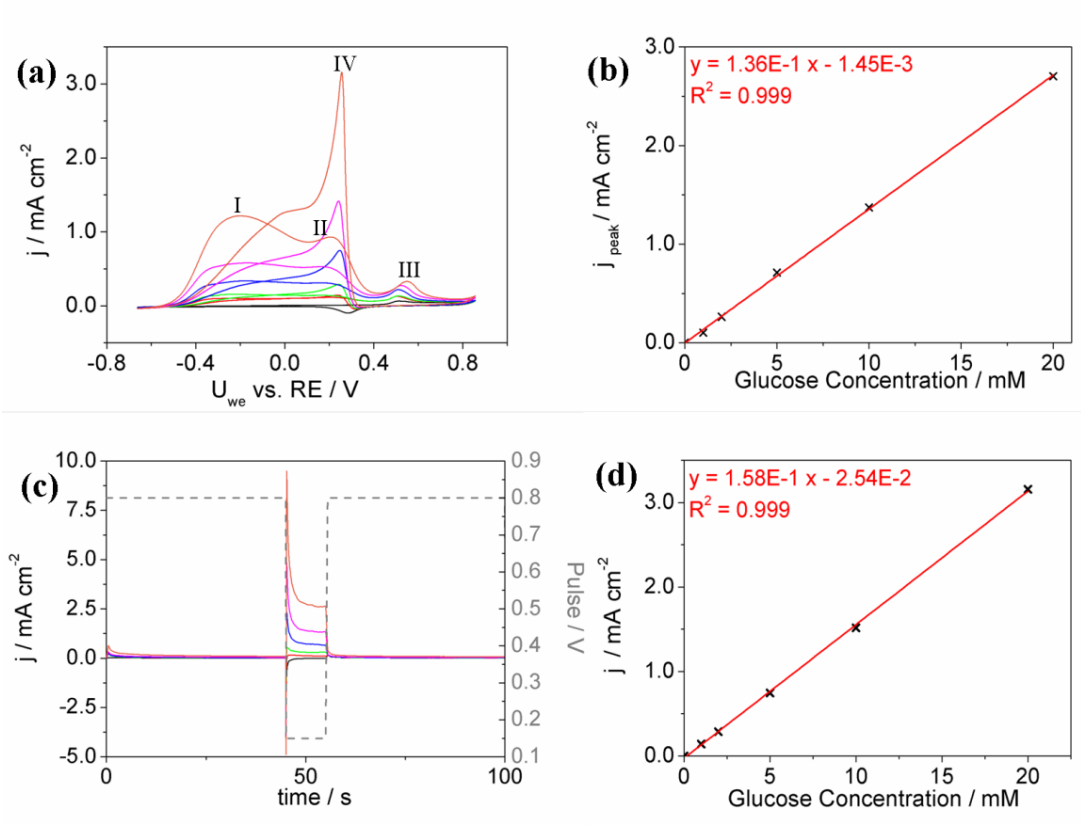

Figure 20. (a) Cyclic voltammograms (20 mV s^{-1} scan rate) and (c) pulsed technique (chronoamperometry) at gold electrode in 50 mM buffer (K_2HPO_4/K_3PO_4), at pH 11.5 and different glucose concentrations: (black) electrolyte, (red) 1 mM glucose, (green) 2 mM glucose, (blue) 5 mM glucose, (pink) 10 mM glucose, (orange) 20 mM glucose. Calibration curves of (b) cyclic voltammetry and (d) of pulsed technique.

In these conditions (Figure 20b) it is evident the linear relationship existing between cathodic oxidative peak current density and glucose concentration in the investigated range. The same phenomenon in similar conditions has been previously outlined by Makovos *et al.* [33].

The preparation of the circuits to perform CVs and to analyze the peak current value in an actual application is complex [27], therefore the next logical step was to develop and optimize a pulsed two-step electrochemical technique which would be easier to realize in practical applications. In the first step (0.8 V vs. RE, 40 s), gold hydroxide is generated, followed by the second step (0.15 V vs. RE, 15 s), where gold hydroxide is reduced and glucose sensing performed. Potential and step time have been optimized for the operating conditions. In Figure 1c is reported one of the ten cycles performed for each glucose concentration to evaluate the reproducibility of the measurement. Even with this type of measurement, we obtained a highly linear relationship

between glucose concentration and current density as reported in Figure 20d. In this case the stationary current value vs. glucose concentration is reported instead of the peak current value, since it is more reproducible and easier to measure in a real device application.

After proving the efficiency of the pulsed technique at pH 11.5, the next step was to test it at pH 7.4, (blood pH) while keeping all other parameters constant.

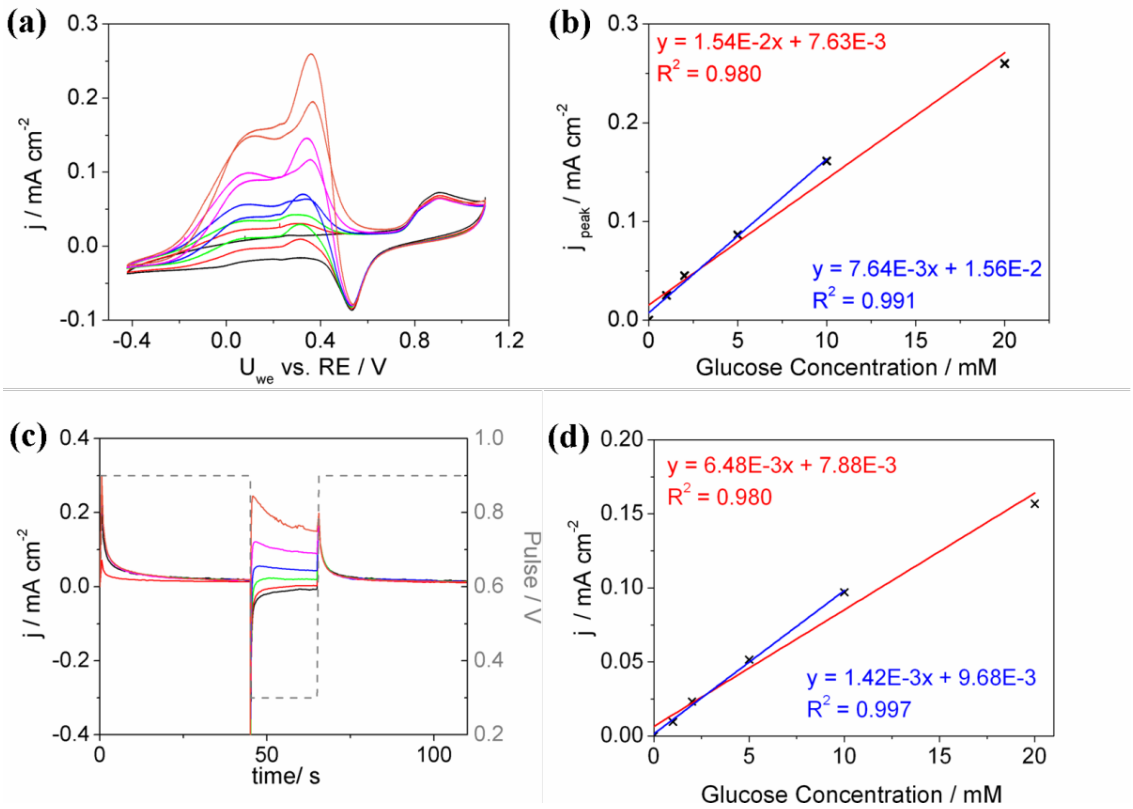

Figure 21. (a) Cyclic voltammograms (20 mV s^{-1} scan rate) and (c) pulsed technique (chronoamperometry) at gold electrode in 50 mM buffer (K_2HPO_4/KH_2PO_4), at pH 7.4 (blood pH) and different glucose concentrations: (black) electrolyte, (red) 1 mM glucose, (green) 2 mM glucose, (blue) 5 mM glucose, (pink) 10 mM glucose, (orange) 20 mM glucose. Calibration curves of (b) cyclic voltammetry and (d) pulsed technique (peak current density vs. glucose concentration).

In Figure 21a the cyclic voltammograms in the same glucose concentration range are reported. The current output is lower with respect to the previous conditions, and therefore the sensitivity on the return peak is also lower. Moreover, (Figure 21b) at higher glucose concentrations the response is not linear. This is probably due to the lower OH^- concentration that limits the gluconate formation, as previously discussed.

Despite this, the pulsed technique has been tested in these conditions (Figure 21c). Changing the pH requires a modification in the steps potentials, as both the gold hydroxide and return peak potentials are pH dependent. In this case, the gold hydroxide is generated at 0.9 V vs. RE (40 s) and the subsequent reduction/sensing step performed at 0.3 V (15 s). Thus it was demonstrated

that it is possible to apply the pulsed method at blood pH, though the sensitivity and linearity range are diminished (Figure 21d).

The following step was to test the method in the presence of 100 mM potassium chloride at pH 7.4 buffered with 50 mM K_2HPO_4/KH_2PO_4, thus partially recreating the physiological conditions of human blood. In this case, in both CV and the pulsed technique, instead of the oxidative peak in the cathodic scan, a reduction process is observed. In the presence of chlorides, it is well known that gold is oxidized to $AuCl_4^-$, a reaction that takes place at a lower potential than $Au(OH)_3$ formation. In the cathodic scan the gold tetrachloroaurate, previously generated in the anodic scan, is reduced (Scheme 2).

However, upon analyzing the Pourbaix diagram of gold in the presence of chlorides [50], it is evident that at pH values higher than 9, gold hydroxide is the most stable phase, even in the presence of up to a 2 M chloride concentration. Therefore, it is not necessary to remove all the chlorides from the solution in order to perform the sensing step, but it is enough to locally increase the pH to over 9. On the basis of these considerations, a four-step, three electrode (silver gauze, gold pin and platinum counter electrode) measurement has been performed. The optimized operating conditions are reported in Scheme 3.

Three Electrode Four Step Pulsed Technique

1st step: Chloride Removal

WE (Ag): $Ag + Cl^- \rightarrow AgCl(s) + e^-$

CE (Pt): $H_2O + 2e^- \rightarrow H_2 + 2OH^-$

pH from 7.4 to 11.5 (10% of Cl^- removed)

2nd step: Gold Hydroxide Formation

WE (Au): $Au + 3OH^- \rightarrow Au(OH)_3 + 3e^-$

CE (Pt): $H_2O + 2e^- \rightarrow H_2 + 2OH^-$

3rd step: Reduction of Gold Hydroxide and Glucose Sensing

WE (Au):

$Au(OH)_3 + 3e^- \rightarrow Au + 3OH^-$

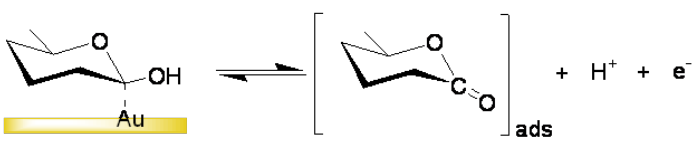

CE (Pt): $H_2O + 2e^- \rightarrow H_2 + 2OH^-$

4th step: Chloride Regeneration

WE (Ag): $AgCl(s) + e^- \rightarrow Ag + Cl^-$

CE (Pt): $2H_2O \rightarrow O_2 + 2H^+ + 2e^-$

Scheme 3. Four-step pulsed electrochemical detection schematic.

The first step is a chronopotentiometry step, (I= 10 mA) in which a silver gauze working electrode is oxidized to silver chloride, while water is reduced at the platinum counter electrode. In the overall reaction, for every chloride ion removed, one hydroxide ion is generated; therefore in order to shift the solution pH from 7.4 to 11.5 it is necessary to remove only 10% of the chlorides present in the solution. Thus the charge flow needs to be controlled, and it depends on the volume of solution employed (in our case we used 15 ml of solution and the charge was limited to 5 mC). The second step corresponds to the first one of the pulsed technique described above, in which the gold pin electrode surface is oxidized to gold hydroxide (0.7 V vs. RE, 40 s) and subsequently reduced (0.3 V vs. RE, 15 sec) in the third step: once the gold surface is regenerated, glucose can re-adsorbed and the oxidative peak is generated. In this case, both the peaks observed in the CV (Figure 22a) and the steady state current, in the pulsed technique, (Figure 22b) show linear dependence, with very high correlation coefficient values, on glucose concentration in the investigated range, coupled with high sensitivity. In the last (fourth) step, the silver electrode (partially covered with silver chloride from step 1) is reduced and regenerated, ready for the next sensing.

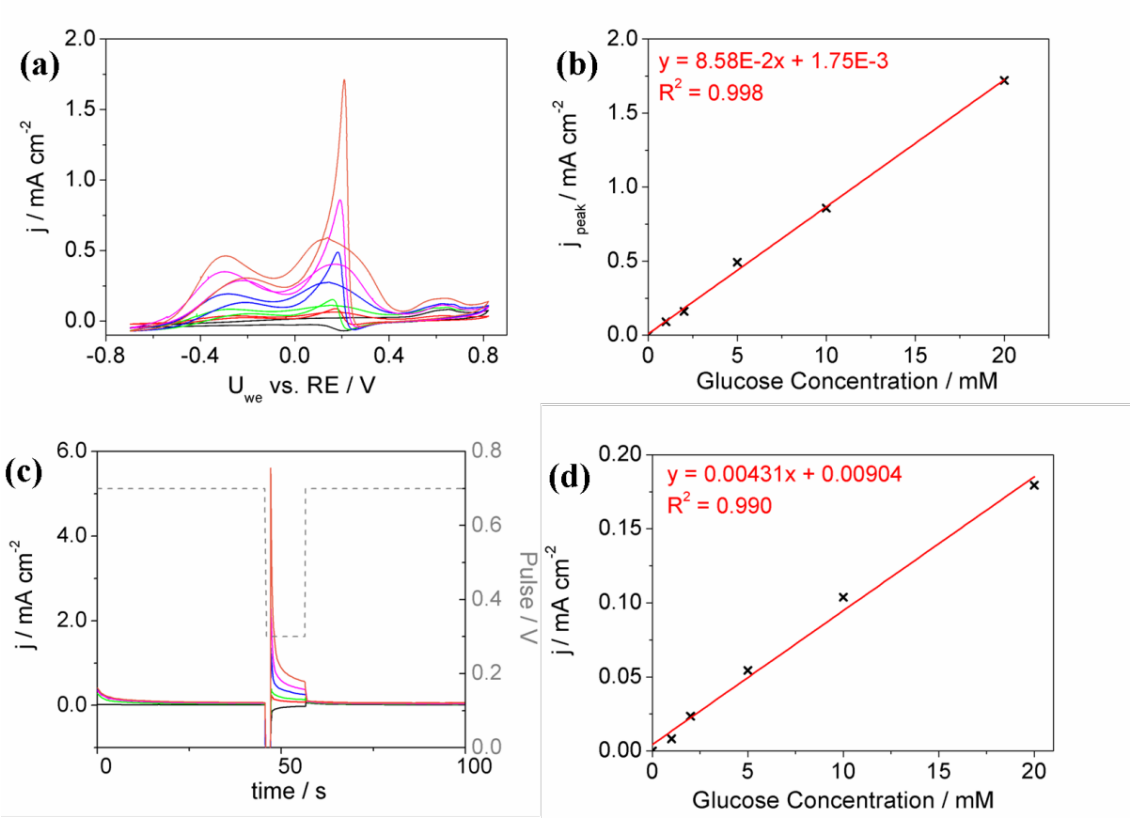

Figure 22. (a) Cyclic voltammograms (20 mV s^{-1} scan rate) and (c) pulsed technique (chronoamperometry) of a 50 mM buffer (K_2HPO_4/KH_2PO_4) pH 7.4, 100 mM NaCl solution at different glucose concentrations after chloride removal step: (black) electrolyte, (red) 1 mM glucose, (green) 2 mM glucose, (blue) 5 mM glucose, (pink) 10 mM glucose, (orange) 20 mM glucose. Calibration curves of (b) cyclic voltammetry technique and (d) pulsed technique (peak current density vs. glucose concentration).

3.3.2 Conclusions

For the first time, an electrochemical method for determining glucose in the presence of chlorides is proposed; it shows higher accuracies and sensitivities than enzymatic methods. All the materials employed (silver, platinum and gold) are fully compatible with in vivo sensing applications. At the present the method has been tested in 15 ml of solution and needs long steps time. The next step in the implementation of this technique is the realization of a miniaturized device in which each step time would be drastically reduced. Further studies on the effect of other poisons of the gold catalyst are also required.

CHAPTER IV: GLUCOSE-GLUCONATE FUEL CELLS

Chapter IV: Glucose-gluconate fuel cells

In this chapter the direct non-enzymatic electrooxidation of glucose will be discussed and the concept of glucose-gluconate fuel cells introduced. The optimization of the operating conditions of a commercial, platinum based anode material in order to selectively oxidize glucose to gluconate will be presented. The promising electrocatalyitic properties of gold nanoparticles towards glucose electrooxidation in aqueous alkaline solutions will be demonstrated and applied to the development of a new anode material obtained by electrodepositing gold nanoparticles on a carbon nanotubes conformally coated polyester textile current collector deeply described in chapter VI.

4.1 Introduction

At the beginning of the eighties, the substitution of hydrogen with different feeds was considered in fuel cell technology. The direct methanol or ethanol-air cells (DMFC) investigated with pioneering attempts about twenty years before attracted again the attention of the scientific community [51]. The approach was fascinating not only for the promising experimental results but even for the availability of large renewable primary energy sources (*i.e.* sugar) in the case of ethanol. According to this strategy, the possibility to feed fuel cells with carbohydrate solutions was considered. Hydrogen or ethanol was directly produced in the cell by catalytic reformers or metabolic degradations (biological fuel cells) [52].

The presence of one or more intermediate steps between the fuel primary energy source and the electrochemical oxidized species lowers the energy efficiency with respect to the direct oxidation process of the carbohydrate molecules; therefore fuel cells operating with direct sugar oxidation should have higher efficiency. Furthermore, the carbohydrates are not only renewable and widely available energy sources, but they also present other advantages with respect to hydrogen or ethanol (*i.e.* safe storage and easy delivery).

The investigation of direct carbohydrate oxidation fuel cells started in 1964 [53] and continued as a promising approach to autonomous energy supply for medical implants [8] until the coming of the lithium batteries, a dozen years later.

About ten years ago, the studies concerning the direct glucose oxidation fuel cells recovered strength owing to the development of nanostructured electrodes [54,55] with high electrocatalytic performance for glucose oxidation in aqueous solution. The few results obtained using both alkaline [54-56] or proton conducting membrane [57] electrolytes are often unreliable and scattered as well as the related anode reaction is far from well defined. These shortcomings are probably due

to the technological and engineering approaches used by the authors [58,59]; in fact the experimental work was mainly devoted to the evaluation of the electrical cells' performance (power densities) by short-circuiting experiments rather than investigating the fundamental aspects of the electrochemical process. A more systematic study of the thermodynamics and kinetics of glucose electrooxidation should provide useful data for better evaluating the energy performances, which will be absolutely necessary to guide the exploitation of the direct glucose oxidation or abiotically catalyzed fuel cells [8].

4.2 Glucose –gluconate fuel cell

The direct oxidation of glucose to produce electrical energy has been widely investigated because of renewability, abundance, high energy density and easy handling of the carbohydrate. Most of the previous studies have been conducted in extreme conditions in order to achieve complete glucose oxidation to CO_2, neglecting the carbohydrate chemical instability that generally leads to useless by-products mixtures. The partial oxidation to gluconate, originally studied for implantable fuel cells, has the advantage of generating a commercially valuable chemical (see paragraph 4.3). Therefore the idea is to develop a new gluconate synthetic method where the electric energy generated improves the energy efficiency of the entire plant.

4.3 Gluconic acid and derivatives

Gluconic acid is a crystalline solid (Mw = 196.16), (m.p. 131°C), $[\alpha]_D^{20}$ = -6,7°. It is a mild strength acid with a K_a(25°C) = $2.5 \cdot 10^{-4}$, very soluble in water and in alcoholic solutions and completely immiscible in ether and in the majority of organic solvents.
In aqueous solution it is in equilibrium with its lactones (γ-gluconolactone e δ-gluconolactone) in a ratio depending on concentration and temperature.
Due to the difficulties of synthesis in the crystalline form it is usually commercialized in aqueous solutions at 50% by weight (d_4^{25} = 1.24 g/ml). It is usually stored in stainless steel tanks.

4.3.1 Uses and applications

The main applications of gluconic acid are due to its peculiar properties: it is a weak acid able to dissolve oxides, hydroxides and carbonates of polyvalent cations, without attacking metallic surfaces.
This property is further enhanced by the ability of forming water-soluble complexes with these

cations. Gluconic acid is particularly indicated to remove calcareous deposits or rust from metal and other surfaces, included beer and milk residues on galvanized iron, magnesium alloys and stainless steel. Moreover it is employed in the textile industry together with magnesium salts, as stabilizer in peroxidic bleaching baths.

Considering its physiological compatibility, D-gluconic acid is also used in both food and pharmaceutical industry. Low concentrations (0.02-0.1%) of the substance promote sucrose inversion, preventing fructose from further reactions. In many applications, the 1,5-lactone is a convenient substitute of the free acid: this offers particular advantages for long term acidic conditions, for example for the preparation of pickles and frankfurter sauces or in the conservation of fresh sauces. Another application is as yeasting agent in baking.

If compared with other complexing agents of both inorganic and organic origin, gluconic acid, its lactone and salts have another advantage: they are easily and quickly degraded by a biological wastewater treatment.

4.3.2 Gluconates

The most important gluconate is sodium gluconate, which water solubility as a function of temperature is reported in the following table.

T (°C)	0	20	50	80	100
g ml^{-1}	0,43	0,60	0,85	1,33	1,60

Sodium gluconate, as the free acid, forms complexes with metallic cations, which stability often increase considerably with the pH. This salt has cleaning properties very useful on many surfaces. Together with sodium carbonate and hydroxide solutions it is used to remove fats and corrosion products from aluminum, rust from iron, superficial oxides form copper and copper alloys and to engrave aluminum.

Strongly alkaline baths of gluconate allows the removal of superficial zinc coating and are characterized by the ability to remove a lot of zinc and so from a long duration. Alkaline solutions of gluconate at 95-100 °C are used to remove varnish and dyes, without damaging the surfaces underneath. Gluconate is also useful in surface pretreatments, for example in depositing a brazing coating of nickel-cobalt on aluminum, or in baths required for the preparation of smooth and shining surfaces of nickel, tin and zinc, substituting the highly toxic cyanide ion. Mixtures of gelatine and sodium gluconate are used as pasting agents in the paper industry granting higher acidic resistance. The textile industry uses gluconate (sometimes in combination

with polyphosphates) to separate polyesteric or polyammidic textiles or to treat the natural cellulose fibers.

4.3.3 Sodium gluconate

Sodium gluconate is a component of commercial detergents: due to its absolute stability towards hydrolysis at high temperatures and pH (below 11); for its chelating properties it is used for example in cleaning aluminum bottles or surfaces.
In the concrete industry sodium gluconate is very effective as retardant of the drying process; the addition of 0.02-0.2% by weight with respect to the concrete generates very homogeneous cements with improved mechanical resistance to water an ice. Thus gluconate gives better rheological properties, improved plasticity when dry despite the decreased water content.
Complexes of gluconate with aluminum, iron, zinc and, in a slower way, with chrome can be degraded by simple precipitation of the hydroxides. The metallic ions released during the degradation are removed from the waste water by precipitation or adsorption on the sludge.
Tracking elements are usually administered as gluconates, considering that these compounds are quickly absorbed by the organism and well tolerated, for example calcium gluconate is used in calcium therapy as well as iron for iron/therapy.

4.3.4 Synthesis methods

For commercial purposes, D-gluconic acid and its salts are exclusively prepared by oxidation of glucose or of raw material containing glucose. The oxidation methods can be electrochemical or biochemical.

- *Electrochemical oxidation*

The electrochemical procedure is characterized by problems related mainly to halogens oxidation potentials. In this process glucose solutions containing about the 10% in moles of bromides are electrolyzed at current densities ranging from 1 to 20 A dm^{-2}. In order to neutralize the acid generated, carbonates and hydroxides are added. The coulombic efficiencies are in the order of 80-86%. This process is not competitive due to the high cost of electricity.

- *Enzymatic oxidation*

The conversion of glucose to gluconic acid involves plain reactions.

The first one is catalyzed by glucose oxidase (β-D-glucose: oxygen-1-oxoreductase), as shown in Scheme 4.

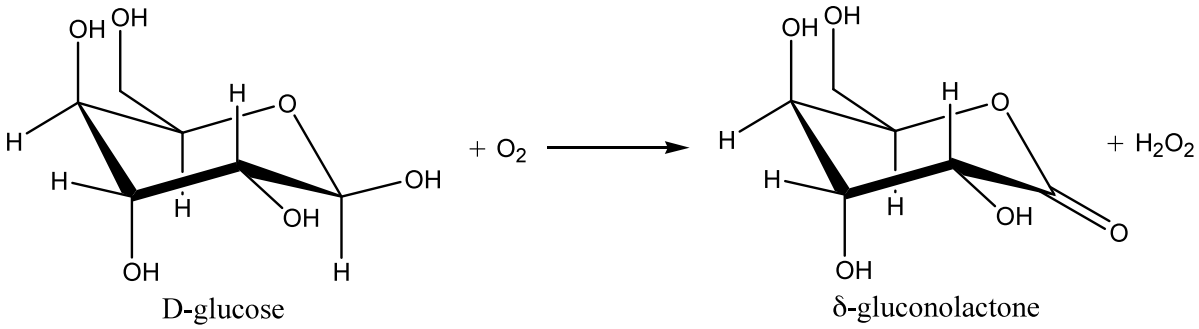

Scheme 4. Glucose enzymatic oxidation.

From the scheme it can be observed that it requires 1 oxygen mole per glucose mole consumed. One mole of δ-gluconolactone is produced per mol of substrate spontaneously converted to gluconat by hydrolysis and one mole of H_2O_2 that can be removed from the reaction media by using a catalase.

Glucose oxidase (GOx) has been isolated for the first time by Muller in 1928 from a concentrated solution of *aspergillus niger,* a flavoprotein (containing FAD as prostetic group), characterized by a high selectivity towards β-D-glucose oxidation.

From a practical point of view the fermentative process for gluconic acid production with aspergillus niger has to respect the following conditions:

- High glucose concentration (110-250 g/l)
- Low nitrogen concentration in solution (max. 20 mM)
- Low phosphites concentration (max. 20 mM)
- Sufficient amounts of transition elements compounds, for example manganese sulfate (in a concentration range 0.7-13 mM), able to regenerate the micelles that produces GOD.
- The pH of the solution needs to be in the range 4.5-6.5. Below pH 3 glucose oxidase loses it catalytic activity.
- High aeration speed, preferably obtained through applied pressures of about 4 bar.

4.3.5 Economical aspects

The production of gluconic acid its derivatives is nowadays estimated around 60000 t/y. The 85% is in the form of gluconate.

4.4 Optimizing operating conditions and electrochemical characterization of glucose-gluconate alkaline fuel cells [60]

In the present study we optimized fuel composition and operating conditions in order to selectively oxidize glucose to gluconate, maximizing the power density output of a standard commercial platinum based anode material (FC01 Mini Fuel Cell by Electro-Chem-Technic, see. Appendix D). Deep electrochemical characterizations concerning reversible potential, cyclic voltammetry and overpotential measurements have been carried out at 25°C in the D-(+)-glucose concentration range $1.0 \cdot 10^{-2}$ – 1.0 M. NMR and EIS investigation clarify the role of the buffer in enhancing the electrochemical performance.
The aim was to also produce an actual benchmark for the evaluation of upcoming electrode materials.

4.4.1 Electrode Reversible Potential Measurements

It is well known that glucose is unstable in aqueous alkaline solution and degrades into complex mixtures [49,61,62]. Nevertheless glucose electrochemical oxidation is favored at high pH values [55]. In order to establish the optimum operating pH at which the carbohydrate degradation takes place, the glucose concentration in aqueous solutions as a function of time was measured. From each solution some aliquots were sampled and analyzed by HPLC: no variation in composition was observed for pH values equal or less than 11. As a consequence, a buffered solution (0.5 M Na_2HPO_4, pH 10.5), purged by N_2 flux was used as electrolyte in the anodic compartment. The role of the buffer will be discussed in detail later in the text.
In these buffered solutions the equilibrium electrode potential (E_{rev}) of the anode was measured versus the SCE. In such operating conditions the electrode potentials, after two hours of equilibration time, were very reproducible (± 1 mV) and stable; constant values for 70 hours or more were observed. As the glucose concentration rises, the electrode potential becomes more and more negative, their values versus the logarithm of glucose concentration show a straight line correlation with a change in the slope taking place at about $5.5 \cdot 10^{-2}$ M (see Figure 23).
The number of electrons consumed per molecule of glucose, *n*, obtained from the two slopes are equal to 0.22 ([glucose] < $5.5 \cdot 10^{-2}$ M) and 1.4 ([glucose] > $5.5 \cdot 10^{-2}$ M). The extremely low value of *n* obtained for low glucose concentrations may be explained by the simultaneous occurrence of two reactions at the anode: glucose oxidation and oxygen reduction. In fact, even if the solution is purged with nitrogen some traces of oxygen still remain. In such conditions the measured potential is a mixed potential (partially due to the kinetics of both the reactions).

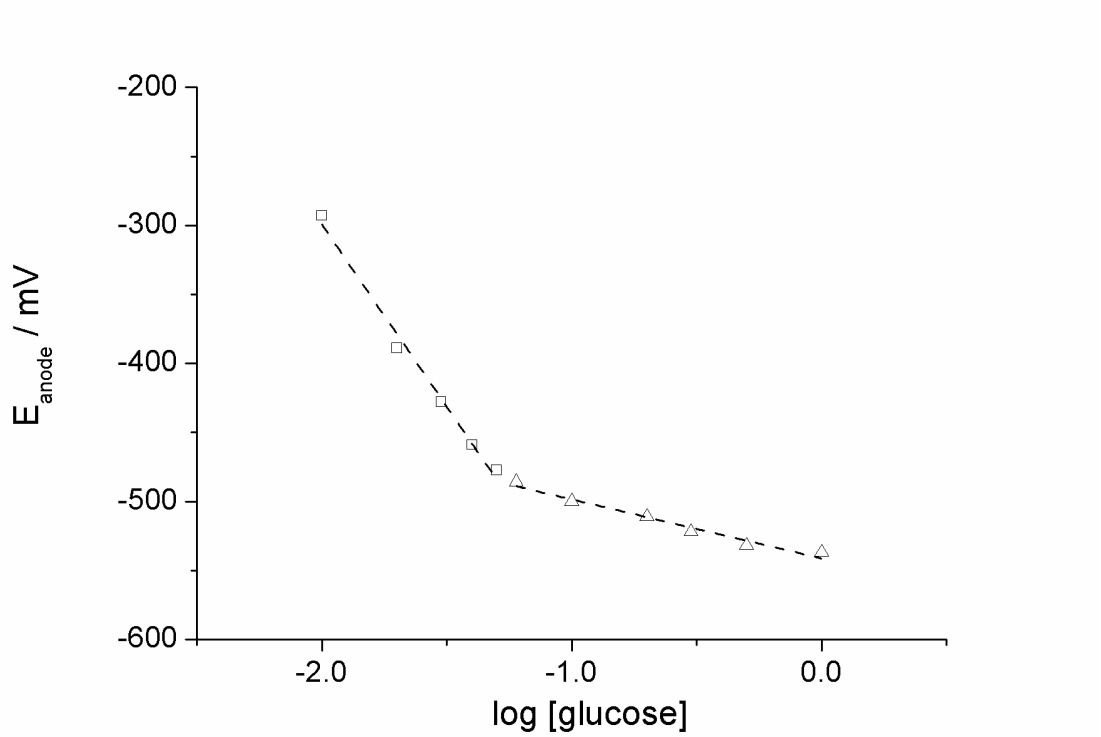

Figure 23. Reversible anode (commercial platinum based material) potential as a function of the glucose concentration, at pH = 10.5 and room temperature.

Naturally, when the concentration of glucose is sufficiently high, the oxygen reduction rate is negligible with respect to the exchange current of glucose oxidation. The value of *n* at high concentration, 1.4, is probably the result of a partial oxidative adsorption of glucose (*n* = 1) and partial oxidation of glucose to gluconate (*n* = 2), following the mechanism of electrooxidation of glucose on platinum electrodes proposed by Beden et.al [9]. Another possible explanation for the slope change at different glucose concentrations may be the variation in the elemental redox reaction, as previously reported [63]. Nevertheless, the low value of *n* for low concentrations makes this hypothesis unrealistic. By fitting the curve in Figure 23 at high glucose concentration, the value for the standard redox potential, E_0, of glucose electrooxidation at pH 10.5 and room temperature was evaluated to be -0.5412 V (vs. SCE).

4.4.2 Current-Voltage Characterization

The measurements were performed using plain and buffered solutions. In the former case before the electrolyte decomposition potential, the anode voltage (*V*) versus current density (*j*) shows (see Figure 24) the typical behavior associated to the charge transfer overpotential (η).

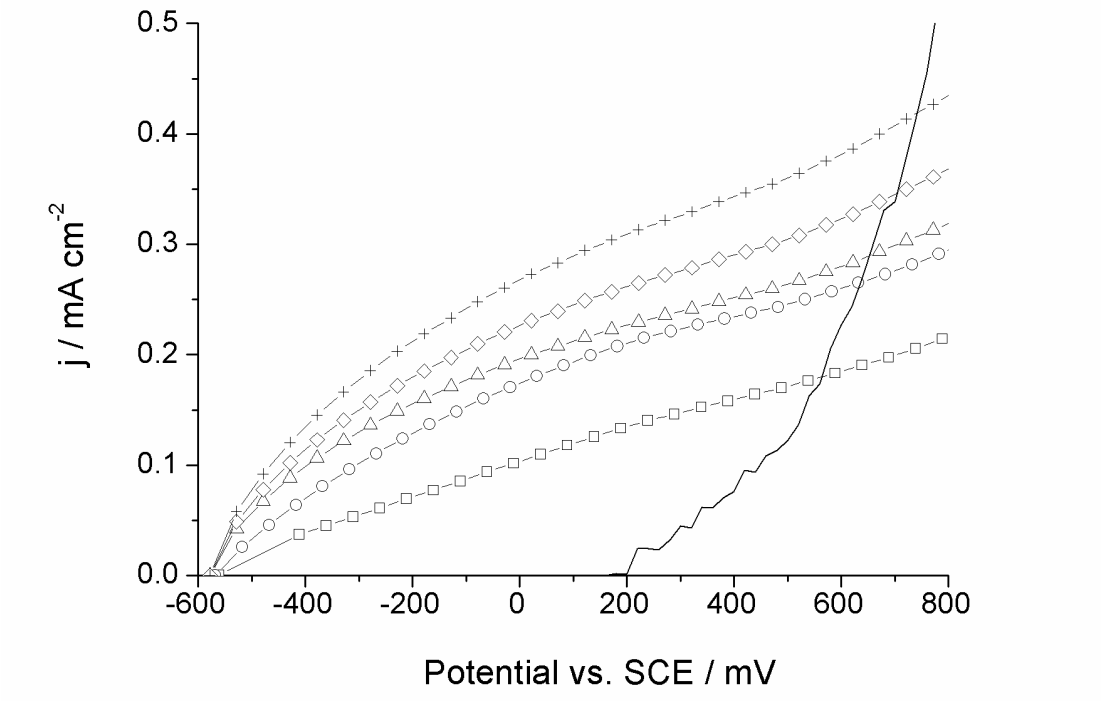

Figure 24. I-V characteristic of the commercial platinum based anode material at pH = 10.5 and different D-glucose concentration: (□) = 100 mM, (○) = 200 mM, (Δ) = 300 mM, (◊) = 400 mM, (+) = 500 mM and (—) = KOH solution (at pH = 10.5).

In fact, η vs. j has a straight line correlation at the lowest applied voltages, while the Tafel equation describes the electrode behavior at the higher values. Two Tafel can be identified (Figure 25), which are associated to the two main steps of the electrooxidation of glucose.

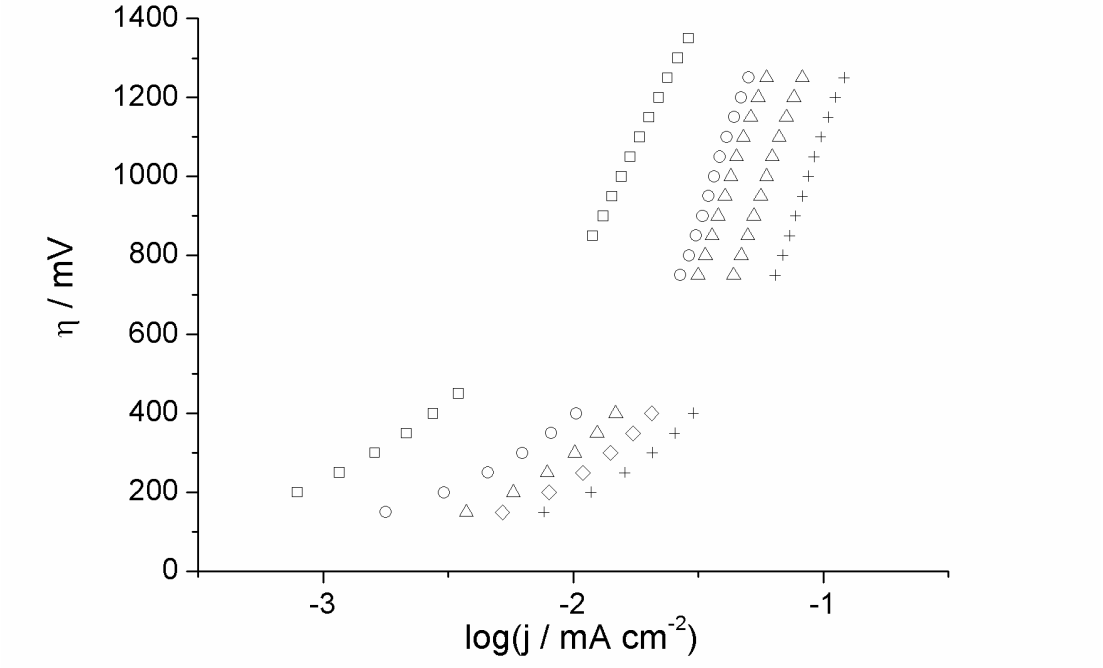

Figure 25. Overpotential as a function of the current density, at pH =10.5 and different glucose concentration: (□) = 100 mM, (○) = 200 mM, (Δ) = 300 mM, (◊) = 400 mM and (+) = 500 mM.

After the initial oxidative adsorption of glucose to the platinum surface (step 1, Figure 26), the adsorbed intermediate is further oxidized to δ-gluconolactone (step 2, Figure 26). In step 3 δ-gluconolactone is desorbed and then hydrolyzed to gluconate.

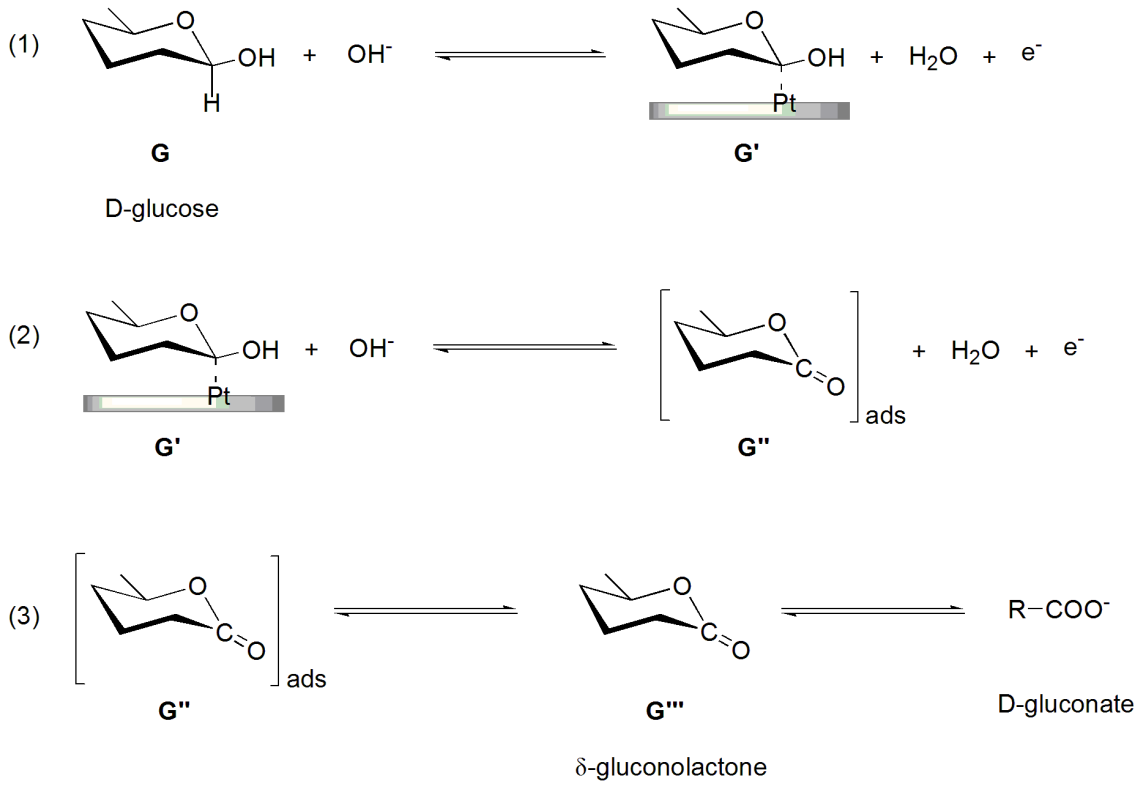

Figure 26. Proposed mechanism at platinum electrodes. G = D-glucose (β-D-glucopyranose formed predominantly in water), G'= dehydrogenated glucose (intermediate generated by anomeric carbon dehydrogenation), G''= δ-gluconolactone, G'''= D-gluconate. Adapted from [11].

From the shape of the I-V curve, it appears that the limiting steps are the two electrochemical reactions, while the desorption of the gluconolactone is relatively fast. This observation can be deduced by the fact that no peak is observed in the I-V curve. If the electrochemical steps were limiting, the adsorbed products would slow down the reaction rate at higher surface coverage, and therefore one or more peaks should appear in the I-V curve.

In the presence of the buffer (Figure 27) the reaction rates of the electrochemical steps change. In fact, two maxima appear which are indicative of two faster electrochemical steps and a slow desorption of the gluconolactone (see the previous explanation). Moreover, it is observed that the peak maxima positions in the potential scale do not vary with the concentration of glucose while the peak current densities do. The maxima locations in the potential scale depend on the buffer concentration as shown in Figure 28, in particular the higher is the concentration of the buffer the more cathodic is the potential, and at the same time the intensity of the peak increases.

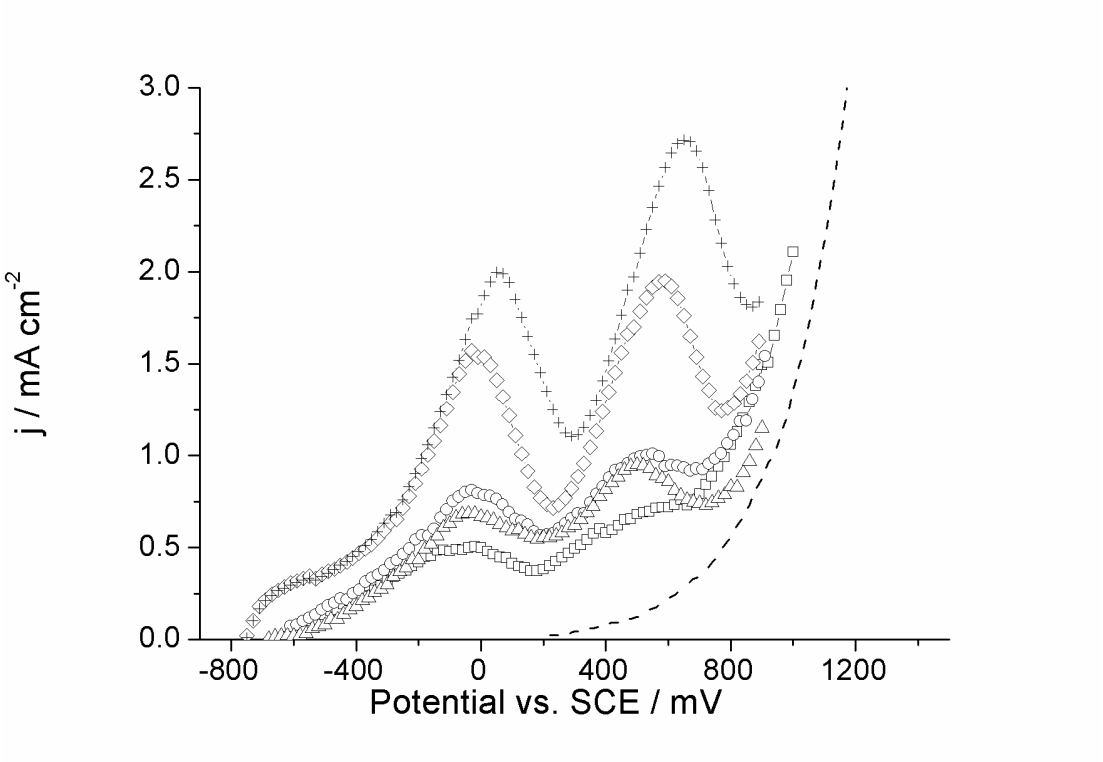

Figure 27. I-V characterization of the commercial platinum based anode material in buffered solution (pH = 10.5) at different D-glucose concentrations: (□) = 100 mM, (○) = 200 mM, (Δ) = 300 mM, (◊) = 400 mM and (+) = 500 mM and (---) = buffered electrolyte.

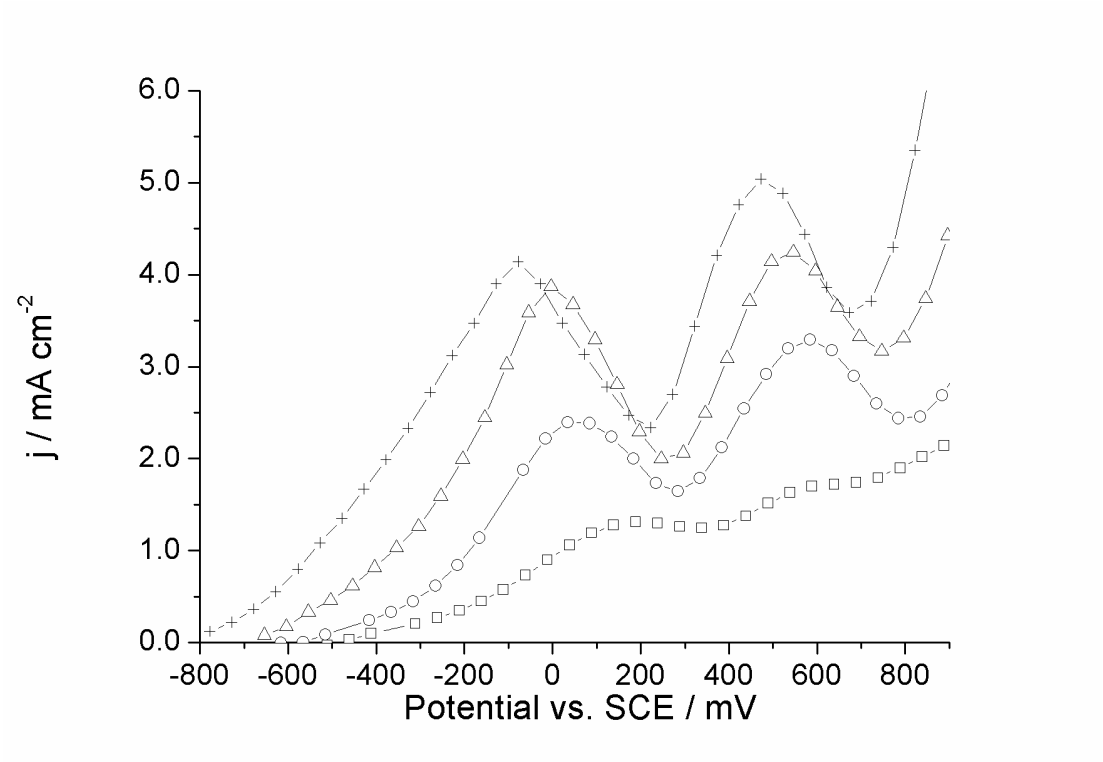

Figure 28. I-V characterization of the commercial platinum based anode material in 500 mM D-glucose solution at different buffer concentrations: (□) = 50 mM, (○) = 250 mM, (Δ) = 500 mM and (+) = saturated solution.

The cathodic shift of the maxima is quite exclusively due to the shift of the reversible reaction potential, thus indicating that the reaction is now changed and that the buffer is a reactant. We presume that the following electrochemical steps are now taking place:

$$G + PO_4^{3-} = G' + HPO_4^{2-} + e^-$$

$$G' + PO_4^{3-} = G'' + HPO_4^{2-} + e^-$$

as consequence the OCV is dependent on the concentration of PO_4^{3-}.

At pH = 10.5, the amount of PO_4^{3-} in the solution is around 1% of the total amount of Na_2HPO_4.

Thus, in the case of the buffered solution, the limiting reactant is the phosphate ion.

We can conclude that the buffer has multiple roles in the final performances of the anode:

- it changes the reaction rates and steps;
- it increases the conductivity of the solution (see below paragraph 4.3.2.4);
- it increases the amount of β form of glucose (see below paragraph 4.3.2.3);
- it may adsorb at the surface of platinum and subtract active sites for the electrooxidation of glucose as already highlighted at gold electrodes[12] .

4.4.3 NMR Measurements

NMR measurements were performed to study the possible interaction between D-glucose and Na_2HPO_4. Two solutions were prepared and let equilibrate for one hour before the experiment: solution A containing D-glucose 0.5 M in d-H_2O and solution B with D-glucose 0.5 M and Na_2HPO_4 0.5 M in d-H_2O, pH = 10.5 (pH adjusted with d-NaOH). The [β]/[α] ratio was calculated in the two samples by the ratio of the integrations of corresponding H-1 (anomeric) signals in the proton spectra.

H-1(α) is a doublet (J = 3.7 Hz) at 5.02 ppm, and H-1(β) is a doublet (J = 8.0 Hz) at 4.44 ppm. In solution A (containing only glucose) [β]/[α] is 0.46, while in solution B (containing the phosphate) [β]/[α] is 1.87. The ^1H and ^{13}C spectra of solutions A and B did not display any difference in the signal chemical shifts or in the coupling constant values, thus indicating that neither covalent bonds nor tight sugar-phosphate complexes are formed in these conditions.

However, only a consistent increase in the β-anomeric form was observed by adding phosphate. A solution containing a lower glucose concentration (0.01 M) and the same buffer amount (0.5 M) presents higher value of anomers concentration ratio ([β]/[α] = 2.2).

Proton spectra of a set of solutions with glucose 0.5 M and increasing concentrations of bibasic phosphate, covering a range from 0.05 M to 1 M, showed that the [β]/[α] ratio is almost independent of phosphate concentrations (an average value of 1.92 was found in all

experiments); 24 hours later the same solutions gave similar results.

It has been already reported that the β form of glucose exhibits a higher electrochemical reactivity toward electrooxidation at gold electrodes compared to the α form[64]. Nevertheless we want to stress that the increase in [β]/[α] with the phosphate buffer cannot alone take into account the electrochemical results.

Moreover, both NMR and HPLC of solutions after polarization showed the presence of the only gluconate and no other by-products.

4.4.4 Electrochemical Impedance Spectroscopy (EIS)

EIS measurements were used to understand the role of the phosphate buffer on the conductivity of the solution and on the reaction mechanism. The solution conductivity also influences the amount of usable electrode. In fact, higher solution conductivities permit easier current transport inside the electrode and consequently a higher portion of the electrode to be active. The measurement can be used to optimize the thickness of the electrode as a function of the working conditions.

EIS measurements were performed in solutions having different buffer concentrations and constant glucose amounts. For each solution the experimental results (reported in Figure 29 as Nyquist plot) show, at high frequency, an arc whose origin lies on the real axis (uncompensated ohmic resistance) followed by a capacitive distorted semicircle.

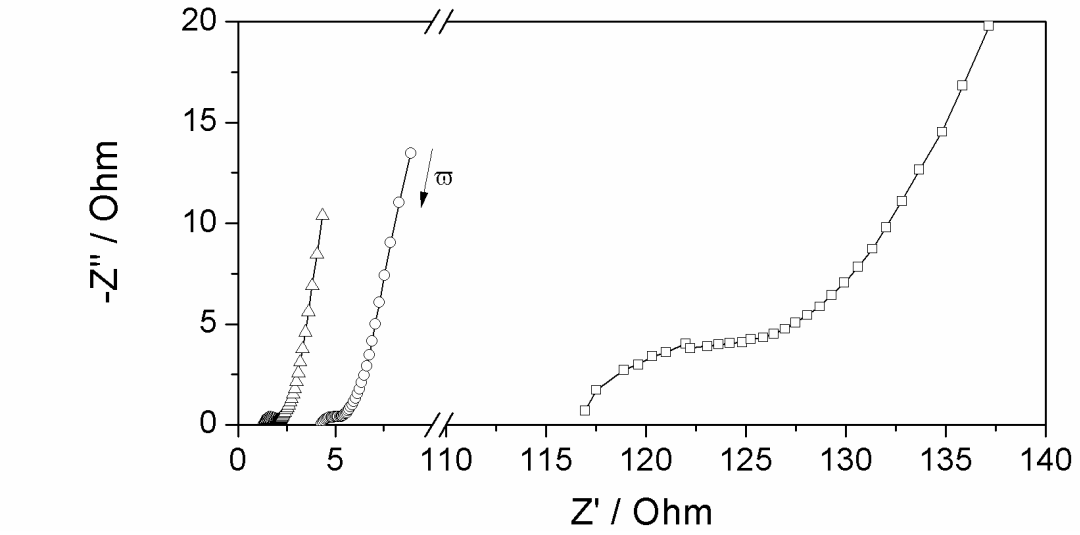

Figure 29. Nyquist plot obtained at pH = 10.5 with constant glucose amount (50 mM) and different buffer concentrations: (□) = 0 mM; (○) = 50 mM; (Δ) = 500 mM. Spectra were collected at OCV using a perturbation potential of 10 mV in the frequency range 20000 - 0.10 Hz.

Fitting of the impedance spectra was performed by using the equivalent circuit reported in the following Figure 30 and the theory of porous electrode [65].

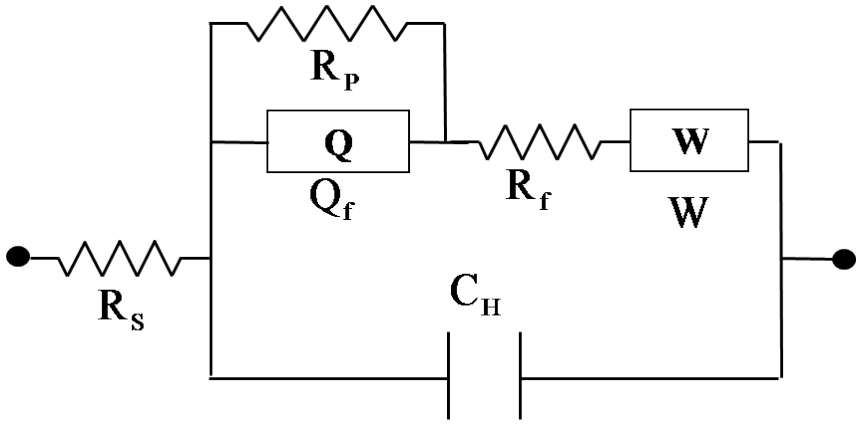

Figure 30. Equivalent circuit of the platinum/electrolyte interface in presence of glucose.

In Table 3 the fitting parameters and the standard deviations are reported.

Table 3. Fitting parameters and standard deviations

$[Na_2HPO_4]$ mM	R_{el} Ω cm^2	R_p Ω cm^2	C_{dl} F cm^{-2}	R_{ad} Ω cm^2	C_{ad} F cm^{-2}	W S s$^{0.5}$ cm^2	R_{ct} Ω cm^2	χ^2
0	115	31.9	0.00325	2.83	0.168	0.0732	16000	0.00010
50	4.17	3.54	0.00398	0.280	0.139	0.313	348	0.00021
500	1.14	3.02	0.00153	0.224	0.177	0.525	300	0.00015

By increasing the buffer concentration, the electrolyte resistance, in the bulk and in the pores, and the adsorption and charge transfer resistances decrease. The double layer capacitance, as expected and the adsorption capacitance remains quite constant. The latter is proportional to the number of active sites in the platinum particles, and therefore it is expected to not be dependent on the concentration of the buffer. The higher conductivity of the buffered electrolytes permits better use of the active material inside the pores of the electrode. The charge transfer resistance is in good agreement with the value of exchange current densities observed from the I-V curves.

4.4.5 Energy Performance

To roughly evaluate the energy performance of the FC01 Mini Fuel Cell, some connection – disconnection cycles were carried out. After reaching the OCV the two electrodes were

connected to an electrical resistance (R) and afterwards disconnected when the electrical potential reached steady-state conditions. Such procedure was repeated consecutively for several times.

In each connection – disconnection step, the voltage (see Figure 31) showed a sudden drop immediately after the connection of the cell to the resistance, followed by a slow fall until it reached a nearly constant value.

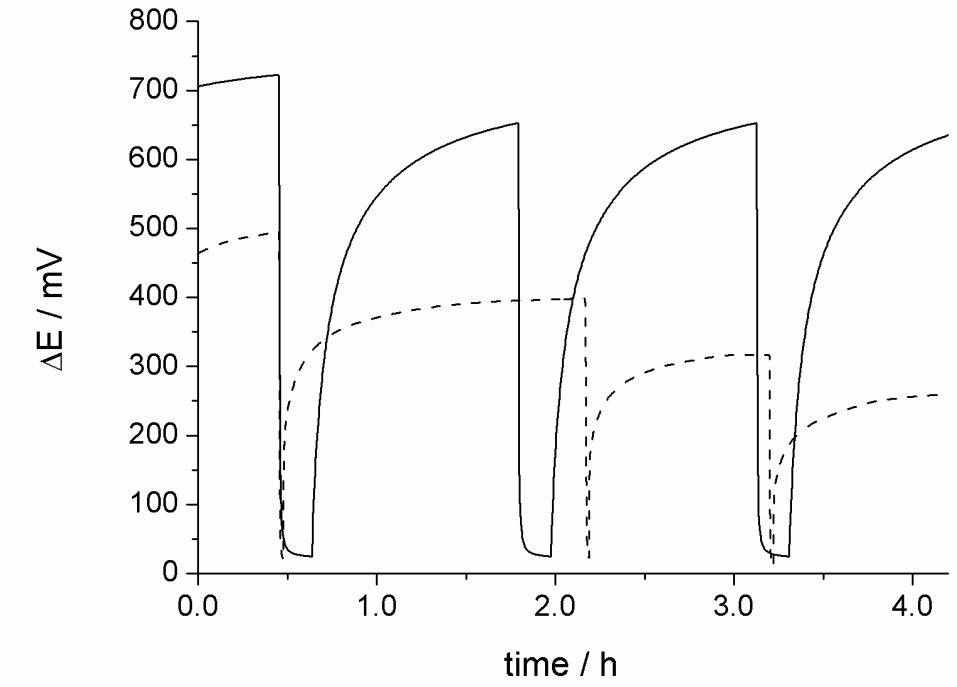

Figure 31. Typical behavior of the fuel cell voltage as a function of time during consecutive connection-disconnection cycles. Glucose solution concentration 500 mM, pH = 10.5, with (—) and without (---) buffer and R = 10 Ω.

Opening the circuit, the potential after a fast increase went slowly back to the initial OCV values which were achieved only in the buffered solutions. The same behavior was observed with different electrical resistance and their values of course influenced the short-circuit potentials. It was also observed that the presence of the buffer not only supports the recovery of the OCV to early values but it increases the potentials in the short-circuit conditions, enhancing the energy performances. The power density was evaluated to be about 50 μW cm^{-2}.

4.4.6 Discussion and Conclusions

In the present study the operating conditions for achieving reproducible and constant OCV values have been found. In particular, the proper pH and the presence of the buffer not only

stabilize the reversible anode potential, but also promote higher cell voltages during the energy supply.

The buffer has multiple roles in the final performances of the anode: it changes the reaction rates and steps; it increases the amount of β form of glucose (see below paragraph 4.4.3); it increases the conductivity of the solution (see below paragraph 4.4.4); it may adsorb at the surface of platinum and subtract active sites for the electrooxidation of glucose as already highlighted at gold electrodes.

NMR measurements highlight relatively larger β-anomeric percentages only at the lowest sugar concentrations as well as the chemical analyses by HPLC of solutions after their electrolysis showed the presence of the only gluconic acid, the decrease of the glucose amount and no other by-products. The anode potential, stabilized by the buffer presence, depends on the glucose chemical potential which has to be fixed either constantly replenishing with fresh reactant (flooded flow cell) the cell or having saturated glucose solutions.

Moreover the presence of the Na_2HPO_4 not only stabilizes the potential, but also improves the electrochemical performances of the anode in term of exchange current density. Such behavior is not ascribable to the chemical interaction with glucose, as shown by NMR measurements, but to the interaction with the anode material as indicated by the decrease of all the resistive components in the EIS measurement.

The results obtained with the tested commercially available anode (50 $\mu W\ cm^{-2}$) are far from satisfactory even by comparison to the literature and represents a benchmark for the evaluation of upcoming electrode materials.

4.5 Nanostructured gold electrodes as anode in glucose-gluconate fuel cells [66]

The electrocatalytic properties of nanostructured gold electrodes towards glucose electrooxidation in KOH were investigated by cyclic voltammetry and compared with commercially available polycrystalline gold electrode. These electrodes were prepared by depositing gold nanoparticles from a sol onto different carbonaceous conductive supports: glassy carbon, carbon cloth and graphite paper. The gold sol was prepared reducing an aqueous solution of tetrachloroauric acid with sodium borohydride. In order to improve the gold nanoparticles adhesion, a surface treatment of the supports with warm concentrated nitric acid was performed. Gold on treated carbon cloth turned out to be a very promising anode for glucose electrooxidation. In order to better understand the glucose oxidation, its pH dependence as well as sorbitol (the glucose reduction product) electrooxidation were investigated.

4.5.1 Introduction

Glucose oxidation on bare gold electrode was investigated in the past by polarization method, cyclic voltammetry [29,31,33,67] and more recently by large amplitude Fourier transformed alternating current voltammetry [68]. It has been demonstrated that, among different materials, it is the most active in alkaline solutions [67]. Moreover, it has been demonstrated that gold electrocatalytic activity is strongly influenced from the pH and composition of the electrolyte. In weak alkaline solution ($7 < pH \leq 10.5$) the capability of gold to oxidize glucose depends mainly on the presence of appropriate buffer solution [33] while no results are reported by using diluted alkali. From the reported studies, it became evident that the role of the buffering compounds (either phosphate or carbonate) is not merely the pH stabilization because their interaction with the sugar unit plays an important role. At higher pH (≥ 11) due to the presence of KOH gold is quite electrocatalytic active and the dependence of the oxidation reaction with the pH has been investigated [67]. The oxidation of glucose in strong alkaline media is particularly interesting in sugar-fed fuel cell [55]. On the other hand the chemical instability of glucose during oxidation at high pH values and its degradation kinetics were widely investigated in the past years [69] showing the formation of complex mixtures of high and low molecular weight carboxylates and aldehydes rather than simple gluconate.

The proposed mechanism of glucose electrooxidation on gold electrode, based on the previous studies of gold redox and electrocatalytic behavior in aqueous media [70,71], embodies a fast chemisorption step followed by dehydrogenation and simultaneous decomposition of the organic molecule [67]. An interesting aspect of glucose voltammograms on gold is the oxidative peak during cathodic scan [29,31,33] which has been explained taking in account the role of oxygen anions desorbed from the metal surface [33].

More recently, several works have been devoted to the optimization of the electrode performance in sensors or fuel cells through chemical and morphological modification of gold electrodes [23,27,37,44,69]. In particular, the highest efficiency of glucose oxidation has been obtained using modified gold nanoparticles at moderate alkaline pH values [27].

The aim of this work is to investigate the electrocatalytic performances of gold nanoparticles towards glucose electrooxidation in alkaline solutions and to compare the results with those of commercial polycrystalline gold, in order to show the nanostructured electrodes potentialities as anodic catalytic material in glucose alkaline fuel cells (AFC). For this purpose, gold nanoparticles have been deposited on glassy carbon (GC) and on high surface area materials such as carbon cloth and graphite paper. For experimental details see Appendix D.

4.5.2 Results and Discussion

Nanoparticle morphology. The deposition of gold nanoparticles from the sol provides low metal loading on glassy carbon support: no difference between loaded and pristine substrate is observed to the naked eye. The determination of such a low gold surface area is very problematic: different electrochemical and physical methods (such as chronoamperometry, BET etc.) were unable to appreciate the small difference between impregnated and pristine surface areas.

Hence, SEM images were employed to evaluate particles distribution (Figure 32a) and size (Figure 32b) to roughly estimate the gold surface area.

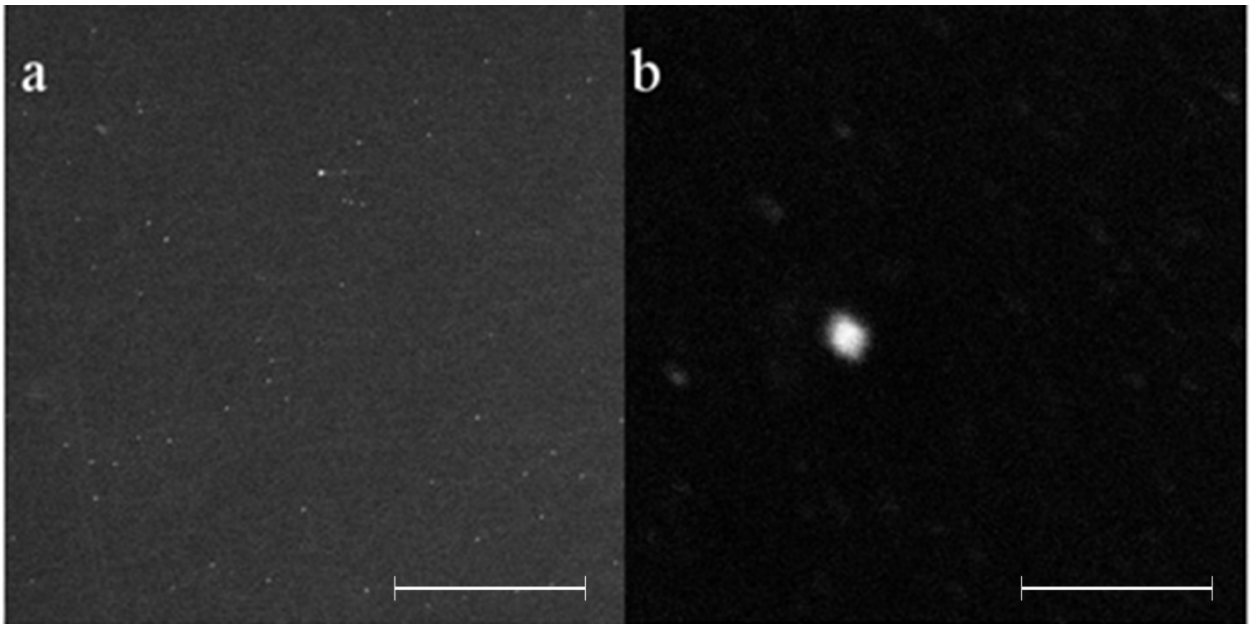

Figure 32. SEM images of gold nanostructured electrode: (a) 13.46 kx, marker 10 µm; (b) 144.59 kx, marker 1 µm.

Assuming pseudo-spherical shape with average diameter of 100 nm (see Figure 32b), and estimating a distribution of $12 \cdot 10^6$ Au particle/cm^2, the gold surface would cover 0.1% of the glassy carbon plate. Thus, the nanosized gold active area is evaluated around $1 \cdot 10^{-4}$ cm^2, that is about 300 times lower than the geometric area of polycrystalline electrode ($3.14 \cdot 10^{-2}$ cm^2).

4.5.3 Electrochemistry of gold nanoparticles on glassy carbon tip

The activation/stabilization CV scans of nanosized electrode on glassy carbon pin show the well known behavior of gold when employed in strong acidic solution [72] (Figure 33 red curve).

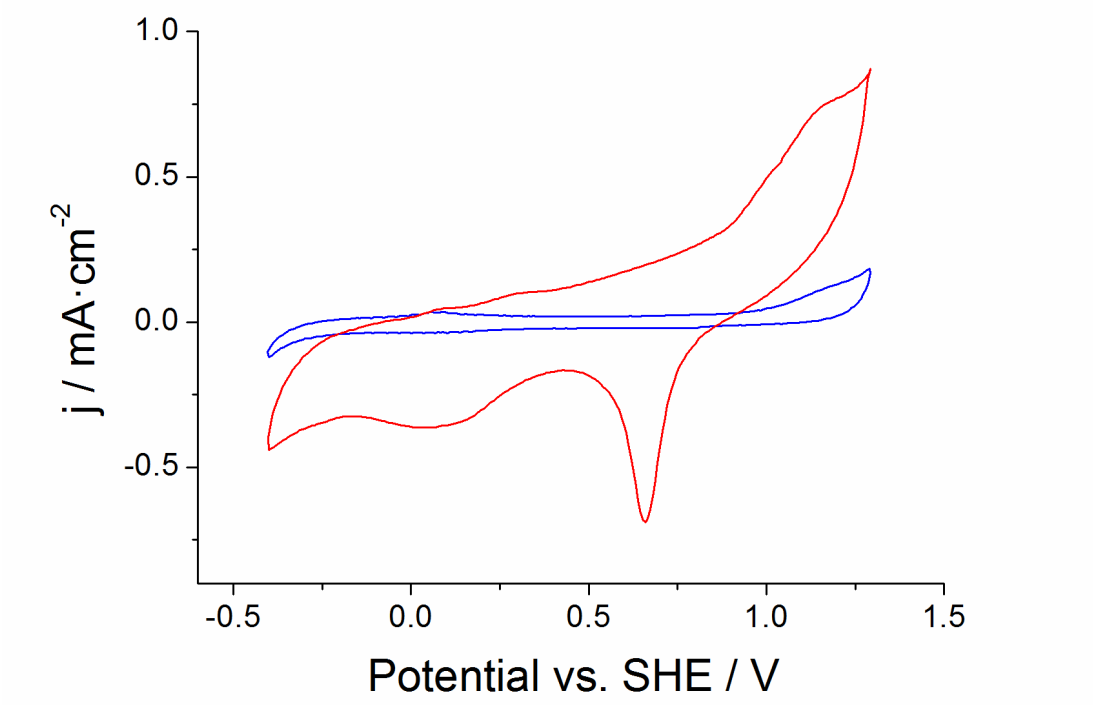

Figure 33. Cyclic voltammograms in H_2SO_4 0.25 M of: (red curve) the gold nanoparticles on glassy carbon and (blue curve) pristine glassy carbon; scan rate 100 mV s^{-1}, 20th cycle.

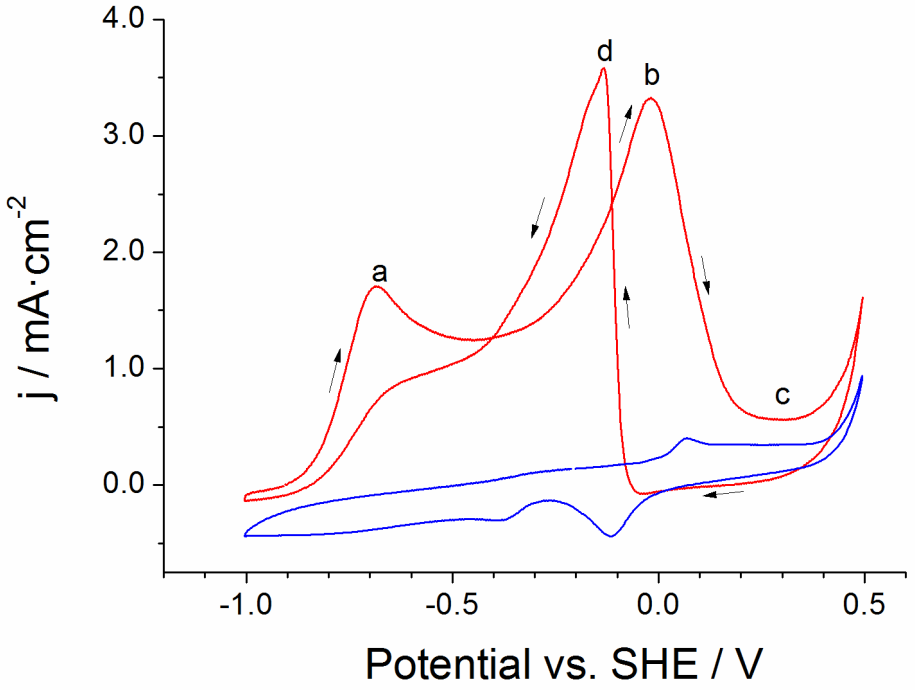

Figure 34. Cyclic voltammograms of the nanostructured gold electrode in: 0.1 M KOH (blue curve) and 0.1 M KOH plus 10 mM glucose (red curve) solutions; scan rate 100 mV s^{-1}, 10th cycle.

The oxidation process at high potential (1.1 V) is due to the formation of superficial oxide layer onto the gold surface; the layer is then reduced during the cathodic sweep at potentials around 0.65 V. No significant differences were detected between two successive scans after 15 cycles. The unloaded glassy carbon electrode does not show electrochemical processes in the potential

range investigated (Figure 33 blue curve).

When cycled in alkaline solution (Figure 34 blue curve), the nanosized gold electrode presents two oxidation and one reduction processes. The anodic peaks at 0.2 and 0.7 V are usually attributed to the OH^- oxidative adsorption [29,37] and the formation of oxide layer Au-O, respectively; Au-O is then reduced at -0.1 V during the chatodic scan [37].

The polycrystalline commercial electrode shows curves qualitatively similar in both acidic and alkaline solutions.

4.5.4 Glucose oxidation by gold nanoparticles on glassy carbon tip

The CV curve of nanosized electrode in glucose alkaline solution shows three clear electrochemical processes during the anodic sweep and one during the cathodic return scan (Figure 34, red curve). The peak a (-0.7 V) was attributed by many authors to dehydrogenation of anomeric carbon under adsorption control [16,73,74]. The dehydrogenation of the anomeric carbon peak was deeply investigated by Beden, *et al.* on Pt electrode [9,64]. In particular, it was outlined that when the solution was prepared and kept at low temperature (2°C) this peak became remarkably high; in fact at low temperature, in alkaline medium (NaOH 0.1M) the β-D-glucose quickly becomes the main species in solution (as determined by GC-MS). Voltammetric investigations proved that β-D-glucose is the most active anomer due to the planar approach of the molecule to the electrode surface. Furthermore it is important to note that this peak shifts of about 600 mV toward lower potential with respect to the polycrystalline platinum. The higher oxidation potential on Pt is probably due to the hydrogen adsorption that hindered that of the glucose; this phenomenon is negligible on the gold surface.

A second electrochemical process can be observed at 0.0 V in Figure 34 red curve, peak b; this peak has a large left shoulder due to several oxidative processes taking place in the potential range -0.3-0.0 V. Beden *et al.* described the processes on Pt electrode at low temperature (2°C) and found out that the oxidation of the previously adsorbed intermediate follows two possible routes: at $E < 0.1$ V, it is oxidized as weakly adsorbed gluconate, either linked by two oxygen or by only one oxygen (at $-0.2 < E < 0.1$ V) whereas the second route is observed at $0.1 < E < 1.1$ V, when glucose is oxidized as weakly adsorbed δ-gluconolactone. At 25°C we observed a convolution of all these peaks in peak b: it is however evident that, in any case, the oxidation product is always gluconate in these conditions.

Around 0.2 V (Figure 34 red curve, zone c) gold surface oxidation occurs as it is possible to argue by comparison between the CV curves in the presence and absence of glucose. Xie *et al.* [37] demonstrated the formation of Au/oxygen specie in the 0.2 V region by quartz crystal

microbalance analysis coupled with electrochemical apparatus. Furthermore they pointed out that glucose can be oxidized at the metal gold surface but not at Au oxide surface, so the current decreases at potential higher than 0.3 V.

The oxidative peak in the CV reductive scan (Figure 34 red curve, peak d), already observed in several reported studies [27,29,37] is obtained as soon as the oxide layer is reduced. The mechanism for the oxidation during the cathodic sweep was firstly proposed by Liu and Makovos: the oxide layer is reduced to generate free O^{2-} anions which react with glucose to give gluconic acid, and then the Au surface undergoes re-oxidation by OH^- in solution [29]. No electrochemical processes were detected in the glucose solution using the unloaded glassy carbon electrode (Figure 34, blue curve).

4.5.5 Comparison between nanoparticles and commercial gold pin electrode

When compared to the commercial polycrystalline electrode, nanostructured gold particles exhibit better performances in terms of current density output and also a shift towards lower potentials of the oxidation processes (Figure 35).

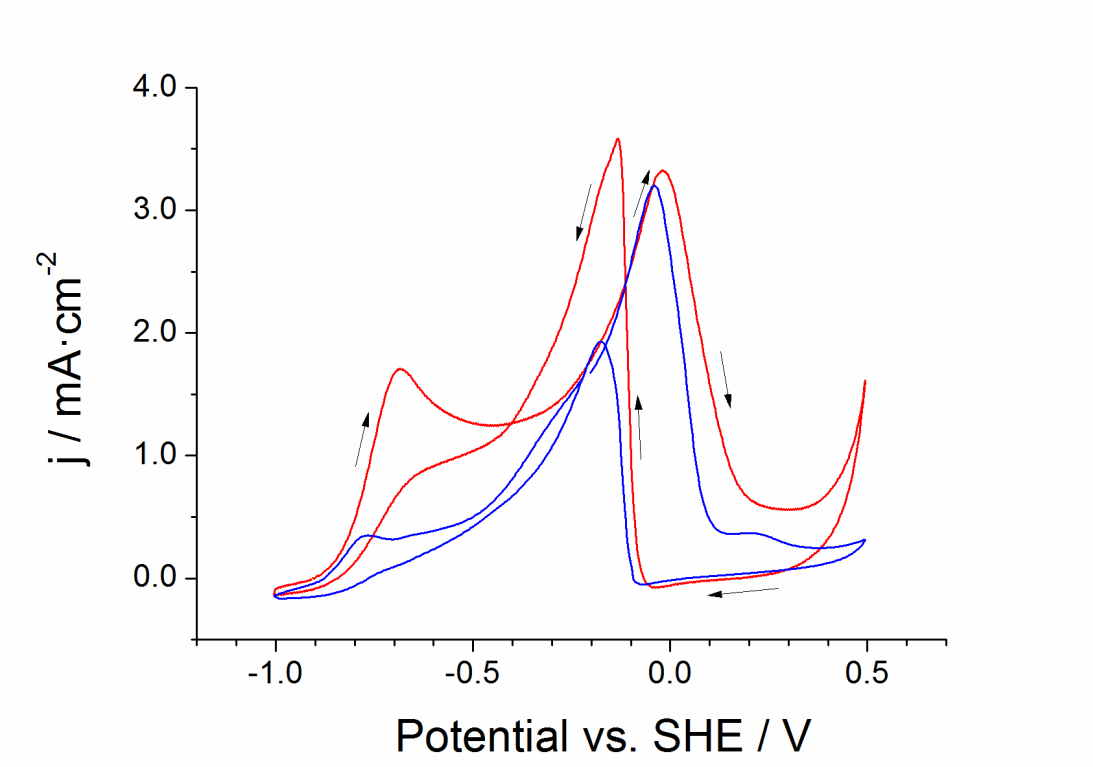

Figure 35. Cyclic voltammograms in 10 mM glucose, 0.1 M KOH solution of: polycrystalline (blue curve) and nanostructured (red curve) gold electrode; scan rate 100 mV s^{-1}, 10th cycle.

It is important to underline that in both cases the current densities were referred to the geometrical surface area. In the case of the polycrystalline gold pin the real surface area was

measured by chronoamperometry [75] using different electroactive species ($Fe(CN)_6^{4-}$, $Fe(CN)_6^{3-}$ and Ag^+): no difference with respect to the geometrical one was pointed out. Since the effective area of the gold nanoparticles is about one hundred times lower, as previously discussed, the actual current density of the nanoparticle electrode should be at least two orders of magnitude higher. Moreover it is interesting to observe the large increment in the peak current density of peak a (see Figure 35) current density attributed to the presence of more defective sites on the surface of gold nanoparticles. It is well known, in fact, that surface reactions usually require lower activation energy in presence of defective sites (*i.e.* kink atom, adatom, edge adatom, etc.); as a consequence, the nanoparticles should have an intrinsic large number of defects which are responsible for glucose oxidative adsorption.

4.5.6 pH effect on glucose oxidation

In order to understand the role of pH on glucose electrooxidation we have firstly investigated the behavior of a commercial gold electrode. CV scans in KOH electrolyte solutions (Figure 36) show that the oxidation of the gold surface slightly depends on the pH as well as its onset and peak position lay around -0.35/0.0 and 0.05/0.10 V, respectively.

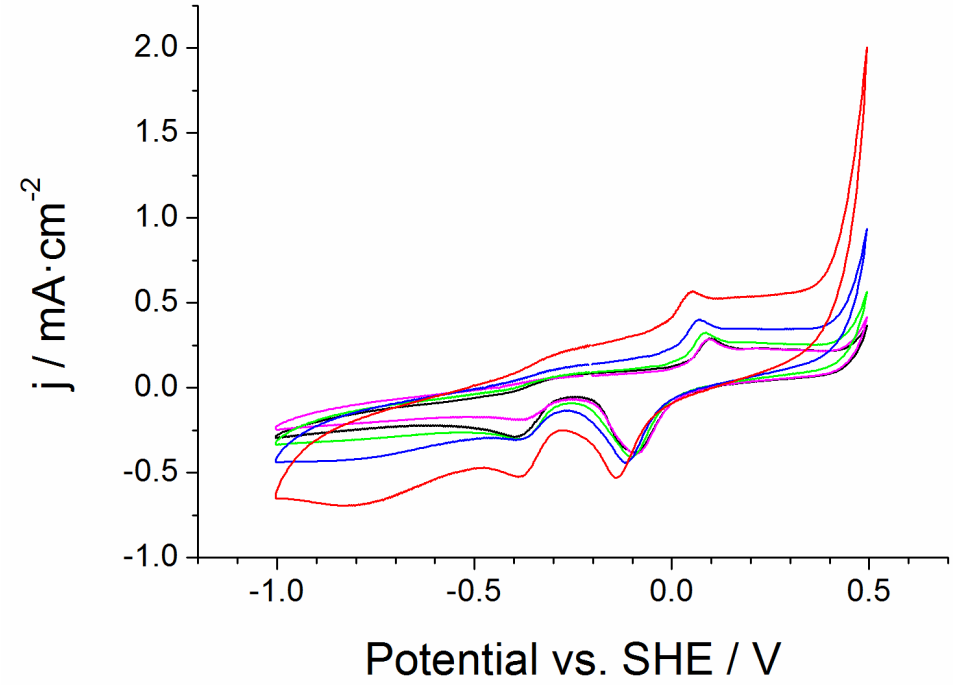

Figure 36. Cyclic voltammograms of the polycrystalline gold electrode at different pHs: (red curve) = 14.0, (blue curve) = 13.5, (green curve) = 13.0, (purple curve) = 12.5, (black curve) = 12.0 scan rate 100 mV s^{-1}, 10th cycle.

As the pH increases, the glucose oxidation peak (b) moves towards lower potential meaning that

the reaction becomes more favorable, while the adsorption peak (a) maintains about the same potential (Figure 37).

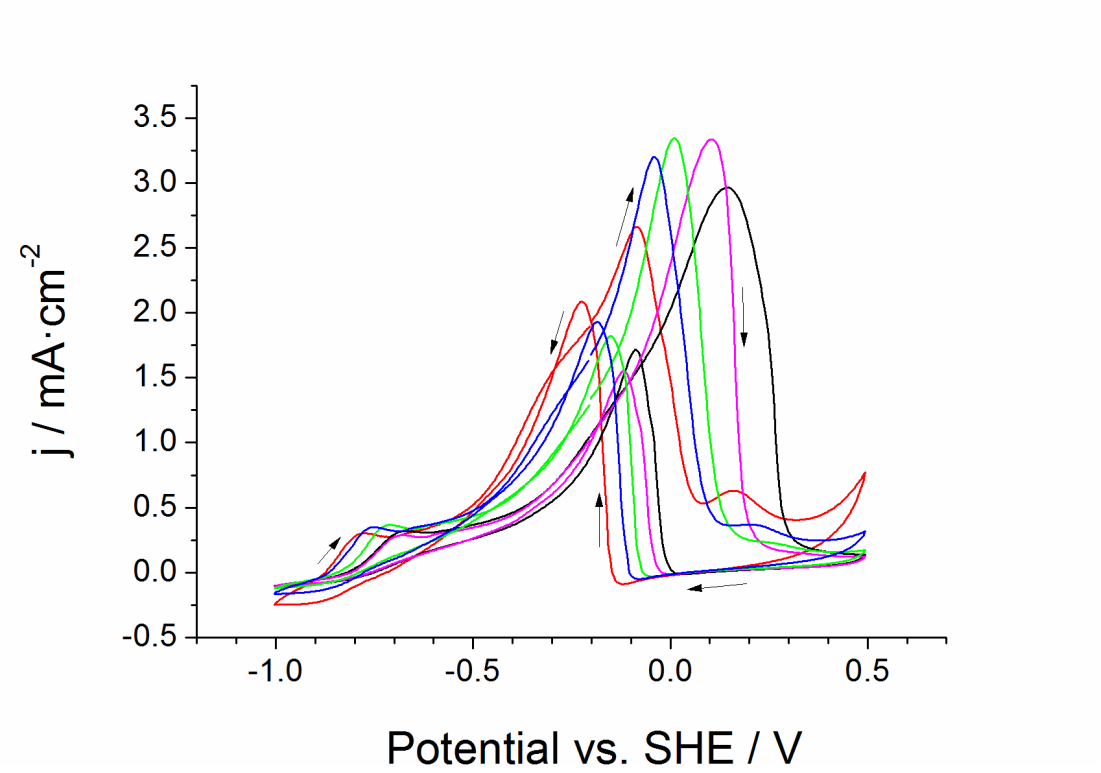

Figure 37. Cyclic voltammograms of the polycrystalline gold electrode in 10 mM glucose at different pHs: (red curve) = 14.0, (blue curve) = 13.5, (green curve) = 13.0, (purple curve) = 12.5, (black curve) = 12.0; scan rate 100 mV s^{-1}, 10th cycle.

The fact that gold surface electrochemical process (peak a) is only slightly influenced by pH suggests that the strong pH dependence of glucose oxidation peak (b) potential is relative to an interaction with OH^- in solution. Such interaction is probably the nucleophilic attack of OH^- to glucose carbonyl group in linear form with the formation of an intermediate strongly interacting with the Au electrode surface. These observations might prefigure an electrooxidation reaction like that proposed by Rossi *et al.* [76] where the chemical oxidation of glucose in presence of molecular oxygen involves a two electrons mechanism with the formation of gluconate and hydrogen peroxide.

4.5.7 Sorbitol electrochemistry

Sorbitol represents the reduction product of glucose in which the aldehydic group is substituted with the alcoholic function. Due to the lack of the carbonilic group, sorbitol cannot give the six ring close configuration and it does not present any anomeric carbon. It seems, therefore, interesting to compare sorbitol and glucose oxidation at the polycrystalline gold electrode. The

comparison between the CV of the two molecules (Figure 38) points out the absence of the low potential process in the case of sorbitol, thus confirming the attribution of the peak a in Figure 34.

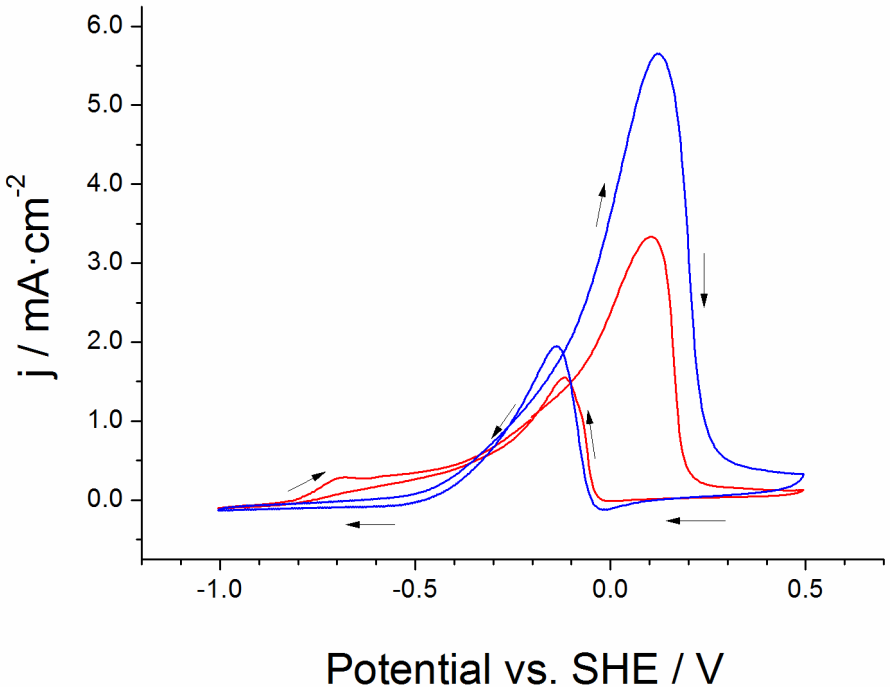

Figure 38. Cyclic voltammograms of polycrystalline gold electrode in 10 mM glucose and 0.1 M KOH solutions of glucose (red curve) and sorbitol (blue curve); scan rate 100 mV s-1, 10th cycle.

Sorbitol shows a large oxidation peak at 0.1 V, the same potential value attributed to the glucose peak b in Figure 34. The peak shape is very similar, the current density of the process is almost twofold; this could be due to the oxidation of the primary $–CH_2OH$ functions, which are two in sorbitol but just one in glucose. The chemical stability of sorbitol in strong alkaline solution allows a better analysis of the uncontaminated oxidation products after the electrolysis at 0.1 V. Preliminary HPLC analysis point out that electrochemical oxidation produces of sorbitol gives not only gluconic acid, the most abundant product, but also other chemical species.

4.5.8 Glucose oxidation on different carbonaceous conductive supports: effect of nitric acid treatment

To test the glucose oxidation on large electrodes for practical applications, we have investigated the behavior of different carbon based substrates impregnated with the gold nanoparticles. The low metal loading obtained with the impregnation method is probably due to the very smooth and hydrophobic surface of the GC support, which reduces the nanoparticles adhesion and meanwhile explains the presence of large particles.

In order to improve the gold surface area three different carbonaceous conductive supports (GC plate, carbon cloth and graphite paper) were studied and compared. All the supporting materials underwent a treatment with warm (70°C) concentrated (65%) nitric acid before the subsequent impregnation of colloidal gold sol.

It is known that oxidation of carbon surfaces can offer not only a more hydrophilic surface structure, but also a larger number of oxygen-containing functional groups as quantitatively measured by Boehm's method [77]. Among different oxidant agents (such as hydrogen peroxide and potassium permanganate), nitric acid is considered the most active reagent for generating a larger number of carboxyl and lactone groups [78].

In Figure 39 is reported the CV of pristine (red curve), treated (blue curve) and treated with gold nanoparticles (green curve) carbon cloth. Remarkable increase (about one order of magnitude) of the flowing current was observed for treated sample, probably due to the improved hydrophilicity of the support that permits a better contact between substrate and electrode surface.

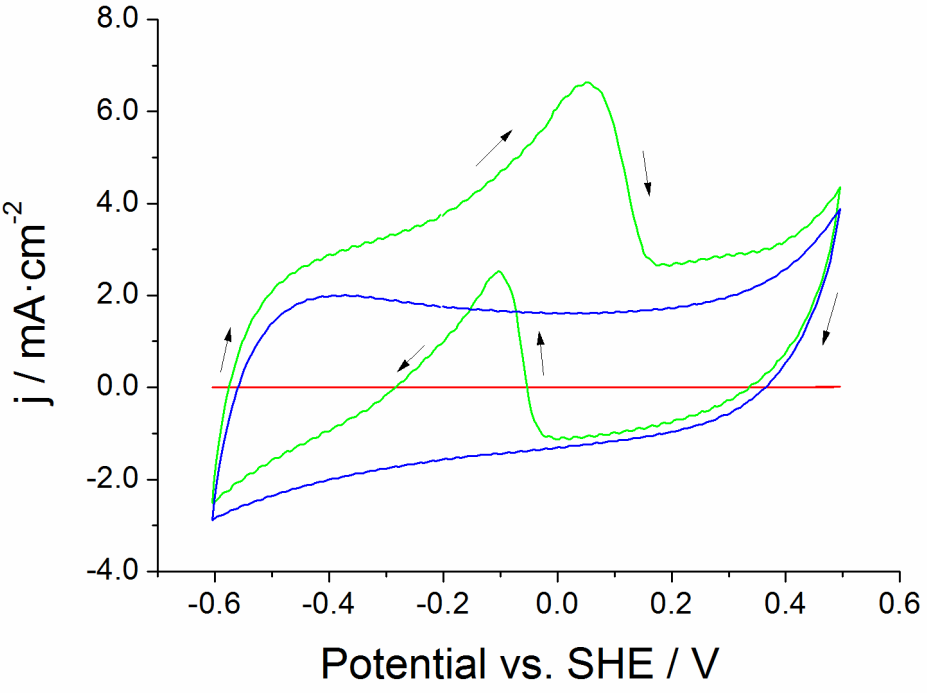

Figure 39. Cyclic voltammograms in 10 mM glucose and 0.1 M KOH solution of: (red curve) pristine, (blue curve) nitric acid treated and (green curve) nitric acid treated with gold nanoparticles carbon cloth electrode, having the same size; scan rate 100 mV s^{-1}, 10th cycle.

The presence of gold particles further increases the current density. Similar behavior was also remarked for both glassy carbon and graphite paper substrates.

In Figure 40 are compared the performances of the three carbonaceous conductive supports after the nitric acid treatment and gold sol impregnation; GC shows certainly the worst performance.

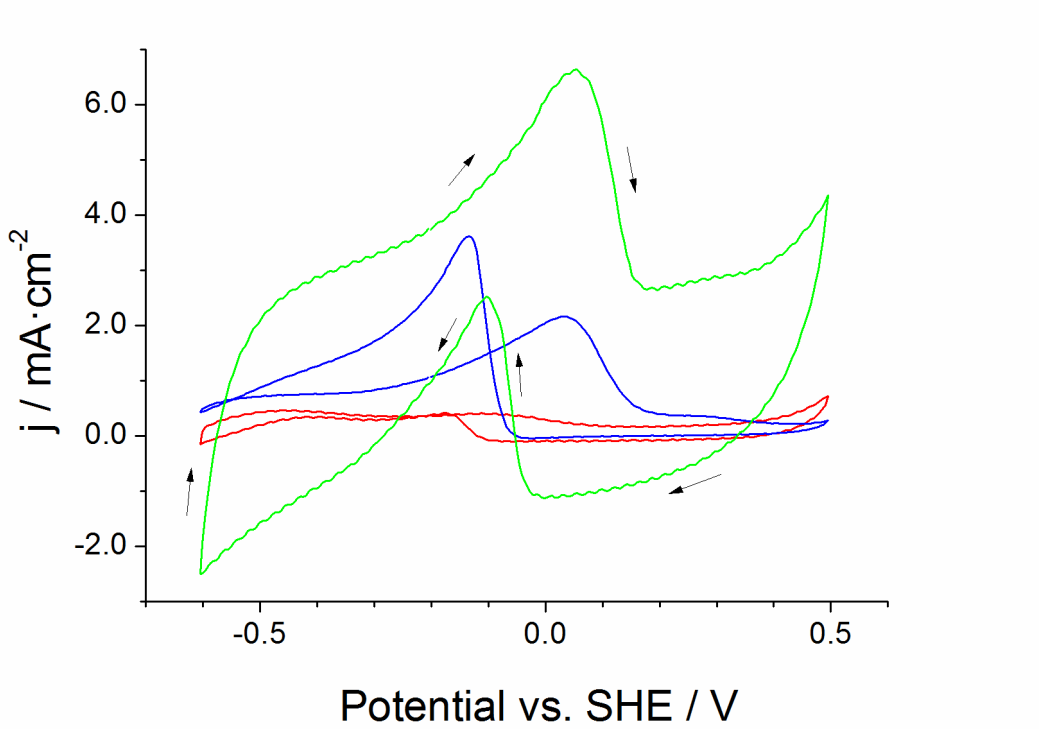

Figure 40. Cyclic voltammograms in 10 mM glucose and 0.1 M KOH solution of: (red curve) glassy carbon, (blue curve) graphite paper, (green curve) carbon cloth electrode; scan rate 100 mV s^{-1}, 10th cycle.

The oxidative peak potential on both graphite paper and carbon cloth lies at around the same value (0.0 V), but the current density of the latter (about 7.0 mA cm^{-2}) is four times higher.
Gold nanoparticles on carbon cloth seems to be a very promising anode material for glucose electrooxidation.

4.5.9 Conclusions

A nanostructured gold electrode was obtained, on the surface of a glassy carbon tip, depositing the noble metal from a colloidal dispersion, prepared by aqueous tetrachloroauric acid reduction. The gold particles (average size 100 nm and electrode surface area about $1 \cdot 10^{-4}$ cm^2) generate better electrocatalytic properties with respect to commercially available polycrystalline electrode for glucose oxidation. The evaluation of the oxidation peak as a function of the pH outlines the strong improvement of substrate reactivity increasing the OH^- concentration. Moreover, the oxidation of sorbitol, the reduced form of glucose, confirmed the attribution of the peak at -0.75 V to the anomeric carbon oxidation.
A very strong increment of the electrode performance in glucose oxidation was obtained by improving the total gold nanoparticles amount which was achieved using carbon cloth-support. With such electrode the current densities raises up to 7 mA cm^{-2}.

4.6 Gold on CNT-cotton anode material for glucose fuel cell

On the basis of the previous studies, we proposed a new anode material for glucose-gluconate direct oxidation fuel cells prepared by electrodepositing gold nanoparticles onto a conductive textile, realized by conformally coating single walled carbon nanotubes (SWNT) on a polyester textile substrate described in detail in chapter VI. The electrodeposition conditions have been developed in order to obtain a uniform distribution of gold nanoparticles in the 3D porous structure of the textile. The reaction conditions (pH, electrolyte composition and glucose concentration) have been optimized in order to obtain the highest oxidation rates. The electrochemical characterization has been carried out by cyclic voltammetry.

4.6.1 Conductive textile fabrication

For all the information regarding the conductive textile preparation and characterization, please refer to chapter VI.

4.6.2 Surface modification

- *Surfactant removal*

The material as prepared is highly hydrophilic due to the surfactant (sodium dodecylbenzenesulfonate, SDBS) sill present on the surface. However it needs to be removed in order to avoid side reactions. Washing with abundant deionized (DI) water and pressing with a grid is sufficient to remove the surfactant. We deeply described the procedure in Chapter VI.

- *SWNT-textile pretreatment*

After the SDBS removal the textile exhibits hydrophobic behavior which would be incompatible with its application in a water based electrolyte. To improve the surface hydrophilicity and remove the last traces of surfactant the textile is dipped into 4 M HNO_3 solution for about 2 h, washed with DI water, treated with glacial acetic acid for 2 more hours and washed again with DI in order to completely remove the acid. Treating the nanotubes with nitric acid and glacial acetic acid introduces a larger number of oxygen-containing functional groups such as carboxyl, lactones and phenols and creates more hydrophilic surface structure [79]. The treatment has two other advantages: it helps to remove impurities, such as catalytic metal particles responsible for self discharge problems [80] and induces hole doping, which decreases the resistivity of the nanotubes [81-83].

4.6.3 Results and discussion

A treated textile sizing 1x1 cm was used as working electrode (WE) while a platinum gauze was used as counter electrode in the presence of a Ag/AgCl/Cl^- 3.5M reference electrode (RE). A 20 mM solution of $AuCl_3$ was employed as gold precursor in the presence of 0.6 M HCl as supporting electrolyte.

The electrodeposition was carried out with a cronoamperometry technique, fixing the potential at -0.6 V vs. RE, limiting the charge at 2C. At this potential both gold deposition and hydrogen evolution can take place, the coulombic efficiency being around 15%. It is probably the formation of hydrogen bubbles at the conductive textile substrate that accounts for the small nanoparticles formation.

When dipped in the aqueous solution the conductive cotton tends to expand (thickness of around 1 mm); in order to obtain a uniform deposition of gold nanoparticles along the entire cross section of the electrode a cell geometry with two counter electrodes was employed (schematized in Figure 41, insert).

Figure 41a shows SEM images of the as prepared substrate. The gold particles have a mean diameter of about 100 nm; smaller particles can be obtained decreasing the deposition potential, nevertheless their performances in terms of current output tend to decrease each cycle, probably due to particle aggregation. Figure 41a and Figure 41b shows the exterior and interior part of the textile demonstrating a uniform particle distribution in the whole cross section.

The performances of the as prepared SWNT/textile electrodes were tested in a 100 mM NaF solution with 100 mM buffer (Na_2HPO_4/Na_3PO_4, pH 11.5) as electrolyte and in the presence of 10 mM glucose as the substrate. Each component of the electrolyte was especially designed on the basis of the mechanism of glucose electrooxidation at gold electrodes previously reported (see chapter 2).

The role of each component of the solution is here discussed.

- pH 11.5. It is well known that glucose is unstable in aqueous alkaline solution and degrades into complex mixtures [49]. Nevertheless glucose electrooxidation is favored at high pH values [55]. 11.5 is the threshold pH value above which glucose is unstable in the operating conditions adopted.
- Buffer (NaH_2PO_4/NaH_2PO_4). The buffer has multiple effects on the reaction. The main function is to keep a constant pH value near the gold surface; in fact during the oxidation OH^- ions are consumed, decreasing the pH near the electrode and therefore diminishing the current output. It also adsorbes at gold surface, decreasing the active sites for glucose oxidation, and improves the conductivity of the solution. At 100 mM the buffering effect is predominant.

- NaF. It has the great advantage of not adsorbing at gold electrodes, thus not interfering with the first step of glucose electrooxidation, glucose oxidative adsorption as demonstrated by EIS in paragraph 2.2.2. A simple explanation can be identified in the hard-soft acid and base theory; in fact, being gold a soft acid and fluoride a strong base their interaction is very weak.

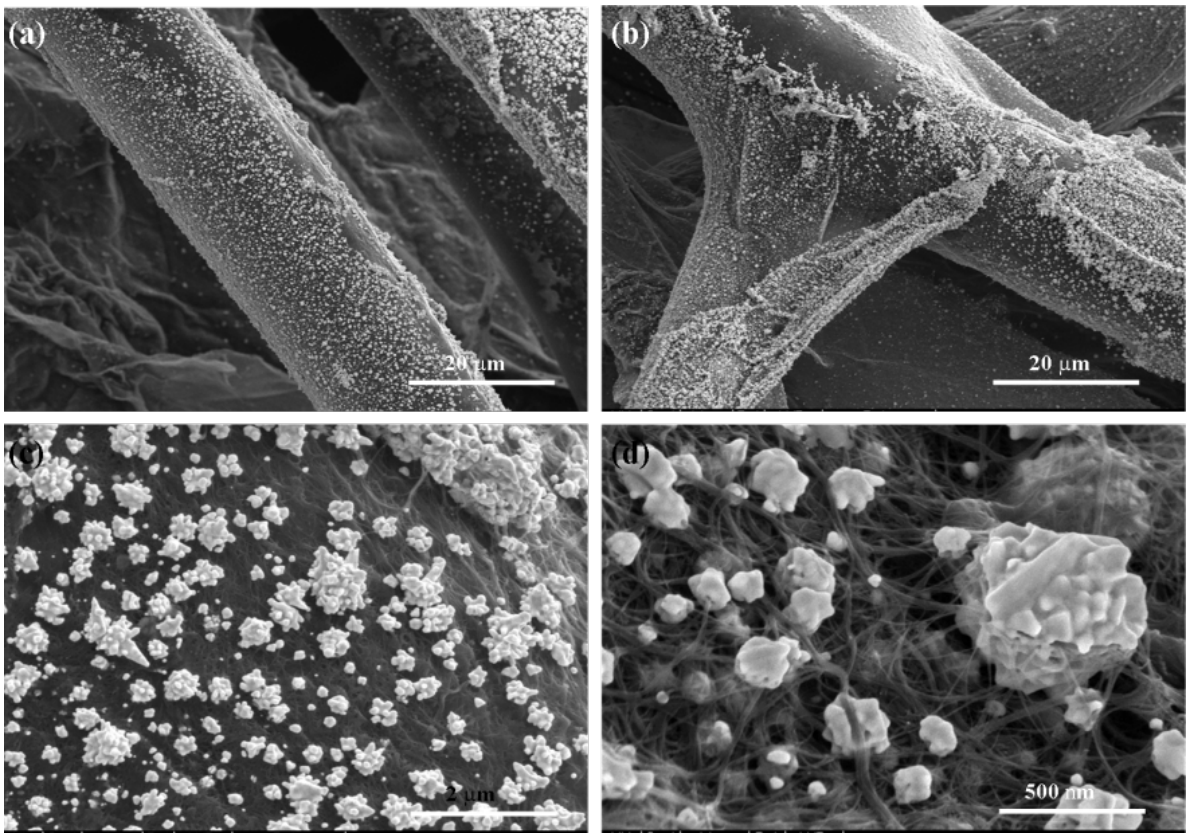

Figure 41. SEM images of the WNT textile after gold electrodeposition. (a) outside of the material, (b) inside, (c) gold nanoparticles uniform distribution and (d) intimate electrical contact between nanotubes and gold nanoparticles.

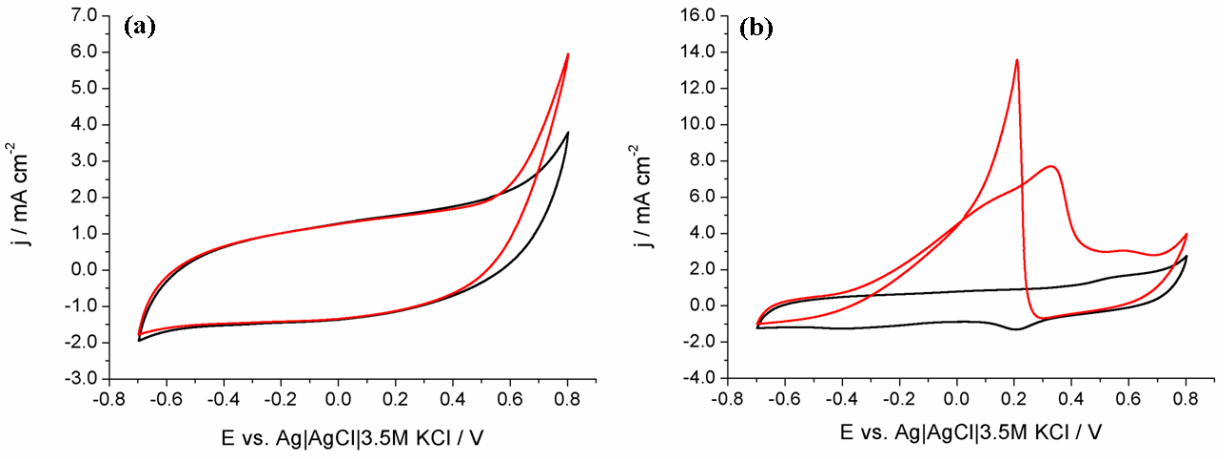

Figure 42. Cyclic voltammetries in 100 mM NaF, 100 mM buffer (Na_2HPO_4/Na_3PO_4), pH 11.5 solution of (a) SWNT/textile in the absence (black curve) and the presence (red curve) of 10 mM glucose (b) Au-SWNT/textile in the absence (black curve) and the presence (red curve) of 10 mM glucose.

Figure 42a shows the cyclic voltammetry of the conductive textile before gold electrodeposition in presence and absence of glucose; as one can observe the SWNT are not active for glucose electrooxidation in the potential range investigated. In Figure 42b in the absence of glucose (black curve) we can see two electrochemical processes relative to gold hydroxide formation and reduction. The broad shape of the peak as well as the sharp and intense oxidative peak in the cathodic scan (red curve) are proofs of the uniform distribution of nanoparticles along the entire cross section of the material. The current density output of this material (Figure 42b, red curve) is much higher than the previously reported anodes.

4.6.4 Conclusions

In the present study we proposed a new anode material for glucose-gluconate fuel cells prepared by electrodepositing gold nanoparticles on a conformally SWNT coated polyester textile. The deposition conditions have been optimized in order to obtain a uniform distribution of nanoparticles. The 3D porous structure of the textile matrix allows a better diffusion of the reactants while the microscale porous structure of the nanotubes coating improve nanoparticle adhesion. The current output per geometrical surface area is much higher than the previously proposed materials, prefiguring a potential application as anode in glucose gluconate fuel cell.

CHAPTER V: MICROBIAL FUEL CELLS

Chapter V: Microbial fuel cells

Microbial fuel cells (MFCs) harness the metabolism of microorganisms, converting chemical potential energy into electrical energy[84,85,86,87,88]. Applications include energy recovery not only from carbohydrates but also from waste, such as organic matter in wastewater[89,90,91], marine sediment[92,93], or human excrement in space[94].

After a brief introduction concerning such devices, the preparation and characterization of highly conductive and macroporous electrodes, fabricated from a carbon nanotube (CNT)-cotton composite for high-performance MFCs, will be described. The conductance of the CNT-cotton fiber is about 2000 S cm^{-1}, double that of a commercial carbon fiber. The macroporous structure of the intertwined CNT-cotton fibers creates an open 3-dimensional space for growth, enabling efficient mass transfer and internal colonization by a diverse microflora. The rough surface of CNT-cotton fibers and the secondary 3-dimenisional structure of CNT layers, with connections between CNTs and microbial nanowires, facilitate electron transfer from exoelectrogens to the CNT-cotton anode. A MFC equipped with a CNT-cotton anode has major performance advantages over one equipped with a commercial carbon cloth one: the conductivity between the CNT-cotton anode and the electrolyte is 10 times greater, power density is 64% higher, and energy recovery efficiency is 75% greater.

5.1 Microbial fuel cells [95]

Microbial fuel cells (MFCs) are devices that use bacteria as the catalysts to oxidize organic and inorganic matter to generate electrical energy (Figure 43). The device must be capable of having the substrate oxidized at the anode replenished, either continuously or intermittently; otherwise, the system is considered to be a biobattery. Electrons can be transferred to the anode by electron mediators or shuttles, by direct membrane associated electron transfer, or by so-called nanowires produced by the bacteria, or perhaps by other as yet undiscovered means. Chemical mediators, such as neutral red or anthraquinone-2,6-disulfonate (AQDS), can be added to the system to allow electricity production by bacteria unable to otherwise use the electrode. If no-exogenous mediators are added to the system, the MFC is classified as a "mediator-less" MFC even though the mechanism of electron transfer may not be known.

In most MFCs the electrons that reach the cathode combine with protons that diffuse from the anode through a separator and oxygen provided from air; the resulting product is water. Chemical oxidizers, such as ferricyanide or Mn (IV), can also be used although these must be replaced or regenerated. In the case of metal ions, such as Mn that are reduced from Mn (IV) to

Mn (II), bacteria can help to catalyze the reoxidation of the metal using dissolved oxygen.

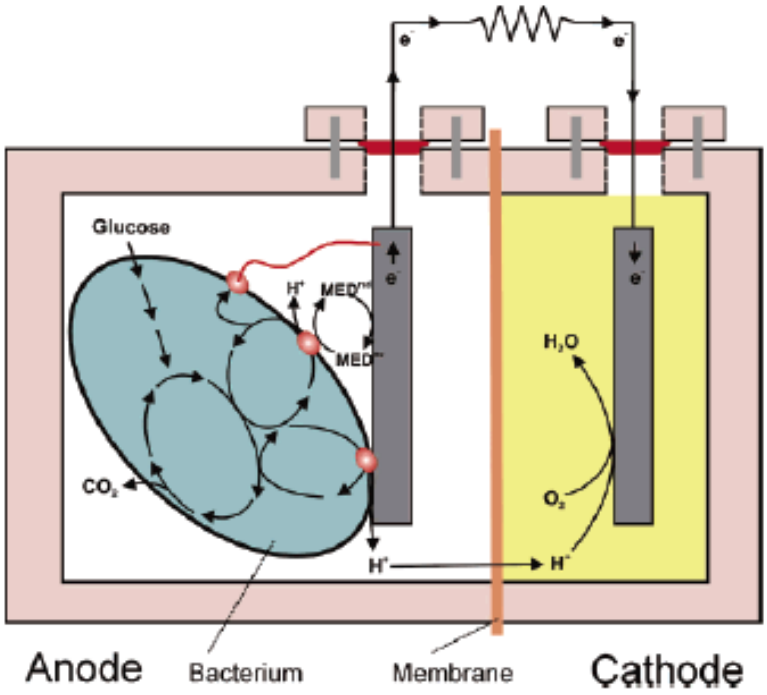

Figure 43. Operating principles of a MFC (not to scale). A bacterium in the anode compartment transfers electrons obtained from an electron donor (glucose) to the anode electrode. This occurs either through direct contact, nanowires, or mobile electron shuttles (small spheres represent the final membrane associated shuttle). During electron production, protons are also produced in excess. These protons migrate through the cation exchange membrane (CEM) into the cathode chamber. The electrons flow from the anode through an external resistance (or load) to the cathode where they react with the final electron acceptor (oxygen) and protons.

Microbially catalyzed electron liberation at the anode and subsequent electron consumption at the cathode, when both processes are sustainable, are the defining characteristics of an MFC. Using a sacrificial anode consisting of a slab of Mg alloy does not, for example, qualify the system as an MFC as no bacteria are needed for catalyzing the oxidation of the fuel. Systems that use enzymes or catalysts not directly produced in situ by the bacteria in a sustainable manner are considered here as enzymatic biofuel cells and are well reviewed elsewhere.

MFCs operated using mixed cultures currently achieve substantially greater power densities than those with pure cultures. In one recent test, however, an MFC showed high power generation using a pure culture, but the same device was not tested using acclimated mixed cultures and the cells were grown externally to the device. Community analysis of the microorganisms that exist in MFCs has so far revealed a great diversity in composition. We believe, based on existing data, and new data from our individual laboratories, that many new types of bacteria will be

discovered that are capable of anodophilic electron transfer (electron transfer to an anode) or even interspecies electron transfer (electrons transferred between bacteria in any form).
MFCs are being constructed using a variety of materials, and in an ever increasing diversity of configurations. These systems are operated under a range of conditions that include differences in temperature, pH, electron acceptor, electrode surface areas, reactor size, and operation time. Potentials are reported with different reference states, and sometimes only under a single load (resistor).

5.1.1 MFC Designs

Many different configurations are possible for MFCs (Figure 44 and Figure 45).

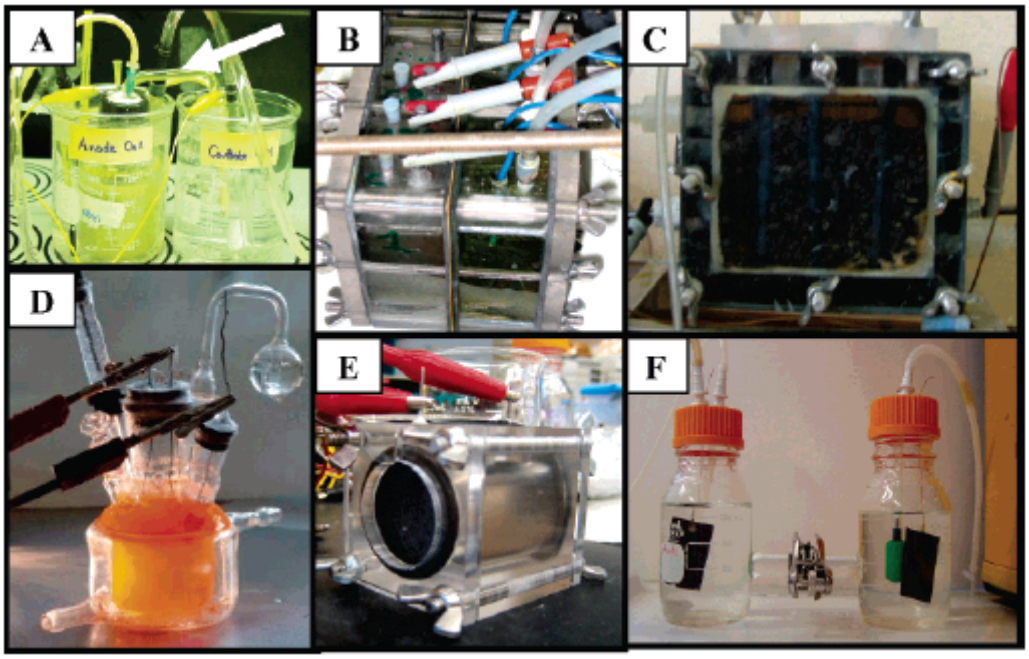

Figure 44. Types of MFCs used in studies: (A) easily constructed system containing a salt bridge (shown by arrow); (B) four batch-type MFCs where the chambers are separated by the membrane (without a tube) and held together by bolts (7); (C) same as B but with a continuous flow-through anode (granular graphite matrix) and close anode-cathode placement; (D) photoheterotrophic type MFC; (E) single-chamber, air-cathode system in a simple "tube" arrangement; (F) two-chamber H-type system showing anode and cathode chambers equipped for gas sparging.

A widely used and inexpensive design is a two chamber MFC, built in a traditional "H" shape, consisting usually of two bottles connected by a tube containing a separator which is usually a cation exchange membrane (CEM) such as Nafion or Ultrex, or a plain salt bridge (Figure 44a, f). The key to this design is the membrane, that must allow protons to pass between the

chambers (the CEM is also called proton exchange membrane, PEM), but optimally not the substrate or electron acceptor in the cathode chamber (typically oxygen).

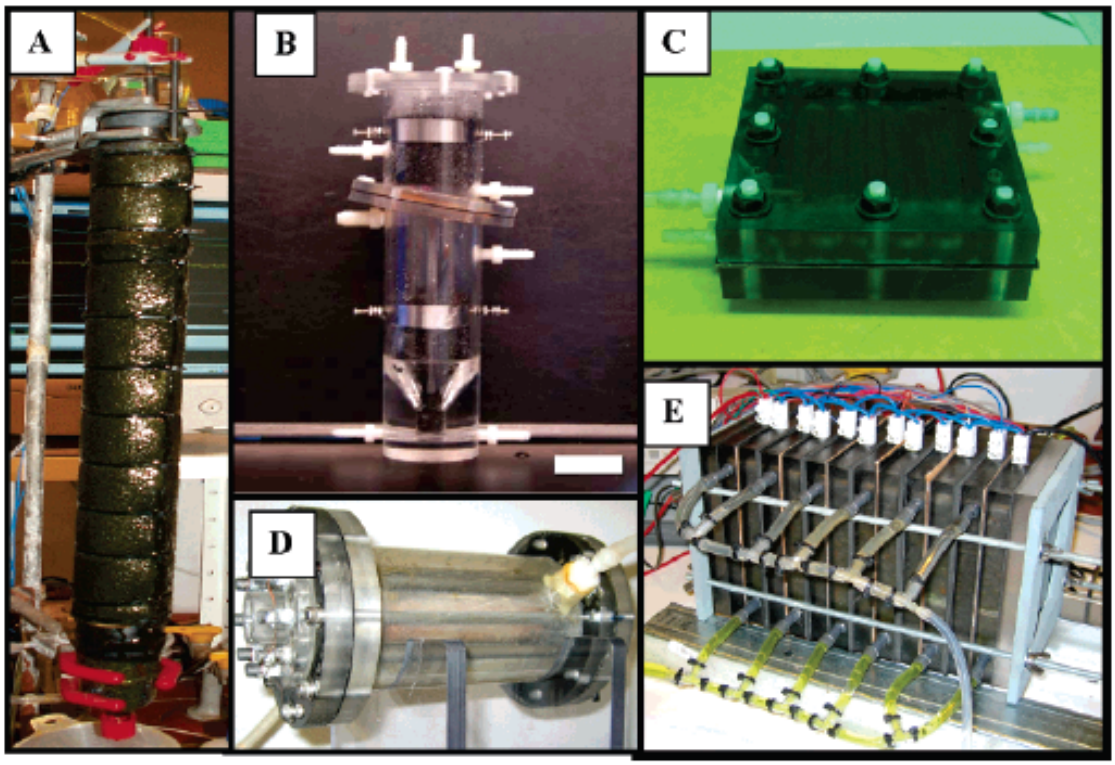

Figure 45. MFCs used for continuous operation: (A) upflow, tubular type MFC with inner graphite bed anode and outer cathode; (B) upflow, tubular type MFC with anode below and cathode above, the membrane is inclinated; (C) flat plate design where a channel is cut in the blocks so that liquid can flow in a serpentine pattern across the electrode; (D) single-chamber system with an inner concentric air cathode surrounded by a chamber containing graphite rods as anode; (E) stacked MFC, in which 6 separate MFCs are joined in one reactor block.

In the H-configuration, the membrane is clamped in the middle of the tubes connecting the bottle (Figure 44f). As long as the two chambers are kept separated, they can be pressed up onto either side of the membrane and clamped together to form a large surface (Figure 44b). An inexpensive way to join the bottles is to use a glass tube that is heated and bent into a U-shape, filled with agar and salt (to serve the same function as cation exchange membrane), and inserted through the lid of each bottle (Figure 44a). The salt bridge MFC, however, produces little power due the high internal resistance observed.

H-shape systems are acceptable for basic parameter research, such as examining power production using new materials, or types of microbial communities that arise during the degradation of specific compounds, but they typically produce low power densities. The amount of power that is generated in these systems is affected by the surface area of the cathode relative

to that of the anode and the surface of the membrane. The power density (*P*) produced by these systems is typically limited by high internal resistance and electrode-based losses (see below). When comparing power produced by these systems, it makes the most sense to compare them on the basis of equally sized anodes, cathodes, and membranes.

Using ferricyanide as the electron acceptor in the cathode chamber, the power density increases due to the availability of a good electron acceptor in high concentrations. Furthermore the ferricyanide dissolves oxygen (H-design reactor with the Nafion CEM) and increases the power by 1.5 to 1.8 times compared to a Pt-catalyst cathode. The highest power densities so far reported for MFCs have been obtained with ferricyanide at the cathode. While ferricyanide is an excellent catholyte in terms of system performance, unfortunately it must be chemically regenerated and its use is not sustainable in practice. Thus, the use of ferricyanide is restricted to fundamental laboratory studies. It is not essential to place the cathode in water or in a separate chamber when using oxygen at the cathode. The cathode can be placed in direct contact with air (Figure 44e, Figure 45c,d), either in the presence or absence of the membrane. In one system a kaolin clay-based separator and graphite cathode were joined to form a combined separator-cathode structure. Much larger power densities have been achieved using oxygen as the electron acceptor when aqueous-cathodes are replaced with air-cathodes. In the simplest configuration, the anode and cathode are placed on either side of a tube, with the anode sealed against a flat plate and the cathode exposed to air on one side, and water on the other (Figure 44e). When a membrane is used in this air-cathode system, it serves primarily to keep water from leaking through the cathode, although it also reduces oxygen diffusion into the anode chamber. The utilization of oxygen by bacteria in the anode chamber can result in a lower Coulombic efficiency (see below). Hydrostatic pressure on the cathode will make it leak water, but that can be minimized by applying coatings, such as polytetrafloroethylene (PTFE), to the outside of the cathode that permit oxygen diffusion but limit bulk water loss.

Several variations on these basic designs have emerged in the effort to increase power density or provide for continuous flow through the anode chamber (in contrast to the above systems which were all operated in batch mode).

Systems have been designed with an outer cylindrical reactor with a concentric inner tube that is the cathode (Figure 45d), and with an inner cylindrical reactor (anode consisting of granular media) with the cathode on the outside (Figure 45a). Another variation is to design the system like an upflow fixed-bed biofilm reactor, with the fluid flowing continuously through porous anodes toward a membrane separating the anode from the cathode chamber (Figure 45b). Systems have been designed to resemble hydrogen fuel cells, where the CEM is sandwiched

between the anode and cathode (Figure 45c). To increase the overall system voltage, MFCs can be stacked with the systems shaped as a series of flat plates or linked together in series (Figure 45e).

5.1.2 Sediment MFCs

By placing one electrode into marine sediments rich in organic matter and sulfides, and the other in the overlying oxic water, electrical energy can be generated at sufficient levels (up to 28 mW m^{-2}) to power some marine devices.

Graphite disks can be used for the electrodes, although platinum mesh electrodes have also been exploited. "Bottle brush" cathodes used for seawater batteries may hold the most promise for long-term operations of unattended systems as these electrodes provide a high surface area and are made of noncorrosive materials. Sediments have also been placed into H-tube configured two-chamber systems to allow investigation of the bacterial community.

5.1.3 Modifications for Hydrogen Production

By "assisting" the potential generated by the bacteria at the anode with a small potential by an external power source (>0.25 V), it is possible to produce hydrogen at the cathode. These reactors, called bioelectrochemically assisted microbial reactors (BEAMRs) or biocatalyzed electrolysis systems, are not true fuel cells, however, as they are operated to produce hydrogen, not electricity. Through modifications of the MFC designs described above (to contain a second chamber for capturing the hydrogen gas), it should be possible to develop many new systems for hydrogen production.

5.1.4 Materials of Construction

<u>Anode</u>

Anodic materials must be conductive, biocompatible, and chemically stable in the reactor solution. Metal anodes consisting of noncorrosive stainless steel mesh can be utilized, but copper is not useful due to the toxicity of even trace copper ions to bacteria. The most versatile electrode material is carbon, available as compact graphite plates, rods, or granules, as fibrous material (felt, cloth, paper, fibers, foam), and as glassy carbon.

The simplest anode materials are graphite plates or rods as they are relatively inexpensive, easy to handle, and have a defined surface area; much larger surface areas are achieved with graphite felt electrodes (0.47 m^2g^{-1}, GF series, GEE Graphite limited, Dewsbury, UK). However, not all

the indicated surface area will necessarily be available to bacteria.

Carbon fiber, paper, foam, and cloth (Toray) have been extensively used as electrodes. It has been shown that current increases with overall internal surface area in the order carbon felt > carbon foam > graphite. Substantially higher surface areas are achieved either by using compact materials like reticulated vitreous carbon (RVC; ERG Materials and Aerospace Corp., Oakland, CA) which is available with different pore sizes, or by using layers of packed carbon granules (Le Carbone, Grimbergen, Belgium) or beads. In both cases maintaining high porosity is important to prevent clogging. The long term effect of biofilm growth or particles in the flow on any of the above surfaces has not been adequately examined.

To increase the anode performance, different chemical and physical strategies have been followed. Park *et al.* incorporated Mn(IV) and Fe(III) and used covalently linked neutral red to mediate the electron transfer to the anode.

Electrocatalytic materials such as polyanilins/Pt composites have also been shown to improve the current generation through assisting the direct oxidation of microbial metabolites.

Directing the water flow through the anode material can be used to increase power. Cheng *et al.* found that flow directed through carbon cloth toward the anode, and decreasing electrode spacing from 2 to 1 cm, increased power densities (normalized to the cathode projected surface area) from 811 to 1540 mW m^{-2} in an air-cathode MFC. The increase was thought to be due to restricted oxygen diffusion into the anode chamber, although the advective flow could have helped with proton transport toward the cathode as well.

Increased power densities have been achieved using RVC in an upflow anaerobic sludge blanket (UASB) type MFC or in granular anode reactors with ferricyanide cathodes. Flow through the anode has also been used in reactors using exogenous mediators.

Cathode

Due to its good performance, ferricyanide ($K_3[Fe(CN)_6]$) is very popular as experimental electron acceptor in microbial fuel cells. The greatest advantage of ferricyanide is the low overpotential using a plain carbon cathode, resulting in a cathode working potential close to its open circuit potential. The greatest disadvantage, however, is the insufficient reoxidation by oxygen, which requires the catholyte to be regularly replaced. In addition, the long term performance of the system can be affected by diffusion of ferricyanide across the CEM and into the anode chamber.

Oxygen is the most suitable electron acceptor for MFCs due to its high oxidation potential, availability, low cost (it is free), sustainability, and the lack of a chemical waste product (water

is formed as the only by-product). The choice of the cathode material greatly affects performance, and is varied based on application. For sediment fuel cells, plain graphite disk electrodes immersed in the seawater above the sediment have been used. Due to the very slow kinetics of the oxygen reduction at plain carbon, and the resulting large overpotential, the use of such cathodes restricts the use of this noncatalyzed material to systems that can tolerate low performance. In seawater, oxygen reduction on carbon cathodes has been shown to be microbially supported. Such microbially assisted reduction has also been observed for stainless steel cathodes which rapidly reduces oxygen when aided by the bacterial biofilm.

To increase the rate of oxygen reduction, Pt catalysts are usually used for dissolved oxygen or open-air (gas diffusion) cathodes. To decrease the costs for the MFC the Pt load can be kept as low as 0.1 mg cm^{-2}. The long term stability of Pt needs to be more fully investigated, and there remains a need for new types of inexpensive catalysts. Recently, noble-metal free catalysts that use pyrolyzed iron(II) phthalocyanine or CoTMPP have been proposed as MFC cathodes.

Membrane

The majority of MFC designs require the separation of the anode and the cathode compartments by CEMs. Exceptions are naturally separated systems such as sediment MFCs or specially designed single-compartment MFCs. The most commonly used CEM is Nafion (Dupont Co., USA), which is available from numerous suppliers (e.g., Aldrich and Ion Power, Inc.). Alternatives to Nafion, such as Ultrex CMI-7000 (Membranes International Incorp., Glen Rock, NJ) also are well suited for MFC applications and are considerably more cost-effective than Nafion. When CEMs are used in MFCs, it is important to recognize that it may be permeable to chemicals such as oxygen, ferricyanide, other ions, or organic matter used as the substrate. The market for ion exchange membranes is constantly growing, and more systematic studies are necessary to evaluate the effect of the membrane on performance and long-term stability.

5.1.5 Distinguishing Methods of Electron Transfer

Presence of Mediators

Bacteria can reduce activation losses by increasing their extracellularly oriented mediation capacity.

Three pathways are discerned at this point: direct membrane complex mediated electron transfer, mobile redox shuttle mediated electron transfer, and electron transfer through conductive pili, also referred to as nanowires.

Cyclic voltammetry (CV) offers a rapid and proven method to discern whether bacteria use

mobile redox shuttles to transfer their electrons, or pass the electrons "directly" through membrane associated compounds. For CV, the reference electrode is placed in the anode chamber of the MFC close to the anode (working electrode); the counter electrode (e.g., platinum wire) is preferably placed in the cathode chamber, but can also be placed in the anode chamber. A potentiostat is used to obtain the scan of potential.

For bacterial suspensions, a scan rate of 25 mV s^{-1} appears to be reasonable based on the work of several researchers. For the analysis of mediators in biofilms, however, this scan rate needs to be decreased, possibly to 10 mV s^{-1} and lower. This decrease can affect the accuracy of peak discrimination as the peaks tend to broaden.

The extent of the redox mediation and the midpoint potentials can be determined through analysis of (*i*) the MFC derived culture within its medium; (*ii*) the MFC culture after centrifugation and resuspension in physiological solution; and (*iii*) the supernatant of the centrifuged MFC culture. If a peak is found both in case (*i*) and (*ii*), it indicates a shuttle which is membrane associated. If a peak is found in case (*i*) and (*iii*), it indicates that a mobile, suspended shuttle is present. The size of the peaks, as integrated upon the voltammogram does not correlate unequivocally to the extent of the membrane associated electron transfer and the mobile shuttle mediated electron transfer. This is caused by the restricted accessibility of the membrane associated shuttles for oxidation/reduction by the working electrode.

Presence of Nanowires

Electrically conductive bacterial appendages known as nanowires have only recently been discovered so their structure(s) are therefore not well studied or understood. Pili produced by some bacteria have so far been shown to be electrically conductive using scanning tunneling electron microscopy. There is no data at the present time whether nanowires can be detected or can be distinguished from adsorbed chemical shuttles via standard electrochemical methods such as CV. If electron shuttles associate with non-conductive pili, or if the pili are covered with metal precipitates, they will be included in the CV measurements as membrane associated shuttles or may appear to be nanowires using STM. If redox shuttles are enclosed within the pilus' tubular structure they are unlikely to be detected using CV. Additional research will be needed to determine the best methods for detecting nanowires and determining their importance relative to other methods of electron transfer from cells to electrodes.

Outlook

MFC designs need improvements before a marketable product will be possible. Both the issues

identified above and the scale-up of the process remain critical issues. Most of the designs reviewed here cannot be scaled to the level needed for a large wastewater treatment plant which requires hundreds of cubic meters of reactor volume. Either the intrinsic conversion rate of MFCs will need to be increased, or the design will need to be simplified so that a cost-effective, large-scale system can be developed. Designs that can most easily be manufactured in stacks, to produce increased voltages, will be useful as the voltage for a single cell is low.

The success of specific MFC applications in wastewater treatment will depend on the concentration and biodegradability of the organic matter in the influent, the temperature, and the absence of toxic chemicals. Materials costs will be a large factor in the total reactor costs. Mainly anodic materials commonly used in MFC reactors, such as graphite foams, reticulated vitreous carbon, graphite, and others, are quite expensive. Simplified electrodes, such as carbon fibers, may alleviate these electrode costs. The use of expensive catalysts for the cathode must also be avoided.

Another crucial aspect is the removal of non-carbon based substrates from the waste streams: nitrogen, sulfur, and phosphorus containing compounds often cannot be discharged into the environment at influent concentrations.

Similarly, even particulate organic compounds will need to be removed and converted to easily biodegradable compounds, as part of an effective wastewater treatment operation.

Applications

One of the first applications could be the development of pilot-scale reactors at industrial locations where a high quality and reliable influent is available. Food processing wastewaters and digester effluents are good candidates. To examine the potential for electricity generation at such a site, consider a food processing plant producing 7500 kg/d of waste organics in the effluent. This represents a potential for 950 kW of power or 330 kW assuming 30% efficiency. At an attained power of 1 kW m^3, a reactor of 350 m^3 is needed, which would roughly cost 2.6 MEuros, at current prices. The produced energy, calculated on the basis of 0.1 Euros per kWh, is worth about 0.3 M Euros per year, providing a ten-year payback without other considerations of energy losses or gains compared to other (aerobic) technologies. Moreover, decreased sludge production could substantially decrease the payback time.

In the long term more dilute substrates, such as domestic sewage, could be treated with MFCs, decreasing society's need to invest substantial amounts of energy in their treatment. A varied array of alternative applications could also emerge, ranging from biosensor development and sustained energy generation from the seafloor, to biobatteries operating on various

biodegradable fuels.

While full-scale, highly effective MFCs are not yet within our grasp, the technology holds considerable promise, and major hurdles will undoubtedly be overcome by engineers and scientists. The growing pressure on our environment, and the call for renewable energy sources will further stimulate development of this technology, leading soon we hope to its successful implementation.

5.1 Three-Dimensional Carbon Nanotube-Cotton Anode for High-Performance Microbial Fuel Cells

The basic operation of microbial fuel cells (MFCs) is like that of other fuel cells (Figure 46a): oxidation of an electron donor at an anode releases electrons that pass through an external circuit to a cathode where an oxidant, such as oxygen, is reduced. In MFCs, however, oxidation at the anode is mediated by "exoelectrogens"[88], microorganisms that transfer electrons to an electrode. Transfer of electrons may occur by direct contact between redox-active membrane-bound proteins and the electrode surface, by diffusion of secreted redox-active molecules that ferry electrons between the electrode surface and the cell, or by conduction through microbially-generated nanowires that link cells to the electrode surface[87,88,96]. Criteria for optimal electrode performance include high conductivity, chemical stability, large specific surface area, biocompatibility, and resistance to decomposition. To date, most researchers have employed anodes consisting of plain carbon materials, such as carbon cloth[97], carbon paper[98], graphite brush[99], etc, and modified carbon base materials[100]. These materials are functional, but the efficiency of electron transfer limits power ouput[101].

Carbon nanotubes (CNTs) are promising for use in electrodes because of their extraordinary high conductivity, mechanical flexibility, and large specific surface area[102,103]. A possible concern is biocompatibility: CNTs could be inhibitory or even toxic to microorganisms[104,105], but most evidence suggest otherwise. Microorganisms can grow in media containing CNTs, forming CNT-microorganism clusters[106]. In recent test of CNT-modified anodes, MFC performance was enhanced[107,108,109]. A plausible hypothesis is that CNTs facilitate electron transfer from the exoelectrogens to the anode, but supporting evidence is lacking.

A highly conductive and macroporous CNT-cotton composite was fabricated through a simple and scalable process: dipping-drying of a cotton cloth in aqueous CNT ink (1.6 mg CNT/mL)[110]. CNTs conformally coated the fibers (Figure 46b, c, d).

The conductance of single CNT-cotton fiber is comparable to a bundle of approximate 200 commercial carbon fibers (Figure 46e). If the CNT-cotton fiber is treated as a uniform

conductive material, its conductance is about 2000 S cm^{-1}, double that of a carbon fiber. The CNTs follow the surface morphology of the intertwined fibers, creating a 3-dimensional space favorable for colonization (Figure 46c).

The CNT-cotton was installed as the anode in a classic H-shaped two-chamber MFC (Figure 47). Its performance and colonization were then evaluated. MFCs were inoculated with domestic wastewater and fed glucose. The uncolonized CNT-cotton was initially inactive (Figure 48a).

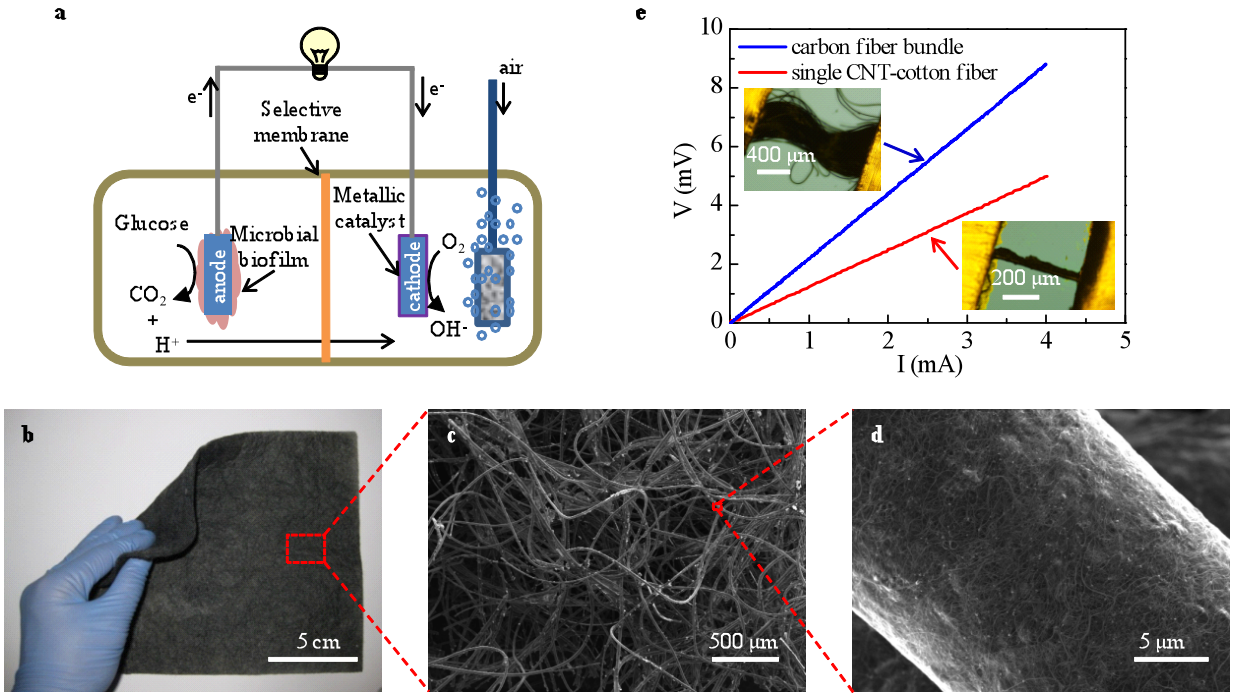

Figure 46. Microbial fuel cell (MFC) and CNT-cotton composite. a, Schematic of the classic MFCs, showing the basic mechanism of current generation in MFCs. b, A 15 cm × 15 cm piece of CNT-cotton with sheet resistance of 4 ohm/sq^{-2}. c, Scanning electron microscope (SEM) image of the CNT-cotton surface showing the open macroporous structure. d, SEM image of single cotton fiber conformally coated with CNTs. The diameter of the CNT-cotton fiber is about 20 μm. e, I-V curve of the conductivity measurement, displaying that single CNT-cotton fiber is comparable to a bundle of approximate 200 commercial carbon fibers.

After twelve days of operation, the operating voltage increased to greater than 0.3 V through a 1 kΩ resistor (Figure 48b), indicating successful startup[88]. During this period, the anode was colonized, and the anode compartment became turbid (Figure 47). Scanning electron microscope (SEM) image (Figure 48c) provided evidence of colonization and biocompatibility. A cyclic voltammogram (Figure 48a) demonstrated significant positive current peak for glucose oxidation, evidence of exoelectrogenic activity.

Figure 47. A set of lab scale classic H-shaped two-chamber MFC. Anode is CNT-cotton and cathode is carbon cloth with a platinum catalyst layer. Anode and cathode chambers are separated by an ion exchange membrane. Domestic wastewater is used as the inoculum. Anode is fed with glucose and cathode camber is continuously purged with air using a diffusion stone. The loading is a 1 kΩ resistor. The turbidity in the anode chamber (left) is caused by the growth of microorganisms.

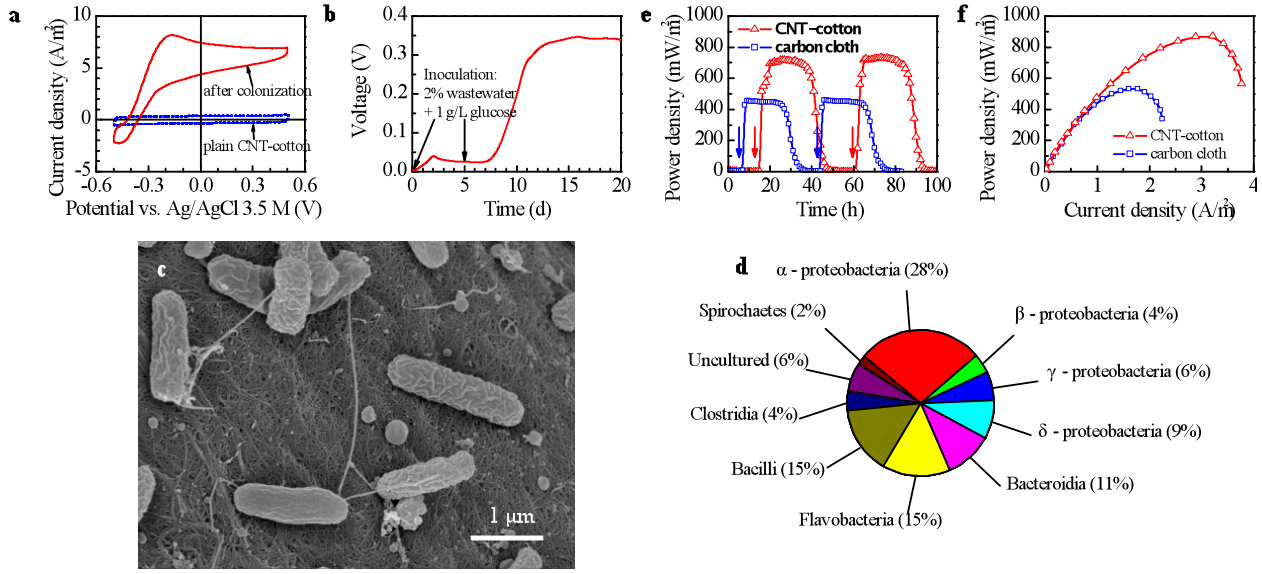

Figure 48. Startup of the MFC equipped with CNT-cotton anode and its performance versus carbon cloth anode. a, Cyclic voltammograms for the CNT-cotton anode before and after colonization. Positive current indicated glucose oxidation. b, Voltage generation of the MFC across a 1 kΩ external resistor. The operating voltage higher than 0.3 V indicated successful startup. c, Scanning electron microscope image of the microorganisms on the CNT layer. d, Structure of the microbial community on CNT-cotton anode. e, Steady power generation with a 1 kΩ loading resistor. Arrows indicate glucose feeding (200 mg L^{-1}). Power outputs were normalized to the projective surface area of anode. f, Polarization curve, showing that the maximum power density of the MFC prepared with the CNT-cotton anode was 64% higher than that with the carbon cloth anode.

While the cotton fiber provided mechanical support, the sole electro-active material present was CNTs. These results confirm that CNTs alone can function as an anode. A sample of the biofilm attached to a piece of CNT-cotton anode was then analyzed by extracting DNA and preparing a 16S rRNA gene clone library. The results revealed a diverse community (Figure 48d), including species previously reported in MFCs, and related to *Geobacter*, *Rhodopseudomonas*, *Ochrobactrum*, *Comamonas*, *Enterobacter* (Figure 49)[111,112,113,114,115]. Steady operation of this MFC was achieved for more than 4 months.

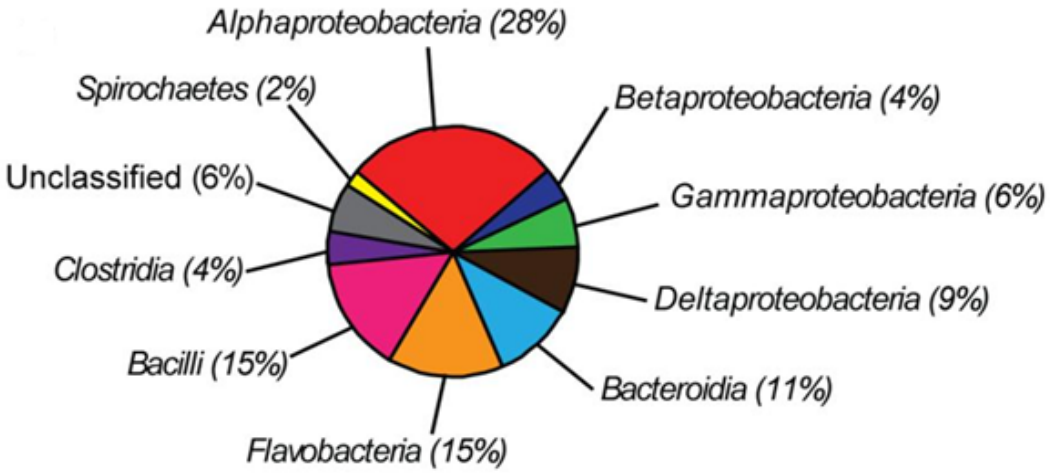

Figure 49. Microbial community developed on CNT-cotton anode.

To better evaluate the performance of CNT-cotton anode, an MFC with a CNT-cotton anode was operated in parallel with an MFC in the same configuration but with a commercial carbon cloth anode. Both MFCs were loaded with a 1 kΩ external resistor and intermittently fed glucose (200 mg L^{-1}). Steady power generation cycles were achieved after 1 month of operation (Figure 48e). As shown in Figure 48d, for a 1 kΩ loading resistance, the power density of the MFC equipped with a CNT-cotton anode was 59% higher than that of a MFC equipped with a carbon cloth anode (733 mW m^{-2} vs. 461 mW m^{-2}). Under identical operating conditions, the maximum power density of the MFC prepared with a CNT-cotton anode was 64% higher (870 mW m^{-2} vs. 531 mW m^{-2}), as determined by the polarization curve (Figure 48f). The total electric energy generation can be calculated by integrating the power-time curve. The results show that the MFC equipped with a CNT-cotton anode produced 75% more energy from the same mass of added glucose. These data strongly indicate that a CNT-cotton anode enables superior performance. Several factors may contribute to the superior performance of a CNT-cotton anode. The CNT-cotton is much more porous than commercial carbon cloth, consisting of regularly woven carbon fibers (Figure 51). Greater porosity provides more open space for colonization.

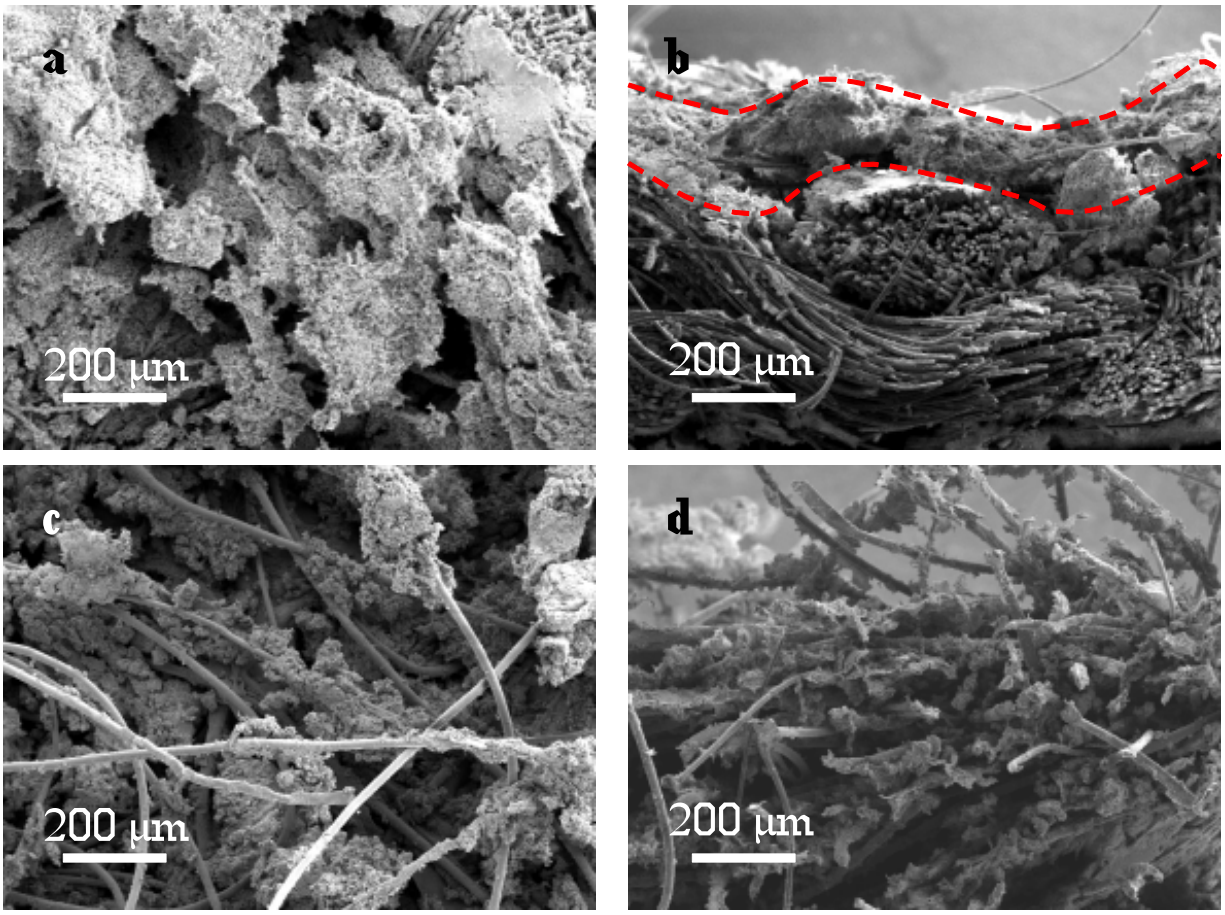

Figure 50. Three-dimensional open macroporous structure of the CNT-cotton anode. Scanning electron microscope (SEM) images were taken for both the projective surfaces (a, c) and the transections (b, d). a, b, biofilm is largely restricted to the outer surface of the carbon cloth anode (area between two broken lines in b), with few microorganisms present on the interior fibers. c, d, SEM images displaying that a microbial biofilm wrapped uniformly around each CNT-cotton fiber, including both exterior and interior fibers.

After 50 days of operation, thick biofilms covered the anodes of both MFCs. In the case of carbon cloth anode, however, the colonization was largely restricted to the outer surface of the anode, with few microorganisms present on the interior fibers (Figure 50a, c). For the CNT-cotton MFC anode, a microbial biofilm wrapped uniformly around each CNT-cotton fiber, including both exterior and interior fibers (Figure 50b, d). Nearly all of the fibers in the CNT-cotton anode were thus capable of collecting current whereas only the coated outer fibers were capable of doing so in the case of the carbon cloth anode.

The CNT-cotton anode also had high electron transfer efficiency. All of the 3 pathways of electron transfer from exoelectrogen to anode are facilitated by the particular structure and property of the CNT layer (Figure 52a).

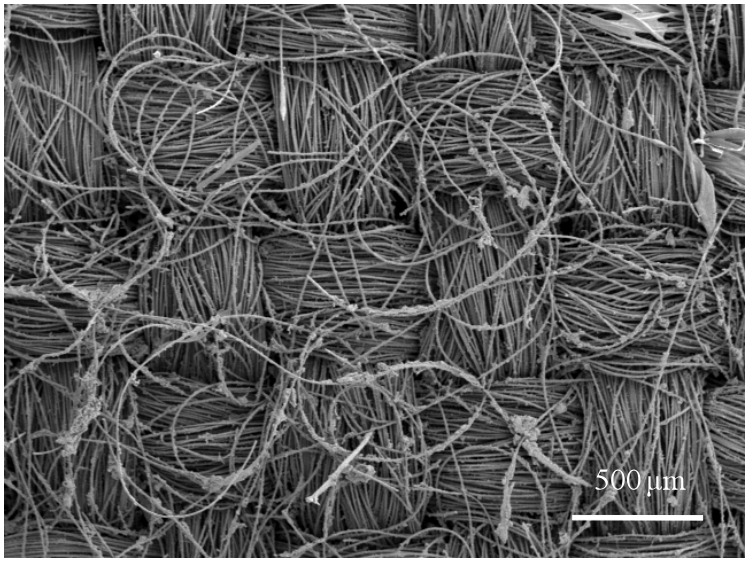

Figure 51. Projective surface of carbon cloth anode.

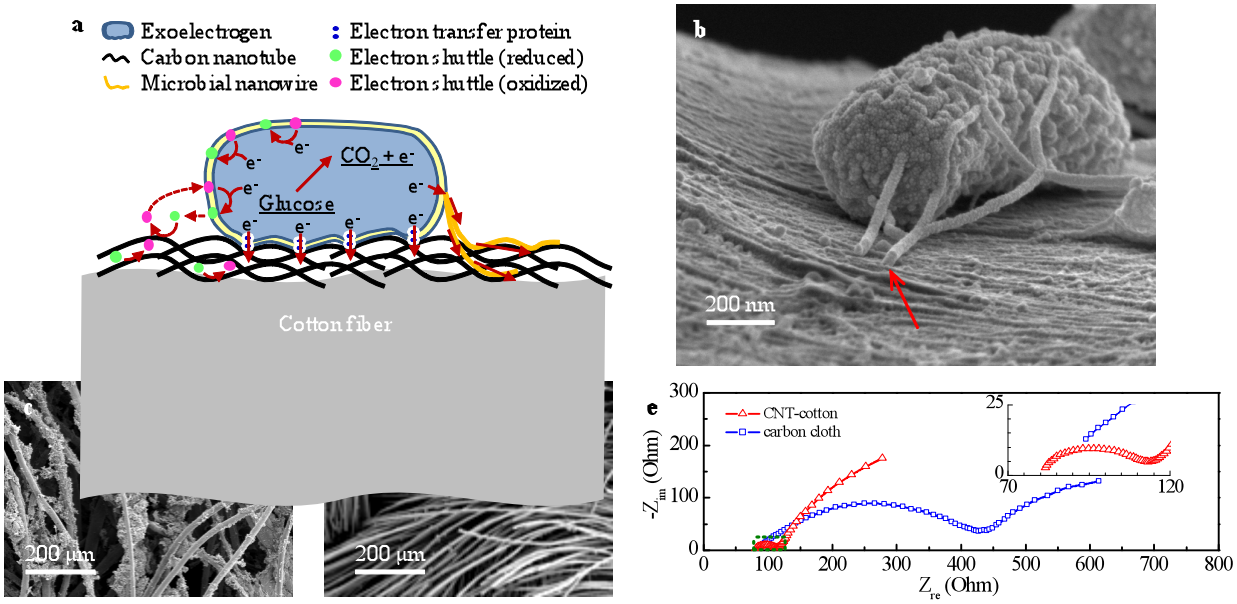

Figure 52. Electron transfer from exoelectrogens to a CNT-cotton anode. a, Schematic showing three different pathways of electron transfer from exoelectrogen to a CNT-cotton anode. b, Scanning electron microscopy image of a microbial nanowire extends from cell membrane and penetrates into the CNT layer. Arrow indicates the nanowire. c, d, SEM image of the CNT-cotton anode (c) and the carbon cloth anode (d) after 5 minutes of bath sonication (100 W) and 10 seconds of vortex agitation (2700 rpm). A biofilm is still visible on the CNT-cotton fibers (c), but not on the carbon cloth fibers (d), suggesting stronger mechanical binding to CNT-cotton anode. e, Nyquist curve of the electrochemical impedance spectroscopy test for the microbial fuel cells equipped with the CNT-cotton anode and the carbon cloth anode, respectively. The area within the green square is magnified in an insert graph. The electron transfer resistance between the CNT-cotton anode and the electrolyte, indicated by the diameter of the first semicircle of the Nyquist curve, is only 10% of the resistance between the carbon cloth anode and the electrolyte (approximately 30 Ω vs. 300 Ω).

First, the CNT coating makes the surface of CNT-cotton fibers rough. For single microorganism with fixed size, the rough surface of CNT-cotton fiber provides more contact area than the smooth surface of a carbon cloth fiber, resulting in stronger mechanical bonding and more efficient electron transfer between cell membranes and the anode.

Secondly, the coated CNTs themselves form a secondary 3-dimensional porous structure with high active surface area enabling collection of electrons from electron mediators or shuttles in the electrolyte. Finally, CNTs display strong interactivity with microbial nanowires. A great number of nanowires were observed under SEM (Figure 53).

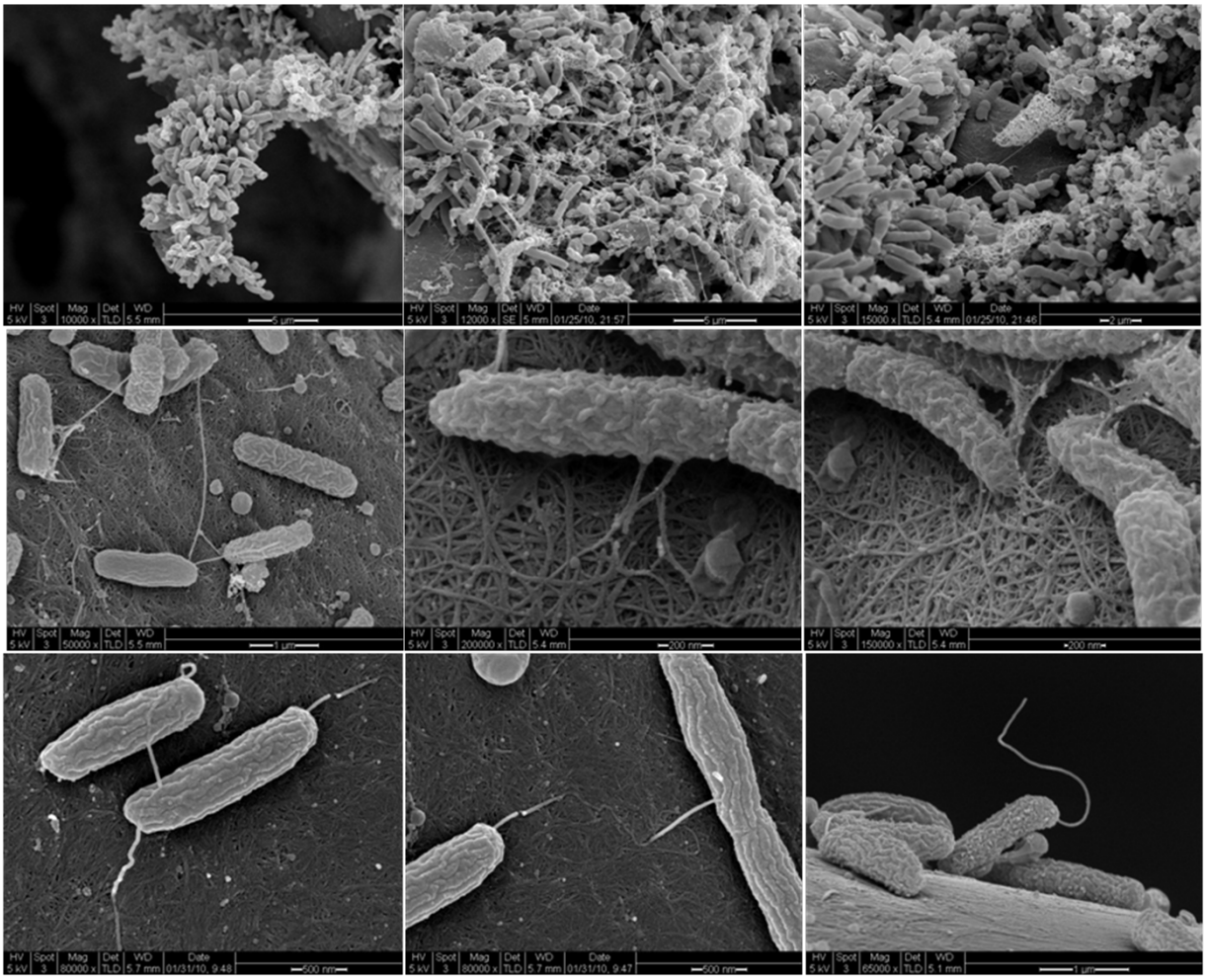

Figure 53. Scanning electron microscopy image of the biofilm covering the CNT-anode.

These nanowires (or pili) tethered cells to the anode surface, facilitating maintenance of a stable biofilm[116]. Nanowires are also known to be conductive and provide a third route for electron transfer[117,118]. The diameter of the observed nanowires was around 5 nm within the range of CNTs. Size compatibility improves prospects for interaction. Some nanowires compactly attach to the CNT layer, with a segment longer than 1 μm.

Figure 52b shows a nanowire bridging the gap between CNTs and penetrating into the anode surface. This would not be possible for the solid surface of carbon cloth fibers. Interacting with CNTs likely enhances nanowires' function as tethers and electron conductors, further improving the mechanical binding and electrical conductivity between microorganisms and anode materials.

A simple experiment was performed to assess mechanical binding to the CNT-cotton anode. Samples covered by mature microbial biofilms (Figure 50a, c) were removed from both CNT-cotton anode and the carbon cloth anode. The samples were sonicated in phosphate buffer solution for 5 minutes and then subjected to vortex agitation for 10 seconds. A biofilm remained visible on the CNT-cotton fibers (Figure 52), but not on the carbon fibers (Figure 52d), suggesting stronger mechanical binding to the CNT-cotton anode. Stronger mechanical binding shortens distances between microorganisms and the anode, decreasing electron transfer resistance.

Direct measurement of electrical resistance between anode materials and microorganisms is difficult, but we can obtain some information regarding conductivity between anode materials and electrolyte through electrochemical impedance spectroscopy (EIS) tests. EIS tests were performed to both CNT-cotton anode and carbon cloth anode under conditions of steady power generation. The results show that the electron transfer resistance between the CNT-cotton anode and electrolyte is only 10% of that between the carbon cloth anode and the electrolyte, as indicated by the diameters of the first semicircles of the Nyquist curves in Figure 52e. This 10-fold improvement in conductance decreased the overall internal resistance of the MFC outfitted with a CNT-cotton anode (400 Ω) to only 40% of that measured for a carbon cloth anode (1000 Ω).

The CNT-cotton anode is promising for high-performance MFCs due to its 3-dimensional macroporous structure and compatibility with CNTs. Further improvements are needed in the structure and properties of the support material (cotton in this case). Nevertheless, the results suggest a novel approach to electrode design and will facilitate design of MFCs for energy recovery during treatment of domestic and industrial wastewaters.

5.2 Microbial Fuel Cells Cathodes

As previously outlined, microbial fuel cell (MFC) is a promising technology for wastewater treatment due to its capability of recovering electric energy during the removal of organic pollutants [88,89,96,119]. Air is considered to be the most suitable oxidant for field scale MFCs, because it is free and inexhaustible [120,121]. However, the oxygen reduction efficiency is highly

constrained by the specific operating conditions of MFCs, such as ambient temperature and mostly neutral pH [120,122,123]. Thus, cathode performance often limits the power output of MFCs [122,124]. Moreover, cathode usually accounts for the greatest part of the total capital cost of a MFC, mainly because of the use of precious metal catalyst like Pt [125]. Therefore, improving the cathode performance decreasing the catalyst loading represents a critical issue for researchers working on MFCs [120].

According to the different cathode configurations, MFCs are classified in two categories: aqueous-cathode and air-cathode devices. In an aqueous-cathode MFC, the cathode is immerged in an electrolyte purged with air, thus oxygen is dissolved in the electrolyte [122], while for an air-cathode MFC one side of the cathode is directly exposed to air and gas phase oxygen works as electron donor [89]. A common opinion is that aqueous-cathode MFCs do not perform as well as air-cathode MFCs [96]. However, most of the previous studies on aqueous-cathode MFCs employed cathode prepared by coating a carbon supported catalyst paste onto a carbon cloth (CC) substrate [122,126-130]. This cathode configuration, widely used in chemical fuel cells, is actually designed for oxygen reduction in the gas phase. An aqueous-cathode MFC may also achieve high performance if the cathode can be well designed for reduction of oxygen dissolved in the electrolyte. Moreover, some modified MFC technologies prefer an aqueous-cathode. For examples, in a microbial desalination cell, catholyte is essential for collecting the cations, e. g. Na^+, transported through the cation exchange membrane from the salt water [131]. Therefore, while most current studies focus on optimizing air-cathodes [132-134], improving aqueous-cathode is also meaningful.

To catalyze oxygen reduction, catalysts must have simultaneous access to oxygen, electrons, and protons [102]. The catalytic surface area having this triple-access, termed as electrochemically active surface area (ECAS), is directly related to the cathode performance [135]. In a conventional air-cathode, the carbon support, e.g. carbon black, provides the electron pathway, while a Nafion membrane works as the electrolyte, providing proton conduction. The porous structure of the composite electrode processes high interfacial surface area with gas phase to facilitate oxygen transfer [102,135,136]. In an aqueous-cathode system, since both proton and oxygen come from the aqueous electrolyte, the structure design is much easier. However, an open porous structure, with pore sizes larger than that of conventional air-cathodes, is preferred for an easier access of the electrolyte.

5.3 CNT-Textile with Electrodeposited Pt Nanoparticles for High-performance MFC Cathode

In this study, we propose a new composite cathode prepared by electrochemically depositing Pt

nanoparticles onto a highly conductive carbon nanotube (CNT)-textile substrate, previously studied by our research group as electrode in batteries, supercapacitors, as well as the anode in MFCs [110].

5.3.1 Materials and Methods

Electrode preparation

The CNT-textile was fabricated through a simple and scalable dipping-drying process previously described in details [110]. A CNT-textile sheet with thickness of ~1 mm was cut into a 1 cm × 3 cm piece, and then treated with nitric acid (4 M, 2 hours) and glacial acetic acid (2 hours) successively before the Pt deposition. These acid treatment processes increase the sample's hydrophilicity and produce oxygen-rich functional groups on the originally inert CNT surface acting as nucleating sites for Pt deposition [137,138]. The electrochemical deposition process was performed in a four-neck flask containing chloroplatinic acid (H_2PtCl_6, 0.019 M) and hydrochloric acid (HCl, 0.6 M) as electrolyte [137]. CNT-textile was the working electrode with only 1 cm × 1 cm dipped into the electrolyte. Two Pt meshes, one on each side of the CNT-textile, were used as counter electrodes in order to optimize the current lines and have a uniform Pt distribution in the whole current collector (see paragraph 4.6.3). The deposition was performed potentiostatic technique, fixing the potential at -0.6 V vs. a double junction Ag|AgCl|KCl (3.5M) reference electrode (RE) limiting the charge at 600 mC [137]. Three control samples with the same geometric surface area were also prepared: a plain CC, a plain CNT-textile, and a commercial CC with Pt painting (CC-Pt). All these four electrode samples were tested in parallel.

Electrode characterization

The morphology of electrode surfaces was investigated using a field emission scanning electron microscope (FEI XL30 Sirion SEM). Pt loadings were measured by an IRIS advantage inductively coupled plasma atomic emission spectroscopy (ICP-AES) system. The average sizes of Pt particle on different electrodes were calculated by Debye Scherrer equation, based on the X-ray Diffraction (XRD) test results [137,138]. ECSAs were characterized using electrochemical method, in which the ECSAs were proportional to the hydrogen adsorption-desorption capability of the electrode [135]. Oxygen reduction efficiencies were tested by performing liner staircase voltammetry (LSVs) at a step-sweep rate of 10 mV per 10 seconds from 0.5 to -0.5 vs. a double junction Ag|AgCl|KCl (3.5M) reference electrode. The electrolyte is PBS (see next section)

simulating the working condition in aqueous-cathode MFCs [122]. The electrolyte was saturated with oxygen under ambient pressure and temperature before the tests.

MFC construction and characterization

All cathode samples were investigated in an H-shaped two-chambers MFC with a CNT-textile anode (1 cm × 1 cm). The MFC was inoculated with domestic wastewater and has been operated for 6 months to obtain mature biofilm on the anode. An anion exchange membrane (AMI-7001, Membranes International Inc., NJ) was used as the separator. Catholyte was a phosphate buffer solution (PBS, 100 mM, pH 7) comprised of $NaH_2PO_4 \cdot H_2O$ (4.90 g L^{-1}), Na_2HPO_4 (9.15 g L^{-1}), KCl (0.26 g L^{-1}), and NH_4Cl (0.62 g L^{-1}) [122]. Anolyte contains glucose (1 g L^{-1}), mineral solution (12.5 mL L^{-1}), vitamin solution (5 mL L^{-1}), and the same PBS as that used for catholyte [122,139]. The cathode chamber was continuously purged with air using a diffusion stone (flow rate ~0.1 L min^{-1}). Polarization curves obtained from the same LSVs described before were applied to evaluate the MFC performance. Power and current densities were normalized by the projected surface area of the cathode (2 cm^2). All experiments were conducted at room temperature.

5.3.2 Results and discussion

CNT-textile-Pt composite

The plain surface of CNT-textile is shown in Figure 54A.

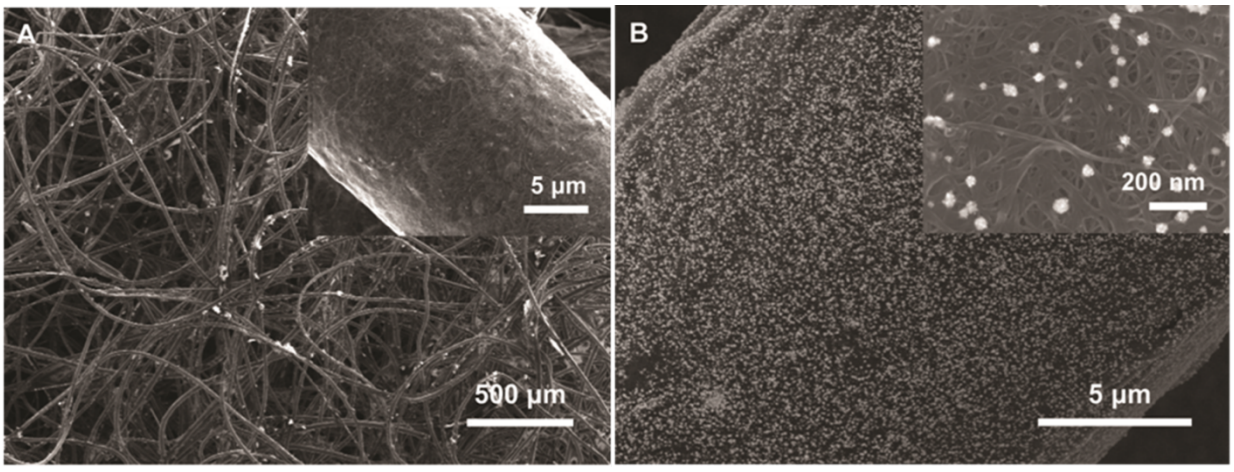

Figure 54. (A) SEM of the surface of plain CNT-textile displaying the macroscale porous structure and the conformal CNT coating. (B) SEM of the CNT-textile-Pt with Pt loading of 0.048 mg cm^{-2}.

The randomly intertwined textile fibers form an open macroscale porous structure. The conformally coated CNTs make the CNT-textile highly conductive, with a sheet resistance of 4

Ω sq^{-1} [110]. The acid treatment creates many oxygen-rich functional groups on the CNT surface, working as active sites for Pt reduction and nucleation [137,138]. Since Pt particles were deposited by an electrochemical method, only the sites with electronic access were covered with Pt particles. Therefore, the electron pathways to all the catalysts are guaranteed. As shown in Figure 54B, the deposited Pt particles are uniformly distributed along the CNT textile backbone making the Pt particles easy to access by the electrolyte containing oxygen and proton. Thus, in CNT-textile-Pt, almost every Pt particle has triple-access for oxygen reduction.

Oxygen reduction activity and MFC performance

The oxygen reduction activity of the cathode samples were characterized by LSV as previously described. As shown in Figure 55, CNT-textile-Pt cathodes generate much larger current of reduction than CC-Pt, indicating superior oxygen reduction activity.

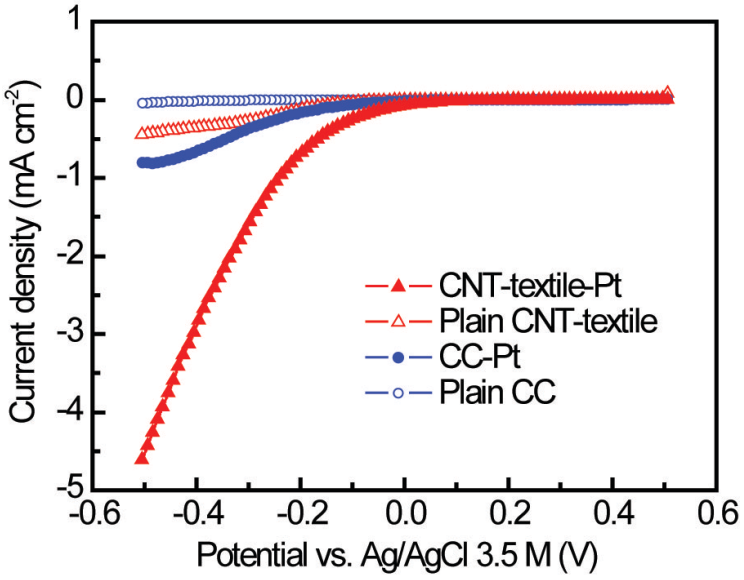

Figure 55. LSV results showing the oxygen reaction activities of different cathodes.

While oxygen reduction by the plain CC is almost negligible, the plain CNT-textile also reveals certain oxygen reduction activity, resulting from the catalytic activity of CNTs that has been reported by several studies. Power densities of the MFCs equipped with different cathodes were shown in Figure 56.

In accordance with the results of oxygen reduction, the CNT-textile-Pt cathode shows much better performance than the CC-Pt cathode. The maximum power density of the MFC with CNT-textile-Pt cathode is 837 mW m^{-2}, 2.14 times of that achieved with CC-Pt cathode (391 mW m^{-2}). The MFC prepared with the plain CNT-textile cathode also generates a maximum power density of 177 mW m^{-2}. Even though removing this contribution of the CNTs, the CNT-

textile-Pt cathode still show better performance than the CC-Pt cathode, which indicates that the Pt in CNT-textile-Pt provides greater catalytic activity.

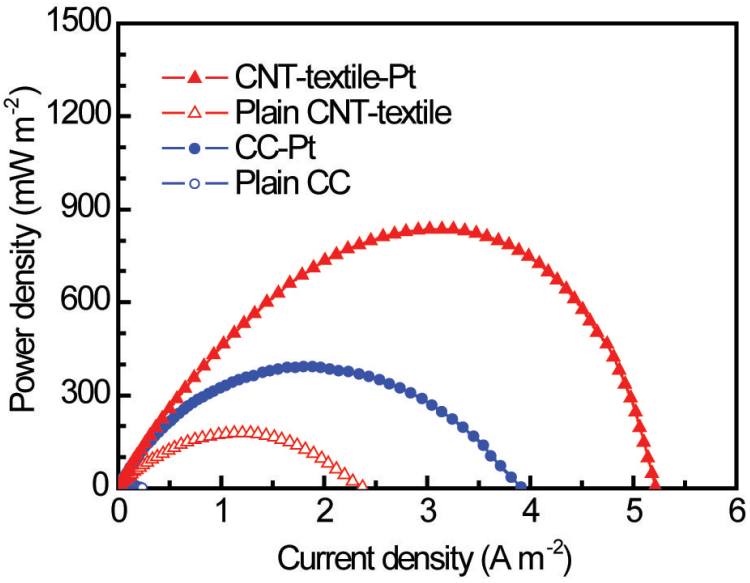

Figure 56. Polarization curves of MFCs with different cathodes. Power densities are normalized by the project surface area of electrodes.

Electrode properties

Pt loadings of the CNT-textile-Pt and CC-Pt cathodes, determined by ICP-AES measurement, are shown in Table 4. Characterization of CNT-textile-Pt cathodes compared with CC-Pt.

The Pt loadings were controlled by the charge applied during electrochemical deposition. However, only part of the applied charges (15.9% in this study), defined as coulombic efficiency (CE), is effective for Pt deposition [137]. The Pt loading of the CNT-textile-Pt cathode is 0.048 mg cm^{-2}, only 19.3% of the commercial CC-Pt cathode (0.249 mg cm^{-2}). While many studies have been focused on using alternative catalyst, such as activated carbon, stainless steel, Ni, Fe, Co, Mn, Cu, etc [121,123,140-143], decreasing Pt loading provides a more direct approach to reduce the capital cost of the cathode.

Table 4. Characterization of CNT-textile-Pt cathodes compared with CC-Pt.

	CNT-textile-Pt	CC-Pt
Charge applied (mC)	600	N/A
Pt Loading (mg cm^{-2})	0.048	0.249

Coulombic efficiency (%)	15.9	N/A
Average size of Pt nanoparticles (nm)	9.2	2.6
Theoretical surface area (cm^2 Pt cm^{-2} electrode)	14.5	262.5
Active surface area (cm^2 Pt cm^{-2} electrode)	7.79	0.92
Surface area utilization efficiency (%)	53.6	0.4

The particle sizes of Pt seem to vary from several nanometers to less than 100 nm. However, the bright dots displayed in the scanning micrographs are actually clusters of several Pt nanoparticles with smaller size (Figure 54B, insert). The average sizes of Pt nanoparticles on different electrode samples can be calculated from XRD results, and then with the average particle sizes and total Pt loading, the theoretical overall Pt surface area can be estimated. As shown in Table 4. Characterization of CNT-textile-Pt cathodes compared with CC-Pt., the CNT-textile-Pt samples have less Pt surface area than the CC-Pt due to the lower loading and larger particle size. However, the ECSAs of CNT-textile-Pt, which are more relevant to the catalytic performance, are larger than that of CC-Pt. This result is accordance to the different MFC performances achieved by these two cathodes. Comparing the surface area utilization efficiency, the CNT-textile-Pt is two orders better than the CC-Pt (53.6% vs. 0.4%), suggesting the well design of our CNT-textile-Pt cathode. The reason for the large active surface lost of the CC-Pt cathode may include: 1) isolated Pt particles with no electronic pathway are formed [135]; 2) some Pt particles located in small or closed-end pores are not accessible for the electrolyte; 3) the hydrophobic surface of the CC-Pt hinders the electro-electrolyte contact.

5.3.3 Conclusions

A new CNT-textile-Pt cathode specially designed for aqueous-cathode MFCs was obtained by electrochemically depositing Pt nanoparticles on a macroporous CNT-textile substrate. This CNT-textile-Pt cathode shows surface area utilization efficiency two orders of magnitude higher than the commercial CC-Pt cathode. Assisted by the additional catalytic activity of CNTs, an MFC equipped with CNT-textile-Pt cathodes achieve higher power density (2.14-fold) with lower Pt loading (19.3%). Moreover, the synthesis process of CNT-textile-Pt is simple and scalable. Thus, CNT-textile-Pt is promising to function as cathodes for large scale high performance aqueous-cathode MFCs.

CHAPTER VI: CONDUCTIVE ENERGY TEXTILES

Chapter IV: Conductive Energy Textiles

Recently there is strong interest in lightweight, flexible and wearable electronics to meet the technological demands of modern society. Integrated energy storage devices of this type are a key area that is still significantly underdeveloped. Here, we describe wearable power devices using everyday textiles as the platform. With an extremely simple "dipping and drying" process using single-walled carbon nanotube (SWNT) ink, we produced highly conductive textiles with conductivity of 125 S cm^{-1} and sheet resistance less than 1 Ω/sq. Such conductive textiles show outstanding flexibility and stretchability, and demonstrate strong adhesion between the SWNTs and the textiles of interest. Supercapacitors (SC) made from these conductive textiles show high areal capacitance, up to 0.48 F cm^{-2}, and high specific energy. We demonstrate the loading of pseudocapacitor materials into these conductive textiles that leads to a twenty four-fold increase of the areal capacitance of the device. These highly conductive textiles can provide new design opportunities for wearable electronics and energy storage applications.

6.1 Stretchable, porous and conductive energy textiles

Wearable electronics represent a developing new class of materials with an array of novel functionalities, such as flexibility, stretchability and lightweight, which allow for many applications and designs previously impossible with traditional electronics technology. High-performance sportswear, wearable displays, new classes of portable power and embedded health monitoring devices are some examples of these novel applications.[144-146] All these electronic applications require lightweight, wearable power conversion and storage devices. The ideal wearable power would incorporate textile as a component. Previously, studies have been done for integrating nanoscale materials into textiles to improve the clothing colors, anti-odor function, UV protection and human biomonitoring.[147-149] In our work, we conformally coat single-walled carbon nanotubes (SWNTs) on cellulose and polyester fibers to make porous conductors. The fabrication process is simple and scalable, similar to those widely used for dyeing fibers and fabrics in the textile industry. The SWNT coating makes these textiles highly conductive, with sheet resistance less than 1 Ω/sq. The conductive textiles (e-Textile) show outstanding mechanical and chemical properties. Their porous structure allows high mass loading of materials which increases the performance of energy storage devices. When conductive textiles are used as electrodes and standard textiles are used as separators, fully stretchable SCs are demonstrated which will significantly benefit the development of wearable and stretchable electronics.[150]

6.1.1 *"Dyeing" textile with SWNT ink*

Textile fibers, such as cellulose or polyester, have a hierarchical structure with complicated surface morphology, functional groups such as hydroxyl groups, and high porosity.[151] For example, each cotton fiber is comprised of multiple individual cotton fibrils, which are in turn composed of multiple microfibrils, bundled together. The microfibrils are made of poly-D glucose chains, usually arranged in crystalline, or partially crystalline, domains. (Figure 57(a)).

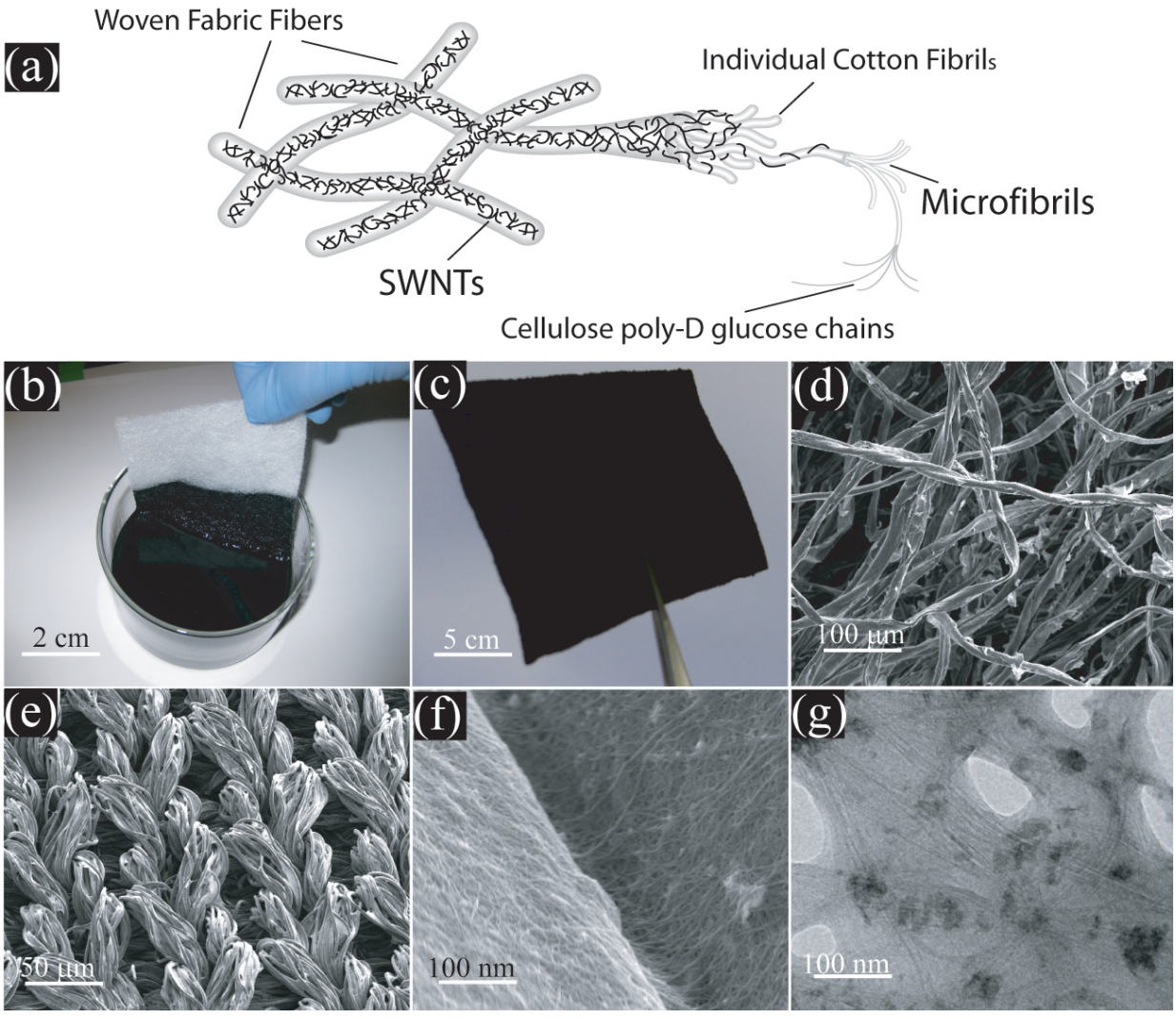

Figure 57. Porous textile conductor fabrication. (a) Schematic of SWNTs wrapping around cellulose fibers to for a 3D porous structure. (b) Conductive textiles are fabricated by dipping textile into an aqueous SWNT ink followed by drying in oven at 120 C for 10 minutes. (c) A thin, 10 cm by 10 cm textile conductor based on a fabric sheet with 100% cotton and Rs of 4 Ω/sq. (d) SEM image of coated cotton reveals the macroporous structure of the cotton sheet coated with SWNTs on the cotton fiber surface. (e) SEM image of fabric sheet coated with SWNTs on the fabric fiber surface. (f) High magnification SEM image shows the conformal coating of SWNT covering and bridging between the fabric fibers. (g) TEM image of SWNTs on cotton fibers.

This structure allows the fibers to absorb large amounts of water, or other polar solvents, which causes the fibers to swell when placed in such solutions. The interaction of these polymeric fibers with SWNTs is facilitated by these properties, as well as several properties of the SWNTs themselves. SWNTs are mechanically flexible, which allows them to conform to the shape of the polymer fibers. Also, the interactions of SWNTs with polymer fibers have been widely studied. SWNTs have been proven to have large van der Waals interactions with many types of polymers, and SWNTs and cellulose fibers exhibit the large van de Waals forces which are demonstrated in other SWNT-polymer composites.[152-154] Furthermore, acid treated SWNTs have carboxyl functional groups on the surfaces and the ends, which can form strong hydrogen bonds with the hydroxyl groups in the cellulose fibers.[152-154] Due to the mechanical flexibility of SWNTs and the high surface area of cellulose fibers, together with the large water absorption of the fibers, surface contact between SWNTs and cellulose fibers is maximized. Upon contact, large van der Waals forces and hydrogen bonding occurs, which binds the SWNTs very tightly to the cellulose. Figure 72(b) shows a schematic of SWNTs wrapping around cellulose fibers to create a 3D porous structure. To realize such structure, a ink with well dispersed SWNTs is prepared by dispersing 1.6 mg/mL laser ablation tubes in water with 10 mg/mL sodium dodecylbenzenesulfonate (SDBS) as surfactant.[155] Then a textile is dipped into the black SWNT ink. Due to the strong absorption, the textile is quickly coated by the SWNT ink. The textile with SWNT ink is subsequently dried in oven at 120°C for 10 minutes to remove water. A highly conductive textile is achieved through this simple dipping and drying process. Textiles investigated in this study include cotton sheet (Figure 72(a)) and woven polyester fabric (see Supporting Information). Figure 72(c) shows a conductive fabric with sheet resistance (R_s) of ~4 Ω/sq. These highly conductive textiles retain their texture and structure after SWNT coating, and feel the same as the original material. This fabrication process can be easily applied to other ink made of nanostructured materials and scaled up with roll-to-roll techniques using slot-die or curtain coating processes.[156] SEM images of Figure 72(d) and Figure 72(e) reveal the macro porous structures of a cotton sheet and a fabric, respectively. Conformal coating of SWNTs onto the fibers was observed for both the cotton and the fabric (Figure 72(f)). This conformal coating is a result of the mechanical flexibility of individual SWNTs and the strong binding energy between SWNTs and the cotton fibers,[157] and accounts for the high conductivity of the textile. Previous studies have shown that SWNT films have micro scale porosity which is required to maximize the electrical double layer capacitance.[158] The microporous structure on top of the macroporous textile leads to what we call a double porous structure. Such double porous structures facilitate the easy access of electrolyte ions to the SWNTs, which is essential

for high power SC applications. TEM images taken on SWNT-cotton fiber hybrids (Figure 57(g)) show the SWNTs are well bonded to the fiber and forming cross-linked networks, which provide conducting pathways.

Such porous textile conductors demonstrate excellent electrical, mechanical and chemical resistance performance.

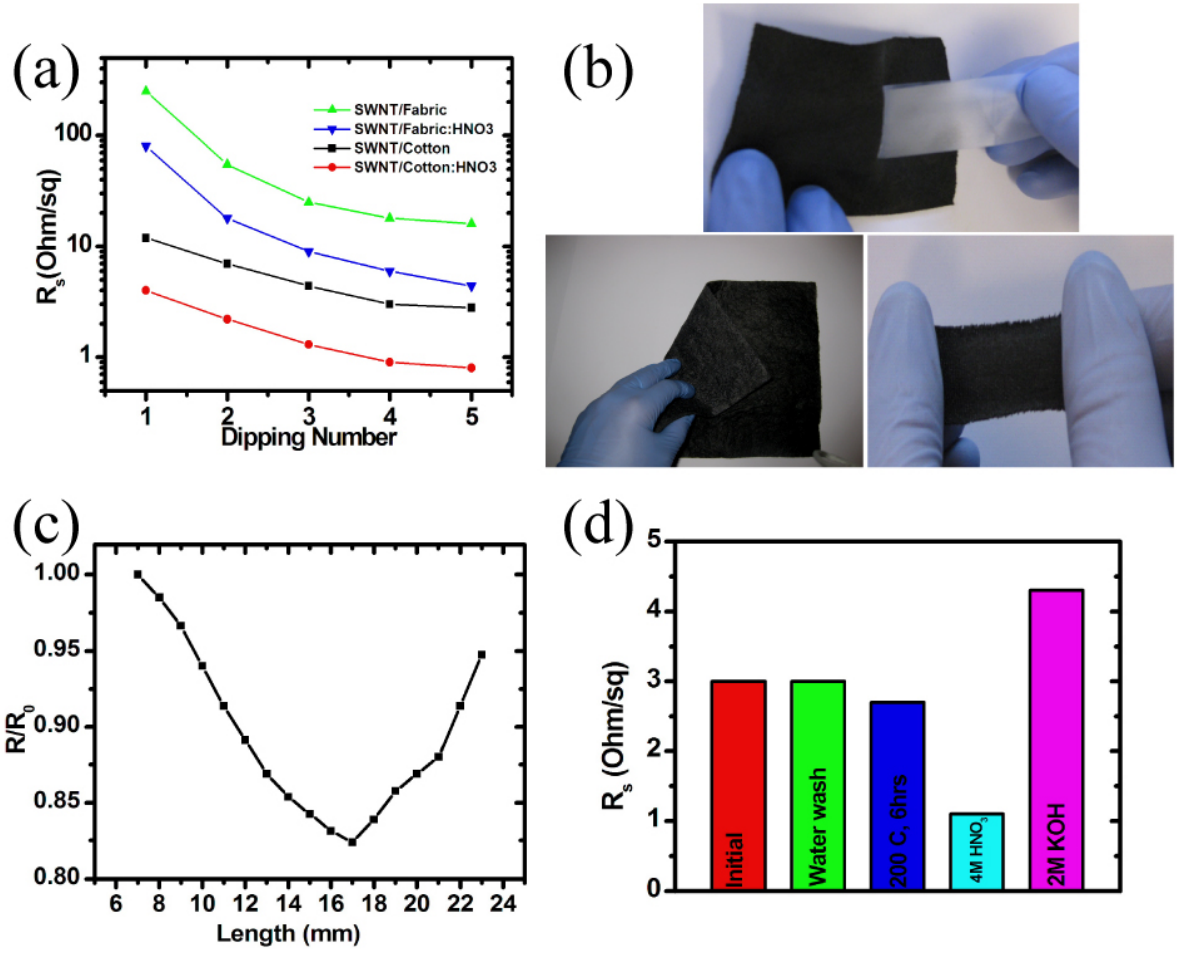

Figure 58. Properties of textile conductors. (a) Sheet resistance of fabric and cotton sheet after SWNT coating, which shows the same values on both faces for either fabric or cotton. The sheet resistances decrease by a factor of approximately 3 after HNO_3 treatment. (b) Excellent mechanical properties of conductive textile: strong adhesion between SWNTs and textile (passing the scrotch tape test), foldable and stretchable. (c) The SWNT coated textiles show unusual stretching properties. The film sheet resistance decreases as the SWNT/fabric is stretched up to 240% of its initial length, after which the resistance starts to increase. (d) SWNT/cotton is resistant to water washing, thermal treatment at 200 C for 6 hours, 4 M HNO_3 acid and 2 M KOH.

Figure 53(a) shows that the conductance increases as the dipping number in SWNT ink increases. The R_s difference for cotton and fabric with different dipping number is due to the SWNT ink absorption difference for cotton and fabric per area (Figure 59).

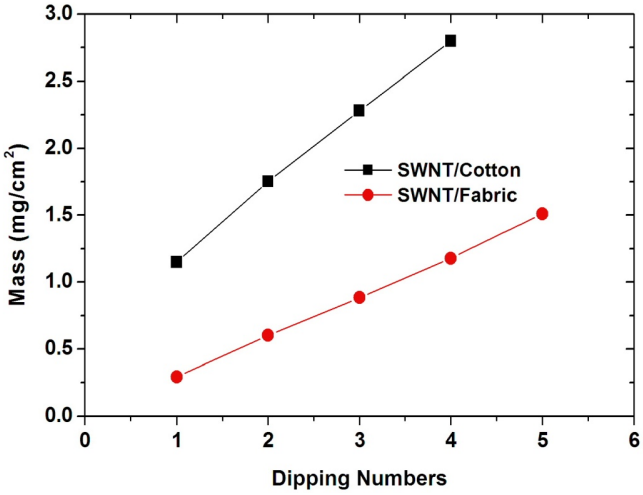

Figure 59. The amount of ink absorbed per area by the cotton sheet or fabric sheet with different dipping numbers.

Soaking the conductive cotton sheets in 4M nitric acid for a half followed by blowing dry can wash away the surfactant molecules and induce hole doping[159-161] which resulted in decrease of their R_s by approximately three times. The thickness of cotton sheets decreases from ~2 millimeter to ~ 80 micrometers with mechanical pressing, which changes the electrical conductivity from 5 to ~ 125 S cm^{-1}. Conductive textiles with a large range of conductance could be achieved by tuning the SWNT ink concentration and dipping number.

The conductive textiles show outstanding mechanical properties: strong binding between SWNTs to the textile, foldability and stretchability. The mechanical adhesion tests for SWNTs to cotton by the standard tape test and by washing in water show no visible nanotubes in the solution, or on the tape, and no conductivity degradation of the sample. In the water-washing test, the conductive cotton is soaked in water, then squeezed and wrung out. SWNTs stick well to the cotton without peeling or dissociating and precipitating in water (Figure 60(b)). These tests suggest that SWNTs strongly adhere to the cotton fibers, which are critical for wearable electronic and power devices. Such strong binding may be due to the following reasons:

1) A large van der Waals force and a hydrogen bonding exist between SWNTs and the textile fibers.[157]
2) The flexibility of SWNTs allow them to be conformally adhered to the surface of cotton fibers which maximize the surface contact area between SWNTs and textile fibers.[162]

The superior mechanical adhesion of SWNTs on cotton is essential for high-speed roll-to-roll fabrication and energy storage device stability. To test the stretchability, the resistance of a fabric sample with a dimension of 2.5 cm by 7 cm e-Fabric is monitored as it is being loaded in tension using a tensile tester. More detailed information can be found in Appendix D.

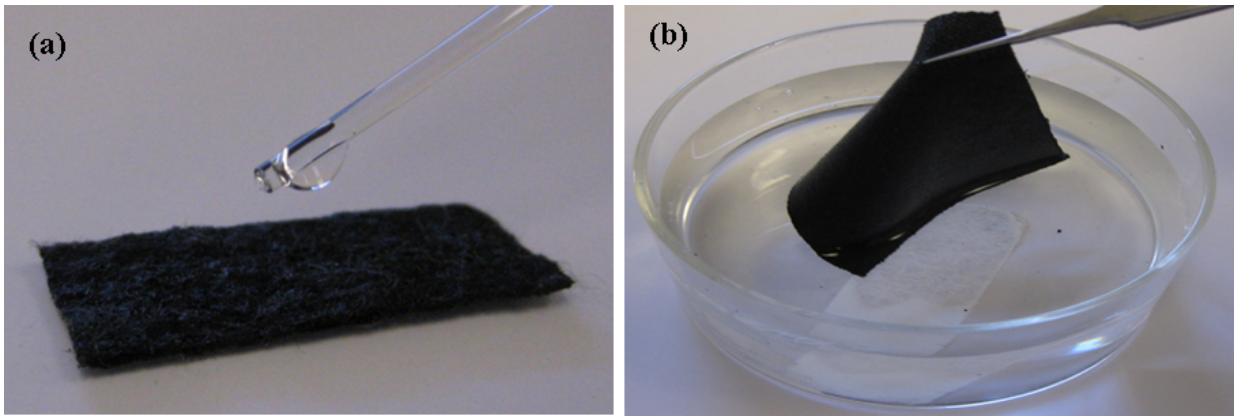

Figure 60. (a) A SWNT/cotton shows high water and organic electrolyte absorption due to the porous structure (left top), and (b) excellent binding between SWNTs and cotton fibers allows the conductive textile to pass the washing in water.

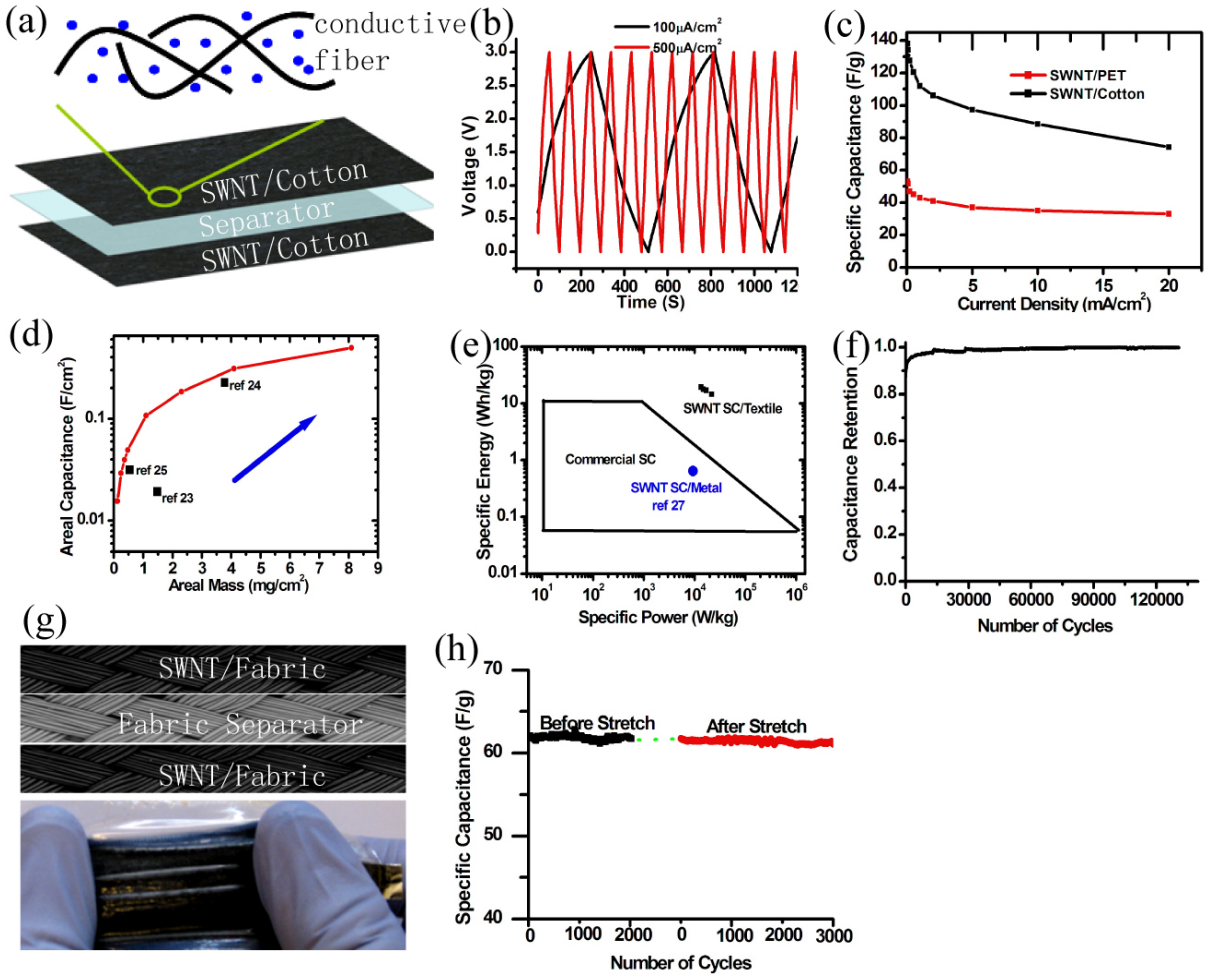

Figure 61. Organic SC with porous textile conductor. (a) SC structure with porous textile conductors as electrodes. The porous structure facilitates the accessibility of electrolyte. (b) SC performance comparison between SWNTs on PET and SWNTs on cotton. (c) Areal capacitance increases with areal mass loading of SWNTs. Comparison with previous studies shows that our porous conductors allow the highest mass loading and highest areal capacitance. The current used is 200 μA cm^{-2}. (d) Ragone plot of commercial SCs, SWNT

SC on metal substrates, and SWNT SC on porous conductors including all the weight. (e) Cycling stability of a SC with porous textile conductor. (f) The schematic drawing of the stretchable SCs with SWNT/fabric as electrodes and with stretchable fabric as the separator (top). A SC under 120% strain (bottom). (g) The specific capacity for a stretchable SC before and after stretching to 120% strain for 100 cycles. The current density is 1 mA cm^{-2}.

In contrast to stretchable conductors reported by others[150,163,164] in which the conductivity decreases with stretching, as our SWNT-fabric is stretched, the conductance increases. It is remarkable that the conductance keeps increasing until the strain reaches a value of 140%, *i.e.* the fabric is stretched to 2.4 times of its original length. This increase in conductance is due to the improvement of the mechanical contacts between fabric fibers which leads to the better electrical contacts for SWNTs. As the strain increases further, the conductance starts to decrease, which is likely due to severe inhomogeneous deformation at large strains, as well as the reduced cross sectional area. Such stretchability of conductive textile could enable various stretchable electronic devices.[163] Fibers in cotton and fabric as well as SWNTs, are known to be resistant to acid, base and organic solvents.[165] Therefore, conductive textiles should also show the same chemical resistance.

Figure 58(d) shows the R_s for e-Cotton after being exposed to water washing, thermal treatment at 200 °C for 6 hours, 4M HNO_3 acid for 30 minutes and 2M KOH for 30 minutes, respectively. Only 2M KOH slightly increases the R_s of conductive cotton, while the others actually decrease the R_s possibly due to the surfactant washing or doping nanotubes. [159-161] The chemical stability of the e-Textile allows a wide range of operations of energy storage devices when the porous textile conductor is used.

6.1.2 Porous textile conductor for energy storage

Porous textile conductor with SWNT coating was tested as both active charge storage electrodes and current collectors in SCs. Figure 61(a) shows the schematic drawing of the SC tested, where 1M $LiPF_6$ electrolyte is used. The porous structure of conductive cotton facilitates the access of electrolyte to SC electrode materials, *i.e.* SWNTs. We tested the SC performance under galvanostatic cycling with a variety of currents (Figure 61(b)). The linear voltage-time profile confirms the charging and discharging of the SCs. To evaluate the advantage of using porous textiles over flat plastic substrates, SCs were assembled and tested with a SWNT loading of 0.24 mg cm^{-2} on a conton sheet and on a Polyethylene terephthalate (PET) substrate. The specific capacitance of SC with porous textiles is around 2-3 times better than that with PET substrates in the range of current density 20 μA cm^{-2} – 20 mA cm^{-2} (Figure 61(c)). 140 F g^{-1} at 20 μA cm^{-2}

and 80 F g^{-1} at 20 mA cm^{-2} are achieved in our conducting textiles, which are comparable to the highest specific capacitance achieved with SWNTs as electrode materials.[158] The higher SC capacitance with SWNTs on textile is likely due to its better ion access in the porous structure. We also use the porous structure to load SWNTs with high mass in our SCs, up to 8 mg cm^{-2}. The areal capacitance increases with the areal mass (Figure 61(d)).[166,167] Compared with the reported values using SWNT electrodes in the literature, our SCs reached much higher areal mass loading and areal capacitance with respect to geometric area of the device. Our devices achieve an areal capacitance equal to 0.48 F cm^{-2}, the highest value reported for SWNTs and close to commercial values. [166,167] [168]

Gravimetric energy density and power are important parameters for SCs in large-scale energy storage. Heavy metal strips are widely used as current collectors in commercial SCs, with light-weight plastic and paper substrate emerging as their replacements.[158,166,167,169] The reported energy density and power density for SWNT electrodes in literature normally only includes the mass of SWNT, which is only ~ 4-10% of the total weight of the device.[166] Due to the light weight of cotton at~ 12 mg cm^{-2}, and the high mass loading of SWNTs allowed by the porous structure of cotton, the weight percentage of SWNTs in our full device is up to ~ 30%. In the Ragone plot (Figure 61(e)), the mass of electrode materials (~ 16 mg cm^{-2}), the cotton (~ 24 mg cm^{-2}), electrolyte (~6 mg cm^{-2}) and separator (~ 2 mg cm^{-2}) are all included in our complete SC device. The reference data indicated by the blue dot is by Niu *et al.*,[170] which is also based on the total mass of the full SC. Our SCs have >10 times higher specific energy than both SCs on metals and commercial SCs at the same specific power. For example, the specific energy reaches a high value of 20 Wh kg^{-1} at a specific power of 10 kW kg^{-1}. The specific power can be further improved by reducing the overall resistance down to ~ 0.1 Ω[171] through means of coating the textiles with even more conductive inks, such as inks that incorporate small amount of metal nanowires. Our textile SC devices show also extremely good cycling stability, with only 2% variation and change in capacitance over a remarkably large cycle number of 130,000 cycles (Figure 61 (f)). The initial increase of the specific capacitance upon cycling is likely due to the improvement in wetting of the SWNTs by the electrolyte. This cycling performance meets the requirements for commercial applications.[172] By using stretchable fabric sheets, instead of cotton sheets, as both the electrode substrates and the separator (Figure 61(g)), we were able to fabricate a fully stretchable SC. Figure 61(h) displays the specific capacitance of for a SC before and after being stretched up to 120% strain 100 times. The mass loading of SWNT is 0.24 mg cm^{-2} and the specific capacitance for the stretchable SC is 62 F g^{-1} at 1 mA cm^{-2}. We observed no change in the specific capacitance after stretching. The stretchable SCs show high Coulomb

efficiency (> 99%) and good cycling stability, < 6% decrease after 8000 cycles, which could be improved with better device sealing. Our stretchable SCs are attractive for the powering up the emerging stretchable or wearable electronics.[163]

One approach to further increase the specific energy of SWNT SCs is to incorporate pseudocapacitor materials having high reversible specific capacitance such as MnO_2, RuO_2 or conducting polymers.[173,174] Previously, pseudocapacitor materials were either mixed with SWNTs which significantly decreases the film conductivity, or coated on the surface of SWNTs but with only very small mass loading, ~ 0.03-0.2 mg cm^{-2} to maintain good electrical contact with SWNTs.[175,176] In our case, as shown in the schematic in Figure 63(a), MnO_2 was uniformly electrodeposited on the SWNTs. This was effective in significantly increasing the mass loading of the pseudocapacitor, while maintaining contact between SWNTs and providing a good electrical conduction path. MnO_2 was deposited along the conducting path which allows its intrinsically good contact with the SWNTs. Here the conductive cotton is without mechanical pressing to use its fluffy structure effectively (Figure 63(b)). The open structure of cotton allows excellent deposition of the MnO_2 conformally along the fibers (Figure 62).

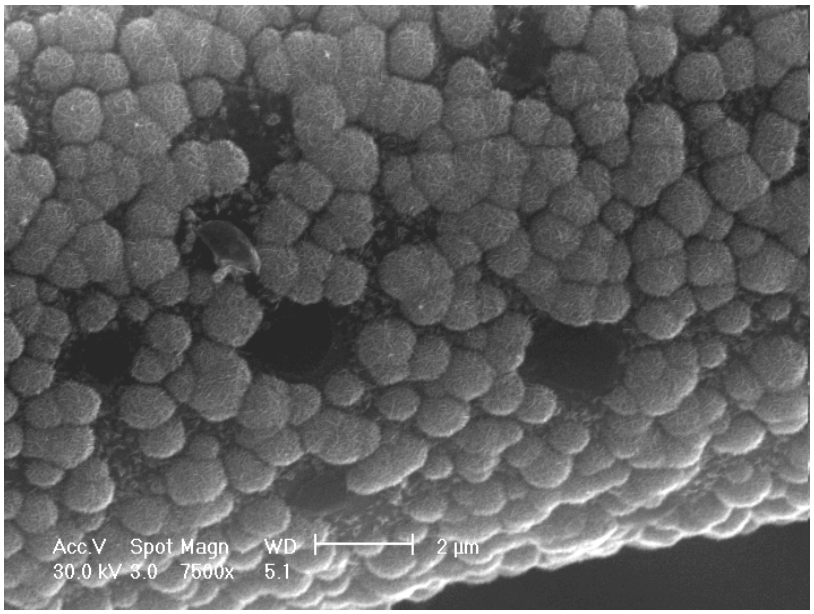

Figure 62. SEM image showing the conformal coating of MnO_2 on top of the cotton fibers inside the cotton sheet.

The deposition is observed not only on the surfaces of the SWNT/cotton but also inside the layers of cotton fibers. The conductive cotton was pelt apart and SEM was taken for the interior cotton (Figure 63(c)). Conformal coating of MnO_2 on cotton fiber surface is observed, and the peeling leads to the partial delamination of MnO_2 from the cotton fibers (Figure 63(c)).

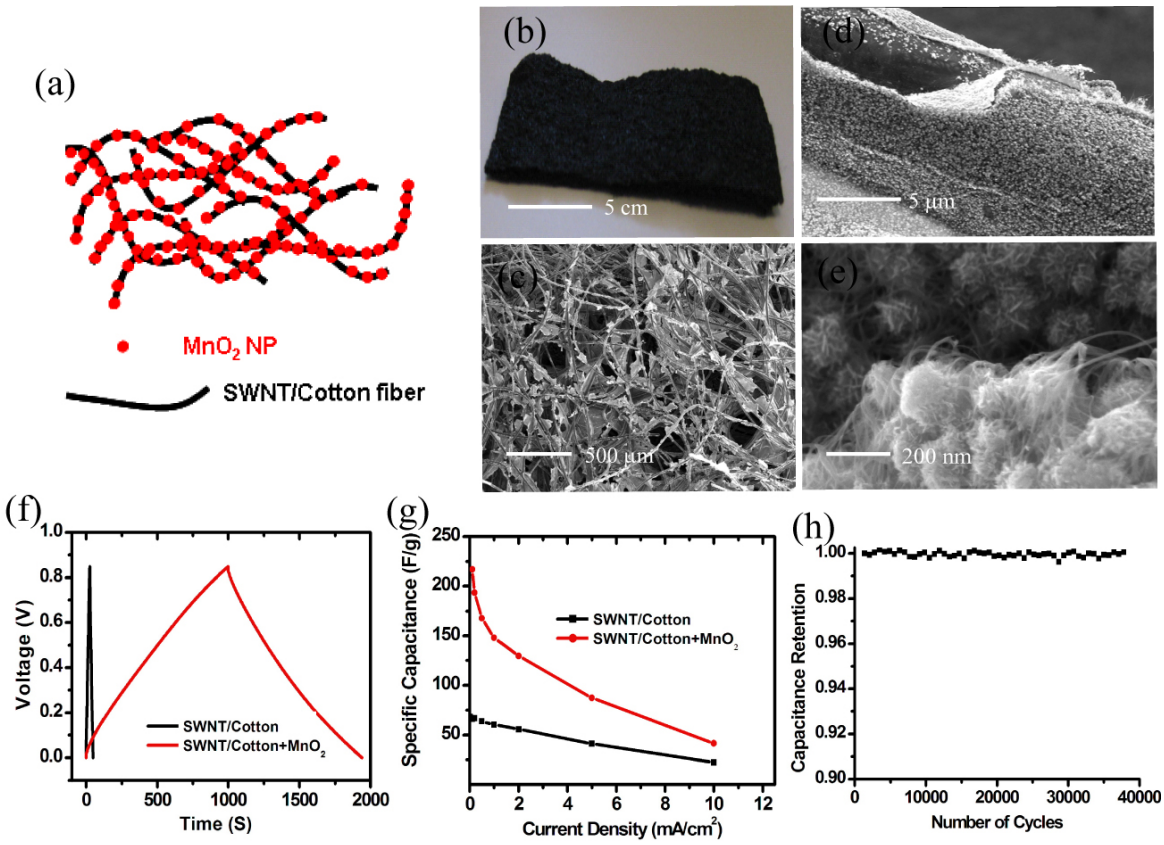

Figure 63. Loading pseudocapacitor or battery materials in porous conductor. (a) Schematic drawing of electrodeposition of MnO_2 onto the SWNT coated textile fibers. Due to the porous structure, the MnO_2 particles are coated on all the textile fibers including those in the interior of the textile. (b) A photo of MnO_2 coated SWNT/Cotton. (c) SEM of a top view of conductive textile after MnO_2 coating. (d) SEM of cotton fibers inside the textile after peeling the fiber layers apart, which shows that the MnO_2 nanoparticles coated the fibers in the interior of the textile, not just the surface layers. (e) High magnification SEM image showing the flower structure of MnO_2 particles on SWNTs. (f) Charge-discharge of aqueous SC with SWNT/cotton electrodes and 2M Li_2SO_4 as the electrolyte with current of 20 μA cm^{-2}. The areal capacitance increases by twenty four-fold after MnO_2 deposition. (g) Specific capacitance of SWNT/cotton with and without MnO_2 for different discharge current densities. (h) Cycling stability of a SC with SWNT-MnO_2 nanoparticles and porous textile conductor.

Figure 63(e) reveals the flower structure of MnO_2 particles deposited on the SWNT surfaces. The MnO_2 nanoparticles are entangled with the SWNTs which ensures good electrical contacts between them. To demonstrate the feasibility of this pseudocapacitor approach for wearable power devices, SCs of SWNT/cotton with MnO_2 were tested with a 2M aqueous Li_2SO_4 electrolyte. In this particular SC, the mass density is 0.24 mg cm^{-2} for SWNTs and is 1.60 mg/cm^2 for the MnO_2 which is 50 times higher than the reported value in literature.[175] The time required to charge the SCs for SWNT/cotton after MnO_2 deposition is significantly increased, suggesting a large charge capacity increase. (Figure 63(f)). The areal capacitance with respect to

the device increases by 24 folds after MnO_2 deposition. In literature, the electrodepostion of oxides typically increase the capacitance by a factor of less than 6.[177] The areal capacitance of device reaches 0.41 F cm^{-2} which is much higher than reported values with SWNT electrodes.[166,167] [168] The specific capacitance data, considering the mass of both SWNTs and MnO_2 is plotted in Figure 63(g). The specific capacitance when including both mass of CNT and MnO_2 increases by a factor of four with MnO_2 deposition. Note that the specific capacitance of SWNTs here with Li_2SO_4 electrolyte is lower than the values in Figure 61(b), which is likely due to the better wetting between the organic electrolyte and SWNTs. Such wearable SCs with salt electrolyte also show excellent cycling stability (Figure 63(h)), with negligible change between the initial and the final specific capacitance over 35,000 cycles. No change is observed between the initial and the final specific capacitance when compared after 35,000 cycles

6.1.3 Conclusions

In this study we report the use of porous conductive textiles as a platform for energy storage device applications. Such porous conductor allows the high mass loading of electrode materials and excellent access of electrolyte to those materials, which leads to outstanding device performance. Such textile-based power will boost the development and application of wearable electronics. With lightweight and cheap cotton or fabrics and existing textile fabrication infrastructure, large-scale energy storage with low material and processing costs is also feasible. When combined with inks of other functional materials, other types of electronics could be created, such as wearable solar cells and batteries. These porous conductors with excellent properties will find a wide range of applications.

6.2 Aqueous Supercapacitors on Conductive Cotton

Wearable electronics is a combination of the advantages of both electronics and fabric. Here we report wearable supercapacitors using cotton fabric as an essential component. Carbon nanotubes are conformally coated onto the fibers, leading to a high conductive interconnecting network. This porous carbon nanotube coating functions as both active material and current collector in this supercapacitor. Aqueous lithium sulfate is used as the electrolyte in the devices, because it presents no safety concerns for human use. The supercapacitor shows high specific capacitance (~ 70-80 F g^{-1} at 0.1 A g^{-1}) and cycling stability (negligible decay after 35,000 cycles). The extremely simple design and fabrication process make it applicable for providing power in practical electronic devices.

6.2.1 Introduction

Wearable electronics represent a developing new class of devices with an array of novel functionalities, which make them ideal for immerging applications such as high-performance sportswear, wearable displays, new classes of portable power and embedded health monitoring devices [178] [145] [146]. All these electronic applications require lightweight, wearable power conversion and storage devices. Textile is a flexible and porous material made by weaving or pressing natural or synthetic fibers, which gives it important properties such as flexibility, stretchability and lightweight. Thus the ideal wearable power would incorporate textile as a component. Among textiles, cotton has the advantage to be an inexpensive natural fiber, which is highly hydrophilic and light.

In this work, we conformally coat single-walled carbon nanotubes (SWNTs) onto cellulose fibers to make porous conductors. The fabrication process is simple and scalable, similar to those widely used for dyeing fibers and fabrics in the textile industry, and already studied by our group in a recently reported paper [179]. The SWNT coating makes these textiles highly conductive, with sheet resistance less than 1 Ω/sq. The conductive textiles show outstanding mechanical and chemical properties. Their porous structure and high surface area are particularly interesting for supercapacitor applications. Different from our previous studies, we report the performance of a symmetric SWNT/cotton supercapacitor in safe aqueous electrolyte, whose conditions are fully compatible with wearable device applications.

6.2.2 CNT ink fabrication

10 mg mL^{-1} SDBS surfactant was dissolved in DI water with the help of bath sonication. Then, laser ablation SWNTs were dispersed in the surfactant solution to a concentration of 1.6 mg mL^{-1}. After bath sonication for 5 minutes, the CNT dispersion was probe-sonicated for 30 minutes at 200 W (VC 505, Sonics Inc).

6.2.3 CNT-Cotton preparation procedure

A fluffy cotton sheet with thickness of ~ 1-2 mm is dipped into the SWNT ink and immediately removed. Due to the strong absorption, the ink quickly coats the textile. The textile with SWNT ink is subsequently dried in oven at 120 °C for 10 minutes to remove water. The mass of the SWCNT is obtained by the weight difference before and after the soaking of the cotton sheet. This process is repeated to increases the SWNT loading in the cotton: Figure 64 shows the accumulated ink mass absorbed per cm^2 by the cotton with different numbers of soaking times.

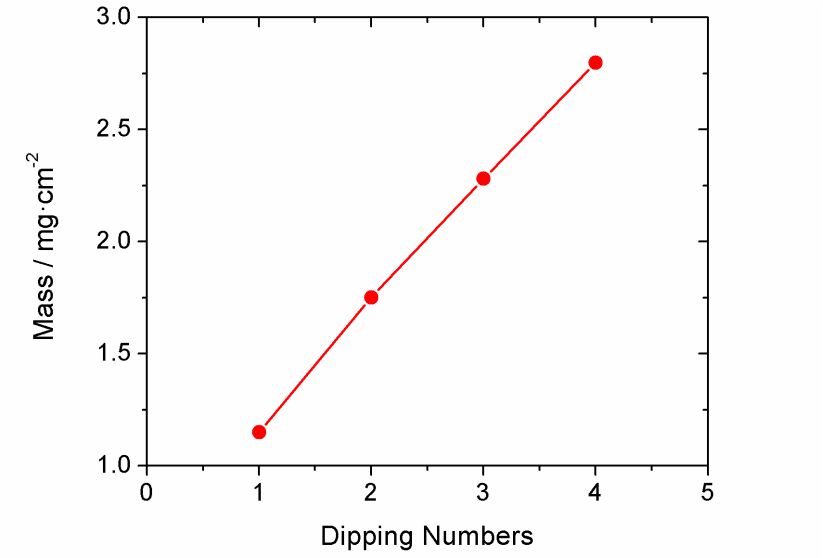

Figure 64. The amount of ink absorbed per area by the cotton sheet at different dipping numbers.

A small variation (<5%) of absorbed ink mass per area is observed when repeating the process.

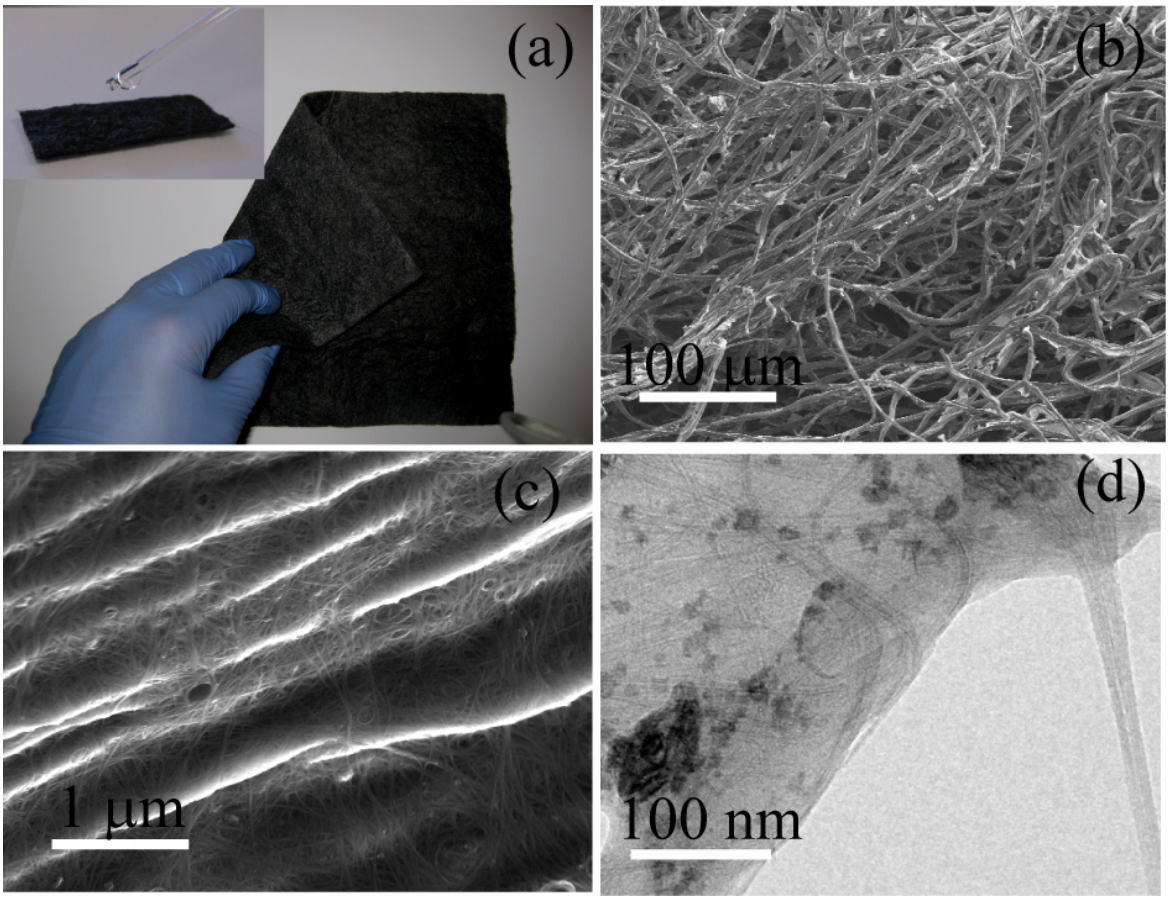

Figure 65. (a) A 15 cm by 15 cm foldable textile conductor based on a cotton sheet with sheet resistance of 2 Ω/sq. The water drop test on SWNT coated cotton shows the highly hydrophilic surface. (b) SEM image of cotton sheet coated with SWNTs. (c) Higher magnification of sample from (b) to show conformal coating of CNTs on cotton surface. (d) TEM of SWNTs on cotton fiber. There is no evidence of SWNTs agglomeration.

SEM images of Figure 65(b) reveal the macro porous structure of a cotton sheet and Figure 65(c) the conformal coating of SWNTs onto the fibers. This conformal coating is a result of the mechanical flexibility of the individual SWNTs and the strong binding energy between SWNTs and cotton fibers [157], accounting also for the high conductivity of the textile. Previous studies have shown that SWNT films have micro scale porosity which is required to maximize the specific capacitance [158]. The microporous structure on top of the macroporous textile leads to what we call a "double porous structure" that facilitates the easy access of electrolyte ions to the SWNTs, which is essential for high power SC applications. TEM images of the SWNT-cotton fiber (Figure 65(d)) show that the SWNTs are well bonded to the fiber, forming a cross-linked network, which provide conducting pathways.

Such porous textile conductors demonstrate excellent electrical, mechanical and chemical resistance performance [179] suggesting that the SWNTs adhere very strongly to the cotton fibers, which is critical for wearable electronic and power devices. Such strong binding may be due to the following:

1) The Large Van der Waals force and hydrogen bonding existing between SWNTs and the textile fibers [157].

2) The flexibility of SWNTs allow them to be conformally adhered to the surface of cotton fibers, maximizing the surface contact area between SWNTs and textile fibers [162].

3) The cotton fiber structure is comprised of multiple individual cotton fibrils, which are in turn composed of multiple microfibrils, bundled together. The microfibrils are made of poly-D-glucose chains, usually arranged in crystalline, or partially crystalline, domains. This structure allows the fibers to absorb large amounts of water, or other polar solvents.

The superior mechanical adhesion of SWNTs on cotton is essential for high-speed roll-to-roll fabrication and energy storage device stability.

6.2.4 Surfactant removal

The material prepared as previously mentioned is highly hydrophilic, due to the surfactant still present on the surface. However it needs to be removed to avoid side reactions, which generates irreversible specific charge and self-discharge phenomena. The surfactant removal is essential for the final device performance, especially its cyclability and coulombic efficiency. Washing with abundant DI water and pressing with a grid is sufficient to remove the surfactant. A simple rule of thumb to evaluate if all the surfactant has been removed is to press the fabric and see if bubbles are produced.

6.2.5 CNT-Cotton pretreatment

After the SDBS removal the textile exhibits a hydrophobic behavior which would be incompatible with its application in a water based electrolyte. To improve the surface hydrophilicity and remove the last traces of surfactant the textile is dipped into a 4M HNO_3 solution for about 6h and then washed again with DI water to remove the acid. Treating the nanotubes with nitric acid introduces a larger number of oxygen-containing functional groups such as carboxyl, lactones and phenols and creates a more hydrophilic surface structure [79]. The nitric acid treatment also has two other advantages: it helps to remove impurities, such as amorphous carbon and catalytic metal particles (both of which contribute to self discharge problems) [80]; the treatment also induces hole doping, which decreases the resistivity of the nanotubes [81 82 83]. Fig. 2(a) shows the wettability test of the substrate after the acid treatment.
As mentioned, the acid wash is also the final step in the surfactant removal process. To prove the success of the washing process in removing all the surfactant it is enough to observe the OCV value against the RE. If the value lies around 0.0 V vs. RE this means that there is still some surfactant left, and it is necessary to repeat the washing process. The observed OCV value is due to an unidentified secondary reaction involving the surfactant. If the value lies around 0.4 V vs. RE, we can be sure that all the surfactant has been eliminated and proceed with the electrochemical tests.

6.2.6 Electrochemical test

The performances of the CNT-cotton electrodes previously prepared were tested in an aqueous 2M Li_2SO_4 solution. The electrolyte was chosen for the following reasons:

1) Sulfates conjugate electrochemical stability in the potential range investigated and they are inexpensive.
2) Among the sulfates, lithium sulfate has the advantage of a higher solubility in water, as compared to the less expensive sodium and potassium salts.
3) A 2M solution of lithium sulfate has an acidic pH (around 3.2); a slow H^+ ionsorption has been reported in the literature, granting an additional capacity [180].

Before each measurement the electrolyte was purged with nitrogen gas for 30 min to remove the dissolved oxygen which could give rise to an irreversible specific charge. All the measurements were performed under nitrogen atmosphere.

6.2.7 Results and discussion

Figure 66 reports galvanic cycles (100 µA cm^{-2}) of the SWCNT/Cotton material at 4 different CNT loadings (0.12, 0.24, 0.36, 0.47 mg cm^{-2}), corresponding to 4 subsequent "dip and dry" steps. From now on we will refer to them as cotton #1, #2, #3, #4. As one can observe, the specific charge (represented by the area underneath the curves) increases with the CNT loading.

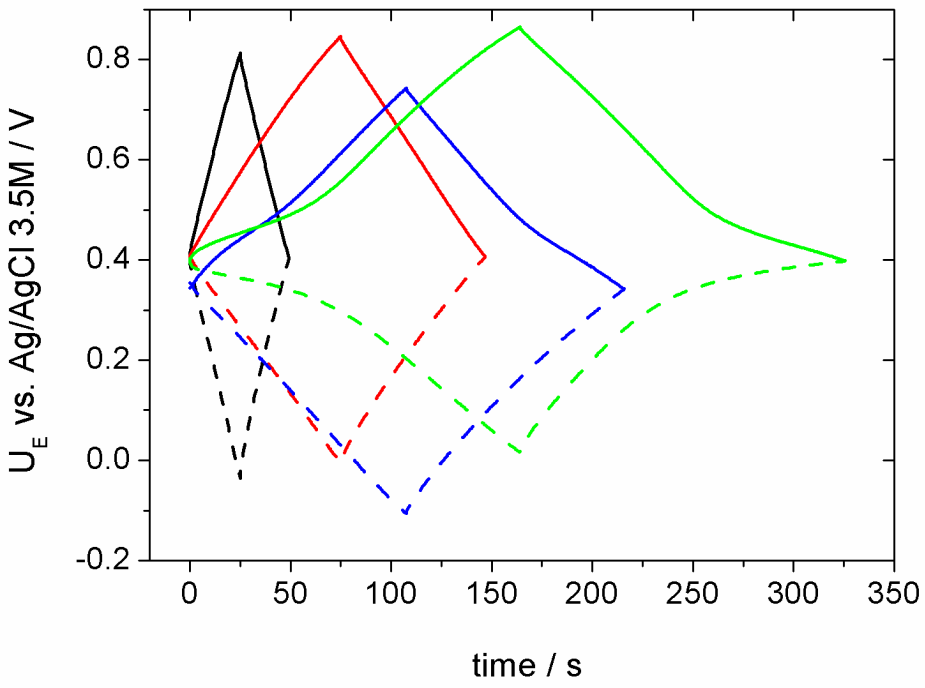

Figure 66. Galvanostatic cycling at apparent current density of 0.1 mA cm^{-2} for working (continuous) and counter (dotted) SWNT/cotton electrodes vs. Ag/AgCl 3.5M in 2M Li_2SO_4 electrolyte, at different mass loading. Black curve – cotton #1 (0.12 mg cm^{-2}), red curve – cotton #2 (0.24 mg cm^{-2}), blue curve – cotton #3 (0.36 mg cm^{-2}), green curve – cotton #4 (0.47 mg cm^{-2}).

In the presence of a reference electrode the behavior of both positive and negative electrodes can be monitored during the cycling. With this approach some irreversible behavior in the cathodic side can be easily identified during the first few cycles: the reason is the low hydrogen evolution overpotential on CNT, as already reported in the literature [180]. Moreover, the shape of the curve, especially the one relative to the high CNT loadings, suggests the presence of a slow ionsorption, granting an additional specific charge at low scan rates.

To deeply investigate this phenomenon, the differential curves are reported in Figure 67 for the current intensity of 100 µA. We want to stress that at higher mass loading (lower specific current) a peak appears in the positive electrode of the supercapacitor around 0.4 V vs. Ag/AgCl 3.5M. This peak is evidence of an electrochemical adsorption or an ionsorption process that occurs slowly; at higher specific current it disappears.

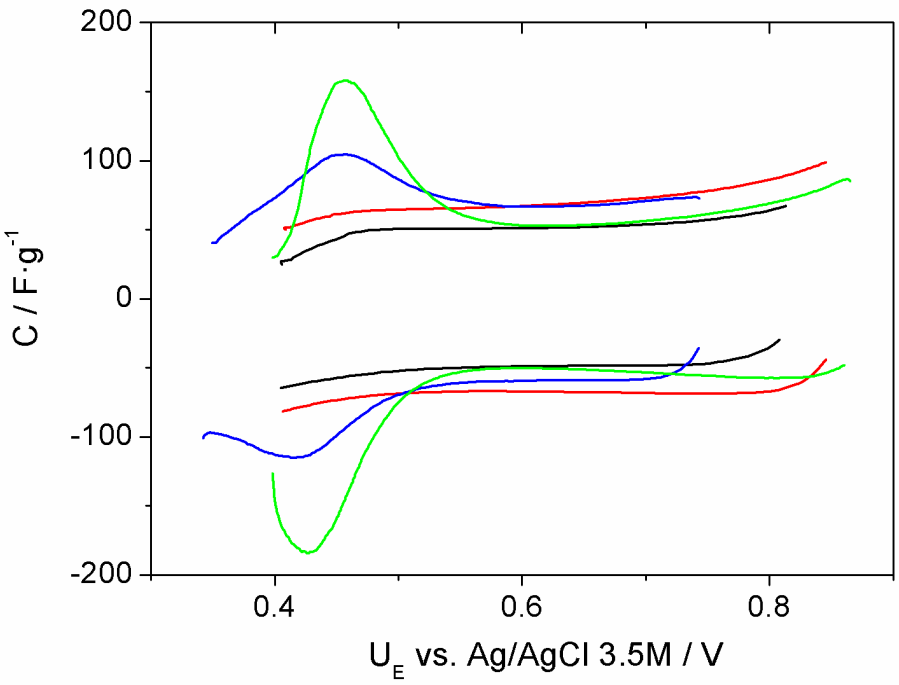

Figure 67. Differential curves relative to the positive electrode at different SWNT loading. Black curve – cotton #1 (0.12 mg cm^{-2}), red curve – cotton #2 (0.24 mg cm^{-2}), blue curve – cotton #3 (0.36 mg cm^{-2}), green curve – cotton #4 (0.47 mg cm^{-2}).

The electrochemical adsorption/ionsorption is even more evident in the Nyquist plots of the EIS performed on the electrodes. From the shape of the Nyquist plot and the value of the impedance at different mass loading, we can obtain the following information:

1) The distorted capacitive semicircle at high frequencies is evidence of a current distribution along the thickness of the electrode and of an electrochemical process different from the simple double layer charging/discharging [181 182 183].
2) The increase in the capacitive part of the impedance after the high frequency semicircle is due to the blocking nature of the electrochemical process, thus indicating that it is an adsorption or an ionsorption.
3) The small difference in the value of the imaginary part of the impedance at low frequencies between the different mass loadings suggests that the electrochemical process is limited by the transport in the pores of the adsorbed species. Also the inflection point (*) at low frequencies is indicative of such phenomenon.
4) After reaching a mass loading of 0.24 mg·cm^{-2}, the internal resistance of the supercapacitor is due to the transport of ions in the electrolyte.

From all the previous consideration, we presume that the ionsorption is due to the H_3O^+. In fact, there are four main species in solution: Li^+, SO_4^{--}, H_3O^+ and OH^-. The Li^+ and SO_4^{--} are present

in such a high concentration that their ionsorption shouldn't be transport limited. Among H_3O^+ and OH^-, the latter is present in such a low concentration that it is unable to justify all the specific charge under the peak in Figure 67, green curve. Thus it is concluded that the hydronium ionsorption is responsible for the phenomenon.

In Figure 68 are reported the specific capacitances at various specific currents. The curve representing the lowest CNT content shows the worst performances in terms of specific capacitance (55 F g^{-1}) and capacitance retention at higher specific currents: this behavior is due to the low electrical conductivity of the substrate (as also indicated by the Nyquist plot, Figure 69).

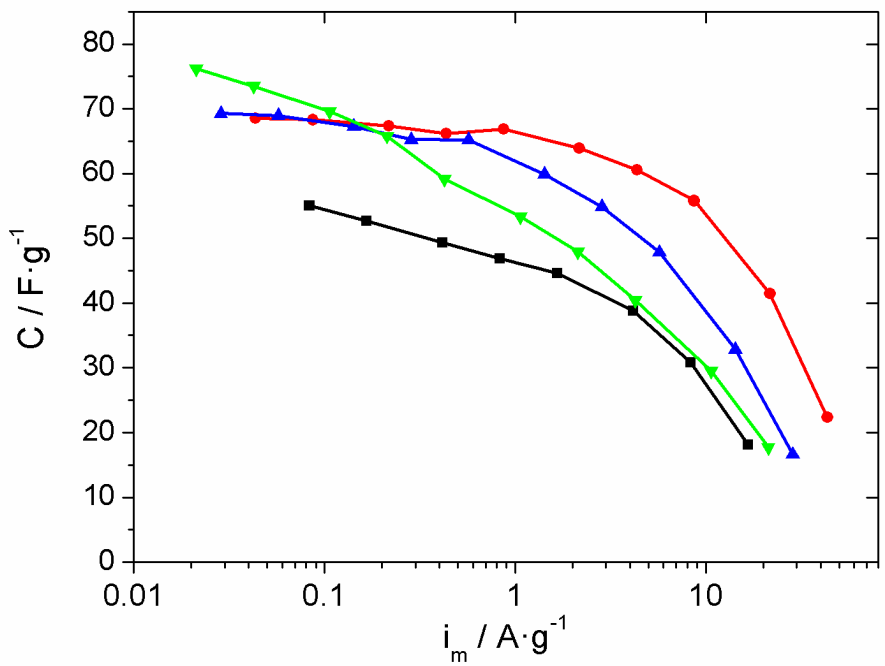

Figure 68. Specific capacitance versus specific current for SWNT/cotton electrodes at different SWNT loading. Black curve – cotton #1 (0.12 mg cm^{-2}), red curve – cotton #2 (0.24 mg cm^{-2}), blue curve – cotton #3 (0.36 mg cm^{-2}), green curve – cotton #4 (0.47 mg cm^{-2}).

At this mass loading, the CNT content is insufficient to form a good interconnecting network. For sample cotton #2 the specific capacitance increases to about 70 F g^{-1} and it is quite constant in the current range from 10 µA g^{-1} to 1 mA g^{-1}.

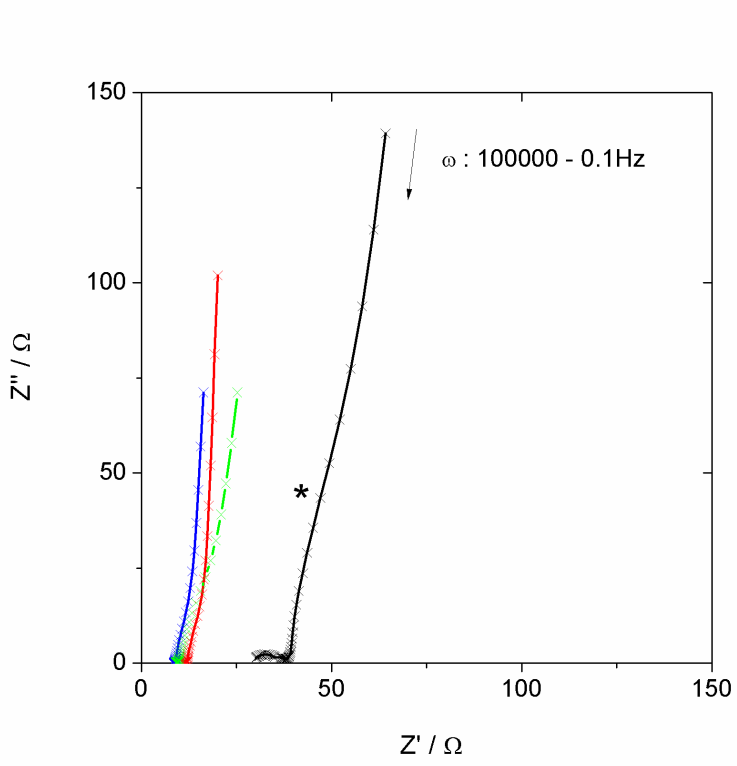

Figure 69. Nyquist plot of supercapacitors with different SWNT loading. Black curve – cotton #1 (0.12 mg cm^{-2}), red curve – cotton #2 (0.24 mg cm^{-2}), blue curve – cotton #3 (0.36 mg cm^{-2}), green curve – cotton #4 (0.47 mg cm^{-2}).

Comparing cotton #2 and cotton #3, it is found that the performances are quite similar, in terms of maximum specific capacitance, but the specific capacitance decreases at lower current values in sample cotton #3. For cotton #4 the initial specific capacitance is higher (around 80 F g^{-1}), but it continuously decreases with the current. This behavior can be interpreted by using the framework of the theory of current density distribution in porous electrodes. This theory can be summarized by the following equation:

$$\frac{\partial^2 \Delta\Phi}{\partial x^2} = \frac{\rho_s I}{af} \qquad \text{(Equation 1)}$$

where $\mathbf{\Delta\Phi}$ is the potential drop at the solid/liquid interface, **x** represents the position within? the porous electrode, ρ_s is the resistivity of the electrolyte solution, **a** the characteristic length of the porous electrode, **f** the void fraction, and **I** the current density at the solid/liquid interface (which is dependent on the position **x**). The characteristic length, **a**, increases by increasing the ratio between the volume of the electrode and the active surface area, V/A. Equation (1) is valid when

the electric resistance of the solid phase in the porous electrode is negligible. The behavior of the electrodes at different current densities is better understood when the areal capacitance with respect to the mass loading is reported (see Figure 70).

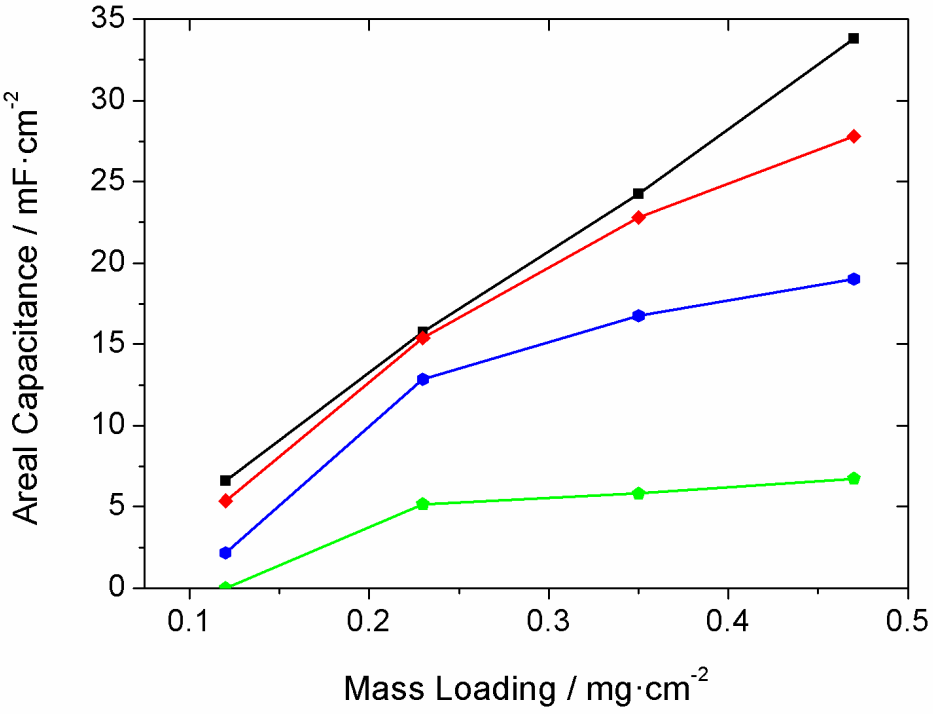

Figure 70. Areal capacitance versus mass loading for different apparent current densities: black curve – cotton #1 (0.01 mA cm^{-2}), red curve – cotton #2 (0.2 mA cm^{-2}), blue curve – cotton #3 (2 mA cm^{-2}), green curve – cotton #4 (10 mA cm^{-2}).

When the apparent current density (the current density per geometrical area) is low (black curve), Equation (1) reduces to a constant current density distribution along the pores of the electrode, and therefore, the areal capacitance increases linearly with the mass loading. By increasing the apparent current density, the electrodes with a larger **a** value (lower mass loading) still charge homogeneously, while the one with lower **a** (higher mass loading) show a distribution of current density, and consequently a distribution of surface charge. As observed in Figure 70 for the curves b-d, the higher the apparent current density, the stronger the deviation from linearity. The deviation from linearity is always reducing the maximum amount of areal capacitance. Depending on the application, the optimal loading is easily predicted.

In Figure 71 the cycling stability of the SWNT/cotton#2 device was tested at an absolute current of 1 mA·cm^{-2}; no fading was observed after 35,000 cycles. The coulombic efficiency at the 35,000th cycle is higher than 99% and the specific capacitance value lies around 45 F g^{-1}.

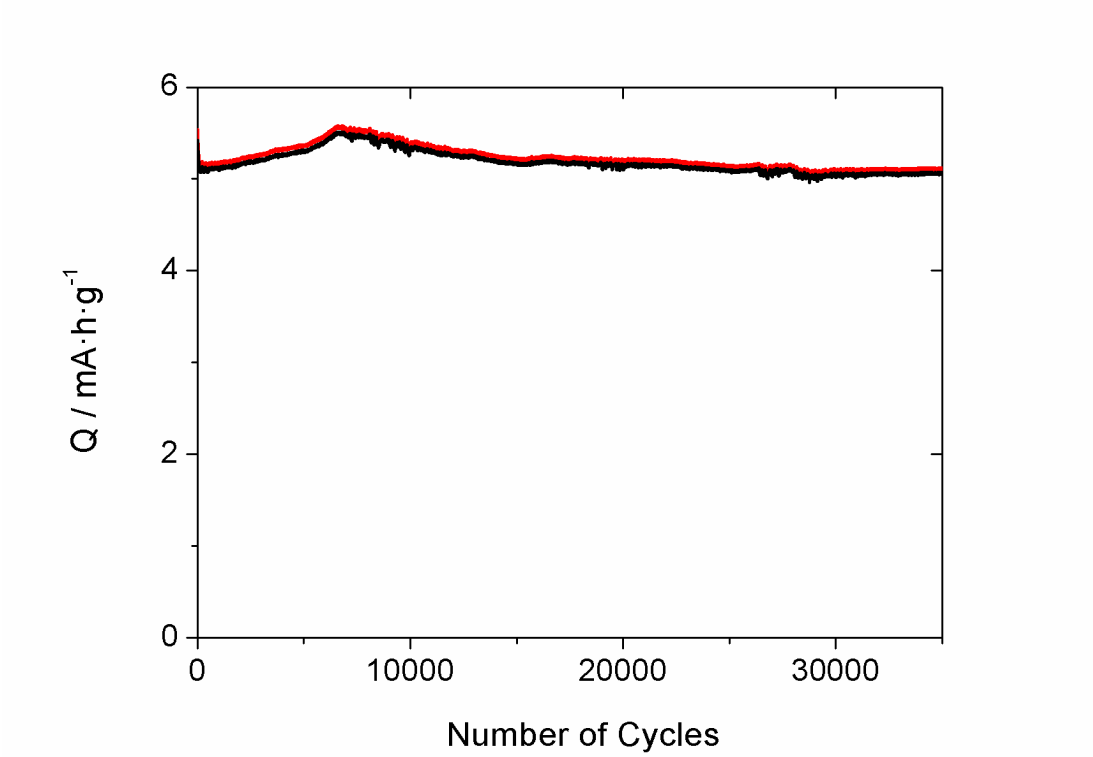

Figure 71. Cycling stability of SWNT/cotton #2 supercapacitor device in 2M Li_2SO_4 aqueous electrolyte at 1 mA cm^{-2} apparent current density.

6.2.8 Conclusions

In the present study we reported a supercapacitor using a conformally coated SWNT/cotton fabric as both active material and current collector (resistance lower than 1 Ω/sq). We demonstrated excellent cycling performances (good capacity retention after 35,000 cycles) and high specific capacitances (70-80 F g^{-1} at 0.1 mA cm^{-2}). The device as prepared is fully wearable: from textile (cotton) to the lithium sulfate electrolyte, which is compatible with the human body. It can also be integrated into wearable devices. By means of impedance spectroscopy and differential curves, we highlighted an additional reversible capacitance due to a slow ionsorption process.

Potential improvements in the future need to be directed towards an asymmetric supercapacitor; the hydrogen evolution overpotential limits the operative voltage range, and therefore the achievable high power limit.

CONCLUSIONS

The complex oxidation of glucose at the surface of gold electrodes was studied in detail in different conditions of pH, buffer and halide concentration. As observed in previous studies, an oxidative current peak occurs during the cathodic sweep showing a highly linear dependence on glucose concentration, when other electrolyte conditions are unchanged. The effect of the different conditions on the intensity of this peak has stressed the limitations of the previously proposed mechanisms. A mechanism able to explain the presence of this oxidative peak was proposed in which the key step is the competitive adsorption at the active sites of the ionic species present in the solution (phosphate buffer, chlorides and OH^-) and the substrate (glucose). Simulations of the proposed mechanism have supported the plausibility of the mechanism.

The application of the above mentioned peak in blood glucose sensing has been hindered by the presence of inhibitors: chlorides amino acids and human albumin. Among them chlorides are the most problematic because of their high concentration in the blood (about 0.1 M) and the difficulty inherent in trying to separate them from glucose. In order to overcome this problem we developed a four-step, three electrode (silver gauze, gold pin and platinum counter electrode) technique. In the first step a silver gauze working electrode is oxidized to silver chloride, while water is reduced at the platinum counter electrode. In the overall reaction, for every chloride removed, a hydroxide ion is generated shifting the solution pH from 7.4 to 11.5. In the second step the gold pin electrode surface is oxidized to gold hydroxide and subsequently reduced in the third step: once the gold surface is regenerated, glucose can be re-adsorbed and oxidized giving rise to the sensing peak. In the last (fourth) step, the silver gauze (partially covered with silver chloride from step 1) is reduced and regenerated, ready for the next sensing. For the first time, an electrochemical glucose sensor able to work in the presence of chlorides and with higher accuracies and sensitivities than an enzymatic device was proposed. All the materials used in the prototype (silver, platinum and gold) are fully bio-compatible thus prefiguring an application in implantable glucose sensors, the future glucose meters technology.

The direct oxidation of glucose to produce electrical energy has been widely investigated because of renewability, abundance, high energy density and easy handling of the carbohydrate. Most of the previous studies were conducted in extreme conditions in order to achieve complete glucose oxidation to CO_2, neglecting the carbohydrate chemical instability that generally leads to useless by-products mixtures. Instead the partial oxidation to gluconate, originally studied for implantable fuel cells, has the advantage of generating a commercially valuable chemical. For this reason, we started optimizing fuel composition and operating conditions in order to

selectively oxidize glucose to gluconate, maximizing the power density output of a standard commercial platinum based anode material. A deep electrochemical characterization concerning reversible potential, cyclic voltammetry and overpotential measurements have been carried out at 25°C in the D-(+)-glucose concentration range $1.0 \cdot 10^{-2}$ to 1.0M. NMR and EIS investigation clarified the role of the buffer (Na_2HPO_4/NaH_2PO_4) in enhancing the electrochemical performance: it changes the reaction rates and steps; it increases the amount of β form of glucose; it increases the conductivity of the solution; it may adsorb at the platinum surface of platinum and subtract active sites for the electrooxidation of glucose as already highlighted for gold electrodes. Moreover the presence of the buffer not only stabilizes the potential, but also improves the electrochemical performances of the anode in term of exchange current density. Such behavior is not ascribable to the chemical interaction with glucose, as demonstrated by NMR measurements, but to the interaction with the anode material as indicated by the decrease of all the resistive components in the EIS measurement.

In order to improve the anode performance of the previously discussed glucose-gluconate FCs, the electrocatalytic properties of nanostructured gold electrodes were investigated, by cyclic voltammetry, and compared with commercially available polycrystalline gold electrodes. These nanostructured electrodes were prepared by depositing gold nanoparticles from a colloidal dispersion (sol) onto different carbonaceous conductive supports: glassy carbon, carbon cloth and graphite paper. The gold sol was prepared reducing an aqueous solution of tetrachloroauric acid with sodium borohydride. The gold particles (average size 100 nm) exhibit better electrocatalytic properties with respect to commercially available polycrystalline electrode for glucose oxidation. A surface treatment of the carbonaceous conductive supports with warm concentrated nitric acid resulted in an improved adhesion of the gold nanoparticles. Gold on treated carbon cloth turned out to be a very promising anode for glucose electrooxidation. On the basis of the information acquired in the above mentioned studies, we came out with a new anode for glucose-gluconate direct oxidation fuel cells prepared by electrodeposition of gold nanoparticles on what we called a “conductive energy textile” realized by conformally coating polyester textile substrates with single walled carbon nanotubes (SWNT).The electrodeposition conditions have been optimized in order to obtain uniform distribution of gold nanoparticles in the 3D porous structure of the conductive textile. The electrochemical characterization, carried out by means of cyclic voltammetry, showed higher current densities with respect to the previously reported materials.

I also worked on microbial glucose electrooxidation applied to microbial fuel cells. As a new member in the fuel cell family, microbial fuel cells (MFCs) are devices that convert chemical

energy into electrical energy by the catalytic activity of microorganisms. The most promising application of this technology is to harvest energy from undesirable fuel sources, such as the organic matter in domestic wastewater, marine sediment, or human excrement in space. A novel carbon nanotube-cotton (CNT-cotton) composite material with high conductivity and high porosity was proposed to be used as anode for achieving high-performance MFCs. Scanning electron microscope (SEM) images of microorganisms growing on the CNT layer provided the direct evidence to support the biocompatibility of the CNTs and their feasibility to be used as the anode in MFCs. The randomly intertwined CNT-cotton fibers create a 3D active space for biofilm growth, and meanwhile, the incompact macroporous structure allows efficient mass transfer for microbial metabolism inside the anode. Furthermore, the coated CNTs significantly improve the mechanical binding as well as the electrical conductivity between the exoelectrogenic microorganisms and the CNT-cotton anode. Compared to commercial carbon cloth anode, the CNT-cotton anode achieves 64% higher power density and 75% higher energy recovery efficiency in MFCs.

Air is considered to be the most suitable oxidant for field scale MFCs, because it is free and inexhaustible. However, the oxygen reduction efficiency is highly constrained by the specific operating conditions of MFCs, such as ambient temperature and mostly neutral pH. Thus, cathode performance often limits the power output of MFCs. Moreover, cathode usually accounts for the greatest part of the total capital cost of a MFC, mainly because of the use of precious metal catalyst like Pt. Therefore, improving the cathode performance decreasing the catalyst loading represents a critical issue for researchers working on MFCs. A new CNT-textile-Pt cathode specially designed for aqueous-cathode MFCs was obtained by electrochemically depositing Pt nanoparticles on a macroporous CNT-textile substrate. This CNT-textile-Pt cathode shows two orders higher of surface area utilization efficiency than the commercial carbon cloth (CC)-Pt cathode. Assisted by the additional catalytic activity of CNTs, the MFCs equipped with CNT-textile-Pt cathodes achieve higher power density (2.14-fold) with lower Pt loading (19.3%). Moreover, the synthesis process of CNT-textile-Pt is simple and scalable. Thus, CNT-textile-Pt is promising to function as cathodes for large scale high performance aqueous-cathode MFCs.

In parallel to glucose electrooxidation a new stretchable, porous conductive energy textile has been developed. Recently there is strong interest in lightweight, flexible and wearable electronics to meet the technological demands of modern society. Integrated energy storage devices of this type are a key area that is still significantly underdeveloped. We developed wearable power devices using everyday textiles as the platform. With an extremely simple

"dipping and drying" process using single-walled carbon nanotube (SWNT) ink, we produced highly conductive textiles with conductivity of 125 S cm^{-1} and sheet resistance less than 1 Ω/sq. Such conductive textiles show outstanding flexibility and stretchability, and demonstrate strong adhesion between the SWNTs and the textiles of interest. Supercapacitors (SC) made from these conductive textiles show high areal capacitance, up to 0.48 F cm^{-2}, and high specific energy. We demonstrated that the loading of pseudocapacitor materials into these conductive textiles leads to a twenty four-fold increase of the areal capacitance of the device.

Moreover, supercapacitors have been fabricated using the conductive energy textile as both active material and current collector (resistance lower than 1 Ω/sq). The device has excellent cycling performance (good capacity retention after 35,000 cycles) and high specific capacitance (70–80 F g^{-1} at 0.1 mA cm^{-2}). The as prepared device is fully wearable since both the textile (cotton) and the lithium sulfate electrolyte are compatible with the human body. It can also be integrated into wearable devices. By means of impedance spectroscopy and differential curves, we have highlighted an additional reversible capacitance due to a slow ionsorption process.

APPENDIX

Appendix A: glucose properties

Glucose	
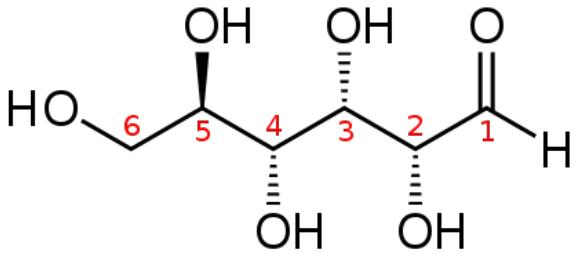	
Properties	
Molecular formula	$C_6H_{12}O_6$
Molar mass	180.16 g mol^{-1}
Exact mass	180.063388
Density	1.54 g cm^{-3}
Melting point	α-D-glucose: 146°C β-D-glucose: 150°C
Solubility in water	91 g/100 ml (25 °C)
Solubility in methanol	0.037 M
Solubility in ethanol	0.006 M
Solubility in tetrahydrofuran	0.016 M
Thermochemistry	
Standard enthalpy of formation $\Delta_f H^0_{298}$	-1271 kJ mol^{-1}
Standard enthalpy of combustion $\Delta_c H^0_{298}$	- 2805 kJ mol^{-1}
Standard molar entropy S^0_{298}	209.2 JK^{-1} mol^{-1}

Appendix B: constituents of human blood (adapted from [184])

Blood accounts for 7% of the human body weight, with an average density of approximately 1060 kg/m^3, very close to pure water's density of 1000 kg/m^3.

The average adult has a blood volume of roughly 5 liters, composed of plasma and several kinds of cells (*corpuscles*); these formed elements of the blood are erythrocytes (red blood cells), leukocytes (white blood cells), and thrombocytes (platelets). By volume, the red blood cells constitute about 45% of whole blood, the plasma constitutes about 54.3%, white cells constitute 0.7%.

Cells

One microliter of blood contains:

- *4.7 to 6.1 million (male), 4.2 to 5.4 million (female) erythrocytes:* in mammals, mature red blood cells lack a nucleus and organelles. They contain the blood's hemoglobin and distribute oxygen. The red blood cells (together with endothelial vessel cells and other cells) are also marked by glycoproteins that define the different blood types. The proportion of blood occupied by red blood cells is referred to as the hematocrit, and is normally about 45%.
- *4,000-11,000 leukocytes:* White blood cells are part of the immune system; they destroy and remove old or aberrant cells and cellular debris, as well as attack infectious agents (pathogens) and foreign substances.
- *200,000-500,000 thrombocytes:* thrombocytes, also called *platelets*, are responsible for blood clotting (coagulation). They change fibrinogen into fibrin. This fibrin creates a mesh onto which red blood cells collect and clot, which then stops more blood from leaving the body and also helps to prevent bacteria from entering the body.

Plasma

About 55% of whole blood is blood plasma, a fluid that is the blood's liquid medium, which by itself is straw-yellow in color. The blood plasma volume totals of 2.7 – 3.0 liters in an average human. It is essentially an aqueous solution containing 92% water, 8% blood plasma proteins, and trace amounts of other materials. Plasma circulates dissolved nutrients, such as glucose, amino acids, and fatty acids (dissolved in the blood or bound to plasma proteins), and removes waste products, such as, carbon dioxide, urea, and lactic acid.

Other important components include:

Serum albumin

Blood-clotting factors (to facilitate coagulation)

Immunoglobulins (antibodies)

Lipoprotein particles

Various other proteins

Various electrolytes (mainly sodium and chloride)

The term **serum** refers to plasma from which the clotting proteins have been removed. Most of the proteins remaining are albumin and immunoglobulins.

Constitution of normal blood	
Parameter	Value
Hematocrit	45 ± 7 (38 – 52%) for males 42 ± 5 (37 – 47%) for females
pH	7.35 – 7.45
pO_2	10 – 13 kPa (80 – 100 mm Hg)
pCO_2	4.8 – 5.8 kPa (35 – 45 mm Hg)
HCO_3^-	21 mM – 27 mM
Oxygen saturation	Oxygenated: 98 – 99% Deoxygenated: 75%

The normal pH of human arterial blood is approximately 7.40 (normal range is 7.35 – 7.45), a weakly alkaline solution. Blood that has a pH below 7.35 is too acidic, whereas blood pH above 7.45 is too alkaline. Blood pH, partial pressure of oxygen (pO_2), partial pressure of carbon dioxide (pCO_2), and HCO_3 are carefully regulated by a number of homeostatic mechanisms, which exert their influence principally through the respiratory system and the urinary system in order to control the acid-base balance and respiration. Plasma also circulates hormones transmitting their messages to various tissues. The list of normal reference ranges for various blood electrolytes is extensive.

Appendix C: Diabetes Mellitus (adapted from [185])

Diabetes mellitus, often simply referred to as diabetes—is a condition in which a person has high blood sugar, either because the body does not produce enough insulin, or because cells do not respond to the insulin that is produced. This high blood sugar produces the classical symptoms of polyuria (frequent urination), polydipsia (increased thirst) and polyphagia (increased hunger).

There are three main types of diabetes:

- *Type 1 diabetes*: results from the body's failure to produce insulin, and presently requires the person to inject insulin.
- *Type 2 diabetes*: results from insulin resistance, a condition in which cells fail to use insulin properly, sometimes combined with an absolute insulin deficiency.
- *Gestational diabetes*: is when pregnant women, who have never had diabetes before, have a high blood glucose level during pregnancy. It may precede development of type 2 DM.

Other forms of diabetes mellitus include congenital diabetes, which is due to genetic defects of insulin secretion, cystic fibrosis-related diabetes, steroid diabetes induced by high doses of glucocorticoids, and several forms of monogenic diabetes.

All forms of diabetes have been treatable since insulin became available in 1921, and type 2 diabetes may be controlled with medications. Both type 1 and 2 are chronic conditions that usually cannot be cured. Pancreas transplants have been tried with limited success in type 1 DM; gastric bypass surgery has been successful in many with morbid obesity and type 2 DM. Gestational diabetes usually resolves after delivery. Diabetes without proper treatments can cause many complications. Acute complications include hypoglycemia, diabetic ketoacidosis, or nonketotic hyperosmolar coma. Serious long-term complications include cardiovascular disease, chronic renal failure, retinal damage. Adequate treatment of diabetes is thus important, as well as blood pressure control and lifestyle factors such as smoking cessation and maintaining a healthy body weight.

As of 2000 at least 171 million people worldwide suffer from diabetes, or 2.8% of the population. Type 2 diabetes is by far the most common, affecting 90 to 95% of the U.S. diabetes population.

Definition

The term diabetes, without qualification, usually refers to diabetes mellitus, which roughly

translates to excessive sweet urine (known as "glycosuria"). Several rare conditions are also named diabetes. The most common of these is diabetes insipidus in which large amounts of urine are produced (polyuria), which is not sweet (insipidus meaning "without taste" in Latin).
The term "type 1 diabetes" has replaced several former terms, including childhood-onset diabetes, juvenile diabetes, and insulin-dependent diabetes mellitus (IDDM). Likewise, the term "type 2 diabetes" has replaced several former terms, including adult-onset diabetes, obesity-related diabetes, and non-insulin-dependent diabetes mellitus (NIDDM). Beyond these two types, there is no agreed-upon standard nomenclature. Various sources have defined "type 3 diabetes" as: gestational diabetes, insulin-resistant type 1 diabetes (or "double diabetes"), type 2 diabetes which has progressed to require injected insulin, and latent autoimmune diabetes of adults (or LADA or "type 1.5" diabetes).

Classification

Most cases of diabetes mellitus fall into three broad categories: type 1, type 2, and gestational diabetes. A few other types are described.
Type 1 diabetes
Type 1 diabetes mellitus is characterized by loss of the insulin-producing beta cells of the islets of Langerhans in the pancreas leading to insulin deficiency. This type of diabetes can be further classified as immune-mediated or idiopathic. The majority of type 1 diabetes is of the immune-mediated nature, where beta cell loss is a T-cell mediated autoimmune attack. There is no known preventive measure against type 1 diabetes, which causes approximately 10% of diabetes mellitus cases in North America and Europe. Most affected people are otherwise healthy and of a healthy weight when onset occurs. Sensitivity and responsiveness to insulin are usually normal, especially in the early stages. Type 1 diabetes can affect children or adults but was traditionally termed "juvenile diabetes" because it represents a majority of the diabetes cases in children.

Type 2 diabetes
Type 2 diabetes mellitus is characterized by insulin resistance which may be combined with relatively reduced insulin secretion. The defective responsiveness of body tissues to insulin is believed to involve the insulin receptor. However, the specific defects are not known. Diabetes mellitus due to a known defect are classified separately. Type 2 diabetes is the most common type.
In the early stage of type 2 diabetes, the predominant abnormality is reduced insulin sensitivity.

At this stage hyperglycemia can be reversed by a variety of measures and medications that improve insulin sensitivity or reduce glucose production by the liver. As the disease progresses, the impairment of insulin secretion occurs, and therapeutic replacement of insulin may sometimes become necessary in certain patients.

Gestational diabetes

Gestational diabetes mellitus (GDM) resembles type 2 diabetes in several respects, involving a combination of relatively inadequate insulin secretion and responsiveness. It occurs in about 2%–5% of all pregnancies and may improve or disappear after delivery. Gestational diabetes is fully treatable but requires careful medical supervision throughout the pregnancy. About 20%–50% of affected women develop type 2 diabetes later in life.

Even though it may be transient, untreated gestational diabetes can damage the health of the fetus or mother. Risks to the baby include macrosomia (high birth weight), congenital cardiac and central nervous system anomalies, and skeletal muscle malformations. Increased fetal insulin may inhibit fetal surfactant production and cause respiratory distress syndrome. Hyperbilirubinemia may result from red blood cell destruction. In severe cases, perinatal death may occur, most commonly as a result of poor placental perfusion due to vascular impairment. Labor induction may be indicated with decreased placental function. A cesarean section may be performed if there is marked fetal distress or an increased risk of injury associated with macrosomia, such as shoulder dystocia.

A 2008 study completed in the U.S. found that more American women are entering pregnancy with preexisting diabetes. In fact the rate of diabetes in expectant mothers has more than doubled in the past 6 years. This is particularly problematic as diabetes raises the risk of complications during pregnancy, as well as increasing the potential that the children of diabetic mothers will also become diabetic in the future.

Other types

Pre-diabetes indicates a condition that occurs when a person's blood glucose levels are higher than normal but not high enough for a diagnosis of type 2 diabetes. Many people destined to develop type 2 diabetes spend many years in a state of pre-diabetes which has been termed "America's largest healthcare epidemic."

Some cases of diabetes are caused by the body's tissue receptors not responding to insulin (even when insulin levels are normal, which is what separates it from type 2 diabetes); this form is

very uncommon. Genetic mutations (autosomal or mitochondrial) can lead to defects in beta cell function. Abnormal insulin action may also have been genetically determined in some cases. Any disease that causes extensive damage to the pancreas may lead to diabetes (for example, chronic pancreatitis and cystic fibrosis). Diseases associated with excessive secretion of insulin-antagonistic hormones can cause diabetes (which is typically resolved once the hormone excess is removed). Many drugs impair insulin secretion and some toxins damage pancreatic beta cells. The ICD-10 (1992) diagnostic entity, malnutrition-related diabetes mellitus (MRDM or MMDM, ICD-10 code E12), was deprecated by the World Health Organization when the current taxonomy was introduced in 1999.

Following is a comprehensive list of other causes of diabetes:

• Genetic defects of β-cell Function
  o Maturity onset diabetes of the young (MODY)
  o Mitochondrial DNA mutations
• Genetic defects in insulin processing or insulin action
  o Defects in proinsulin conversion
  o Insulin gene mutations
  o Insulin receptor mutations
• Exocrine Pancreatic Defects
  o Chronic pancreatitis
  o Pancreatectomy
  o Pancreatic neoplasia
  o Cystic fibrosis
  o Hemochromatosis
  o Fibrocalculous pancreatopathy
	• Endocrinopathies
	  o Growth hormone excess (acromegaly)
	  o Cushing syndrome
	  o Hyperthyroidism
	  o Pheochromocytoma
	  o Glucagonoma
	• Infections
	  o Cytomegalovirus infection
	  o Coxsackievirus B
	• Drugs
	  o Glucocorticoids
	  o Thyroid hormone
	  o β-adrenergic agonists

Signs and symptoms

The classical symptoms of diabetes are polyuria (frequent urination), polydipsia (increased thirst) and polyphagia (increased hunger). Symptoms may develop rapidly (weeks or months) in type 1 diabetes while in type 2 diabetes they usually develop much more slowly and may be subtle or absent.

Prolonged high blood glucose causes glucose absorption, which leads to changes in the shape of the lenses of the eyes, resulting in vision changes; sustained sensible glucose control usually returns the lens to its original shape. Blurred vision is a common complaint leading to a diabetes diagnosis; type 1 should always be suspected in cases of rapid vision change, whereas with type 2 change is generally more gradual, but should still be suspected.

People (usually with type 1 diabetes) may also present with diabetic ketoacidosis, a state of metabolic dysregulation characterized by the smell of acetone; a rapid, deep breathing known as Kussmaul breathing; nausea; vomiting and abdominal pain; and an altered states of consciousness.

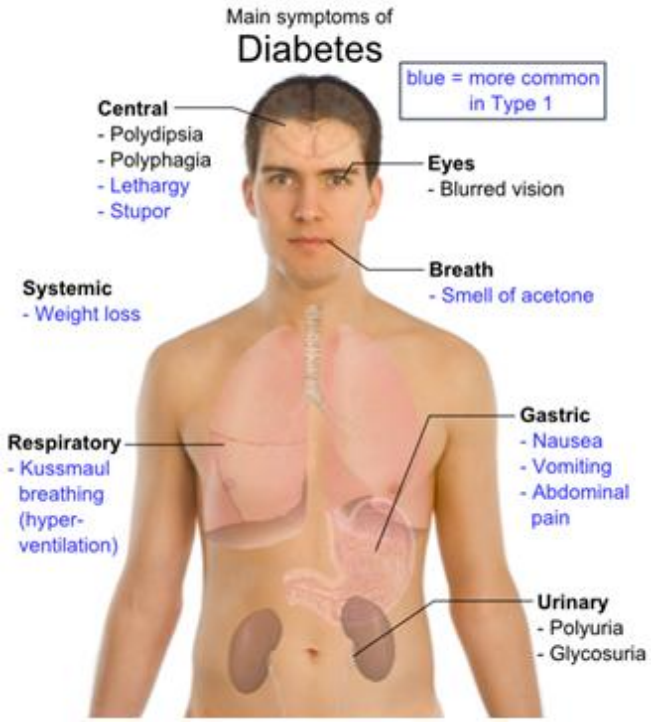

Figure 72. Overview of the most significant symptoms of diabetes.

A rarer but equally severe possibility is hyperosmolar nonketotic state, which is more common in type 2 diabetes and is mainly the result of dehydration. Often, the patient has been drinking extreme amounts of sugar-containing drinks, leading to a vicious circle in regard to the water loss. A number of skin rashes can occur in diabetes that are collectively known as diabetic dermadromes.

Causes

The cause of diabetes depends on the type. Type 2 diabetes is due primarily to lifestyle factors and genetics.

Type 1 diabetes is also partly inherited and then triggered by certain infections, with some evidence pointing at Coxsackie B4 virus. There is a genetic element in individual susceptibility to some of these triggers which has been traced to particular HLA genotypes (*i.e.*, the genetic "self" identifiers relied upon by the immune system). However, even in those who have inherited the susceptibility, type 1 diabetes mellitus seems to require an environmental trigger.

Pathophysiology

Insulin is the principal hormone that regulates uptake of glucose from the blood into most cells (primarily muscle and fat cells, but not central nervous system cells). Therefore deficiency of insulin or the insensitivity of its receptors plays a central role in all forms of diabetes mellitus.

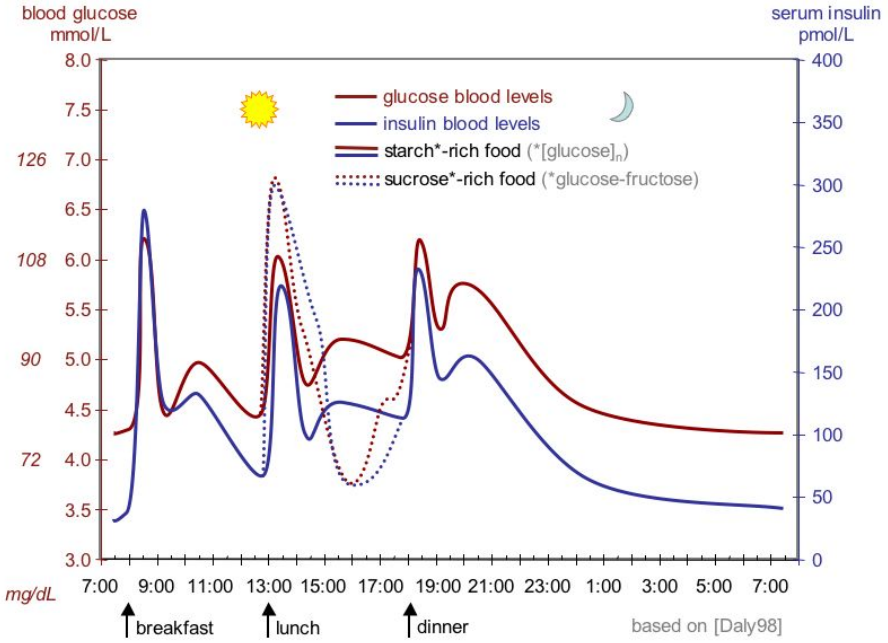

Figure 73. The fluctuation of blood sugar (red) and the sugar-lowering hormone insulin (blue) in humans during the course of a day with three meals. One of the effects of a sugar-rich vs a starch-rich meal is highlighted.

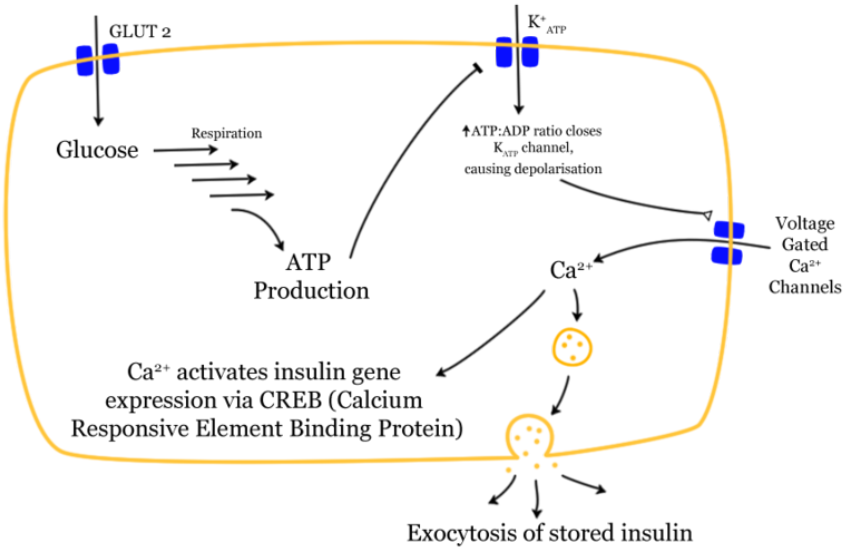

Figure 74. Mechanism of insulin release in normal pancreatic beta cells. Insulin production is more or less constant within the beta cells, irrespective of blood glucose levels. It is stored within vacuoles pending release, via exocytosis, which is primarily triggered by food, chiefly food containing absorbable glucose. The chief trigger is a rise in blood glucose levels after eating.

Humans are capable of digesting some carbohydrates, in particular those most common in food; starch, and some disaccharides such as sucrose, are converted within a few hours to simpler forms most notably the monosaccharide glucose, the principal carbohydrate energy source used by the body. The most significant exceptions are fructose, most disaccharides (except sucrose and in some people lactose), and all more complex polysaccharides, with the outstanding exception of starch. The rest are passed on for processing by gut flora largely in the colon. Insulin is released into the blood by beta cells (β-cells), found in the Islets of Langerhans in the pancreas, in response to rising levels of blood glucose, typically after eating. Insulin is used by about two-thirds of the body's cells to absorb glucose from the blood for use as fuel, for conversion to other needed molecules, or for storage.

Insulin is also the principal control signal for conversion of glucose to glycogen for internal storage in liver and muscle cells. Lowered glucose levels result both in the reduced release of insulin from the beta cells and in the reverse conversion of glycogen to glucose when glucose levels fall. This is mainly controlled by the hormone glucagon which acts in the opposite manner to insulin. Glucose thus forcibly produced from internal liver cell stores (as glycogen) re-enters the bloodstream; muscle cells lack the necessary export mechanism. Normally liver cells do this when the level of insulin is low (which normally correlates with low levels of blood glucose).

Higher insulin levels increase some anabolic ("building up") processes such as cell growth and duplication, protein synthesis, and fat storage. Insulin (or its lack) is the principal signal in converting many of the bidirectional processes of metabolism from a catabolic to an anabolic direction, and vice versa. In particular, a low insulin level is the trigger for entering or leaving ketosis (the fat burning metabolic phase).

If the amount of insulin available is insufficient, if cells respond poorly to the effects of insulin (insulin insensitivity or resistance), or if the insulin itself is defective, then glucose will not have its usual effect so that glucose will not be absorbed properly by those body cells that require it nor will it be stored appropriately in the liver and muscles. The net effect is persistent high levels of blood glucose, poor protein synthesis, and other metabolic derangements, such as acidosis. When the glucose concentration in the blood is raised beyond its renal threshold (about 10 mmol/L, although this may be altered in certain conditions, such as pregnancy), reabsorption of glucose in the proximal renal tubuli is incomplete, and part of the glucose remains in the urine (glycosuria). This increases the osmotic pressure of the urine and inhibits reabsorption of water by the kidney, resulting in increased urine production (polyuria) and increased fluid loss. Lost blood volume will be replaced osmotically from water held in body cells and other body compartments, causing dehydration and increased thirst.

Diagnosis

2006 WHO Diabetes criteria		
Condition	**2 hour glucose**	**Fasting glucose**
	mmol/l(mg/dl)	mmol/l(mg/dl)
Normal	<7.8 (<140)	<6.1 (<110)
Diabetes mellitus	≥11.1 (≥200)	≥7.0 (≥126)

Diabetes mellitus is characterized by recurrent or persistent hyperglycemia, and is diagnosed by demonstrating any one of the following:

- Fasting plasma glucose level ≥ 7.0 mmol/L (126 mg/dL).
- Plasma glucose ≥ 11.1 mmol/L (200 mg/dL) two hours after a 75 g oral glucose load as in a glucose tolerance test.
- Symptoms of hyperglycemia and casual plasma glucose ≥ 11.1 mmol/L (200 mg/dL).
- Glycated hemoglobin (Hb A1C) ≥ 6.5%.

A positive result, in the absence of unequivocal hyperglycemia, should be confirmed by a repeat of any of the above-listed methods on a different day. It is preferable to measure a fasting glucose level because of the ease of measurement and the considerable time commitment of formal glucose tolerance testing, which takes two hours to complete and offers no prognostic advantage over the fasting test. According to the current definition, two fasting glucose measurements above 126 mg/dL (7.0 mmol/L) is considered diagnostic for diabetes mellitus.

People with fasting glucose levels from 100 to 125 mg/dL (5.6 to 6.9 mmol/L) are considered to have impaired fasting glucose. Patients with plasma glucose at or above 140 mg/dL (7.8 mmol/L), but not over 200 mg/dL (11.1 mmol/L), two hours after a 75 g oral glucose load are considered to have impaired glucose tolerance. Of these two pre-diabetic states, the latter in particular is a major risk factor for progression to full-blown diabetes mellitus as well as cardiovascular disease.

Management

Diabetes mellitus is a chronic disease which is difficult to cure. Management concentrates on keeping blood sugar levels as close to normal ("euglycemia") as possible without presenting undue patient danger. This can usually be with close dietary management, exercise, and use of

appropriate medications (insulin only in the case of type 1 diabetes mellitus. Oral medications may be used in the case of type 2 diabetes, as well as insulin).
Patient education, understanding, and participation is vital since the complications of diabetes are far less common and less severe in people who have well-managed blood sugar levels. Wider health problems may accelerate the deleterious effects of diabetes. These include smoking, elevated cholesterol levels, obesity, high blood pressure, and lack of regular exercise.

Lifestyle modifications

There are roles for patient education, dietetic support, sensible exercise, with the goal of keeping both short-term and long-term blood glucose levels within acceptable bounds. In addition, given the associated higher risks of cardiovascular disease, lifestyle modifications are recommended to control blood pressure in patients with hypertension, cholesterol in those with dyslipidmia, as well as exercising more, smoking less or ideally not at all, consuming a recommended diet. Patients with foot problems are also recommended to wear diabetic socks, and possibly diabetic shoes.

Support

In countries using a general practitioner system, such as the United Kingdom, care may take place mainly outside hospitals, with hospital-based specialist care used only in case of complications, difficult blood sugar control, or research projects. In other circumstances, general practitioners and specialists share care of a patient in a team approach. Optometrists, podiatrists/chiropodists, dietitians, physiotherapists, nursing specialists (e.g., DSNs (Diabetic Specialist Nurse)), nurse practitioners, or Certified Diabetes Educators, may jointly provide multidisciplinary expertise. In countries where patients must provide for their own health care (e.g. in the US, and in much of the undeveloped world).
Peer support links people living with diabetes. Within peer support, people with a common illness share knowledge and experience that others, including many health workers, do not have. Peer support is frequent, ongoing, accessible and flexible and can take many forms—phone calls, text messaging, group meetings, home visits, and even grocery shopping. It complements and enhances other health care services by creating the emotional, social and practical assistance necessary for managing disease and staying healthy.

Prognosis

Diabetes doubles the risk of vascular problems, including cardiovascular disease.

According to one study, women with high blood pressure (hypertension) were three times more likely to develop type 2 diabetes as compared with women with optimal BP after adjusting for various factors such as age, ethnicity, smoking, alcohol intake, body mass index (BMI), exercise, family history of diabetes, etc. The study was conducted by researchers from the Brigham and Women's Hospital, Harvard Medical School and the Harvard School of Public Health, USA, who followed over 38,000 female health professionals for ten years.

Except in the case of type 1 diabetes, which always requires insulin replacement, the way type 2 diabetes is managed may change with age. Insulin production decreases because of age-related impairment of pancreatic beta cells. Additionally, insulin resistance increases because of the loss of lean tissue and the accumulation of fat, particularly intra-abdominal fat, and the decreased tissue sensitivity to insulin. Glucose tolerance progressively declines with age, leading to a high prevalence of type 2 diabetes and postchallenge hyperglycemia in the older population. Age-related glucose intolerance in humans is often accompanied by insulin resistance, but circulating insulin levels are similar to those of younger people. Treatment goals for older patients with diabetes vary with the individual, and take into account health status, as well as life expectancy, level of dependence, and willingness to adhere to a treatment regimen. Glycated hemoglobin is better than fasting glucose for determining risks of cardiovascular disease and death from any cause.

Epidemiology

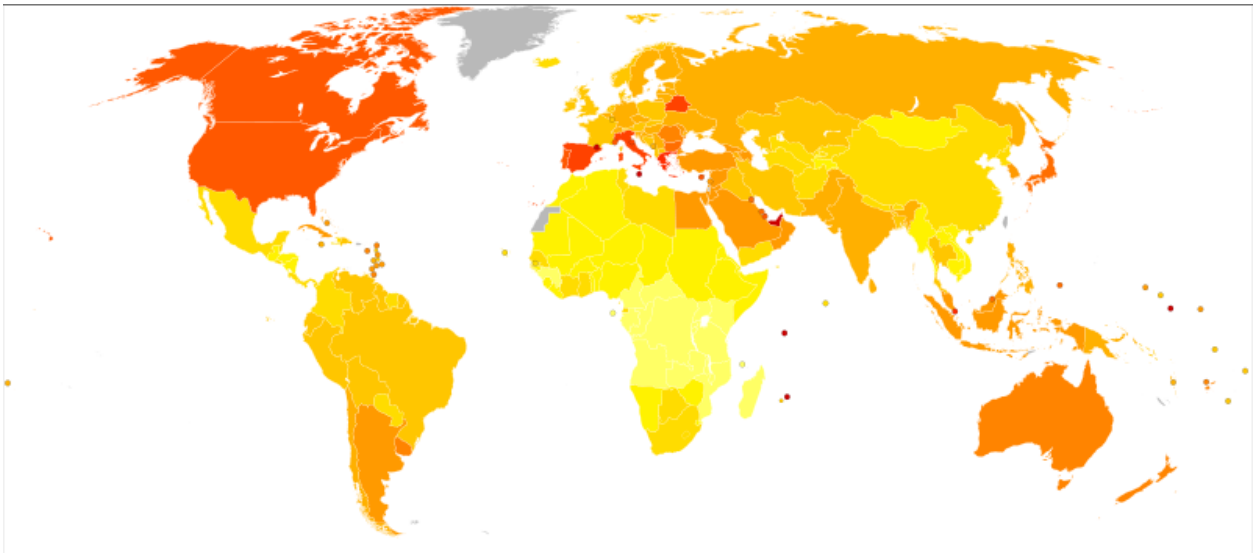

Figure 75. Prevalence of diabetes worldwide in 2000 (per 1000 inhabitants). World average was 2.8%.

no data ≤ 7.5 7.5–15 15–22.5 22.5–30 30–37.5 37.5–45 45–52.5 52.5–60 60–67.5 67.5–75 75–82.5 ≥ 82.5

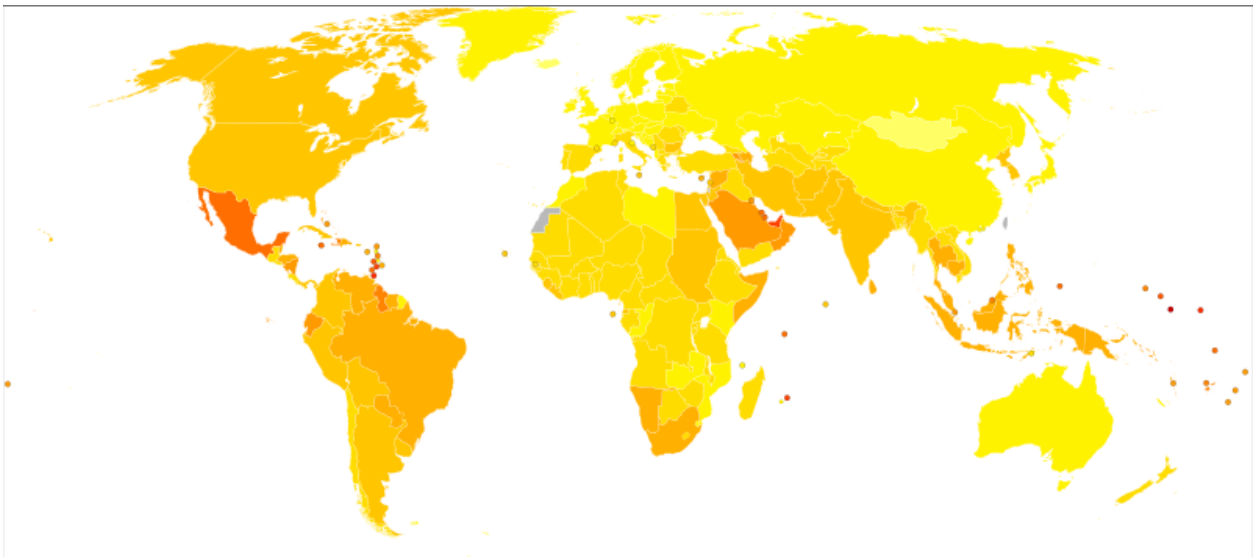

Figure 76. Disability-adjusted life year for diabetes mellitus per 100,000 inhabitants in 2002.

no data **≤ 100** **100-200** **200-300** **300-400** **400-500** **500-600** **600-700** **700-800** **800-900** **900-1000** **1000-1500** **≥ 1500**

In 2000, according to the World Health Organization, at least 171 million people worldwide suffer from diabetes, or 2.8% of the population. Its incidence is increasing rapidly, and it is estimated that by 2030, this number will almost double. Diabetes mellitus occurs throughout the world, but is more common (especially type 2) in the more developed countries. The greatest increase in prevalence is, however, expected to occur in Asia and Africa, where most patients will probably be found by 2030. The increase in incidence of diabetes in developing countries follows the trend of urbanization and lifestyle changes, perhaps most importantly a "Western-style" diet. This has suggested an environmental (*i.e.*, dietary) effect, but there is little understanding of the mechanism(s) at present, though there is much speculation, some of it most compellingly presented. For at least 20 years, diabetes rates in North America have been increasing substantially. In 2008 there were about 24 million people with diabetes in the United States alone, from those 5.7 million people remain undiagnosed. Other 57 million people are estimated to have pre-diabetes. The Centers for Disease Control has termed the change an epidemic. The National Diabetes Information Clearinghouse estimates that diabetes costs $132 billion in the United States alone every year. About 5%–10% of diabetes cases in North America are type 1, with the rest being type 2. The fraction of type 1 in other parts of the world differs. Most of this difference is not currently understood. The American Diabetes Association cite the 2003 assessment of the National Center for Chronic Disease Prevention and Health Promotion (Centers for Disease Control and Prevention) that 1 in 3 Americans born after 2000 will develop diabetes in their lifetime.

According to the American Diabetes Association, approximately 18.3% (8.6 million) of Americans age 60 and older have diabetes. Diabetes mellitus prevalence increases with age, and the numbers of older persons with diabetes are expected to grow as the elderly population increases in number. The National Health and Nutrition Examination Survey (NHANES III) demonstrated that, in the population over 65 years old, 18% to 20% have diabetes, with 40% having either diabetes or its precursor form of impaired glucose tolerance.

Indigenous populations in first world countries have a higher prevalence and increasing incidence of diabetes than their corresponding non-indigenous populations. In Australia the age-standardised prevalence of self-reported diabetes in Indigenous Australians is almost 4 times that of non-indigenous Australians. Preventative community health programs such as Sugar Man (diabetes education) are showing some success in tackling this problem.

History

The term diabetes (Greek: διαβήτης, diabētēs) (pronounced /ˌdaɪ.əˈbiːtiːz/ or /ˌdaɪ.əˈbiːtɨs/; /mɨˈlaɪtəs/ or /ˈmɛlɨtəs/) was coined by Aretaeus of Cappadocia. It was derived from the Greek verb διαβαίνειν, diabaínein, itself formed from the prefix dia-, "across, apart," and the verb bainein, "to walk, stand." The verb diabeinein meant "to stride, walk, or stand with legs asunder"; hence, its derivative diabētēs meant "one that straddles," or specifically "a compass, siphon." The sense "siphon" gave rise to the use of diabētēs as the name for a disease involving the discharge of excessive amounts of urine. Diabetes is first recorded in English, in the form diabete, in a medical text written around 1425. In 1675, Thomas Willis added the word mellitus, from the Latin meaning "honey", a reference to the sweet taste of the urine. This sweet taste had been noticed in urine by the ancient Greeks, Chinese, Egyptians, Indians, and Persians. In 1776, Matthew Dobson confirmed that the sweet taste was because of an excess of a kind of sugar in the urine and blood of people with diabetes. Diabetes mellitus appears to have been a death sentence in the ancient era. Hippocrates makes no mention of it, which may indicate that he felt the disease was incurable. Aretaeus did attempt to treat it but could not give a good prognosis; he commented that "life (with diabetes) is short, disgusting and painful." Sushruta (6th century BCE) identified diabetes and classified it as Medhumeha. He further identified it with obesity and sedentary lifestyle, advising exercises to help "cure" it. The ancient Indians tested for diabetes by observing whether ants were attracted to a person's urine, and called the ailment "sweet urine disease" (Madhumeha). The Chinese, Japanese and Korean words for diabetes are based on the same ideographs (糖尿病) which mean "sugar urine disease".

In medieval Persia, Avicenna (980–1037) provided a detailed account on diabetes mellitus in The Canon of Medicine, "describing the abnormal appetite and the collapse of sexual functions," and he documented the sweet taste of diabetic urine. Like Aretaeus before him, Avicenna recognized a primary and secondary diabetes. He also described diabetic gangrene, and treated diabetes using a mixture of lupine, trigonella (fenugreek), and zedoary seed, which produces a considerable reduction in the excretion of sugar, a treatment which is still prescribed in modern times. Avicenna also "described diabetes insipidus very precisely for the first time", though it was later Johann Peter Frank (1745–1821) who first differentiated between diabetes mellitus and diabetes insipidus.

Although diabetes has been recognized since antiquity, and treatments of various efficacy have been known in various regions since the Middle Ages, and in legend for much longer, pathogenesis of diabetes has only been understood experimentally since about 1900. The discovery of a role for the pancreas in diabetes is generally ascribed to Joseph von Mering and Oskar Minkowski, who in 1889 found that dogs whose pancreas was removed developed all the signs and symptoms of diabetes and died shortly afterwards. In 1910, Sir Edward Albert Sharpey-Schafer suggested that people with diabetes were deficient in a single chemical that was normally produced by the pancreas—he proposed calling this substance insulin, from the Latin insula, meaning island, in reference to the insulin-producing islets of Langerhans in the pancreas.

The endocrine role of the pancreas in metabolism, and indeed the existence of insulin, was not further clarified until 1921, when Sir Frederick Grant Banting and Charles Herbert Best repeated the work of Von Mering and Minkowski, and went further to demonstrate they could reverse induced diabetes in dogs by giving them an extract from the pancreatic islets of Langerhans of healthy dogs. Banting, Best, and colleagues (especially the chemist Collip) went on to purify the hormone insulin from bovine pancreases at the University of Toronto. This led to the availability of an effective treatment—insulin injections—and the first patient was treated in 1922. For this, Banting and laboratory director MacLeod received the Nobel Prize in Physiology or Medicine in 1923; both shared their Prize money with others in the team who were not recognized, in particular Best and Collip. Banting and Best made the patent available without charge and did not attempt to control commercial production. Insulin production and therapy rapidly spread around the world, largely as a result of this decision. Banting is honored by World Diabetes Day which is held on his birthday, November 14.

The distinction between what is now known as type 1 diabetes and type 2 diabetes was first clearly made by Sir Harold Percival (Harry) Himsworth, and published in January 1936.

Despite the availability of treatment, diabetes has remained a major cause of death. For instance, statistics reveal that the cause-specific mortality rate during 1927 amounted to about 47.7 per 100,000 population in Malta.

Other landmark discoveries include:

- Identification of the first of the sulfonylureas in 1942
- Reintroduction of the use of biguanides for Type 2 diabetes in the late 1950s. The initial phenformin was withdrawn worldwide (in the U.S. in 1977) due to its potential for sometimes fatal lactic acidosis and metformin was first marketed in France in 1979, but not until 1994 in the US.
- The determination of the amino acid sequence of insulin (by Sir Frederick Sanger, for which he received a Nobel Prize)
- The radioimmunoassay for insulin, as discovered by Rosalyn Yalow and Solomon Berson (gaining Yalow the 1977 Nobel Prize in Physiology or Medicine)
- The three-dimensional structure of insulin (PDB 2INS)
- Dr Gerald Reaven's identification of the constellation of symptoms now called metabolic syndrome in 1988
- Demonstration that intensive glycemic control in type 1 diabetes reduces chronic side effects more as glucose levels approach 'normal' in a large longitudinal study, and also in type 2 diabetics in other large studies
- Identification of the first thiazolidinedione as an effective insulin sensitizer during the 1990s

In 1980, U.S. biotech company Genentech developed human insulin. The insulin is isolated from genetically altered bacteria (the bacteria contain the human gene for synthesizing human insulin), which produce large quantities of insulin. Scientists then purify the insulin and distribute it to pharmacies for use by diabetes patients.

Society and culture

The 1990 "St Vincent Declaration" was the result of international efforts to improve the care accorded to those with diabetes. Doing so is important both in terms of quality of life and life expectancy but also economically—expenses due to diabetes have been shown to be a major drain on health-and productivity-related resources for healthcare systems and governments.

Several countries established more and less successful national diabetes programmes to improve treatment of the disease.

A study shows that diabetic patients with neuropathic symptoms such as numbness or tingling in feet or hands are twice as likely to be unemployed as those without the symptoms.

Appendix D: supplementary information

Paragraph 2.2: Mechanism of glucose electrooxidation at gold electrodes

D(+)-Glucose (dextrose) anhydrous, potassium chloride, sodium fluoride, PBS (phosphate buffer solution: 100 mM NaCl, 10 mM KCl, 10 mM KH_2PO_4 and 10 mM K_2HPO_4), potassium phosphate dibasic and potassium phosphate monobasic were purchased from Sigma Aldrich. A gold pin electrode (Surface Area 0.0314 cm^2) and a platinum counter electrode were purchased from Amel Electrochemistry.

Electrochemical characterization was carried out using a BioLogic VMP3 potentiostat-galvanostat multichannel equipped with EIS board. A double junction Ag|AgCl|KCl (3.5 M) reference electrode (RE) was used in the measurement. The double junction was employed to prevent OH^- diffusion and reaction at the Ag/AgCl interface; additionally, the RE potential was monitored after each measurement to confirm that no change had taken place.

Before each measurement, the gold pin electrode surface was activated and stabilized in 0.1 M KOH by CV scans at 100 mV s^{-1} between -0.7 and 0.8 V vs. RE until stable voltammograms were observed (about 20 scans). All the measurements were performed under inert (nitrogen) atmosphere and room temperature.

Paragraph 3.3: A new approach to glucose sensing at gold electrodes

D(+)-Glucose (dextrose) anhydrous, sodium chloride, potassium phosphate dibasic, potassium phosphate monobasic and silver gauze (80 mesh, 0.115mm diameter wire, 99.9% 2x2cm) were purchased from Sigma Aldrich. Gold pin electrode (Surface Area 0.0314cm^2) and platinum counter electrode were purchased from Amel Electrochemistry.

The electrochemical characterization was carried out using a BioLogic VMP3 potentiostat-galvanostat multichannel equipped with EIS board. A double junction Ag|AgCl|KCl (3.5M) reference electrode (RE) was used in the measurement. The double junction was employed to prevent OH^- diffusion and reaction at Ag/AgCl interface; in any case the RE potential was monitored after each measurement.

Before each experiment, the gold pin electrode surface has been activated and stabilized in 0.1 M KOH by CV scans at 100 mV s^{-1} between -0.7 and 0.8 V vs. RE until stable voltammograms have been observed (about 20 scans) [75]. All the measurements have been performed at room temperature under nitrogen atmosphere.

Paragraph 4.4: Optimizing operating conditions and electrochemical characterization of glucose-gluconate alkaline fuel cells

The electrochemical cell was purchased from Electro-Chem-Technic (UK). The cell is specifically designed for small-scale studies with liquid alkaline electrolytes and fuels. It is comprised of a 65 ml fuel and electrolyte compartment that also contains a carbon-supported platinum catalyst together with a PTFE (polytetrafluoroethylene) binder. The electrode is supported on a nickel mesh (catalyst area 17.64 cm^2). The air cathode consists of manganese [as $KMnO_4$ at greater than or equal to 4% (wt of carbon)] on carbon with a PTFE binder and this is also supported on a nickel wire mesh (catalyst area 13.86 cm^2). The surface of the cathode is coated with a gas-permeable layer of PTFE. The nickel mesh supports at both the anode and the cathode are connected to terminals on the cell [56].

The anode material of the cell was electrochemically characterized by equilibrium electrode potential (E_{rev}), current-voltage (I-V), and electrochemical impedance spectroscopy (EIS) measurements as well as the energy performance of the cell investigated. All the experiments were executed at 25.0 ± 0.1 °C. The solutions were prepared using pure deionized water ("Millipore Milli-Q System") and D-(+)-glucose, KOH, and Na_2HPO_4, all from Sigma-Aldrich. Before each experiment the electrochemical cell was washed in sequence with mQ water, 2-propanol, H_2O_2 (3.5 % v/v) and finally again with mQ water.

Electrochemical characterization was carried out using a BioLogic VMP3 potentiostat-galvanostat multichannel equipped with EIS board.

The I-V and EIS experiments were performed by two compartments three electrodes cell with a standard calomel electrode (SCE) and platinum mesh as the reference and counter electrodes, respectively.

The chemical analyses were achieved by HPLC (High Performance Liquid Chromatography) using Shimazu LC-10 with a refractive index RID-10A detector and Varian MetaCarb 87H Plus 300x7.8 mm column; the operating conditions were: H_3PO_4 0.01M as eluant, column temperature of 70°C and flow rate of 0.6 ml/min.

The NMR measurements were carried out by using a Varian Mercury 400 MHz spectrometer and working at 25°C.

Paragraph 4.5: Alkaline glucose oxidation on nanostructured gold electrodes

Colloidal gold was prepared by adding 0.3 mL of a 0.1M $NaBH_4$ (Aldrich) fresh solution to 50 mL of 1 mM tetrachloroauric acid solution (prepared by *aqua regia* dissolution of 99.9999%

gold sponge, Aldrich) and glucose (50:1 molar ratio vs. Au). Water was purified with a Milli-Q system. The nanostructured electrode was then obtained by adsorbing gold particles during 12 h under stirring on the carbonaceous materials as previously reported [76,186]. In the case of the Carbon tip (AMEL) electrode (0.070 cm^2) the surface of the support was mechanical polished, sonicated in ethanol and rinsed with 2-propanol before deposition. Polycrystalline tip Au electrode (AMEL), having 0.0314 cm^2 surface, was used as comparison. The deposition was also performed on larger (30x30 mm) substrate of glassy carbon (ALS Co., Ltd. CODE: 012095), carbon cloth and graphite paper (Hydro2Power S.r.l) by using the same impregnation method. Moreover, the surface of the large substrates was treated with a strong acidic solution to increase the active area.

SEM images of nanoparticles on Glassy carbon plate were obtained at different magnification using a TESCAN VEGA TS5136XM electron microscopy.

Electrochemical characterization was carried out using a PARSTAT 2263 potentiostat-galvanostat. A double junction Ag|AgCl|KCl (3.5M) reference electrode (RE) was used in the measurement. The double junction was employed to prevent OH^- diffusion and reaction at Ag/AgCl interface; in any case the RE potential was monitored after each measurement. All the potential values are reported vs. SHE. Before each measurement, the electrode surfaces were activated and stabilized in 0.25M H_2SO_4 by CV scans at 100 mV s^{-1} between -0.4 and 1.2 V until stable voltammograms have been observed (at least 20 scans). Glucose oxidation was performed by CV in different potassium hydroxide solutions (pH=12-14) with 10mM glucose using a platinum gauze counter electrode in a two compartment (glass frit) cell at scan rate of 100 mV s^{-1} from -1.0 and 0.5 V. The two compartment was used to prevent the diffusion of by-products generated at the counter electrode to the working electrode. Before each electrochemical measurement, all the solutions were degassed by N_2 purging for at least 1h.

Paragraph 5.1: Three-Dimensional Carbon Nanotube-Cotton Anode for High-Performance Microbial Fuel Cells

MFCs construction and operation

H-shaped two-chamber MFCs were constructed by connecting two 150 ml media bottles with 40 mm-diameter tube. Anode was CNT modified cotton cloth (1 cm × 1 cm, projected area of 2 cm^2), or carbon cloth (1 cm × 1 cm, projected area of 2 cm^2, Fuel Cell Earth LLC, MA). Cathode was carbon cloth (2 cm × 5 cm, projected area of 20 cm^2, Fuel Cell Earth LLC, MA) with a catalyst layer (0.5 mg/cm^2 10wt. % Pt on XC-72). Anode and cathode were connected to

external circuit with titanium wire, and all exposed metal surfaces were sealed with a nonconductive epoxy (Dexter, NJ). Anode and cathode compartments were separated by an anion exchange membrane (AEM) (AMI-7001, Membranes International Inc., NJ), which were preconditioned by immersion in a salt solution (NaCl, 1 %) to allow for membrane expansion. The distance between the anode and the cathode was about 11 cm.

Domestic wastewater obtained from Palo Alto Wastewater Treatment Plant was used as the inoculum. The MFC was fed in anode chamber with artificial wastewater, containing glucose (0.2-1.0 g/L), $NaH_2PO_4 \cdot H_2O$ (4.90 g/L), Na_2HPO_4 (9.15 g/L), KCl (0.26 g/L), NH_4Cl (0.62 g/L), mineral solution (12.5 mL/L) and vitamin solution (5 mL/L)[139,121]. Cathode chamber was filled with same media, but without glucose, mineral solution and vitamin solution. Cathode camber was continuously sparged with air using a diffusion stone (100 ml/min). Both chambers were continuously mixed using a magnetic stirrer (200 rpm). The voltage across a 1 kΩ external resistor was recorded by DATAQ-710 data logging system. All experiments were conducted at room temperature.

Electrochemical Characterization

Cyclic voltammetry was performed -0.5 V to 0.5 V (vs. Ag/AgCl) at a scan rate of 10 mV/s. Polarization curves were obtained from linear staircase voltammetry (LSV) test by step-sweeping potential from OCV to the short circuit voltage at a scan rate of 30 mV per 5 minutes. Electrochemical impedance spectroscopy (EIS) was conducted at the open circuit voltage (OCV) over a frequency range of 10^5-0.1 Hz with a perturbation signal of 10 mV, and the results were showed as Nyquist plots.

Scanning electron microscopy (SEM)

The sample pretreatment process is shown as follows: (1) small pieces of the anode were primarily fixed overnight in the fixative containing 0.1 M sodium cacodylate buffer (pH 7.3), 2% glutaraldehyde and 4% paraformaldehyde at 4 ℃, and then washed with the same buffer for 5 mins; (2) the samples were secondary fixed in 1% osmium tetroxide at 4 ℃ for 1-2 hours, and then washed with Milli-Q water for 10 mins; (3) the samples were dehydrated in increasing concentration of ethanol solution (50, 70, 90 and 100%), and critical point dried in 100% ethanol with liquid CO_2; (4) the samples were finally sputter coated with appropriate thickness (0-10 nm) of Au.

DNA extraction, PCR, cloning, and sequencing

After 50 days of operation, genomic DNA was extracted from and carbon nanotube-cotton (CNT) anode samples (0.1 cm^2) in duplicate using the FastDNA Soil DNA Spin Kit (MP Biomedicals, Solon, OH) according to the manufacturer's protocol, except for the initial bead-beating step. A Vortex Adapter (MO BIO laboratories, Inc., Carlsbad, CA) with the Vortex Genie 2T (Scientific Industries, Inc., Bohemia, NY) is used to physically disrupt cells at maximum speed for 15 min. The bacterial 16S rRNA gene was PCR-amplified from the genomic DNA using the bacteria-specific forward primer 8F (5'-AGA GTT TGA TCM TGG CTC AG-3') and the universal reverse primer 1492R (5'-TAC GGY TAC CTT GTT ACG ACT T-3'). Each 25 µL PCR mixture consisted of 0.25 µM of each primer, 1X Fail-Safe PCR buffer F (Epicentre, Madison, WI), 1.25 units of AmpliTaq LD Taq polymerase (Applied Biosystems, Inc., Foster City, CA), and 100-140 ng of genomic template DNA. The PCR temperature profile was as follows: an initial melting step at 94°C for 5 minutes, followed by 35 cycles consisting of 94°C for 45 s, 55°C for 30 s, and 72°C for 90s, with a final extension at 72°C for 10 min. Presence or absence of the expected amplicon was checked via agarose gel electrophoresis. For 16S rRNA gene cloning and sequencing, quadruplicate PCR products were pooled and purified via gel electrophoresis using the QIAquick gel extraction kit (Qiagen Inc., Valencia, CA). Purified PCR products were cloned using the pGEM-T Easy Vector System and transformed into *E. Coli* JM109 competent cells (Promega, Madison, WI), as per the manufacturer's protocol. To confirm the presence of ~1500-bp 16S rRNA gene inserts, *Escherichia coli* transformants were grown overnight at 37°C and used as PCR templates with the T7 and SP6 primers. 48 clones were randomly selected and sequenced from both the T7 and SP6 priming sites on ABI 3100 or 3730 automated sequencers by Elim Biopharmaceuticals, Inc. (Hayward, CA), generating a total of 48 bacterial 16S rRNA gene sequences.

Phylogenetic analysis

Bacterial 16S rRNA gene sequences (~1500 bp) were compared to all available sequences in Genbank using the NCBI BLAST utility (http://www.ncbi.nlm.nih.gov/blast/Blast.cgi) Sequences were subsequently aligned with the GreenGenes NAST utility[187] and imported in the ARB software package[188] to a database of 236,469 16S rRNA sequences included in the November 18, 2008 release of GreenGenes (greengenes.lbl.gov)[189]. A neighbor-joining phylogenetic tree with the Jukes- Cantor correction was generated in ARB based on the multiple alignment of cloned 16S rRNA gene sequences and closely related database samples.

Paragraph 6.1: Stretchable, porous and conductive energy textiles

Part I. Absorption of SWNT ink in cotton and fabric

10 mg/mL SDBS surfactant is dissolved in DI water with the help of bath sonication. Then, laser ablation SWNTs are dispersed in the surfactant solution with 0.8 or 1.6 mg/mL concentrations. After bath sonication for 5 minutes, the CNT dispersion is probe-sonicated for 30 minutes at 200 W power (VC 505, Sonics Inc). Then a fluffy cotton sheet (Cloud 9 dream fleece, Wal-Mart Inc) with thickness of ~1-2 mm is dipped into the SWNT ink and immediately removed. The mass of the ink is obtained by the weight difference before and after the soaking of the cotton sheet. This process is repeated to increases the SWNT loading in the cotton. The same procedure is repeated with a fabric sheet (TX309, The Texwipe Company LLC). A small variation (<5%) of ink mass per area absorbed by cotton or fabric is observed when repeating the process. Due to the high absorption of the cotton and the fabric, the process of absorption is quick and can be easily scaled up with roll to roll coating processes. The conformal coating of the SWNTs is observed, which is possibly due to their mechanical flexibility and large binding energy with textile fibers.

Part II. Properties of conductive textile

The hydrophilic behavior of the conductive cotton allows the good wetting of aqueous electrolyte and polar organic electrolyte commonly used in SCs and batteries. We did the adhesion and washing test of conductive textiles and did not observe a change in conductance. The R_s was measured before and after the adhesion or washing, which remained 4 Ohm/sq for the sample.The tensile test was performed using the MTS Bionix tensile tester, loading the fabric in constant displacement mode. Two metal sheets are clipped to the two ends of the fabric and the resistance is monitored as the fabric is being stretched. The initial width of the fabric is 4 mm and the initial length is 7 mm. At large tensile strains, the width of fabric starts to decreases, or necking occurs, after 120% of engineering strain. For the chemical test, the conductive textiles were washed in water, soaked in 4M HNO_3 for a half hour, or soaked in 2 M KOH for 2 hours. After that, the films were blown dry. R_s was measured before and after the treatment with a four point probe test.

Part III. MnO_2 electrodeposition

MnO_2 deposition was achieved by oxidation of a solution of 0.02 M $Mn(NO_3)_2$ and 0.1 M $NaNO_3$. A costant current of 0.5 mA/cm^2 was applied for 2 h. The cotton/SWNT was used as

electrode. Conformal coating is achieved with MnO_2 particles of about 200-300 nm in dimension.

Paragraph 6.2: Aqueous supercapacitors on conductive cotton

Sodium dodecylbenzene sulfonate (SDBS) and lithium sulfate anhydrous (≥99.99% trace metals basis) were purchased from Sigma Aldrich. Nitric acid (68%) was purchased from EMD Chemicals. Fluffy cotton sheets (Cloud 9 dream fleece) were purchased from Wal-Mart Inc.

Electrochemical characterization was carried out using a BioLogic VMP3 potentiostat-galvanostat multichannel equipped with EIS board. A double junction Ag|AgCl|KCl (3.5M) reference electrode (RE) was used in the measurement. The double junction was employed to prevent OH^- diffusion and reaction at the Ag/AgCl interface; additionally, the RE potential was monitored after each measurement to confirm that no change had taken place. All the measurements were performed under inert (nitrogen) atmosphere and at room temperature.

REFERENCES

1 Wikipedia-Contributors. Glucose. *Wikipedia, The Free Encyclopedia*, doi:http://en.wikipedia.org/wiki/Glucose (2010).

2 Nelson, D. L., Lehninger, A. L. & Cox, M. M. *Lehninger principles of biochemistry*. 3rd edn, (Worth, 2000).

3 Loeb, W. Sugar Decomposition. III. Electrolysis of Dextrose. *Biochem. Z.* **17**, 132-144 (1909).

4 Heller, A. & Feldman, B. Electrochemical Glucose Sensors and Their Applications in Diabetes Management. *Chem. Rev. (Washington, DC, U. S.)* **108**, 2482-2505 (2008).

5 E. Katz, Shipway, A. N. & Willner, I. *Handbook of fuel cells : fundamentals, technology, and applications*. Vol. 1 355 (Wiley, 2003).

6 Chaudhuri, S. K. & Lovley, D. R. Electricity generation by direct oxidation of glucose in mediatorless microbial fuel cells. *Nature Biotechnology* **21**, 1229-1232 (2003).

7 Ekoé*, J. M. *The Epidemiology of diabetes mellitus [print]*. 2nd edn, (Wiley-Blackwell, 2008).

8 Kerzenmacher, S., Ducree, J., Zengerle, R. & von Stetten, F. Energy harvesting by implantable abiotically catalyzed glucose fuel cells. *J. Power Sources* **182**, 1-17 (2008).

9 Beden, B., Largeaud, F., Kokoh, K. B. & Lamy, C. Fourier transform infrared reflectance spectroscopic investigation of the electrocatalytic oxidation of D-glucose: identification of reactive intermediates and reaction products. *Electrochim. Acta* **41**, 701-709 (1996).

10 Corrigan, D. S., Leung, L. W. H. & Weaver, M. J. Single potential-alteration surface infrared spectroscopy: examination of absorbed species involved in irreversible electrode reactions. *Anal. Chem.* **59**, 2252-2256, doi:10.1021/ac00145a009 (1987).

11 Pons, S., Davidson, T. & Bewick, A. Vibrational spectroscopy of the electrode-electrolyte interface: Part IV. Fourier transform infrared spectroscopy: Experimental considerations. *J. Electroanal. Chem.* **160**, 63-71, doi:Doi: 10.1016/s0022-0728(84)80115-1 (1984).

12 Pasta, M., La Mantia, F. & Cui, Y. Mechanism of glucose electroxidation at gold electrodes. *Electrochim. Acta*.

13 Tominaga, M., Nagashima, M., Nishiyama, K. & Taniguchi, I. Surface poisoning during electrocatalytic monosaccharide oxidation reactions at gold electrodes in alkaline medium. *Electrochem. Commun.* **9**, 1892-1898 (2007).

14 Bae, I. T., Yeager, E., Xiang, X. & Liu, C. C. In situ infrared studies of glucose oxidation on platinum in an alkaline medium. *J. Electroanal. Chem. Interfacial Electrochem.* **309**, 131-145 (1991).

15 Ben Aoun, S. & Taniguchi, I. Effective electrocatalytic oxidation of glucose at platinum nanoparticle-based carbon electrodes. *Chem. Lett.* **37**, 936-937 (2008).

16 Yei, L. H. E., Beden, B. & Lamy, C. Electrocatalytic oxidation of glucose at platinum in alkaline medium: On the role of temperature. *J. Electroanal. Chem. Interfacial Electrochem.* **246**, 349-362 (1988).

17 Nikolaeva, N. N., Khazova, O. A. & Vasil'ev, Y. B. Kinetics and mechanism of glucose oxidation on a platinum electrode. *Elektrokhimiya* **19**, 1476-1481 (1983).

18 Nikolaeva, N. N., Khazova, O. A. & Vasil'ev, Y. B. Adsorption of glucose at a platinum electrode. *Elektrokhimiya* **16**, 1227-1230 (1980).

19 Rao, J. R., Richter, G. J., Von Sturm, F. & Weidlich, E. The performance of glucose electrodes and the characteristics of different biofuel cell constructions. *Bioelectrochem. Bioenerg.* **3**, 139-150 (1976).

20 Gebhardt, U., Luft, G., Richter, G. J. & Von Sturm, F. Development of an implantable electrocatalytic glucose sensor. *Bioelectrochem. Bioenerg.* **5**, 607-624 (1978).

21 Tominaga, M. *et al.* Electrocatalytic oxidation of glucose at gold-silver alloy, silver and gold nanoparticles in an alkaline solution. *J. Electroanal. Chem.* **590**, 37-46 (2006).

22 Tominaga, M., Shimazoe, T., Nagashima, M. & Taniguchi, I. Electrocatalytic oxidation of glucose at gold nanoparticle-modified carbon electrodes in alkaline and neutral solutions. *Electrochem. Commun.* **7**, 189-193 (2005).

23 Zhou, Y.-G., Yang, S., Qian, Q.-Y. & Xia, X.-H. Gold nanoparticles integrated in a nanotube array for electrochemical detection of glucose. *Electrochem. Commun.* **11**, 216-219 (2009).

24 Bai, Y., Yang, W., Sun, Y. & Sun, C. Enzyme-free glucose sensor based on a three-dimensional gold film electrode. *Sens. Actuators, B* **B134**, 471-476 (2008).

25 Yu, J.-J., Lu, S., Li, J.-W., Zhao, F.-Q. & Zeng, B.-Z. Characterization of gold nanoparticles electrochemically deposited on amine-functioned mesoporous silica films and electrocatalytic oxidation of glucose. *J. Solid State Electrochem.* **11**, 1211-1219 (2007).

26 Jin, C. & Taniguchi, I. Electrocatalytic oxidation of glucose on gold nanocomposite electrodes. *Chem. Eng. Technol.* **30**, 1298-1301 (2007).

27 Jena, B. K. & Raj, C. R. Enzyme-free amperometric sensing of glucose by using gold nanoparticles. *Chem.--Eur. J.* **12**, 2702-2708 (2006).

28 Tominaga, M., Shimazoe, T., Nagashima, M. & Taniguchi, I. Electro-catalytic oxidation of glucose at carbon electrodes modified with gold and gold-platinum alloy nanoparticles in an alkaline solution. *Chem. Lett.* **34**, 202-203 (2005).

29 Hsiao, M. W., Adzic, R. R. & Yeager, E. G. Electrochemical oxidation of glucose on single crystal and polycrystalline gold surfaces in phosphate buffer. *J. Electrochem. Soc.* **143**, 759-767 (1996).

30 Kokoh, K. B., Leger, J. M., Beden, B., Huser, H. & Lamy, C. "On line" chromatographic analysis of the products resulting from the electrocatalytic oxidation of D-glucose on pure and adatoms modified platinum and gold electrodes. Part II. Alkaline medium. *Electrochim. Acta* **37**, 1909-1918 (1992).

31 Adzic, R. R., Hsiao, M. W. & Yeager, E. B. Electrochemical oxidation of glucose on single crystal gold surfaces. *J. Electroanal. Chem. Interfacial Electrochem.* **260**, 475-485 (1989).

32 Nikolaeva, N. N., Khazova, O. A. & Vasil'ev, Y. B. Main characteristics of glucose electrooxidation on a gold anode. *Elektrokhimiya* **19**, 1042-1048 (1983).

33 Makovos, E. B. & Liu, C. C. A cyclic-voltammetric study of glucose oxidation on a gold electrode. *Bioelectrochem. Bioenerg.* **15**, 157-165 (1986).

34 LaCourse, W. R. & Johnson, D. C. Optimization of waveforms for pulsed amperometric detection of carbohydrates based on pulsed voltammetry. *Anal. Chem.* **65**, 50-55 (1993).

35 Nicol, M. J. The anodic behavior of gold. Part II. Oxidation in alkaline solutions. *Gold Bull.* **13**, 105-111 (1980).

36 Kirk, D. W., Foulkes, F. R. & Graydon, W. F. The electrochemical formation of gold(I) hydroxide on gold in aqueous potassium hydroxide. *J. Electrochem. Soc.* **127**, 1069-1076 (1980).

37 Xiang, C., Xie, Q. & Yao, S. Electrochemical quartz crystal impedance study of glucose oxidation on a nickel hydroxide modified Au electrode in alkaline solution. *Electroanalysis* **15**, 987-990 (2003).

38 Wikipedia-Contributors. Glucose Meters. *Wikipedia, The Free Encyclopedia* (2010).

39 Clark, L. C., Jr. & Lyons, C. Electrode systems for continuous monitoring in cardiovascular surgery. *Annals of the New York Academy of Sciences* **102**, 29-45 (1962).

40 Pasta, M., La Mantia, F. & Cui, Y. A new approach to glucose sensing at gold electrodes. *Electrochem. Commun.* **In Press, Accepted Manuscript**, doi:DOI: 10.1016/j.elecom.2010.07.033.

41 Heller, A. Implanted electrochemical glucose sensors for the management of diabetes. *Annu. Rev. Biomed. Eng.* **1**, 153-175 (1999).

42 Liu, Z., Huang, L., Zhang, L., Ma, H. & Ding, Y. Electrocatalytic oxidation of -glucose at nanoporous Au and Au-Ag alloy electrodes in alkaline aqueous solutions. *Electrochim. Acta* **54**, 7286-7293 (2009).

43 Dursun, Z., Ben Aoun, S. & Taniguchi, I. Electrocatalytic oxidation of D-glucose using a Cd ad-atom-modified Au(111) electrode in alkaline solution. *Turk. J. Chem.* **32**, 423-430 (2008).

44 Jin, C. & Chen, Z. Electrocatalytic oxidation of glucose on gold-platinum nanocomposite electrodes and platinum-modified gold electrodes. *Synth. Met.* **157**, 592-596 (2007).

45 Ben Aoun, S. *et al.* Effect of metal ad-layers on Au(111) electrodes on electrocatalytic oxidation of glucose in an alkaline solution. *J. Electroanal. Chem.* **567**, 175-183 (2004).

46 Watson, D. J. & Attard, G. A. The electro-oxidation of glucose using platinum-palladium bulk alloy single crystals. *Electrochim. Acta* **46**, 3157-3161 (2001).

47 Casella, I. G. & Guascito, M. R. Electrochemical preparation of a composite gold-cobalt electrode and its electrocatalytic activity in alkaline medium. *Electrochim. Acta* **45**, 1113-1120 (1999).

48 Pasta, M., La Mantia, F. & Cui, Y. Mechanism of glucose electrochemical oxidation on gold surface. *Electrochim. Acta* **55**, 5561-5568 (2010).

49 Yang, B. Y. & Montgomery, R. Alkaline degradation of glucose: effect of initial concentration of reactants. *Carbohydr. Res.* **280**, 27-45 (1996).

50 Finkelstein, N. P. & Hancock, R. D. New approach to the chemistry of gold. *Gold Bull.* **7**, 72-77 (1974).

51 McNicol, B. D., Rand, D. A. J. & Williams, K. R. Direct methanol-air fuel cells for road transportation. *J. Power Sources* **83**, 15-31 (1999).

52 Shukla, A. K., Suresh, P., Berchmans, S. & Rajendran, A. Biological fuel cells and their applications. *Current Science* **87**, 455-468 (2004).

53 Bockris, J. O. M., Piersma, B. J. & Gileadi, E. Anodic oxidation of cellulose and lower carbohydrates. *Electrochim. Acta* **9**, 1329-1332 (1964).

54 Jin, C. & Taniguchi, I. Electrocatalytic activity of silver modified gold film for glucose oxidation and its potential application to fuel cells. *Mater. Lett.* **61**, 2365-2367 (2007).

55 Schechner, P., Kroll, E., Bubis, E., Chervinsky, S. & Zussman, E. Silver-Plated Electrospun Fibrous Anode for Glucose Alkaline Fuel Cells. *J. Electrochem. Soc.* **154**, B942-B948 (2007).

56 McGinley, J., McHale, F. N., Hughes, P., Reid, C. N. & McHale, A. P. Production of Electrical Energy from Carbohydrates using a Transition Metal-Catalysed Liquid Alkaline Fuel Cell. *Biotechnol. Lett.* **26**, 1771-1776 (2004).

57 Chan, K.-Y. *et al.* Methods and apparatus for the oxidation of glucose molecules. WO patent 2002047806 (2002).

58 Schechner, P. *et al.* in *Fuel Cell Science, Engineering and Technology--2004, presented at the International Conference on Fuel Cell Science, Engineering and Technology, 2nd, Rochester, NY, United States, June 14-16, 2004.* 491-496.

59 Schechner, P., Bubis, E. & Mor, L. in *International Conference on Fuel Cell Science, Engineering, and Technology, Proceedings, 3rd, Ypsilanti, MI, United States, May 23-25, 2005.* 661-665.

60 Pasta, M. *et al.* Optimizing operating conditions and electrochemical characterization of glucose-gluconate alkaline fuel cells. *J. Power Sources* **In Press, Accepted Manuscript**.

61 De Wit, G., Kieboom, A. P. G. & Van Bekkum, H. Enolization and isomerization of monosaccharides in aqueous alkaline solution. *Carbohydr. Res.* **74**, 157-175 (1979).

62 De Wit, G., Kieboom, A. P. G. & Van Bekkum, H. Ionization and mutarotation of hexoses in aqueous alkaline solution as studied by carbon-13 NMR spectroscopy. *Recueil des Travaux Chimiques des Pays-Bas* **98**, 355-361 (1979).

63 Mor, L., Rubin, Z. & Schechner, P. Measuring open circuit voltage in a glucose alkaline fuel cell operated as a continuous stirred tank reactor. *Journal of Fuel Cell Science and Technology* **5**, 014503/014501-014503/014504 (2008).

64 Largeaud, F., Kokoh, K. B., Beden, B. & Lamy, C. On the electrochemical reactivity of anomers: electrocatalytic oxidation of alpha - and beta -D-glucose on platinum electrodes in acid and basic media. *J. Electroanal. Chem.* **397**, 261-269 (1995).

65 La Mantia, F., Vetter, J. & Novak, P. Impedance spectroscopy on porous materials: A general model and application to graphite electrodes of lithium-ion batteries. *Electrochim. Acta* **53**, 4109-4121 (2008).

66 Pasta, M., Ruffo, R., Falletta, E., Mari, C. M. & Della Pina, C. Alkaline glucose oxidation on nanostructured gold electrodes. *Gold Bull. (London, U. K.)* **43**, 57-64 (2010).

67 Vasil'ev, Y. B., Khazova, O. A. & Nikolaeva, N. N. Kinetics and mechanism of glucose electrooxidation on different electrode-catalysts. Part II. Effect of the nature of the electrode and the electrooxidation mechanism. *J. Electroanal. Chem. Interfacial Electrochem.* **196**, 127-144 (1985).

68 Lertanantawong, B. *et al.* Study of the Underlying Electrochemistry of Polycrystalline Gold Electrodes in Aqueous Solution and Electrocatalysis by Large Amplitude Fourier Transformed Alternating Current Voltammetry. *Langmuir* **24**, 2856-2868 (2008).

69 Corbett, W. M. & Liddle, A. M. The alkaline degradation of glucose and some of its acetyl derivatives. *J. Chem. Soc.*, 531-538 (1961).

70 Burke, L. D. & Nugent, P. F. The electrochemistry of gold: I. The redox behavior of the metal in aqueous media. *Gold Bull. (London)* **30**, 43-53 (1997).

71 Burke, L. D. & Nugent, P. F. The electrochemistry of gold. II The electrocatalytic behavior of the metal in aqueous media. *Gold Bull. (London)* **31**, 39-50 (1998).

72 Nicol, M. J. The anodic behavior of gold. Part I. Oxidation in acidic solutions. *Gold Bull.* **13**, 46-55 (1980).

73 Ernst, S., Heitbaum, J. & Hamann, C. H. The electrooxidation of glucose in phosphate buffer solutions. Part I. Reactivity and kinetics below 350 mV/RHE. *J. Electroanal. Chem. Interfacial Electrochem.* **100**, 173-183 (1979).

74 Ernst, S., Heitbaum, J. & Hamann, C. H. The electrooxidation of glucose in phosphate buffer solutions: kinetics and reaction mechanism. *Ber. Bunsenges. Phys. Chem.* **84**, 50-55 (1980).

75 Bard, A. J. & Faulkner, L. R. *Electrochemical methods : fundamentals and applications*. 2nd edn, (John Wiley, 2001).

76 Comotti, M., Della Pina, C., Matarrese, R., Rossi, M. & Siani, A. Oxidation of alcohols and sugars using Au/C catalysts. *Appl. Catal., A* **291**, 204-209 (2005).

77 Toles, C. A., Marshall, W. E. & Johns, M. M. Surface functional groups on acid-activated nutshell carbons. *Carbon* **37**, 1207-1214 (1999).

78 Li, Y.-H. *et al.* Adsorption of cadmium(II) from aqueous solution by surface oxidized carbon nanotubes. *Carbon* **41**, 1057-1062 (2003).

79 Yu, X. *et al.* Effect of Nitric Acid Treatment on Carbon Nanotubes (CNTs)-Cordierite Monoliths Supported Ruthenium Catalysts for Ammonia Synthesis. *Catal. Lett.* **124**, 168-173 (2008).

80 Tohji, K. *et al.* Purifying single-walled nanotubes. *Nature (London)* **383**, 679 (1996).

81 Parekh, B. B., Fanchini, G., Eda, G. & Chhowalla, M. Improved conductivity of transparent single-wall carbon nanotube thin films via stable postdeposition functionalization. *Appl. Phys. Lett.* **90**, 121913/121911-121913/121913 (2007).

82 Zhou, W. *et al.* Charge transfer and Fermi level shift in p-doped single-walled carbon nanotubes. *Physical Review B: Condensed Matter and Materials Physics* **71**, 205423/205421-205423/205427 (2005).

83 Beaudrouet, E., Le Gal La Salle, A. & Guyomard, D. Nanostructured manganese dioxides: Synthesis and properties as supercapacitor electrode materials. *Electrochim. Acta* **54**, 1240-1248 (2009).

84 Davis, J. B. & H. F. Yarbrough, J. Preliminary Experiments on a Microbial Fuel Cell. *Science* **137**, 615-616 (1962).

85 Dixon, B. Current Thoughts on Microbial Fuel-Cells. *Bio-Technology* **2**, 921-921 (1984).

86 Chaudhuri, S. K. & Lovley, D. R. Electricity generation by direct oxidation of glucose in mediatorless microbial fuel cells. *Nature Biotechnology* **21**, 1229-1232, doi:10.1038/nbt867 (2003).

87 Lovley, D. R. Bug juice: harvesting electricity with microorganisms. *Nature Reviews Microbiology* **4**, 497-508, doi:10.1038/nrmicro1442 (2006).

88 Logan, B. E. Exoelectrogenic bacteria that power microbial fuel cells. *Nature Reviews Microbiology* **7**, 375-381, doi:10.1038/nrmicro2113 (2009).

89 Liu, H., Ramnarayanan, R. & Logan, B. E. Production of electricity during wastewater treatment using a single chamber microbial fuel cell. *Environmental Science & Technology* **38**, 2281-2285, doi:10.1021/es034923g (2004).

90 Daniel, D. K., Das Mankidy, B., Ambarish, K. & Manogari, R. Construction and operation of a microbial fuel cell for electricity generation from wastewater. *International Journal of Hydrogen Energy* **34**, 7555-7560, doi:10.1016/j.ijhydene.2009.06.012 (2009).

91 Ahn, Y. & Logan, B. E. Effectiveness of domestic wastewater treatment using microbial fuel cells at ambient and mesophilic temperatures. *Bioresource Technology* **101**, 469-475, doi:10.1016/j.biortech.2009.07.039 (2010).

92 Bond, D. R., Holmes, D. E., Tender, L. M. & Lovley, D. R. Electrode-reducing microorganisms that harvest energy from marine sediments. *Science* **295**, 483-485 (2002).

93 Tender, L. M. *et al.* Harnessing microbially generated power on the seafloor. *Nature Biotechnology* **20**, 821-825, doi:10.1038/nbt716 (2002).

94 Konikoff, J. J., Reynolds, L. W. & Harris, E. S. Electrical energy from biological systems. *Aerospace Medicine* **34**, 1129-1133 (1963).

95 Logan, B. E. *et al.* Microbial Fuel Cells: Methodology and Technology. *Environmental Science & Technology* **40**, 5181-5192 (2006).

96 Logan, B. E. *et al.* Microbial fuel cells: Methodology and technology. *Environmental Science & Technology* **40**, 5181-5192, doi:10.1021/es0605016 (2006).

97 Cheng, S., Liu, H. & Logan, B. E. Increased power generation in a continuous flow MFC with advective flow through the porous anode and reduced electrode spacing. *Environmental Science & Technology* **40**, 2426-2432, doi:10.1021/es051652w (2006).

98 Kim, J. R., Cheng, S., Oh, S. E. & Logan, B. E. Power generation using different cation, anion, and ultrafiltration membranes in microbial fuel cells. *Environmental Science & Technology* **41**, 1004-1009, doi:10.1021/es062202m (2007).

99 Logan, B., Cheng, S., Watson, V. & Estadt, G. Graphite fiber brush anodes for increased power production in air-cathode microbial fuel cells. *Environmental Science & Technology* **41**, 3341-3346, doi:10.1021/es062644y (2007).

100 Scott, K., Rimbu, G. A., Katuri, K. P., Prasad, K. K. & Head, I. M. Application of modified carbon anodes in microbial fuel cells. *Process Safety and Environmental Protection* **85**, 481-488, doi:10.1205/psep07018 (2007).

101 Kim, B. H., Chang, I. S. & Gadd, G. M. Challenges in microbial fuel cell development and operation. *Applied Microbiology and Biotechnology* **76**, 485-494, doi:10.1007/s00253-007-1027-4 (2007).

102 Wang, C. *et al.* Proton exchange membrane fuel cells with carbon nanotube based electrodes. *Nano Letters* **4**, 345-348, doi:10.1021/nl034952p (2004).

103 Shi, J., Hu, Y. Q. & Hua, Y. X. Self-assembly of platinum nanoparticle/multiwalled carbon nanotube multilayer film on Au substrate electrode. *Electroanalysis* **20**, 1483-1489, doi:10.1002/elan.200804207 (2008).

104 Magrez, A. *et al.* Cellular toxicity of carbon-based nanomaterials. *Nano Letters* **6**, 1121-1125, doi:10.1021/nl060162e (2006).

105 Panessa-Warren, B. J., Warren, J. B., Wong, S. S. & Misewich, J. A. Biological cellular response to carbon nanoparticle toxicity. *Journal of Physics-Condensed Matter* **18**, S2185-S2201, doi:10.1088/0953-8984/18/33/s34 (2006).

106 Morozan, A. *et al.* The biocompatibility microorganisms-carbon nanostructures for applications in microbial fuel cells. *Physica Status Solidi a-Applications and Materials Science* **204**, 1797-1803, doi:10.1002/pssa.200675344 (2007).

107 Qiao, Y., Li, C. M., Bao, S. J. & Bao, Q. L. Carbon nanotube/polyaniline composite as anode material for microbial fuel cells. *Journal of Power Sources* **170**, 79-84, doi:10.1016/j.jpowsour.2007.03.048 (2007).

108 Zou, Y. J. *et al.* A mediatorless microbial fuel cell using polypyrrole coated carbon nanotubes composite as anode material. *International Journal of Hydrogen Energy* **33**, 4856-4862, doi:10.1016/j.ijhydene.2008.06.061 (2008).

109 Tsai, H. Y., Wu, C. C., Lee, C. Y. & Shih, E. P. Microbial fuel cell performance of multiwall carbon nanotubes on carbon cloth as electrodes. *Journal of Power Sources* **194**, 199-205, doi:10.1016/j.jpowsour.2009.05.018 (2009).

110 Hu, L. *et al.* Stretchable, Porous, and Conductive Energy Textiles. *Nano Letters* **10**, 708-714 (2010).

111 Bond, D. R. & Lovley, D. R. Electricity production by Geobacter sulfurreducens attached to electrodes. *Applied and Environmental Microbiology* **69**, 1548-1555, doi:10.1128/aem.69.3.1548-1555.2003 (2003).

112 Zuo, Y., Xing, D. F., Regan, J. M. & Logan, B. E. Isolation of the exoelectrogenic bacterium Ochrobactrum anthropi YZ-1 by using a U-tube microbial fuel cell. *Applied and Environmental Microbiology* **74**, 3130-3137, doi:10.1128/aem.02732-07 (2008).

113 Rezaei, F. *et al.* Simultaneous Cellulose Degradation and Electricity Production by Enterobacter cloacae in a Microbial Fuel Cell. *Applied and Environmental Microbiology* **75**, 3673-3678, doi:10.1128/aem.02600-08 (2009).

114 Xing, D. F., Zuo, Y., Cheng, S. A., Regan, J. M. & Logan, B. E. Electricity generation by Rhodopseudomonas palustris DX-1. *Environmental Science & Technology* **42**, 4146-4151, doi:10.1021/es800312v (2008).

115 Xing, D. F., Cheng, S. A., Logan, B. E. & Regan, J. M. Isolation of the exoelectrogenic denitrifying bacterium Comamonas denitrificans based on dilution to extinction. *Applied Microbiology and Biotechnology* **85**, 1575-1587, doi:10.1007/s00253-009-2240-0 (2010).

116 Reguera, G., Pollina, R. B., Nicoll, J. S. & Lovley, D. R. Possible nonconductive role of Geobacter sulfurreducens pilus nanowires in biofilm formation. *Journal of Bacteriology* **189**, 2125-2127, doi:10.1128/jb.01284-06 (2007).

117 Reguera, G. *et al.* Extracellular electron transfer via microbial nanowires. *Nature* **435**, 1098-1101, doi:10.1038/nature03661 (2005).

118 Gorby, Y. A. *et al.* Electrically conductive bacterial nanowires produced by Shewanella oneidensis strain MR-1 and other microorganisms. *Proceedings of the National Academy of Sciences of the United States of America* **103**, 11358-11363, doi:10.1073/pnas.0604517103 (2006).

119 Rabaey, K. & Verstraete, W. Microbial fuel cells: novel biotechnology for energy generation. *Trends in Biotechnology* **23**, 291-298, doi:10.1016/j.tibtech.2005.04.008 (2005).

120 Zhao, F. *et al.* Challenges and constraints of using oxygen cathodes in microbial fuel cells. *Environmental Science & Technology* **40**, 5193-5199, doi:10.1021/es060332p (2006).

121 Zuo, Y., Cheng, S. & Logan, B. E. Ion exchange membrane cathodes for scalable microbial fuel cells. *Environmental Science & Technology* **42**, 6967-6972, doi:10.1021/es801055r (2008).

122 Oh, S., Min, B. & Logan, B. E. Cathode performance as a factor in electricity generation in microbial fuel cells. *Environmental Science & Technology* **38**, 4900-4904, doi:10.1021/es049422p (2004).

123 HaoYu, E., Cheng, S., Scott, K. & Logan, B. Microbial fuel cell performance with non-Pt cathode catalysts. *Journal of Power Sources* **171**, 275-281, doi:10.1016/j.jpowsour.2007.07.010 (2007).

124 Rabaey, K. & Keller, J. Microbial fuel cell cathodes: from bottleneck to prime opportunity? *Water Science and Technology* **57**, 655-659, doi:10.2166/wst.2008.103 (2008).

125 Rozendal, R. A., Hamelers, H. V. M., Rabaey, K., Keller, J. & Buisman, C. J. N. Towards practical implementation of bioelectrochemical wastewater treatment. *Trends in Biotechnology* **26**, 450-459 (2008).

126 Kim, J. R., Jung, S. H., Regan, J. M. & Logan, B. E. Electricity generation and microbial community analysis of alcohol powered microbial fuel cells. *Bioresource Technology* **98**, 2568-2577, doi:10.1016/j.biortech.2006.09.036 (2007).

127 Logan, B. E., Murano, C., Scott, K., Gray, N. D. & Head, I. M. Electricity generation from cysteine in a microbial fuel cell. *Water Research* **39**, 942-952, doi:10.1016/j.watres.2004.11.019 (2005).

128 Min, B., Kim, J. R., Oh, S. E., Regan, J. M. & Logan, B. E. Electricity generation from swine wastewater using microbial fuel cells. *Water Research* **39**, 4961-4968, doi:10.1016/j.watres.2005.09.039 (2005).

129 Min, B. K., Cheng, S. A. & Logan, B. E. Electricity generation using membrane and salt bridge microbial fuel cells. *Water Research* **39**, 1675-1686, doi:10.1016/j.watres.2005.02.002 (2005).

130 Oh, S. E. & Logan, B. E. Proton exchange membrane and electrode surface areas as factors that affect power generation in microbial fuel cells. *Applied Microbiology and Biotechnology* **70**, 162-169, doi:10.1007/s00253-005-0066-y (2006).

131 Cao, X. *et al.* A new method for water desalination using microbial desalination cells. *Environmental Science & Technology* **43**, 7148-7152, doi:10.1021/es901950j (2009).

132 Cheng, S., Liu, H. & Logan, B. E. Increased performance of single-chamber microbial fuel cells using an improved cathode structure. *Electrochemistry Communications* **8**, 489-494, doi:10.1016/j.elecom.2006.01.010 (2006).

133 Kim, J. R., Premier, G. C., Hawkes, F. R., Dinsdale, R. M. & Guwy, A. J. Development of a tubular microbial fuel cell (MFC) employing a membrane electrode assembly cathode. *Journal of Power Sources* **187**, 393-399, doi:10.1016/j.jpowsour.2008.11.020 (2009).

134 Zuo, Y., Cheng, S., Call, D. & Logan, B. E. Tubular membrane cathodes for scalable power generation in microbial fuel cells. *Environmental Science & Technology* **41**, 3347-3353, doi:10.1021/es0627601 (2007).

135 Takenaka, S., Matsumori, H., Matsune, H., Tanabe, E. & Kishida, M. High durability of carbon nanotube-supported Pt electrocatalysts covered with silica layers for the cathode in a PEMFC. *Journal of the Electrochemical Society* **155**, B929-B936, doi:10.1149/1.2952665 (2008).

136 Taylor, E. J., Anderson, E. B. & Vilambi, N. R. K. Preparation of high-platinum-utilization gas-diffusion electrodes for proton-exchange-membrane fuel-cells. *Journal of the Electrochemical Society* **139**, L45-L46 (1992).

137 Saminathan, K., Kamavaram, V., Veedu, V. & Kannan, A. M. Preparation and evaluation of electrodeposited platinum nanoparticles on in situ carbon nanotubes grown carbon paper for proton exchange membrane fuel cells. *International Journal of Hydrogen Energy* **34**, 3838-3844, doi:10.1016/j.ijhydene.2009.03.009 (2009).

138 Golikand, A. N., Asgari, M., Lohrasbi, E. & Yari, M. Electrocatalytic oxygen reduction on single-walled carbon nanotubes supported Pt alloys nanoparticles in acidic and alkaline conditions. *Journal of Applied Electrochemistry* **39**, 1369-1377, doi:10.1007/s10800-009-9812-7 (2009).

139 Balch, W. E., Fox, G. E., Magrum, L. J., Woese, C. R. & Wolfe, R. S. Methanogens - Re-Evaluation of a Unique Biological Group. *Microbiological Reviews* **43**, 260-296 (1979).

140 Zhao, F. *et al.* Application of pyrolysed iron(II) phthalocyanine and CoTMPP based oxygen reduction catalysts as cathode materials in microbial fuel cells. *Electrochemistry Communications* **7**, 1405-1410, doi:10.1016/j.elecom.2005.09.032 (2005).

141 Cheng, S., Liu, H. & Logan, B. E. Power densities using different cathode catalysts (Pt and CoTMPP) and polymer binders (Nafion and PTFE) in single chamber microbial fuel cells. *Environmental Science & Technology* **40**, 364-369, doi:10.1021/es0512071 (2006).

142 Zhang, F., Cheng, S. A., Pant, D., Van Bogaert, G. & Logan, B. E. Power generation using an activated carbon and metal mesh cathode in a microbial fuel cell. *Electrochemistry Communications* **11**, 2177-2179, doi:10.1016/j.elecom.2009.09.024 (2009).

143 Aelterman, P., Versichele, M., Genettello, E., Verbeken, K. & Verstraete, W. Microbial fuel cells operated with iron-chelated air cathodes. *Electrochimica Acta* **54**, 5754-5760, doi:10.1016/j.electacta.2009.05.023 (2009).

144 Gniotek, K. & Krucinska, I. The basic problems of textronics. *Fibres & Textiles in Eastern Europe* **12**, 13-16 (2004).

145 Lukowicz, P., Kirstein, T. & Troster, G. Wearable systems for health care applications. *Methods Inf. Med.* **43**, 232-238 (2004).

146 Park, S. & Jayaraman, S. Smart textiles: Wearable electronic systems. *Mrs Bulletin* **28**, 585-591 (2003).

147 Hyde, G. K., Park, K. J., Stewart, S. M., Hinestroza, J. P. & Parsons, G. N. Atomic layer deposition of Conformal inorganic nanoscale coatings on three-dimensional natural fiber systems: Effect of surface topology on film growth characteristics. *Langmuir* **23**, 9844-9849 (2007).

148 Shim, B. S., Chen, W., Doty, C., Xu, C. L. & Kotov, N. A. Smart Electronic Yarns and Wearable Fabrics for Human Biomonitoring made by Carbon Nanotube Coating with Polyelectrolytes. *Nano Letters* **8**, 4151-4157 (2008).

149 Hecht, D. S., Hu, L. & Gruner, G. Electronic properties of carbon nanotube/fabric composites. *Current Applied Physics* **7**, 60-63 (2007).

150 Sekitani, T. *et al.* Stretchable active-matrix organic light-emitting diode display using printable elastic conductors. *Nature Materials* **8**, 494-499 (2009).

151 Lewin, M. P., E. . *Handbook of fiber chemistry*. (Marcel Dekker Inc 1998).

152 Pushparaj, V. L. *et al.* Flexible energy storage devices based on nanocomposite paper. *Proceedings of the National Academy of Sciences of the United States of America* **104**, 13574-13577 (2007).

153 Yun, S., Jang, S. D., Yun, G. Y., Kim, J. H. & Kim, J. Paper transistor made with covalently bonded multiwalled carbon nanotube and cellulose. *Applied Physics Letters* **95** (2009).

154 Zhang, H. *et al.* Regenerated-cellulose/multiwalled-carbon-nanotube composite fibers with enhanced mechanical properties prepared with the ionic liquid 1-allyl-3-methylimidazolium chloride. *Advanced Materials* **19**, 698-+ (2007).

155 Islam, M. F., Rojas, E., Bergey, D. M., Johnson, A. T. & Yodh, A. G. High weight fraction surfactant solubilization of single-wall carbon nanotubes in water. *Nano Letters* **3**, 269-273 (2003).

156 Tracton, A. A. *Coating Handbook*. (Marcel Dekker, Inc, 2001).

157 Hertel T.; Walkup, R. E. A., P. . Deformation of carbon nanotubes by surface van der Waals forces. *Phys. Rev. B* **58**, 13870 (1998).

158 An, K. H. *et al.* Supercapacitors using single-walled carbon nanotube electrodes. *Advanced Materials* **13**, 497-+ (2001).

159 Parekh, B. B. F., G.; Eda, G.; Chowalla, M. Improved conductivity of transparent single-wall carbon nanotube thin films via stable postdeposition functionalization. *Appl. Phys. Lett.* **90**, 121913 (2007).

160 Zhou, W. V., J.; Nemes, N. M.; Fischer, J. E.; Borondics, F.; Kamaras, K.; Tanner, D. B. Charge transfer and Fermi level shift in p-doped single-walled carbon nanotubes. *Phys. Rev. B* **71**, 205423 (2005).

161 Geng, H. K., K.; So, K.; Lee, Y.; Chang, Y.; Lee, Y. Effect of Acid Treatment on Carbon Nanotube-Based Conducting Films. *J. Am. Chem. Soc.* **129**, 7758 (2007).

162 Iijima, S. Structural Flexibility of Carbon Nanotubes. *J. Chem. Phys.* **104**, 2089 (1996).

163 Kim, D. H. & Rogers, J. A. Stretchable Electronics: Materials Strategies and Devices. *Advanced Materials* **20**, 4887-4892 (2008).

164 Yu, C. M., C.; Rong, J.; Wei, B.; Jiang, H. Stretchable Supercapacitors Based on Buckled Single-Walled Carbon-Nanotube Macrofilms. *Adv. Mater.* **21**, 1 (2009).

165 Wakelyn, P. J. B., N. R.; French, A. D.; Thibodeaux, D. P. *Cotton Fiber Chemistry and Technology*. (CRC Press, Taylor & Francis Group, 2007).

166 Futaba, D. N. *et al.* Shape-engineerable and highly densely packed single-walled carbon nanotubes and their application as super-capacitor electrodes. *Nature Materials* **5**, 987-994 (2006).

167 M. Kaempgen, C. K. C., J. Ma, G. Gruner. Printable CNT thin film supercap. *Nano. Lett.* **5**, 1872 (2009).

168 Bonnefoi, L. S., P.; Fauvarque, J. F.; Sarrazin, C.; Dugast, A. Electrode optimisation for carbon power supercapacitors. *J. Power Source* **79**, 37 (1999).

169 Hu, L. C., J. W.; Yang, Y.; Jeong, S.; La Mantia, F.; Cui, L.; Cui, Y. Highly Conductive Paper for Energy Storage Devices. *PNAS* **ASAP** (2009).

170 Niu, C. M., Sichel, E. K., Hoch, R., Moy, D. & Tennent, H. High power electrochemical capacitors based on carbon nanotube electrodes. *Applied Physics Letters* **70**, 1480-1482 (1997).

171 Lee, J. Y., Connor, S. T., Cui, Y. & Peumans, P. Solution-processed metal nanowire mesh transparent electrodes. *Nano Letters* **8**, 689-692 (2008).

172 Conway, B. E. *Electrochemical Supercapacitors*. (1999).

173 Subramanian, V., Zhu, H. W. & Wei, B. Q. Synthesis and electrochemical characterizations of amorphous manganese oxide and single walled carbon nanotube composites as supercapacitor electrode materials. *Electrochemistry Communications* **8**, 827-832 (2006).

174 Arabale, G. *et al.* Enhanced supercapacitance of multiwalled carbon nanotubes functionalized with ruthenium oxide. *Chemical Physics Letters* **376**, 207-213 (2003).

175 Abollino, O., Giacomino, A., Malandrino, M., Piscionieri, G. & Mentasti, E. Determination of mercury by anodic stripping voltammetry with a gold nanoparticle-modified glassy carbon electrode. *Electroanalysis* **20**, 75-83 (2007).

176 Wang, Y. Z., I. Electrophoretic Deposition of Manganese Dioxide-Multiwalled Carbon Nanotube Composites for Electrochemical Supercapacitors. *Langmuir* **ASAP** (2009).

177 Deng, G. H. X., X.; Chen, J. H.; Zeng, X. B.; He, D. L.; Kuang, Y. F. . A new method to prepare RuO2 Æ xH2O/carbon nanotube composite for electrochemical capacitors. *Carbon* **43**, 1557 (2005).

178 Gniotek, K. & Krucinska, I. The basic problems of textronics. *Fibres & Textiles in Eastern Europe* **12**, 13-16 (2004).

179 Hu, L. *et al.* Stretchable, Porous, and Conductive Energy Textiles. *Nano Letters*, ACS ASAP.

180 Prosini, P. P., Pozio, A., Botti, S. & Ciardi, R. Electrochemical studies of hydrogen evolution, storage and oxidation on carbon nanotube electrodes. *J. Power Sources* **118**, 265-269 (2003).

181 Newman, J. S. & Tobias, C. W. Theoretical analysis of current distribution in porous electrodes. *J. Electrochem. Soc.* **109**, 1183-1191 (1962).

182 De Levie, R. Porous electrodes in electrolyte solutions. IV. *Electrochim. Acta* **9**, 1231-1245 (1964).

183 Ng, S.-H., La Mantia, F. & Novak, P. A multiple working electrode for electrochemical cells: a tool for current density distribution studies. *Angew. Chem., Int. Ed.* **48**, 528-532 (2009).

184 Wikipedia-Contributors. Constituents of Human Blood. *Wikipedia, The Free Encyclopedia* (2010).

185 Wikipedia-Contributors. Diabetes Mellitus. *Wikipedia, The Free Encyclopedia* (2010).

186 Comotti, M., Della Pina, C., Falletta, E. & Rossi, M. Aerobic oxidation of glucose with gold catalyst: hydrogen peroxide as intermediate and reagent. *Adv. Synth. Catal.* **348**, 313-316 (2006).

187 DeSantis, T. Z., Jr. *et al.* NAST: a multiple sequence alignment server for comparative analysis of 16S rRNA genes. *Nucl. Acids Res.* **34**, W394-399, doi:10.1093/nar/gkl244 (2006).

188 Ludwig, W. *et al.* ARB: a software environment for sequence data. *Nucleic Acids Res.* **32**, 1363 (2004).

189 DeSantis, T. Z. *et al.* Greengenes, a Chimera-Checked 16S rRNA Gene Database and Workbench Compatible with ARB. *Appl. Environ. Microbiol.* **72**, 5069-5072 (2006).

ACKNOWLEDGMENTS

I believe it is clear from my dissertation that my PhD required a multi-subject approach; that's why I worked with many people that I need to acknowledge.

Università degli Studi di Milano

Ho messo piede per la prima volta in Via Celoria Milano ormai otto anni fa: qui ho studiato (tanto), mi sono laureato (trienennale e magistrale) e qui mi sto dottorando, sempre e comunque in Chimica Industriale. Non so se avrò modo di tornarci, le speranze per la mia generazione sono limitate ed il futuro è molto incerto. Quindi colgo l'occasione per ringraziare tutte le persone che qui ho incontrato, con cui ho studiato e lavorato.

In particolare il Prof. Rossi che mi ha iniziato al mondo della ricerca, trasmesso la passione per questo mestiere, mi ha sempre incoraggiato a pensare con la mia testa, dandomi lo spazio di andare a confrontarmi con altre realtà in altri gruppi di ricerca ed in altri campi. Non è da tutti avere questa fortuna.

Un particolare ringraziamento a Cristina ed Ermelinda, le mie correlatrici.

Università degli Studi di Milano-Bicocca

All'U5 di via Cozzi, dipartimento di Scienza dei Materiali sono arrivato all'inizio del mio dottorato. Qui ho tovato un bell'ambiente giovane e dinamico in cui mi sono inserito immediatamente.

Un particolare ringraziamento va al Prof. Mari per avermi accolto nel suo laboratorio ed avermi insegnato che anche la forma non è da trascurare.

Riccardo, il mio mentore: a lui devo molto, non solo perchè è colui che mi ha introdotto all'elettrochimica sperimentale, ma anche per avermi dato l'opportunità di andare a confrontarmi con una realtà come quella di Stanford dove il merito e il duro lavoro è premiato, ridandomi motivazioni che ormai avevo perduto.

Un particolare ringraziamento al Teo, fido compagno di laboratorio, eterno consulente informatico e maniaco dell'ordine alla mia altezza.

Stanford University

I spent almost half of my PhD at Stanford, in the Material Science and Engineering department. Meeting Stanford was mind-blowing: my supervisor Prof. Cui was only 35 years old, his group was huge (about 35 people are working in his lab now) and each member had a different

background: physicians, engineers, material scientists, chemists working together on many projects. I was not used to any of that but I easily got accustomed to this hard working environment that can give a lot of satisfactions.

Let me start by thanking Prof. Cui, he received me in his group giving me the freedom and the possibility to work on different topics.

Prof. Huggins (Bob) and his wife Patty, they welcomed me in their home when I first arrived, helping me in settling down and replenishing me with the vitamin C of the oranges from their beautiful garden.

I'd like to thank all the Cui's group members: I haven't worked with all of them directly, but I followed their researches in the never-ending Wednesday group meetings.

Let me thank Fabio, the pure blood electrochemist: I learned so much from him working together on many projects. I hope and I know we will work together again in the future.

Bing, the carbon nanotubes master: I've never worked with anybody so active and productive. He is always functioning, thinking, on many new ideas. I enjoyed also his Chinese cooking and his always positive mood.

Xing, we worked together on microbial fuel cells: I think we can get a lot of satisfactions from this work.

Heather, my English teacher: my writing skills improved a lot thanks to her.

I need also to thank Jungmee (JM) for all the time we spent together, the lunches at the Tree House (their food is probably the only thing I don't miss), the SF Opera House etc.

Special mention to all the guys from the MSE department: Rodrigo, Leslie, Andreina, Prof. Salleo. The Alan Soccer technicians team, Tommaso, Xavi, Valerio and the South American colony.

All the guys at Stanford beach volley court, Sandro, Joe, Paul, Carolina, Dimitri, Igor for the hours we spent in the beautiful sun of California.

Infine un ringraziamento particolare a tutti i collegiali del Collegio di Milano dove ho vissuto durante il mio primo anno di dottorato. Anche qui la mescolanza di background tra i più diversi ha creato un ambiente culturale vivace che mi ha dato l'opportunità di crescere molto a livello personale.

PUBLICATIONS

[1] **M. Pasta**, F. La Mantia, R. Ruffo, F. Peri, C.D. Pina, C.M. Mari, Optimizing operating conditions and electrochemical characterization of glucose-gluconate alkaline fuel cells, J. Power Sources, (2011), 196(3), 1273-1278.

[2] **M. Pasta**, F. La Mantia, Y. Cui, A new approach to glucose sensing at gold electrodes. Electrochem. Commun. 12, (2010) 1407-1410.

[3] **M. Pasta**, F. La Mantia, L. Hu, H.D. Deshazer, Y. Cui, Aqueous supercapacitors on conductive cotton, Nano Res., 3 (2010) 452-458.

[4] **M. Pasta**, F. La Mantia, Y. Cui, Mechanism of glucose electrochemical oxidation on gold surface, Electrochim. Acta, 55 (2010) 5561-5568.

[5] **M. Pasta**, R. Ruffo, E. Falletta, C.M. Mari, C. Della Pina, Alkaline glucose oxidation on nanostructured gold electrodes, Gold Bull. (London, U. K.), 43 (2010) 57-64.

[6] L. Hu, **M. Pasta**, F. La Mantia, L. Cui, S. Jeong, H.D. Deshazer, J.W. Choi, S.M. Han, Y. Cui, Stretchable, Porous, and Conductive Energy Textiles, Nano Letters, 10 (2010) 708-714.

[7] C. Della Pina, E. Falletta, M. Lo Faro, **M. Pasta**, M. Rossi, Gold-catalysed synthesis of polypyrrole, Gold Bull. (London, U. K.), 42 (2009) 27-33.

[8] Z. Chen, C. Della Pina, E. Falletta, M. Lo Faro, **M. Pasta**, M. Rossi, N. Santo, Facile synthesis of polyaniline using gold catalyst, J. Catal., 259 (2008) 1-4.